NASA CONTRACTOR REPORT

NASA CR-1558

NASA CR-1558

AN ANALYSIS OF FLIGHT TEST DATA ON THE C-141A AIRCRAFT

by J. H. Paterson, W. T. Blackerby,

J. C. Schwanebeck, and W. F. Braddock

Prepared by

LOCKHEED-GEORGIA COMPANY

Marietta, Ga.

for Langley Research Center

NATIONAL AERONAUTICS AND SPACE ADMINISTRATION • WASHINGTON, D. C. • JUNE 1970

AN ANALYSIS OF FLIGHT TEST DATA

ON THE C-141A AIRCRAFT

By J. H. Paterson, W. T. Blackerby, J. C. Schwanebeck,
and W. F. Braddock

CONTENTS

AN ANALYSIS OF FLIGHT TEST DATA

ON THE C-141A AIRCRAFT

by

J. H. Paterson
W. T. Blackerby
J. C. Schwanebeck
W. F. Braddock
Lockheed-Georgia Company

SUMMARY

This study comprises part of a research program to investigate the degree of correlation attainable between flight test measured airplane drag levels and the full scale drag that would be predicted on the basis of wind tunnel data. In this phase of the study the purpose is to analyze available flight test data on the C-141A in much greater detail than heretofore, and to establish the validity of the measured flight test drag.

In achieving this objective, existing flight test results obtained during the Air Force Category I and II testing of the C-141A were used to derive drag polars and minimum profile drag for a rigid airplane, with proper accounting for the effects of aeroelastic distortion on the wing induced and profile drags, and on the airplane trim drag. In addition, the effects of airplane center of gravity location and flight test instrumentation were investigated.

An assessment of the inherent inaccuracies of flight measured thrust and other parameters such as weight, speed, and altitude was made and related to the resulting rigid drag. Scatter of the measured flight test data averages around 3.5 percent of cruise drag and compares with an estimated inaccuracy of 3.3 percent.

An insight into the scale effect on profile drag, defined as skin friction plus form drag, for large subsonic aircraft is provided by the results. The profile drag is shown by the flight test data to vary according to classical skin friction laws throughout the Reynolds Number range from 25 million to 86 million. This implies that the C-141A level of distributed roughness is sufficiently small that a terminal value of skin friction is not sustained.

INTRODUCTION

Drag prediction in recent years has assumed particular importance in the field of subsonic and transonic aerodynamics. The competitive atmosphere generated by operators of jet transport aircraft requires the manufacturer to provide extremely stringent performance guarantees. Thus the task of accurately predicting payload-range characteristics and operating costs of such aircraft has magnified considerably. The implications of an error in predicting aircraft drag are serious for the manufacturer as well as the operator. For example, an increase of one drag count, $\Delta C_D = 0.0001$, or less than 0.40 percent of the cruise drag on the C-5 is equivalent to a reduction of approximately 1,000 pounds of payload for the design mission. In terms of fleet costs for a ten year operating period this amounts to several millions of dollars in lost revenue.

During the last decade, aerodynamic design techniques for estimating drag have certainly improved, but the state-of-the-art still relies on a mixture of semi-empirical methods based on wind tunnel data coupled with flight test information where such data are available. Generally, the approaches to full scale drag estimation fall into two categories: (1) Those manufacturers who have accumulated a great deal of flight test information on a family of aircraft of generally similar configuration, and have produced in parametric form, design charts to predict the performance of the new design. Wind tunnel tests are used to provide incremental data during the configuration development. (2) Some manufacturers believe that with continuing improvements in tunnel tests techniques, the absolute value of drag measured at model scale Reynolds Numbers can be extrapolated to full scale on the basis of classical skin friction laws. This is generally accompanied by a detail model breakdown test to account for component interference and excess profile drag.

Experience has shown that neither of the above methods necessarily guarantees accurately predicted full scale drag. Whereas method (1) may have been successful for a limited family of aircraft, continually changing requirements in the air transport industry are leading to a radically new generation of aircraft. Thus, the old established empirical methods are no longer necessarily applicable. Method (2) has also led, in some cases, to discrepancies between prediction and flight test, usually traceable to inadequate care in wind tunnel test techniques, such as transition fixing, model support system interference, and wall effects, and also, to flight test thrust measurements. More seriously, it has often been the case that discrepancies between prediction and actual flight data have been erroneously ascribed to various sources because of unreliable or misunderstood model and flight data.

As an example of the problems associated with interpreting wind tunnel results, tests reported in reference 1 give force data from three different transonic tunnels on a C-5A model which utilized the same support sting, internal balance, and transition fixing technique in each facility. At cruise conditions, the discrepancy in drag amounted to

0.0010 in C_D between facilities. In spite of these difficulties it is evident that methods for predicting full scale drag should be pursued in the most scientific manner possible. The effort must be made to correlate in detail an accurate wind tunnel measurement with flight data before conclusions can be made on scale effects on profile drag, roughness drag, and drag due to lift.

An initial and vital step in this pursuit is a critical examination of an existing store of drag information surrounding an extensive flight test investigation of a typical subsonic transport. By applying well known, but infrequently used, corrections to such flight test data, together with appropriate Reynolds Number effects, a good correlation between flight results and predictions based on wind tunnel data may be demonstrated. It is the purpose of this study to analyze such data on the Lockheed C-141A aircraft in much greater detail than heretofore, and establish the validity of the measured flight test drag.

The C-141A aircraft has been in service for a number of years with the Air Force. During its design phase extensive wind tunnel testing on several models was conducted. Category I and II performance flight testing was carried out during 1964-1965, from which approximately 200 level flight cruise and climb points were obtained for verification of performance capability. Previous analysis of the flight data to provide handbook information did not justify the rigorous accounting for the effects of airplane center of gravity and aeroelastic distortion, which is essential to establish correlation with prediction techniques. Therefore, the basis for comparison of predicted and flight test drag levels was considered satisfactory at the time by the Lockheed-Georgia Company and the Air Force. The C-141A aircraft is an excellent aircraft for this study for the following reasons:

(a) Post flight test analysis of the total airplane drag data indicate modest scatter and good agreement with previous wind tunnel data.

(b) The unique utilization of four calibrated engines during the flight test program.

(c) It is typical of the current subsonic transport configurations.

(d) The Reynolds Number based on the wing MAC extends from 25 million to 86 million and provides an excellent opportunity to examine Reynolds Number effects.

This report presents the results of this re-analysis of the C-141A flight test drag data and the first phase of a longer term program which will attempt to correlate predicted drag from wind tunnel model tests with the results of this analysis of full scale data.

In this analysis consideration is given to the changes in aircraft load distributions from those experienced on a rigid wind tunnel model brought about by distortions of the structure of a production aircraft under flight load conditions. Allowance is made for configuration differences between the model and the production vehicle due to flight test instrumentation, as well as variances in the trim center of gravity location existing in flight test data.

3

A study of this nature would be incomplete without an examination and assessment of the overall accuracy of the results. Thus the scope of this investigation also includes an evaluation of the method of determining in-flight thrust and the inaccuracies of the various parameters and procedures used in calculating final flight test drag and lift coefficients. During the flight test performance evaluation, generalized thrust data suitable for handbook use were utilized to determine thrust. Consequently, for improved thrust accuracy a re-evaluation of the thrust for each flight test data point was made based on measured engine parameters. Despite this effort, inaccuracies are inherent in any technique which requires extrapolation of model thrust and airflow data to full scale conditions and an attempt is made to estimate this effect on the accuracy of the final drag results. The uncertainties associated with all drag factors are likewise assessed so that an overall prediction of the accuracy of the data is made. Every attempt was made during the study to include all available flight test data which lends itself to determination of cruise configuration drag. Analysis of climb and range mission data normally accumulated during Air Force Category I and II type testing was attempted; however, some of these data do not correlate well with the level flight data and has not been included with the results.

SYMBOLS

A	aspect ratio unless otherwise defined
A_{tail}	horizontal tail aspect ratio
a	NASA mean line designation
a_o	two-dimensional lift curve slope
b	wing span, 159.67 ft.
C_A	vena-contracta area coefficient
C_D	drag coefficient unless otherwise defined
C_{D_i}	wing induced drag coefficient
C_{DP}	primary nozzle discharge coefficient
C_{DF}	fan nozzle discharge coefficient
C_{D_P}	profile drag coefficient
$C_{D_{P_C}}$	compressibility drag
$C_{D_{P_{C_L}}}$	lift dependent profile drag
$C_{D_{trim}}$	trim drag
C_f	skin friction coefficient
CG, cg	center of gravity, percent MAC
C_G	nozzle thrust coefficient

C_{L_A} airplane trimmed lift coefficient

$C_{L_{A-h}}$ airplane tail-off lift coefficient $= C_{L_A} - C_{L_{tail}}$

C_{L_F} fuselage lift coefficient

$C_{L_{tail}}$ tail lift coefficient based on reference area S

C_{L_W} exposed wing lift coefficient

C_m pitching moment

C_V velocity coefficient

ΔC_V difference between model and full scale velocity coefficient

c chord

c_{avg} average chord, S/b

c_d section drag coefficient

c_{d_p} section profile drag coefficient

c_l section lift coefficient

D drag

E error of a variable or parameter

EPR engine pressure ratio

6

e	span efficiency factor = ratio elliptical/non-elliptical induced drag
F_{ABD}	nacelle afterbody drag
F_f	fuel relief factor
F_G	gross thrust
F_N	net thrust
F_{RD}	ram drag
FPR	fan pressure ratio
g	acceleration due to gravity
h	altitude
i_H	horizontal tail incidence
L	lift
M	Mach Number
M_f	Mach Number factor
MAC	mean aerodynamic chord, 266.47 inches
MV	mass flow
N_1	fan rotor speed

7

P	pressure
P_{AM}	ambient pressure
P_{TE}	effective nozzle total pressure
P_{TEX}	nozzle exit total pressure
P_{TM}	measured total pressure
P_{TO}	engine total pressure
$P_{T2.5}$	engine fan discharge pressure
P_{T7}	turbine discharge pressure
ΔP	duct pressure loss including velocity profile loss
ΔP_L	duct pressure loss
ΔP_E	effective duct pressure loss
q	dynamic pressure
RN	Reynolds Number
S	wing area and reference area, 3,228 ft^2
S_H	horizontal tail area, 483.0 ft^2
S_{WET}	wetted area

8

SF	shape factor
t/c	thickness to chord ratio
T_{TO}	free stream total temperature
$T_{T2.5}$	fan discharge temperature
V	velocity, unless otherwise defined
V_O	free stream velocity
W	weight
W_T	total airflow
y	wing spanwise station
y_c/c	camber to chord ratio
α, α_{FRL}	angle of attack = angle between fuselage reference line and relative wind.
α_{TL}	angle between thrust line and fuselage reference line
γ	climb angle
Γ	circulation
Δ	incremental
ϵ	downwash angle at the tail

η non-dimensional spanwise wing parameter, $2y/b$

Λ sweep angle

θ trigonometric substitution for wing spanwise station

ρ density

ϕ nozzle airflow parameter

ψ nozzle thrust parameter

ω induced velocity

Subscripts:

APP   appendage

BLD   bleed

CALC   calculated

corr   corrected

FAN   fan nozzle condition

flex   condition for flexible airplane

fus   conditions for the fuselage

HYS   hysteresis

10

i   induced

IND   indicator

inst   instrumentation

l   local condition

min   minimum

PRI   primary nozzle condition

RED   reduction

rigid   condition for rigid airplane

rigid-flex   conditions between rigid and flexible airplane

$RN=32.5 \times 10^6$ conditions for an $RN = 32.5 \times 10^6$

tail   conditions for the tail

trim   condition for trimmed airplane

wing   conditions for the wing

2D   two dimensional

TEST ARTICLE, PROCEDURE AND
INSTRUMENTATION

Test Article

All C-141A airplane performance test data used in this study were obtained on Production Starlifter 6002 AF S/N 61-2776. The Starlifter, pictured in figure 1, is a long range, subsonic speed, high altitude, swept-wing monoplane aircraft. The aircraft is designed primarily for use as a heavy logistics transport, capable of carrying all types of cargo or personnel.

The aircraft is powered by four calibrated production Pratt and Whitney Aircraft TF 33-P-7 turbofan engines. These engines have twin-spool, axial flow compressors and are flat rated at 21,000 pounds of takeoff thrust.

Table 1 contains the principle dimensions of the C-141A and a general arrangement is shown in figure 2.

Test Procedure

The flight test program, both Category I and Category II, was conducted at Edwards Air Force Base, California, during the period 13 October 1964 through 29 January 1965. Performance data suitable for airplane drag evaluation consist primarily of speed power flights where steady state level flight is maintained. Additional information is available in the form of continuous and sawtooth climbs as well as data recorded during two long range cruise missions.

In order to adequately define the performance of the aircraft, the range of flight test conditions is quite extensive. The tests cover an altitude range from 7100 feet to 40,500 feet, a weight range of 176,800 pounds to 321,500 pounds and a speed range from Mach Number = 0.23 to 0.81. Lift coefficient varies from 0.12 to around 1.0 and the Reynolds Number, based on the wing mean aerodynamic chord, extends from 25 million to 86 million.

Drag data for these flights were computed from the measured parameters by use of the flight performance computer program described in detail in reference 2. This program computes the parameters required for presentation on the time-history plots of the flight test runs and calculates a lift and drag coefficient for each run. The basic equations for lift and drag from figure 3 are

$$L = W \cos \gamma - F_N \sin \left[\alpha_{FRL} + \alpha_{TL} \right]$$

$$D = F_N \cos \left[\alpha_{FRL} + \alpha_{TL} \right] - W \sin \gamma$$

where

$$W = \text{aircraft weight}$$

$$F_N = \text{net thrust}$$

$$\alpha_{FRL} = \text{angle of attack}$$

$$\gamma = \text{angle of climb}$$

$$\alpha_{TL} = \text{angle between thrust line and fuselage reference line}$$

$$= 0.0 \text{ for the C-141A}$$

All climbs, sawtooth and continuous, were flown at forward CG loadings. Continuous data records were taken from start to end of each climb. Climbs were performed with fixed-throttle and each stabilized climb continued until either a minimum of 5 minutes had elapsed or an altitude change of 5000 feet was obtained.

Level flight speed power runs were conducted at various altitudes, speeds, and configurations and at several power settings. The speed power runs were stabilized for approximately 5 minutes before any data records were taken. Double-heading speed power runs were not conducted, but an attempt was made to make these runs in the same air mass.

Inflight time histories of free air temperature, airspeed and altitude were prepared for climbs and speed power runs to determine usability of data pertaining to temperature lapse rate and general smoothness of the test parameters. This made it possible to determine the actual portion of each run exhibiting the smoothest data thus minimizing data reduction time and enabling a determination to be made of the need for immediate repeat runs. By using these inflight data plots, certain runs were discarded which were unsuitable for reduction due to rough air or other difficulties. Thus, all runs reduced were smooth enough for satisfactory computer curve fitting and calculation of C_L and C_D.

The flight performance computer program also performed a "wild" point check on the input data for each run. The program was not allowed to discard actual instrument readings; only those values which had been instrument misread and subsequently verified as such. To accomplish this, the program was first run with the "wild" point routine operative to flag the subject wild points. After rechecking the film, these points were corrected only if they resulted from misread instruments. The program was then resubmitted with the "wild" point routine inoperative.

Standard instrumentation was installed on the test article to measure inflight conditions relative to many facets of aircraft performance. The measurements which are pertinent to the determination of aircraft drag are

Boom airspeed	Engine total pressure (P_{TO})
Boom altitude	
Boom total pressure	Engine fan discharge pressure ($P_{T2.5}$)
Free air temperature	
Angle of pitch	Engine turbine discharge pressure (P_{T7})
Angle of attack	
Rate of climb	Engine fan discharge temperature ($T_{T2.5}$)

The basic instrumentation consisted primarily of two automatic observer panels and two recording oscillographs, sensing devices, signal conditioning units, power supplies, and control systems located in the cargo area.

Instrumentation which changed the external configuration of the aircraft includes a nose mounted airspeed boom system, takeoff and landing camera with fairings located immediately aft of the nose landing gear wheel well, a trailing cone airspeed system attached to the top of the vertical stabilizer, and fuselage clearance skegs and wands for over-rotation warning. A Lockheed-Georgia Company designed data correlation system was installed which gave a precise time relationship between the records taken with the photopanels and oscillographs. This system provided a direct readout on each recorder and data correlation between records to better than 10 milliseconds.

All flight test systems instrumentation and transducers were calibrated in a facility maintained under appropriate military specification requirements. Measurements requiring a system calibration on the aircraft itself were calibrated by flight test techniques using standard calibration procedures. The calibration standards used are traceable to the U.S. Bureau of Standards. Precision of the various indicators is delayed until a later section where the accuracy of the data is discussed in detail.

Initial weight and center of gravity data were derived by using the Edwards Air Force Base weighing facility for accurate pre-flight measurement. Fuel counters were used for gross weight computations during flight and calculation of the center of gravity was accomplished using the standard fuel burnoff sequence. The center of gravity was adjusted for any variance in the standard burnoff sequence due to fuel mismanagement. Post flight weighing verified the fuel counter gross weight and center of gravity data.

Errors in the inflight data derived by use of the fuel counters during testing averaged 0.2 percent of gross weight and 0.25 percent MAC center of gravity. These errors were determined by the post flight weighings and were ratioed into the inflight gross weight and center of gravity data for determination of corrected data.

RESULTS AND DISCUSSION

Aerodynamic Considerations

The validity of any correlation depends on the ability to correctly and accurately identify distinctions between related but widely different sets of information. Correlation of flight test drag data with wind tunnel results thus requires the correlator to enumerate those factors which contribute to the disparity between the two, accurately assess these differences and establish the accuracy of both drag levels. This analysis attempts to develop aircraft drag polars and to establish the variation in minimum profile drag with Reynolds Number throughout the flight range for subsequent correlation with predictions based on wind tunnel data.

The component breakdown of the drag polar for a typical subsonic jet aircraft is diagrammed in figure 4. This shows the complete drag polar as determined from a set of flight test measurements and a representation of the major contributing factors to the total drag. The validity of the total drag polar will be dependent on the measured accuracy of such items as installed engine thrust, aircraft weight, center of gravity location, static pressure and temperature, and airspeed. Since the flight test aircraft does not fly at a constant condition along the drag polar, there are necessary corrections which must be made to normalize measured data which will also affect the accuracy of any final drag values. Further, the absolute level of measured drag will include an excess amount due to flight test instrumentation. These items, as well as additional considerations, will be discussed subsequently.

Examination of figure 4 reveals that any given flight test drag coefficient can be expressed as:

$$C_D = C_{D_{P_{min}}} + C_{D_i} + C_{D_{trim}} + C_{D_{P_{C_L}}} + C_{D_{P_C}} \tag{1}$$

where

$C_{D_{P_{min}}}$ = Minimum profile drag comprising skin friction drag and pressure drag on all aircraft components and drag due to surface roughness. This includes form drag and interference of all external items on the aircraft, including non-production flight test modifications, protuberances, steps, gaps, surface roughness, and leakage drag.

C_{D_i} = Vortex drag corresponding to the spanwise distribution of lift.

15

$C_{D_{trim}}$ = Trim drag which is the additional drag associated with the change in component loads due to the tail load required to offset the pitching moment for a given c.g. position.

$C_{D_{P_{C_L}}}$ = Lift dependent profile drag; this should be small at C_L's near design conditions.

$C_{D_{P_C}}$ = Compressibility drag; wave drag and any shock-induced separation drag, especially significant at off-design conditions. Since the induced and trim drags reflect Mach effects, $C_{D_{P_C}}$ is the compressibility effect on profile drag.

For the purposes of this report, equation (1) will be converted into a convenient reduction form for analysis of $C_{D_{P_{min}}}$. Likewise, a correction equation will be developed for use in deriving drag polar data. Before this is done, further definition and discussion of the components in equation (1) are necessary.

Vortex drag.- In this report vortex drag is calculated, for specific lift coefficients, using the efficiency factor, e, determined from an analysis of the flight measured span load distribution. In this way lift and Mach Number effects on e are included. A summary of the procedures used to compute e is outlined in Appendix A.

Spanwise loads data used for this purpose are based on extensive flight test chordwise pressure distributions and strain gauge measurements obtained as part of the loads survey portion of the C-141A flight test program. During the post-test data analysis these data were normalized in order that they could be expanded for general use at any chosen flight condition. Since loads data are not measured simultaneously with drag, or on the same test aircraft, it is necessary to rely upon these data as the best representation of the actual load distribution produced for a given flight condition. It is believed that this will not introduce any significant errors into the analysis.

Flight pressure distributions were measured only on the exposed portion of the wing and one problem area develops when an attempt is made to describe that portion of the load distribution inboard of the wing fuselage intersection. This becomes especially significant in view of the fact that large changes in load gradient induce correspondingly large changes in local downwash and shed vorticity, thus causing significant changes in wing efficiency factor. Extreme caution must be exercised when extrapolating the exposed wing portion of the load distribution inboard to the theoretical wing root.

In order to achieve consistency in this area, the following method was adopted for this study. From a set of trimmed airplane loads data for a particular flight condition, values were obtained for:

16

$$C_{L_A} = \text{airplane lift coefficient, trimmed}$$

C_{L_A} = airplane lift coefficient, trimmed

C_{L_W} = exposed wing lift coefficient

$C_{L_{tail}}$ = tail lift coefficient required for trim

C_{L_F} = fuselage lift coefficient

$\left(\dfrac{c \mid c}{c_{avg}}\right)_{wing}$ = spanwise load distribution on the wing outboard of the wing-fuselage intersection

where

$$C_{L_A} = C_{L_W} + C_{L_F} + C_{L_{tail}}$$

A third order polynomial was then derived for the fuselage portion of the load curve subject to the constraints:

(1)   The integrated lift coefficient is equal in value to C_{L_F}.

(2)   The gradient at the wing-fuselage intersection is equal to that which exists in the exposed wing data at the intersection.

(3)   The gradient at the theoretical wing root is zero corresponding to a symmetrical flight condition.

Although this procedure is somewhat arbitrary and mechanical in nature it is regarded as a necessary step in accounting for the effect of a large inefficient lift-producing body in combination with the wing. Inaccuracies are inherent in this process especially at the off-design conditions where the carry-over load varies rapidly. However, in the cruise range of lift coefficients the error is only slight and should not detract from the overall analysis.

Trim drag.- In equation form the trim drag is defined as

$$C_{D_{trim}} = \Delta C_{D_{i_{trim}}} + C_{D_{i_{tail}}} + C_{L_{tail}} \tan \epsilon \qquad (2)$$

The first term represents the effect of the trim process on induced drag. An additional amount of lift is generated by the wing-body combination equal to the load on the tail required for trim. The total lift thus generated is sometimes referred to as the tail-off lift since it is the equivalent tail-less airplane lift corresponding to a given tail-on airplane lift.

Thus

$$C_{L_{A-h}} = C_{L_A} - C_{L_{tail}}$$

and since

$$C_{L_A} = C_{L_W} + C_{L_F} + C_{L_{tail}}$$

then

$$C_{L_{A-h}} = C_{L_W} + C_{L_F}$$

The value of the tail-off lift coefficient is seen to be the sum total of the wing and fuselage components. The incremental induced drag due to trim is then

$$\Delta C_{D_{i_{trim}}} = \frac{C_{L_{A-h}}^2}{\pi Ae} - \frac{C_{L_A}^2}{\pi Ae}$$

The tail induced drag, $C_{D_{i_{tail}}}$, is calculated from

$$C_{D_{i_{tail}}} \doteq \frac{\left[C_{L_{tail}} \times S/S_H \right]^2}{\pi A_{tail} \; e_{tail}} \times \frac{S_H}{S} = \frac{C_{L_{tail}}^2 \times S/S_H}{\pi A_{tail} \; e_{tail}}$$

where e_{tail} is computed similarly to e, using flight measured tail spanwise load distributions.

$C_{L_{tail}} \tan \epsilon$ = drag component of the tail lift vector. Examination of figure 3 reveals the origin of this term.

Lift dependent profile drag.- This drag component is necessary in order to extract the final $C_{D_{P_{min}}}$ drag levels for a given flight test drag coefficient. The variation of this component with lift is determined from an analysis of the flight test data and is discussed in further detail in the section, "Equivalent Rigid Profile Drag".

Compressibility drag.- This term is included in order to extend the analysis to those flight test points where Mach Number effects have become significant. In calculating $C_{D_{P_{min}}}$ it is of course necessary first to extract the induced drag. Since this drag is calculated from actual spanwise load distributions as measured, the effects of compressibility on these distributions is reflected in the computed efficiency factor and thus the induced drag. Similarly, the trim drag reflects Mach effects. Consequently, this compressibility drag increment differs from that which is obtained if the compressibility increment is determined on the basis of total drag without recognizing Mach effects on the other drag components. Of course this distinction is basically academic but nevertheless must be recognized to fully understand the true Mach Number effects on induced, trim and profile drag components.

18

For this reason a distinction is made in this report between the compressibility effects on C_{Dp} and C_D. In either case, cross-plots of the flight test data are made to determine the actual compressibility drag rise exhibited by the flight data.

Aeroelastic effects.- Equation (1) states the component breakdown for a typical aircraft drag polar. Ideally this relationship would be the same for both wind tunnel and full scale drag data and scale effects only would constitute the major disparity between the two. This is not the case, however, and aeroelastic effects must be considered. Aeroelastic or flexibility effects refer to the elastic deformation of the structure caused by aerodynamic and inertia loads. The distortions of the aircraft structure result in overall redistribution of the aerodynamic loads and corresponding shifts in aircraft center of pressure. Of particular importance is the deformation of the wing. Under the influence of aerodynamic lift, the wing deflects upward along its elastic axis. For swept wings, such as the C-141A, this results in a reduction in local airfoil section angle of attack compared with the unflexed wing. Since the wing bends normal to the elastic axis, the leading edge of a streamwise section is deflected upward an amount dependent on a more inboard station than is the case for the trailing edge; thus, in the streamwise direction the trailing edge deflects upward more than the leading edge and the section angle of attack is reduced. The amount of reduction varies from zero at the wing root to a maximum at the tip. For high load conditions, a decrease in tip angle of two degrees can occur as shown in figure 5. In this analysis, the C-141A unflexed or rigid configuration is defined as the jig shape.

This effective aerodynamic twisting of the wing or "wash out" directly affects the load generated by the wing since lift is a function of angle of attack. The reduction in local angle of attack along the span reduces the local load with the greatest reduction occuring at the tip. The integrated load which results is less than that of the unflexed wing and this lift loss must be retrieved by increasing the overall airplane angle of attack. Figure 6 illustrates this characteristic for various load conditions on the C-141A.

One result of the wing deformation is the effect of the local changes in angle of attack on the wing profile drag. The magnitude and direction of the change at any local wing station depends on the spanwise location and the amount of wing distortion present, as well as the proximity of the local lift coefficient to its design value.

Another profile drag change arises due to the increase in overall angle of attack required to generate the lift loss on the wing from aerodynamic wash out. This profile drag change occurs over the entire aircraft, however, it is believed that the wing produces the most significant change. The effect on wing profile drag can be obtained from the rigid and flexible span load distributions corresponding to a flight condition but there is no satisfactory method for determining the effect on the fuselage from the flight test data. Wind tunnel test data for the C-141A fuselage indicates a rate of change of $\Delta C_{D_{P_{fus}}} = 0.0001$

per degree angle of attack in the cruise range of lift coefficients. Since the angle of attack changes experienced are generally less than 0.5 degrees over the range of test conditions, the effect on the fuselage should be sufficiently small that it can be excluded from this analysis.

In order to determine the incremental change in wing profile drag due to aeroelastic distortion it is first necessary to compute the profile drag of a rigid wing. Methods currently available are not completely rigorous and are generally invalid where separation or shock waves exist. Nevertheless, various methods can be used to determine incremental changes quite accurately at combinations of C_L and Mach Number where separation and shock wave effects are small. Recent research at NPL, references 3 through 6, and at GELAC, reference 7, indicates that sophisticated means of calculating profile drag changes may be possible based upon improved boundary layer prediction techniques. For the purposes of this analysis, however, use is made of two-dimensional airfoil section data presented in reference 8 for airfoils similar to those used in the C-141A wing. It is recognized that these data were obtained under conditions of natural transition and at a relatively low Reynolds Number thus limiting their application. These data do have the advantage, however, of establishing the effect of camber on NACA modified four-digit series airfoils using an $a = 0.8$ mean line, over the design lift coefficient range of the C-141A airfoils. Since incremental effects due to lift changes are required, and not absolute drag levels, these data are believed satisfactory.

The incremental wing profile drag can be determined by first generating profile drag polars for various wing stations, taking into account the actual thickness and camber of the C-141A wing.

These polars are used in conjunction with the rigid and flexible span load distributions for a particular flight condition. Since these distributions are known for the trimmed airplane, the condition of constant airplane lift coefficient is maintained. By converting the load distribution coefficients to local lift coefficients an increment in local lift coefficient is obtained at any spanwise station; this increment results from both the local wash out angle and the overall shift in airplane angle of attack. In this way, the local profile drag increment obtained is the net effect on wing profile drag due to flexibility.

By applying simple sweep theory the local lift coefficient and airfoil section geometrical characteristics can be converted to equivalent two-dimensional values. For the section lift coefficient,

$$c_{l_{2D}} = \frac{c_l}{\cos^2 \Lambda}$$

The local thickness ratio, t/c, and camber ratio, y_c/c, are corrected for sweep by

$$(t/c)_{2D} = \frac{t/c}{\cos \Lambda}$$

$$(y_c/c)_{2D} = \frac{y_c/c}{\cos \Lambda}$$

For any pair of rigid and flexible spanwise loadings the local lift coefficient incre-
ment is known and, using the profile drag polars obtained above, the corresponding local
incremental profile drag coefficient, Δc_{d_p}, can be determined. The total wing incremental
profile drag is then

$$\Delta C_{D_{P_{wing_{rigid-flex}}}} = \int_0^1 \frac{c_{d_p} c}{c_{avg}} \, d\eta \qquad (3)$$

In addition to the above effects, the alteration of the spanwise load distribution in-
fluences the induced drag since it implies a change in the spanwise distribution of circulation
and therefore in the efficiency factor, e.

As outlined in Appendix A, the value of e is directly related to the spanwise distri-
bution of circulation and any change in the circulation gradient will thus affect the efficien-
cy factor. In the case of the C-141A, the reduction in load near the tip tends to reduce the
efficiency factor, however, this effect is overcome by the resulting load shift onto the body.
The exposed wing lift remains essentially constant although at an increased angle of attack.
The reduced tail load due to the center of pressure shift and the increased angle of attack in-
duce a higher load on the body which tends to improve the gradient over that portion of the
wing span inboard of the wing-fuselage junction. This effect is shown in figure 6.

Finally, the flexibility effect on the trim drag must be included. As has been dis-
cussed previously, the change in spanwise load distribution on a swept wing will shift the
location of the center of pressure and thus alter the tail load required to trim the aircraft.
For the C-141A, the redistribution of spanwise loading, such as that shown in figure 6,
results in reduced tail load. This change must be recognized in the tail induced drag term and
the tail lift vector component.

Understanding of the overall trim process as well as the flexibility effects on trim
drag is enhanced by resorting to a diagram of the major relationships. This is shown in
figure 7 where the lift, pitching moment and drag characteristics are sketched in an exag-
gerated manner. Since the starting point in this analysis is a given trimmed condition cor-
responding to a flight test point, then the airplane lift coefficient, C_{L_A}, and drag coef-
ficient, $C_{D_{flex}}$, are known. What is required is that amount of drag change which the
airplane has undergone to become trimmed in terms of the rigid airplane. At the trimmed
lift coefficient, C_{L_A}, the wing-body is actually carrying an additional amount of lift
equal to the down load on the tail. The amount of tail load is derived from the pitching
moment curve, where the tail-on and tail-off relationships are shown. The C_L versus a
sketch illustrates how the airplane is trimmed at a constant value of C_{L_A}, rigid and flexible.
Tail-on and -off lift curves are shown for both the flexible and rigid airplane. If only the
rigid airplane were being considered, then the tail-off rigid curve shows the amount of

lift, $C_{L_{A-h}}_{rigid}$, being generated at the trim angle of attack, $\alpha_{FRL_{rigid}}$. However, the flexibility effect reduces the lift curve slope so that in order to maintain the same C_{L_A}, the airplane angle of attack increases to $\alpha_{FRL_{flex}}$. There is a corresponding change in the tail-off lift curve. Once again, since the airplane does not "rotate" in flight, the condition of constant angle of attack is imposed and the value $C_{L_{A-h_{flex}}}$ is generated by the wing-body combination.

The trim effect on drag is shown also for both rigid and flexible conditions. The starting point is again at the value C_{L_A}. The condition of constant angle of attack is imposed between the tail-on and tail-off polars. The increment of induced drag, $\Delta C_{D_{i_{trim}}}$, appears on the tail-off polar as the drag difference due to the lift difference, $C_{L_{A-h}} - C_{L_A}$. The remaining increment between the tail-on and tail-off polars is due to the induced drag of the tail and the component, $C_{L_{tail}} \tan \epsilon$. The tail profile drag is considered an increment in the total airplane profile drag and thus is not included in the definition of trim drag, rigid or flexible. Comparison between the rigid and flexible trim drags yields the flexible trim drag increment.

In summary, three effects on drag due to flexibility have been identified as significant: the change in vortex drag, the incremental wing profile drag due to local wing distortion, and the effect on trim drag. The equation for the rigid drag coefficient in terms of the measured flight drag coefficient, $C_{D_{flex}}$, can then be written:

$$C_{D_{rigid}} = C_{D_{flex}} + \Delta C_{D_{rigid-flex}} \tag{4}$$

where

$$\Delta C_{D_{rigid-flex}} = \Delta C_{D_{i_{rigid-flex}}} + \Delta C_{D_{P_{wing_{rigid-flex}}}} + \Delta C_{D_{trim_{rigid-flex}}}$$

and

$$\Delta C_{D_{i_{rigid-flex}}} = \left(\frac{C_{L_A}^2}{\pi A e}\right)_{rigid} - \left(\frac{C_{L_A}^2}{\pi A e}\right)_{flex}$$

$$\Delta C_{D_{P_{wing_{rigid-flex}}}} = \text{incremental wing profile drag as defined by equation (3)}$$

$$\Delta C_{D_{trim_{rigid-flex}}} = C_{D_{trim_{rigid}}} - C_{D_{trim_{flex}}}$$

The trim drag flexibility increment can be further defined as

$$\Delta C_{D_{trim_{rigid-flex}}} = \Delta C_{D_{i_{trim_{rigid-flex}}}} + \Delta C_{D_{i_{tail_{rigid-flex}}}} + \Delta \left(C_{L_{tail}} \tan \epsilon \right)_{rigid-flex}$$

$$= \left(\frac{C_{L_{A-h}}^2}{\pi A e} - \frac{C_{L_A}^2}{\pi A e} \right)_{rigid} - \left(\frac{C_{L_{A-h}}^2}{\pi A e} - \frac{C_{L_A}^2}{\pi A e} \right)_{flex}$$

$$+ \left(\frac{C_{L_{tail}}^2 \times S/S_H}{\pi A_{tail} \; e_{tail}} \right)_{rigid} - \left(\frac{C_{L_{tail}}^2 \times S/S_H}{\pi A_{tail} \; e_{tail}} \right)_{flex}$$

$$+ \left(C_{L_{tail}} \tan \epsilon \right)_{rigid} - \left(C_{L_{tail}} \tan \epsilon \right)_{flex}$$

All increments between rigid and flexible conditions are computed holding the total airplane lift coefficient constant.

<u>Trim c.g. and instrumentation drag</u>.- In addition to the above considerations, correction of the drag to a common c.g. position and for instrumentation drag is desirable. Therefore:

$$C_{D_{rigid}}_{\substack{c.g. = .25 \, MAC \\ less \, inst}} = C_{D_{flex}} + \Delta C_{D_{i_{rigid-flex}}} + \Delta C_{D_{P_{wing_{rigid-flex}}}}$$

$$+ \Delta C_{D_{trim_{rigid-flex}}} + \Delta C_{D_{trim_{c.g.}}} - \Delta C_{D_{inst}} \qquad (5)$$

where

$$\Delta C_{D_{trim_{c.g.}}} = \left(C_{D_{trim}} \right)_{c.g. = .25 \, MAC} - \left(C_{D_{trim}} \right)_{c.g. = flight \, c.g.}$$

$$\Delta C_{D_{inst}} = \text{incremental drag due to flight test instrumentation}$$

Equation (5) above is the basis for analyzing flight test drag; however, before proceeding to discuss the results for the C-141A, it is appropriate to consider the method of computing thrust utilized during the C-141A flight test program.

TF 33 Thrust Calculation

The drag data used in this report are based upon an accurate determination of the thrust delivered in flight by four calibrated TF33 engines. A computer program is used to

compute installed engine thrust for the atmospheric conditions and engine parameters recorded during the flight test program. A detailed discussion of the thrust calculation procedure and a description of the computer program can be found in reference 9.

The basic net thrust of the TF33 engine is defined by the equation

$$F_N = F_G - F_{RD} - F_{ABD}$$

where

$$F_G = \text{Gross nozzle thrust}$$

$$F_{RD} = \text{Ram drag}$$

$$F_{ABD} = \text{Nacelle afterbody drag}$$

Nozzle gross thrusts are obtained separately for the fan and primary nozzles. The net thrust equation may be rewritten

$$F_N = F_{G_{PRI}} + F_{G_{FAN}} - F_{RD} - F_{ABD}$$

The gross thrust for the primary and fan nozzles are obtained from the equation

$$F_G = \psi A \, C_G \, P_{AM}$$

where

$$\psi = \text{Nozzle thrust parameter}$$

$$= \frac{F_{G_{IDEAL}}}{A \, P_{AM}}$$

$$A = \text{Nozzle area}$$

$$C_G = \text{Nozzle thrust coefficient}$$

$$= \frac{F_{G_{ACTUAL}}}{F_{G_{IDEAL}}}$$

$$P_{AM} = \text{Ambient pressure}$$

The subscript ACTUAL implies measured values of thrust and airflow; the subscript IDEAL implies theoretical values based on the ratio P_{TOTAL}/P_{STATIC}.

The ram drag is given by the equation

$$F_{RD} = \frac{W_T V_O}{g}$$

where

$$W_T = W_{PRI} + W_{FAN} + W_{BLD} = \text{Total airflow}$$

$$V_O \quad = \quad \text{Free stream velocity}$$

$$g \quad = \quad \text{Acceleration due to gravity}$$

$$W_{BLD} = \quad \text{Bleed flow}$$

Airflow for both the primary and fan nozzles is given by the equation

$$W = \phi C_D A \, P_{AM}/\sqrt{T}$$

where

$$\phi \quad = \quad \text{Nozzle airflow parameter}$$

$$= \quad \frac{W_{A_{IDEAL}} \sqrt{T}}{A \, P_{AM}}$$

$$C_D \quad = \quad \text{Nozzle airflow coefficient}$$

$$= \quad \frac{W_{A_{ACTUAL}}}{W_{A_{IDEAL}}}$$

$$A \quad = \quad \text{Nozzle area}$$

$$P_{AM} \quad = \quad \text{Ambient pressure}$$

$$T \quad = \quad \text{Nozzle air total temperature}$$

Since nacelle afterbody drag is a function of nozzle pressure ratio, it is included in the net thrust calculation. The data were obtained from scale model wind tunnel tests run at the United Aircraft High Speed 8-foot wind tunnel.

The gross thrust coefficient and the nozzle airflow coefficient for both the primary and fan nozzles were developed from engine test stand data and scale model data over the full range of nozzle pressure ratios using the extrapolation procedure discussed later.

The TF33 engine computer program calculates net thrust using these basic equations. Inlet pressure loss, bleed, and power extraction effects are applied to the basic parameters to obtain installed net thrust.

The computer program is written so that net thrust may be calculated by two methods. The Lockheed method calculates gross thrust from the fan and primary nozzle parameters. Ram drag is calculated using the airflow also calculated from the nozzle parameters. The P&WA method calculates gross thrust from nozzle parameters but obtains airflow in the ram drag calculation from a curve of fan rotor speed versus airflow. This introduces fan rotor speed as one of the required inputs to calculate thrust by this method.

Nozzle coefficients.- The Lockheed method for deriving the gross thrust and airflow coefficient comprises a procedure for evaluation of compatible thrust and airflow values and accounts for such variables as Reynolds Number and suppression effects. The accuracies of the method and comparison of the accuracies of the Lockheed and P&WA extrapolation and thrust calculation procedures will be discussed later.

Scale model tests conducted throughout the full operating range of nozzle pressure ratios are used to extend the range of full scale data obtained from static engine test stand calibrations. The full scale data obtained from the test stand are, of course, limited to the range of nozzle pressure ratios available statically.

Preliminary flight tests of the C-141/TF33 indicated a shift in fan pressure ratio with changes in altitude. Examination of the normal engine parameters did not explain this phenomenon. Effects of Reynolds Number changes in the fan duct were considered and found to be a possible explanation.

The various "losses" associated with nozzle flows are illustrated in figures 8 and 9 for nozzle gross thrust and nozzle mass flow respectively. Friction along the duct walls between the total pressure measuring plane and the nozzle exit results in a boundary layer buildup and an overall pressure drop. These pressures are indicated as P_{TM} (measured) and P_{TEX} (nozzle exit). Also affecting the gas flow and thrust are the velocity profile and vena-contracta. However, an effective pressure (P_{TE}), used by P&WA in extrapolation of coefficients, may be defined which assumes all losses are pressure losses and the velocity profile and vena-contracta are ideal.

In figure 8, curves are shown to illustrate the ideal and actual total gross thrust. Also shown are the pressure-area (PA) terms; the momentum thrust (MV) terms are the differences between the total thrust and the PA terms. In reality, the vena-contracta, a ratio of minimum flow area to the physical area, reduces the velocity at the nozzle exit thereby

26

increasing the static pressure. This increases the actual PA term while reducing the MV term. The points labeled on figure 8 are indications of the following:

Point A: Actual thrust parameter at the measured nozzle pressure ratio.

Point B: Ideal thrust parameter at the measured nozzle pressure ratio.

Point C: Actual thrust parameter at the true nozzle pressure ratio.

Point D: Ideal thrust parameter at the true nozzle pressure ratio.

Point E: Actual and ideal thrust parameter at the effective nozzle pressure ratio.

Point F: Actual PA term at the true nozzle pressure ratio.

Point G: Ideal PA term at the true nozzle pressure ratio.

These points are used in the definitions of the nozzle coefficients as defined below:

A/B = C_G, overall nozzle gross thrust coefficient, ratio of actual to ideal gross thrust at the measured nozzle pressure ratio.

CF/DG = C_V^2, velocity coefficient squared, ratio of actual to ideal momentum at the true nozzle pressure ratio.

F - G = Change in PA term due to vena-contracta.

The nozzle airflow parameter shown in figure 9 is also affected by the vena-contracta and velocity profile. Here, as in the thrust parameter, the vena-contracta reduces the velocity at the nozzle exit which in turn produces a lower velocity coefficient. The points shown in figure 9 and their uses in defining the coefficients are indicated below:

Point A: Actual airflow parameter at measured nozzle pressure ratio.

Point B: Ideal airflow parameter at measured nozzle pressure ratio.

Point C: Actual airflow parameter at the true nozzle pressure ratio.

Point D: Ideal airflow parameter at the true nozzle pressure ratio.

Point E: Actual and ideal airflow parameter at the effective nozzle pressure ratio.

$A/B = C_D$, overall nozzle discharge coefficient, ratio of actual to ideal mass flow at the measured nozzle pressure ratio.

$C/D = C_V$, velocity coefficient, ratio of actual to ideal mass flow at the true nozzle pressure ratio.

Model data analysis.- Data were obtained from a 1/10 scale model with the capability of controlling and independently measuring the flow to the fan and primary nozzles. The measured thrust consisted of that produced by both nozzles. The model simulated the actual production hardware contours from upstream of the measuring station aft to the nozzle exit.

The basic calibration of each nozzle was accomplished by flowing air through that nozzle alone. The other flow path was plugged internally to prevent leakage through the control valves. In the analysis of these tests, the base pressure-area of the non-flowing nozzle was subtracted from the measured thrust. The results of these model tests are shown in figures 10 and 11.

The fan only and primary only data were used to define the effective losses of each nozzle. The effective fan pressure losses for the model fan duct are shown in figure 12. The nozzle gross thrust is affected by momentum, that is, it is dependent upon velocity squared, whereas nozzle flow is affected only by velocity; therefore, the effective losses based on measured thrust are larger than those based on flow.

True losses, of course, vary primarily with velocity and would not exhibit the characteristics shown. The apparent hump in the effective loss is a result of the influence of the vena-contracta on the velocity at the nozzle exit. The data indicated the vena-contracta had no further influence on the losses above a fan nozzle pressure ratio of approximately 2.8. Above this point the nozzle flow exhibits a Prandtl-Meyer expansion from the physical nozzle exit; the vena-contracta is now at the nozzle exit and the area coefficient is 1.0. The remaining losses at this point are the duct pressure loss (ΔP_L) and the loss in the velocity coefficient (C_V). By an iteration process using both flow and thrust data, the ΔP_L and C_V can be determined for this portion of the fan nozzle pressure ratio. The actual step-by-step calculation procedure for this iteration and the remaining calculations for the nozzle coefficients may be found in reference 9.

At nozzle pressure ratios less than 2.8, the minimum flow area moves aft of the physical exit. The velocities in the duct, and therefore the pressure losses, are reduced. Pressure loss curves can be evaluated for various area coefficients, C_A, as shown in figure 13. The area coefficient, C_A, is defined as the ratio of minimum flow area to the physical nozzle area. This calculation is accomplished by fixing the duct friction factor to match the known base point calculated by the above iteration procedure and then accounting for the duct losses as they vary with changes in the ratio of total to static pressure at the nozzle exit. Using the losses defined in figures 8 and 9, the ΔP_L versus C_A relationship in figure 13, and assumed vena-contractas, C_V's can be calculated for both the thrust and airflow data. The process is repeated until both sources produce the same C_V.

28

A similar process is repeated for the primary nozzle. In this case, however, the Reynolds Number effects are considered negligible and the C_V and ΔP_L are combined as a single term. This term is called ΔP and is treated the same as the fan losses.

The final model losses for each of the nozzles are shown in figures 14 through 18. The pressure loss, area and velocity coefficients for the fan duct model are shown in figures 14, 15, and 16 respectively. Figures 17 and 18 show the model primary pressure and velocity loss combination and the area coefficient.

Full scale data analysis.- The data obtained from full scale calibrations are limited to the relatively low nozzle pressure ratio of approximately 1.8 obtained from an engine test stand. To obtain nozzle calibrations for cruise conditions, the full scale static data are extrapolated based on model test results.

Fan nozzle: Full scale altitude test data showed an increase in fan pressure ratio when compared to lower altitude test data. Various possible changes in engine characteristics were considered but could not explain the phenomenon that existed. An examination of changes in fan duct Reynolds Number with changes in altitude revealed that the increase in fan pressure ratio correlated with the increase in fan duct pressure losses. It was found that the static, altitude, and model data could all be related by using the smooth pipe, turbulent flow friction factor based on a Reynolds Number using the hydraulic diameter of the nozzle exit.

Using the basic model data pressure loss curve, figure 14, and the calculated Reynolds Number for various altitudes, the $\Delta P_L/P_{TM}$ for the full scale hardware was constructed as shown in figure 19. The area coefficient for the full scale hardware was assumed to be the same as that for the model when they were operating at the same true nozzle pressure ratio, P_{TEX}/P_{AM}.

The remaining undefined factor for full scale evaluation is the velocity coefficient. Using the thrust data obtained from the static test stand for expansion ratios up to 1.7, and data from figures 14 and 19, the full scale velocity coefficients were calculated. To extrapolate the velocity coefficient, a ΔC_V between the model and full scale was determined. This parameter was relatively flat as shown in figure 20, and, therefore, very easy to extrapolate. Having defined the velocity coefficient for sea level conditions, the problem of obtaining an altitude velocity coefficient remained. Since both the pressure loss and velocity profile are greatly influenced by the boundary layer, the changes in velocity coefficient with altitude were calculated to be proportional to the changes in duct pressure losses with altitude or Reynolds Number as shown in figure 21.

The measured flow obtained from the engine test stand did not reproduce the flow coefficient derived from the above full scale nozzle losses; however, these differences are accounted for as described in the following paragraph.

The differences probably resulted from several sources. In reality, the fan nozzle does not exhaust the flow directly aft; therefore, the velocity coefficient for thrust and airflow will not be identical. Bias errors in both thrust and airflow tend to be reflected in fan parameters. Another possible error could have resulted by using the published thrust coefficient definition of the P&WA hardware which was used in tests to define the Lockheed hardware coefficients. This results because fan thrust and airflow are considered as that which remains after the primary nozzle properties have been calculated.

To obtain the final full scale flow coefficient, the coefficients were first calculated based on figures 14, 19, and 21. Ratios of the altitude to sea level coefficients were then made based on these coefficients. To determine the full range sea level flow coefficient, the measured flow data were used with figure 14 to calculate a ΔP that included the pressure loss and velocity coefficient. This was extrapolated based on a similar model curve. The altitude ratios, determined above, were then applied to the sea level curve to calculate the altitude flow coefficients.

Primary nozzle: The primary nozzle, being relatively short when compared to the fan duct and nozzle, was considered to be independent of Reynolds Number effects. For this reason, the pressure loss and velocity coefficient were not separated for the extrapolation process.

When the primary nozzle is flowing independently of the fan, i.e., the nozzle is flowing without being in the influence of the fan flow, the nozzle is considered to be unsuppressed. The full scale unsuppressed thrust and flow coefficients were extrapolated by using the area coefficient derived from the model and extrapolating the ΔP_L curve based on the ratio of full scale to model pressure losses. The full scale ΔP_L curve is shown as figure 22.

The fan and primary nozzle flows exit in a coaxial, near co-planar arrangement. At low primary nozzle expansion ratios, the fan exhaust, which is coned inward toward the primary flow, reduces the primary flow. The fan flow must be turned back into the axial direction and this is accomplished by forces exerted by the primary flow. The primary flow in turn is suppressed such that the minimum flow area is reduced. Model and full scale data were combined to determine the suppression factor throughout the full operating range. This factor, shown in figure 23, is applied as an additional reduction in the primary nozzle area coefficient. The full scale coefficients are then calculated using the appropriate curves from figures 18, 22, and 23.

Final nozzle coefficients: The full scale fan and primary nozzle coefficients were derived from data obtained from four sets of production hardware run on a slave engine on the engine test stand. These hardware sets were then installed on the airplane to conduct the performance testing. The final full scale nozzle flow and thrust coefficients based on these hardware sets are shown in figures 24 and 25 for the fan and figures 26 and 27 for the primary.

Accuracy of thrust calculation.- The thrust evaluation procedure developed by Lockheed is felt to be superior to that recommended by P&WA in reference 10 because of the additional considerations in the Lockheed method. The P&WA method does not consider the effects of Reynolds Number on the nozzle coefficients, neither does it subdivide the nozzle losses into various definable loss components. The extrapolation of the nozzle coefficients by the Lockheed procedure is made easier and considered more reliable because the extrapolation is based on component losses as opposed to the total losses. The most important factor between the two methods, however, is in the actual net thrust evaluation calculation procedure. The Lockheed calculation uses nozzle conditions to calculate both gross thrust and inlet ram drag (engine airflow); whereas, the P&WA calculation uses nozzle conditions for calculating gross thrust, but uses fan rotor speed to determine engine airflow.

Figure 28 shows the basis for the P&WA extrapolation of the gross thrust coefficient. The relative pressure loss between the model and full scale is calculated for constant values of ψC_G and plotted as shown in figure 29. This pressure loss difference is then extrapolated and used to extend the full scale ψC_G curve. The actual extrapolation shown on figure 29 was determined from the "sea level" fan C_G derived by the Lockheed method. The P&WA extrapolation could easily have produced this curve.

The computer was run to reproduce engine parameters as measured on the engine test stand. The calculated and measured values of thrust and airflow are compared in figures 30 and 31, respectively. These comparisons were found to be quite satisfactory and validated the nozzle coefficients.

The overall nozzle thrust and airflow accuracy of the model and full scale data are in the order of one percent. Using the defined primary nozzle coefficients, the four sets of nacelle hardware showed a variation of only 0.5 percent in the fan coefficients. The manipulation and extrapolation of the averaged coefficients by the Lockheed method added approximately another 0.5 percent error to the definition of total gross thrust and airflow at cruise conditions. The possible errors introduced by improper accounting of Reynolds Number effects are considered to have only a small effect on net thrust because they are largely offset by being used in both the calculation of gross thrust and ram drag. The primary nozzle suppression error in the low power flight region could be as large as approximately one percent, resulting in an additional net thrust error of 0.2 to 0.5 percent. At cruise conditions, however, where the primary nozzle expansion is higher, the suppression factor is almost 1.0 and the error should be negligible.

At cruise conditions the total nozzle gross thrust is twice the magnitude of net thrust. In considering the cruise net thrust error, appropriate factors must be applied to the nozzle gross thrust and airflow errors. Using factors of 2.0 for thrust and 1.0 for airflow, the overall basic net thrust accuracy at cruise due strictly to the reduction, extrapolation and expansion of the nozzle coefficients by the Lockheed method is estimated to be approximately 2.5 percent. This value is based on a root-sum-square analysis. The P&WA method uses fan speed for the evaluation of inlet airflow and does not account for any airflow changes between the uninstalled and completely installed engines. This may result in an error of some magnitude

in calculation of ram drag, and hence net thrust. Based on test data, the P&WA method would increase gross thrust at altitude, where the increase in fan pressure ratio was seen to occur, unless modified in some manner to account for phenomena occuring within the fan ducts. The same data would indicate a decrease in airflow when using the P&WA method. These errors are additive in the net thrust evaluation and thus would result in greater total error.

Flight Test Results

In order to fully investigate the degree of correlation attainable with flight test data, a review of all available C-141A test data was made to provide full and sufficient coverage of a wide range of conditions. Both Category I and II flight test runs were surveyed and only those runs specified by the flight test personnel as being accurate and suitable for cruise configuration drag analysis were selected. Any runs which did not have an accurate definition of aircraft weight, fuel load, and trim condition, as well as the additional parameters required for thrust calculation, were screened out. For the above reasons, all flights selected were part of the Category I test.

Table 2 provides a summary of the 111 runs from the 10 flights chosen. These flights include 60 speed power runs (flights 106, 119, 123, 128, and 129), 21 continuous climb runs (flights 138, 139, and 140), and 30 cruise runs from range missions (flights 187 and 190).

Speed power runs are the best source of data for full scale clean airplane drag due to the nature in which these flights are conducted. Full attention is given to these data in the current analysis. Figure 32 summarizes the drag coefficient, lift coefficient, and Mach Number variations for these flights. Normal cruise conditions for the C-141A are at C_L = 0.38 and M = 0.767. The Reynolds Number range is seen from table 2 to be 24.49 million to 86.37 million based on the wing mean aerodynamic chord, compared with a nominal cruise value of 37.5 million. Three of the speed power runs are observed to occur at lift coefficients in excess of 0.8. These three flights (106-4F, 129-5G, and 129-6R2) were eliminated from the analysis since they do not constitute sufficient data to analyze that portion of the drag polar where extreme separation is known to occur.

Results of Flexible Analysis

In order to assess the aeroelastic effects on drag previously identified it is necessary that the relationship between the rigid and flexible airplane characteristics be developed. As mentioned earlier in the section on vortex drag, extensive flight test pressure and strain gauge data have been analyzed previously, reference 11. These data were correlated with predicted flexible characteristics and a revised set of rigid aerodynamic data derived which,

in conjunction with the elastic characteristics of the structure, are used in a computer program to calculate a complete set of trimmed airplane load distribution data for any flight condition. Output from this program includes non-dimensionalized loads on all components for both rigid and flexible conditions.

It is believed that the use of this program provides the most efficient means of separating and accounting for all the variables present. In order to establish the importance and trends of each variable, a matrix of configurations, shown in table 3, was selected for submission to the program to encompass all flight conditions at which drag data exist. The effect of flexibility on any parameter such as lift coefficient, efficiency factor, or incremental drag at a particular flight test condition can then be obtained by interpolation of the results from the matrix of conditions.

The major variables which influence the magnitude of the flexibility effects are dynamic pressure, lift coefficient and Mach Number, and as can be seen in table 3, the basic series of conditions centers around these variables. Additional conditions were devised to measure the bending relief due to increasing the wing fuel and the effect of center of gravity location. Concurrently, five speed power points were selected to serve as check cases on the overall results. Spanwise distributions for these five cases are shown in figure 33.

Table 3 also contains a summary of the rigid and flexible parameters for each condition. Summary curves and a discussion of the effects follows in the next section. These data serve as the framework for a flexible analysis computer program which performs the interpolation process and combines the drag components for a given flight test condition.

Span efficiency factor.- Rigid efficiency factors, shown in figure 34, were determined for a large range of lift coefficients and Mach Numbers in order to provide a firm basis for the analysis. The airplane does not fly at all the combinations of C_L and M shown in figure 34 and consequently the flexible analysis is limited to the pertinent range of variables. For example, figure 35 shows a comparison of the rigid and flexible efficiency factors for several values of dynamic pressure, q, where the C_L range for each q bounds the available flight data. Since this comparison is made at low speed (M = 0.6), it is also necessary to examine the flexibility effect on e at higher Mach Numbers. This is accomplished in figure 36 for high and low values of C_L and q over the range of test Mach Numbers. Examination of these figures reveals that the flexibility effect is quite significant, especially at low lift coefficients. The reason for this, as discussed earlier in the aeroelastic effects section, is the resultant inboard shift of the wing load onto the fuselage. This tends to improve the total spanwise distribution from an efficiency viewpoint. The fuel load, stored in the wing fuel tanks, affects the dead weight wing twist distribution. This effect tends to relieve the bending due to aerodynamic loading and hence reduces the amount of aeroelastic distortion present at a given condition. Three values of fuel load were chosen, corresponding to low, medium and high fuel load conditions for the purpose of investigating this effect on flexibility. As can be seen in table 3, the effect of fuel load on span efficiency is small, especially in the cruise range of lift coefficients (C_{L_A} = 0.35 to 0.5) where the

change is less than one percent. The effect is slightly larger at low lift coefficients; however, the overall flexibility effect at these conditions is large, as discussed above, thus minimizing the importance of fuel load.

Tail-off lift coefficient.- In order to evaluate the trim drag increment it is essential to know the relationship between the airplane trimmed lift coefficient and the tail-off lift coefficient. Figures 37 and 38 show this relationship as affected by Mach Number and c.g. position for the rigid airplane. Flexibility effects on $C_{L_{A-h}}$ are summarized in figure 39. For the C-141A, these effects are seen to be small at cruise conditions, approximately a one percent reduction in $C_{L_{A-h}}$. At high values of Mach Number and q the amount of reduction may be as high as seven or eight percent; again, these conditions are at low lift coefficients. The influence of Mach Number and fuel load are shown in figure 39 (b) and (c) as factors which are to be applied to the basic reduction curves shown in figure 39 (a). In equation form, for a given $C_{L_{A-h}}$, M and fuel load, the percent reduction of $C_{L_{A-h}}$ is

$$C_{L_{A-h}\,RED} = C_{L_{A-h}\,RED\,\substack{M=.6\\Low\ fuel}} \times M_f \times F_f$$

Tail efficiency factor and downwash.- Tail efficiency factors for use in calculating tail induced drag were determined for varying amounts of tail lift coefficient and Mach Number and the results are shown in figure 40. The flexibility effect on tail induced drag is primarily due to the difference in tail lift coefficient, flexible and rigid. The effect on the tail efficiency factor due to aeroelastic distortion of the tail, similar to that on the wing, while present, is of such magnitude that the tail induced drag change due to tail flexibility can be ignored.

The remaining term in the trim drag which must be considered is the component of tail lift along the drag axis, designated herein as $C_{L_{tail}} \tan \epsilon$. As can be seen from the sketch in figure 3, this component is a forward or thrust producing vector. This is true since the relative wind at the tail is reduced in angle from that at the wing by the downwash angle. The lift-drag axis at the tail is effectively rotated with respect to the lift drag axis at the wing and the tail lift thus has a forward component along the drag axis.

The amount of downwash at the tail as a function of tail-off lift coefficient and for several Mach Numbers is presented in figure 41. Some small effect on downwash due to flexibility is existent as shown in figure 42. The primary result of flexibility on this term is produced by the reduction in tail lift coefficient as was true for tail induced drag.

Wing profile drag increment due to flexibility.- The results of the analysis of the wing profile drag increment due to aeroelastic distortion are presented in figure 43. The analysis was not extended to conditions of C_L and M where large regions of supercritical flow exist on the wing. Since the basis for the analysis is airfoil section data tested under

34

conditions of natural transition, the duplication of shock effects is dubious and thus precludes reliance on the results at these conditions. In table 3, results for the wing profile drag increment are shown only for the $M = 0.6$ cases and at C_L's of 0.55 and below. These data tend to be conservative since the analysis did not include considerations of possible shock-induced separation; also, on the inboard wing panel the isobars gradually become unswept and local increases in lift are felt due to the flexible redistribution of load which would further aggravate compressibility losses. This, however, does not detract materially from the overall analysis since the major emphasis is placed on those test points in an operating range near the minimum profile drag point and at Mach Numbers where such effects should be minimal. The basic data obtained from the low fuel configurations are shown in figure 43 (a) and a factor which approximates the effect of varying amounts of fuel is contained in figure 43 (b).

Results for five selected flights.- The rigid and flexible coefficients obtained from a direct calculation for the five check cases are shown in table 4. A comparison with the results from the interpolation program used to analyze all the flight test points shows good agreement thus validating the interpolation procedure. A step-by-step breakdown of each of the drag components affected by flexibility is presented in this table for the purpose of illustrating the effects as well as comparing the interpolated and calculated results.

Considerations of Other Components

External configuration changes.- The test article was modified in certain ways from the production configuration to suit the peculiar requirements of the performance test programs. These changes are enumerated in table 5 where the estimated drag increment for each item is shown. Figure 44 illustrates the approximate position of the major changes. The wing vortex generators and wing leading-edge stall strips were installed during the flight test program to control the natural stall separation progression and, subsequently, became part of the production airplane. Drag of these items is considered part of the total roughness drag and is not included in the total instrumentation drag increment.

The drag increments shown in table 5 were obtained using conventional methods contained in reference 12, considering the effects of pressure gradients, and boundary layer thickness. A brief discussion follows, outlining the procedures for those items of major significance to the airplane drag.

The drag increment of the nose boom is composed of the skin friction drag of the isolated boom, modified for installation effects. Reference 12 presents data for cylindrical bodies with streamlined head forms in axial flow from which the minimum skin friction value can be determined for the boom. Incremental effects due to mutual interference between the boom and the fuselage are small. An approximation is made based on the effect of the pressure gradient along the boom, as outlined in chapter 8 of reference 12, using the measured static pressures existing on the fuselage nose.

Drag of the takeoff and landing camera is assumed to be that for a faired appendage to a body. This is calculated using the relationship

$$C_{D_{APP}} = C_{D_\pi} \frac{S_\pi}{S} \qquad (6)$$

where C_{D_π} is the drag coefficient for a similar body based on the reference frontal area, S_π.

The drag increment of the two tail skegs may be fairly significant since they are essentially rectangular bodies protruding on the fuselage afterbody where they may contribute to local boundary layer separations. There is no appropriate method to calculate drag due to such separation effects on the aft fuselage however, and a minimum drag value is used based on the drag characteristics of bluff bodies.

Another significant item of drag is due to the trailing static airspeed cone and cable. Drag of the cable was determined from the relationships of reference 12 for wires and cables inclined against the flow direction. This was added to the cone drag estimated for a similar isolated body using equation 6.

Drag of the remaining items in table 5 is rather small even considered in total. Approximations for these items were obtained using methods for excrescence drag given in reference 12.

The total low speed drag increment due to the external changes for flight test operations is estimated to be $\Delta C_{D_{INST}} = 0.00068$.

Incremental drag due to c.g. position.- As can be seen in table 2, variations in the location of the c.g. position of one to two percent MAC occur during most flights. More important, the c.g. position varies significantly from one series of flights to the next, with an overall range of approximately 12 percent MAC. Thus it is necessary to account for these differences by referencing all data to a particular c.g. location. In this report all flight test data has been corrected to trim at a c.g. location of 0.25 MAC. The effect of a shift in c.g. position can be approximated by making use of existing wind tunnel data where such effects were measured. A summary of these effects based on C-141A wind tunnel data, reference 13, is shown in figure 45.

Equivalent Rigid Profile Drag

Analysis of the drag data from the speed power flights was accomplished utilizing a reduction equation derived from equations (1) and (5). Equation (1) can be re-written in terms of the minimum profile drag as:

$$C_{D_{P_{min}}} = C_D - C_{D_i} - C_{D_{trim}} - C_{D_{P_{C_L}}} - C_{D_{P_C}}$$

In order to determine the equivalent rigid profile drag, substitution of the corrections from equation (5) is made for C_D:

$$C_{D_{P_{min_{rigid}}}} = C_{D_{flex}} - C_{D_i} - C_{D_{trim}} - C_{D_{P_{C_L}}} - C_{D_{P_C}}$$
$$\begin{array}{c} c.g. = .25 \text{ MAC} \\ \text{less inst} \end{array} \quad + \Delta C_{D_{i_{rigid-flex}}} + \Delta C_{D_{P_{wing_{rigid-flex}}}}$$
$$+ \Delta C_{D_{trim_{rigid-flex}}} + \Delta C_{D_{trim_{c.g.}}} - \Delta C_{D_{inst}} \qquad (7)$$

All of the components in the above equation can be obtained except the lift dependent profile drag, $C_{D_{P_{C_L}}}$, and the compressibility effect on profile drag, $C_{D_{P_C}}$. In order to facilitate a determination of these values an intermediate value of profile drag was calculated accounting for all components except these two. This term is designated as $C_{D_{P_{rigid}}}^*$. Thus,

$$C_{D_{P_{rigid}}}^* = C_{D_{P_{min_{rigid}}}} + C_{D_{P_{C_L}}} + C_{D_{P_C}}$$
$$\begin{array}{c} c.g. = .25 \text{ MAC} \\ \text{less inst} \end{array}$$

In addition, the Reynolds Number influence on profile drag exists in the data at this point. This influence is brought about by the reduction in boundary layer thickness and attendant skin friction with increasing Reynolds Number. A fairly accurate estimate of this effect is possible from classical skin friction laws with appropriate form or shape factors. The profile drag of each component on the aircraft is calculated from:

$$C_{D_P} = C_f (SF) \frac{S_{WET}}{S}$$

where

C_f = skin friction coefficient at the Reynolds Number based on the component characteristic length.

SF = accounts for the supervelocity resulting from the component shape

S_{WET} = wetted area of the component

S = wing planform area

Although values of SF for various airfoil shapes, thickness/chord ratios and body shapes are available in the literature, reference 12 for example, there is some doubt as to the validity of applying these two-dimensional data to a three-dimensional case. For this reason, the value of SF used for the C-141A is determined as the integrated average of the ratio of local to free stream dynamic pressures. The total airplane profile drag estimate was obtained over the full range of test Reynolds Numbers assuming smooth turbulent flow. The result is shown in figure 46. The intermediate profile drag data were then corrected to a nominal Reynolds Number of 32.5 million using:

$$C^*_{D_{P_{rigid}}}{}_{RN = 32.5 \times 10^6} = C^*_{D_{P_{rigid}}} + \Delta C_{D_{P_{RN}}}$$

where

$$\Delta C_{D_{P_{RN}}} = C_{D_{P_{RN}} = 32.5 \times 10^6} - C_{D_{P_{RN} = flight\ value}}$$

and $\Delta C_{D_{P_{RN}}}$ is obtained from figure 46. It is assumed that within the flight Reynolds Number range the $C_{D_{P_{C_L}}}$ term is independent of RN. The results for the speed power flight test points are plotted versus Mach Number in figure 47. Utilizing these data and the data of figure 32 (b), plots of $C^*_{D_{P_{rigid}}}{}_{RN = 32.5 \times 10^6}$ versus C_{L_A} for several Mach Numbers can be developed as shown in figure 48.

By removing the Mach Number effects thus obtained, $C_{D_{P_C}}$, from the Reynolds Number adjusted data for Mach Numbers above 0.6 it is possible to plot $C_{D_{P_{rigid}}}{}_{RN = 32.5 \times 10^6}{}_{M = 0.6}$ versus $C_{L_{A-h}}$ as shown in figure 49. The tail-off lift coefficient is the appropriate lift variable since trim drag has been removed and the profile drag thus occurs at tail-off lift. At low lift coefficients, where low angles of attack are experienced, a large pressure drag penalty is incurred due to the upsweep of the rear fuselage. At high lift coefficients above $C_L = 0.5$, separation drag becomes an important factor and undoubtedly contributes to the additional profile drag observed. Lack of sufficient data in terms of flight measured drags and span load distributions compound the problem of determining the true profile drag in this high C_L region.

A mean curve is faired through the data based on polynomial curve fit using the method of least squares. This average curve can then be used to adjust all data points for lift effects on profile drag.

Final reduction of the test point drag coefficients to their equivalent rigid minimum profile drag is outlined in table 6, where the data have been segregated by flight category to simplify identification. The results are plotted versus Reynolds Number in figure 50. A mean curve has been faired through the data of figure 50(a) to indicate the Reynolds Number trend. The estimated profile drag variation with Reynolds Number from figure 46 is included in figure 50(a) for comparison purposes.

The variation of profile drag with Reynolds Number from the flight data is seen to differ slightly from that of the estimated data. The increment between the estimated profile drag and actual is termed excess profile drag and is attributed primarily to roughness drag and to separation and interference effects not included in the estimated drag. Since there may be unknown Reynolds Number effects on this excess profile drag, conclusions about the observed flight variation become difficult. In addition, the amount of scatter, although relatively small, and the distribution of the scatter about the mean curve, which affect the shape of the mean line, compound this difficulty.

Most of the data is observed to lie in a band fairly close to the mean line, within approximately $\pm \Delta C_D = .0006$. Five of the points appear to be somewhat separated from the band. Of these points two are at relatively high C_L's, above $C_{L_A} = 0.55$, where it is expected that a great deal more scatter would appear due to separation effects. The remaining three are in the cruise range of C_L's and Mach Number and are believed to be wild points which occur in flight test analysis despite the best engineering efforts. By eliminating the high C_L test points from the analysis as well as the assumed wild points, the profile drag variation appears as shown in figure 51. It is believed that this is the best representation of the minimum profile drag variation with Reynolds Number obtainable from the flight data. It will be observed that these data now exhibit a variation with Reynolds Number which agrees very well with the variation expected from classical skin friction laws. These data indicate that over the range of the flight test Reynolds Numbers at least, the separation and interference drag is constant and not dependent on Reynolds Number. An analysis of the accuracy of these data is discussed in a later section of this report.

For comparison purposes, figures 50 (b) and 50 (c) illustrate the results for the range mission and continuous climb flights. These data lend little credence to the effects illustrated by the speed-power data since the scatter band is somewhat greater and the Reynolds Number range is not sufficient to establish a trend. However, this is not unexpected since the climb data include the additional variables of rate of climb and pilot technique and, in addition, it is difficult to account accurately for the effects of wind shear and temperature gradients. The latter is especially true in the case of the range mission data since these data were obtained over an extremely long distance and time period. Actually, these range mission points appear to be approximately 10 drag counts higher, on the average, than the speed power data and this is attributed directly to wind and temperature gradients not existent in the speed power data. In a later section on the airplane total drag coefficients, this discrepancy is also seen to occur, which indicates that the reduction process to profile

drag levels has not induced this difference. The significance of this is that for purposes of analyzing airplane minimum profile drag, reliance should be placed on only those data where these variables have been either eliminated or minimized.

In the past, flight data on some airplanes have suggested that there exists a terminal value of skin friction, and further that this is due to a critical roughness height related to component length. The turbulent skin friction data of Nikuradse show that terminal values of skin friction are introduced by the degree of distributed roughness existing in the surface. For the C-141A, distributed roughness of the order of 400 micro-inches would be required to cause termination of the decrease in skin friction coefficient with Reynolds Number. Optical measurements of the standard aluminum sheet finish show distributed roughness levels of 60 to 80 micro-inches and modern paint finishes, as measured on the C-141A, produce values in the range of 30 to 50 micro-inches. Thus, there is no reason to expect terminal skin friction values on the basis of measured and calculated allowable distributed roughness and the flight test data confirm the absence of terminal values.

Aircraft Drag Polar Analysis

Use is made of equation (5) to determine a set of equivalent rigid airplane drag coefficients suitable for drag polar analysis. In order to derive sufficient data to establish shapes of drag polars at several Mach Numbers it is necessary to correct the flight test measured drag data to constant conditions of Mach Number, designated M_{corr}, and Reynolds Number, designated RN_{corr}. Thus, equation (5) becomes:

$$
\begin{aligned}
C_{D_{rigid}} \Big|_{\substack{c.g. = .25 \text{ MAC} \\ \text{less inst} \\ M = M_{corr} \\ RN = RN_{corr}}} &= C_{D_{flex}} + \Delta C_{D_{i_{rigid-flex}}} + \Delta C_{D_{p_{wing_{rigid-flex}}}} \\
&+ \Delta C_{D_{trim_{rigid-flex}}} + \Delta C_{D_{trim_{c.g.}}} - \Delta C_{D_{inst}} \\
&+ \Delta C_{D_M} + \Delta C_{D_{RN}} \qquad (8)
\end{aligned}
$$

The first six terms are as defined previously.

$$
\Delta C_{D_M} = C_{D_M} = M_{corr} - C_{D_M} = \text{flight M}
$$

$$
\Delta C_{D_{RN}} = C_{D_{RN}} = RN_{corr} - C_{D_{RN}} = \text{flight RN}
$$

The Mach Number increment is based on an analysis of the flight test data. The increment due to Reynolds Number is based on the estimated skin friction variation for the C-141A aircraft as shown in figure 46.

Mach Number effect on C_D.- A procedure similar to that employed to analyze the Mach Number effects on C_{D_P} was performed on the corrected flight drag values to determine the variation with Mach Number. The speed power points were first corrected using equation (8), without the Mach correction, ΔC_{D_M}, and the resulting data plotted versus Mach Number for each series of flights. The results are shown in figure 52. Figure 53 is the cross-plot of the data at constant Mach Numbers. These data are all corrected to a Reynolds Number of 55 million and a c.g. position of 0.25 MAC. In order to increase the reliability of the curve fairings shown in figure 53 an iteration was performed wherein each flight test point was corrected to several adjacent Mach Numbers where possible, using equation (8) with ΔC_{D_M} included and keeping the corrections as small as possible. Table 7 lists the results of this analysis and figure 54 shows all the points for each Mach Number investigated. These data represent the final drag polars for the flight data corrected to RN = 55 million. A summary plot of the faired curves is shown in figure 55 and a cross-plot of the data versus Mach Number is included in figure 56. The Mach Number effect illustrated in figure 56 is that which is used in the final analysis. In addition, the results for the range mission flights and climb flights are shown separately in figures 57 and 58. The previously faired curves are illustrated on these figures for comparison purposes. It is apparent that the climb data agree quite well with the speed power data, with an additional amount of scatter. The range mission data, however, appear to be shifted approximately 10 counts as discussed previously under the profile drag section.

Reynolds Number effect on C_D.- In addition to the above set of drag polars, an attempt was made to establish polars at several Reynolds Numbers and Mach Numbers. Due to the scarcity of high speed data this was possible only at M = 0.6 and M = 0.7. For purposes of this analysis, the data were grouped into three Reynolds Number bands and corrected to nominal values of RN = 80 million, 55 million and 30 million. In this way, the RN correction applied to any individual point never exceeded that of 15 million and was generally less than 10 million. Further, figure 57 indicates that climb data are useful for drag polar analysis, more so than for profile drag analysis, where the larger amount of scatter over a small Reynolds Number range was not beneficial. Thus the climb data were included in an attempt to increase the number of data points at each Reynolds Number. The final results of this analysis are presented in figure 59. The faired curve for RN = 55 million is that which was derived previously and is shown over the entire C_L range. For the two extreme Reynolds Numbers, however, the data do not extend over a sufficient range to establish the entire polar.

General.- It is not the intent of this report to discuss the statistical treatment of experimental data in any great detail. Reference 14 is a very useful report on the subject as related to aerodynamics and reference 15 contains a comprehensive survey of the accuracy of all sorts of measurements. A few brief definitions and explanations are in order. Accuracy, as the term is applied herein, is defined to be that measure of the reliability of data as regards random errors and biased errors. Random errors are those which cause repeated readings to vary without any apparent reason. These errors are related to the "precision" of the measured data and are separate from biased errors which are defined to be those errors which cause a measurement to be made in error by an unknown fixed amount. Accuracy can be established by statistical methods for a set, or sample, of measured data by assuming a normal distribution of the data about its mean line. Random errors are usually treated in this manner. A standard deviation, which is called sigma, σ, and defined as the radius of gyration of the data about its mean, is calculated and a confidence level assigned in terms of this deviation. Two standard deviations from the mean should encompass 95.4 percent of the data; this represents, however, only an examination of measured results. It is also necessary to predict the expected accuracy in order to conclude the overall accuracy, and establish the validity of the results achieved.

By assuming a normal distribution of errors, whereby the possibility of all errors being in the same direction is remote, the error of a flight test parameter, such as drag coefficient, can be found by combining the errors of all the variables involved. This is represented mathematically as

$$E_V = \sqrt{\left(\frac{V}{a} E_a\right)^2 + \left(\frac{V}{b} E_b\right)^2 + \ldots + \left(\frac{V}{n} E_n\right)^2} \qquad (9)$$

where

$$V = f(a, b, \ldots, n)$$

$$E = \text{error of the variable or parameter}$$

The above is generally referred to as the root-sum-square method.

For this analysis, errors due to instrument indicator accuracy are first determined. These are then combined with thrust sensitivity factors, and the sensitivity of the calculated lift and drag coefficient to measured parameters, to determine the precision of the final calculated coefficients. This represents then the expected random scatter of the flight test data. Additionally, an assessment is made of those errors which have been induced in the calculation and reduction technique. Since these errors are most likely fixed in amount but of unknown direction, they are treated as biased errors. Finally, the random and biased errors are combined so that the overall accuracy can be assessed.

<u>Indicator precision</u>.- Indicator errors due to parallax and instrument vibration were reduced to an insignificant value by proper instrument mounting and a sampling of data at each test condition. Errors that are fixed and inherent of indicators were measured by calibrating the indicators against one or more primary instruments. A curve was then fitted through the calibration points and used to determine the fixed error of each indicator for any data point. The data were then corrected by this value. When the indicator was calibrated from minimum to the maximum value and back to minimum, a difference in readings sometimes existed for any given point. This difference represented the uncertainty of the meter movement, i.e., indicator hysteresis. To select a value to represent the fixed error of the indicator, the mean value of the correction curves for increasing and decreasing quantities was used. This value does not necessarily represent either point on the curve but a compromise of the two values. An error was therefore introduced which was directly proportional to the magnitude of the indicator hysteresis at that point. For each measurement, indicators with small hysteresis were selected.

When several calibrations are performed on the same indicator, a shift in the fixed error may result. This curve shift is a result of indicator wear and an uncertainty error of the primary instrument. This is another error which will add to the uncertainty of the fixed error. By using the root-sum-square method, the uncertainty of fixed error of an indicator can be found as

$$E_{IND} = \sqrt{E_{HYS}{}^2 + E_{CURVE\ SHIFT}{}^2}$$

Typical calibration curves for the airspeed and altimeter indicators are shown in figures 60 and 61. The method is demonstrated by considering the airspeed indicator curves. From calibration curve No. 2, the maximum hysteresis for this indicator is 3 knots. If a data point is taken at this value (400 knots), a fixed correction of +1.5 knots will be added to the indicated reading. The error attributed to the hysteresis will be the mean of the hysteresis at that point, or 1.5 knots. Thus

$$E_{HYS} = 1.5\ knots$$

A shift in the calibration curve occurred from calibration curve No. 1 to calibration curve No. 2. The maximum shift was 1.0 knot at 300 knots, then

$$E_{CURVE\ SHIFT} = 1.0\ knot$$

$$E_{IND} = 1.8\ knots$$

A similar analysis was conducted for all those parameters relative to drag calculation and their calculated values are summarized in table 8.

Thrust accuracy.- In earlier discussions, the inaccuracies built into the engine computer program, i.e., gross thrust coefficient, airflow coefficient, etc., were considered. The inaccuracies associated with the measured engine parameters and their effect on the calculated net thrust are now considered. Random errors, for both Lockheed and P&WA thrust calculation methods, are included for comparison purposes.

The engine parameters measured during flight testing and used in evaluating net thrust are engine pressure ratio (EPR), flight Mach Number (M), altitude (h), free stream total temperature (T_{TO}), fan rotor speed (N_1), and fan pressure ratio (FPR). The fan rotor speed is used as an input only in the P&WA method of computing thrust. An influence coefficient is defined as the percent change in net thrust per percent change in engine parameter. Influence coefficients were calculated for each of the engine parameters over a range of altitudes and Mach Numbers and are tabulated in table 9.

The engine parameters were instrumented and read from a photo panel in the airplane, thus introducing some readability error. The random errors attributed to instrument inaccuracy and readability have been evaluated and are tabulated in table 10.

During the flight test program, FPR was not readily available for some of the tests due to instrumentation failure and other reasons. Instead of deleting these data points, all thrust calculations were made by inputting only EPR, M, h, T_{TO}, and N_1 (for influence coefficients of P&WA method only) into the computer program. In this way, a consistent set of measured engine parameters were retained. When FPR is not input into the computer program, the program calculates FPR from the other engine parameters as described in reference 9. Figure 62 shows the ratio of calculated FPR to measured FPR for a sampling of data points. Based on these data, a random error of ±0.5 percent was chosen for FPR instead of an error based on instrument and readability error.

The thrust error due to the random error of each parameter is found by multiplying the influence coefficient by the random error for that parameter. Combining these thrust errors by the root-sum-square method gives a total thrust error due to engine parameter random error. This total thrust error is tabulated in table 11 for both methods of calculating thrust. The random scatter due to instrumentation accuracies is larger for the P&WA thrust calculation procedure than for the Lockheed method. This is due, primarily, to the calculation of engine airflow independently of nozzle gross thrust in the P&WA method.

In considering the overall thrust accuracy, the error due to the calculation method for thrust discussed earlier in the TF-33 thrust calculation section must be considered with the data scatter error. For the thrust accuracy of individual data points, these errors should be considered as separate and distinct. The error of the calculation method is a bias error since it is repeatable for any given flight condition; however, it may vary significantly with large changes in engine power setting or Mach Number. In the consideration of airplane performance, these large changes in operating conditions may fall on any given portion of the drag polar. Therefore, the drag coefficient would have an effective thrust accuracy which combines the random and bias errors. A value of 2.6 percent for the effective thrust error is obtained by the root-sum-square method.

Overall accuracy.- The accuracy of a particular flight test drag coefficient is influenced not only by thrust inaccuracies but also by other parameters which contribute to the determination of the final drag coefficient. This accuracy is found by combining the results of the thrust accuracy analysis with an analysis of the influence of all parameters which can be identified. This is accomplished separately for the random errors due to instrumentation inaccuracies and bias errors due to calculation methods. An estimate of the overall maximum inaccuracy expected is represented by a combination of the two. First, the equations for the lift and drag coefficients are written

$$C_L = \frac{W \cos \gamma - F_N \sin (\alpha + \alpha_{TL})}{q S}$$

$$C_D = \frac{F_N \cos (\alpha + \alpha_{TL}) - W \sin \gamma}{q S}$$

The above two equations are used in conjunction with equation (9) to evaluate the sensitivity of C_D to an error in each variable considered independently. The instrumentation errors affect the dynamic pressure and Mach Number as well as the calculated thrust. Additionally, errors in weight, angle of attack, and climb angle must be considered. The effect of obtaining a C_D at an incorrect C_L is included by assessing the sensitivity of C_L to the parameters and using the known variations of C_D and C_L. For example, the effect of an error in weight, ΔW, is

$$\Delta C_D = \left(\frac{\partial C_D}{\partial W} + \frac{\partial C_D}{\partial C_L} \frac{\partial C_L}{\partial W} \right) \Delta W$$

Three typical flight conditions were chosen for evaluation of the amount of random error expected in the flight test data. These are given in table 12; also tabulated are the errors for each of the parameters, the total random error and the overall maximum error. The root-sum-square method was used to combine all the errors. Condition number (2), from table 12, is an approximate cruise condition, where $M = 0.775$ and $C_L = 0.35$, and the expected errors are seen to be

Random error in C_D = ± 0.00031

Overall maximum error in C_D = ± 0.00074

In order to assess the actual scatter of the data presented herein, statistical analyses were performed using polynomial curve fits based on the method of least squares. An analysis was performed first on the $C_{D_{P_{min}}}$ data and the results are pictured in figure 63. These data show a two-sigma deviation of ± 0.00078, very close to the maximum predicted deviation. Thus it appears, as stated earlier, that the procedures for computing thrust and reducing the flight measured drag to its profile drag component have introduced additional random errors due to the bias errors of these procedures.

A similar analysis of the drag polar data was limited to an investigation of the amount of scatter existent in the low speed data, $M = 0.6$ and $M = 0.7$, where the greatest concentration of data points occurs. The speed power data of figure 54 (a) and (b) are reproduced in figure 64, together with the previous faired curve, the statistical mean curve and the scatter band. The two-sigma deviations in these data are very nearly the same as those obtained in the profile drag analysis. This indicates that the amount of scatter existent in the test values of C_D has not been affected by the drag reduction process. This conclusion is not certain, however, since some of the corrections such as aeroelastic effects are the same for both drag values. It may be observed that the scatter in the data is no worse in either event and is approximately equal to the amount predicted. The estimated amount of scatter, $\Delta C_D = \pm 0.00074$, is approximately equal to 3.3 percent of cruise drag for the C-141A. The observed scatter ranges from $\Delta C_D = \pm 0.00070$ to $\Delta C_D = \pm 0.00088$, which corresponds to 3.1 and 3.9 percent, respectively, of cruise drag. This averages about 3.5 percent. Reference 14 reports a level of accuracy of 5 percent on thrust measurements as being reasonable without a detailed investigation of the entire flight test procedure. Every attempt has been made in this study to identify and quantify the errors possible throughout the entire process, from obtaining the measured parameters to calculating the final corrected drag coefficients. Therefore, the accuracy level achieved is believed to be representative of that obtainable using conventional flight test methods for large subsonic, transport type, aircraft.

CONCLUSIONS AND RECOMMENDATIONS

This analysis of C-141A flight test drag data has attempted to account for those factors which generally degrade the degree of correlation achievable between wind tunnel and flight data. A set of rigid-airplane drag polars has been derived by accounting for the effects on drag of airplane elastic deformation, center of gravity location, and flight test instrumentation. In addition, the data have been reduced to provide values of equivalent rigid minimum profile drag.

The accuracy of the flight test equivalent $C_{D_{P_{min}}}$ as related to precision or random scatter is established and at cruise conditions is approximately $\pm \Delta C_D = 0.00031$ or approximately ± 1.3 percent of cruise drag. An assessment of the bias errors which may have been induced by the thrust calculation method and the drag reduction technique indicates that the overall inaccuracy of the correlation may be no larger than $\pm \Delta C_D = 0.00074$ or ± 3.3 percent at cruise. These estimated inaccuracies compare favorably with the demonstrated scatter which averages 3.5 percent of cruise drag and is computed by statistical methods. Thus, the degree of accuracy attainable from flight test data is sufficient to provide valid correlation with wind tunnel data.

One important contribution of this study is the substantiation of the scale effect on profile drag. The available flight test data covers a wide range of Reynolds Number, from approximately 25 million to 86 million. The significance of the variation of the rigid $C_{D_{P_{min}}}$ with Reynolds Number is obvious since it implies that terminal values for $C_{D_{P_{min}}}$ may not be reached within the tested range. Predicted values of $C_{D_{P_{min}}}$ for subsonic aircraft, where the design Reynolds Number is much larger than that of the C-141A are thus affected.

Before a true assessment can be made of the actual correlation between the flight test data analyzed herein and wind tunnel data, it is necessary that a complete and reliable set of wind tunnel data be obtained. It is therefore recommended that additional testing of the C-141A model be conducted at high Reynolds Number, under NASA controlled conditions. Such testing should include improved methods of fixing transition and accurate evaluation of model support interference effects.

It is further recommended that analytical studies be conducted concurrent to the above testing to provide additional insight into the methods currently available for the prediction of full scale characteristics from wind tunnel tests. These should include:

(1) Validity of turbulent skin friction expressions with regard to Reynolds Number corrections from model to full scale.

(2) Effect of Reynolds Number on interference and excess pressure drag.

(3) Effect of Reynolds Number on profile drag due to lift, as part of the total wing span efficiency.

(4) Methods for evaluating section profile drag with application to a three-dimensional wing.

APPENDIX A

Estimation of Wing Vortex Induced Drag

It is possible to modify procedures for calculating span load so that the downwash and, hence, the induced drag can be determined for any given wing geometry when the load distribution is known. The normal induced velocity at any section on the wing, y_1, is given by

$$\omega_{(y_1)} = \frac{1}{4\pi} \int_{\frac{-b}{2}}^{\frac{b}{2}} \frac{\frac{d\Gamma_l}{dy}}{y_1 - y} \, dy \qquad (A1)$$

where Γ_l is the local circulation around any section. The angle of incidence of the section is then altered by the induced angle, α_i.

$$\alpha_o = \alpha - \alpha_i \qquad (A2)$$

where

$$\alpha_i = \frac{\omega}{V} \qquad (A3)$$

The induced drag of the section is

$$c_{d_i} = c_l \left[\frac{\omega}{V} \right] \qquad$$

and

$$c_l = \alpha_o \, \alpha_o \qquad (A4)$$

where α_o is the two-dimensional lift curve slope. The circulation, Γ_l, is given by

$$\Gamma_l = \frac{1}{2} c_l c V \qquad (A5)$$

From equation (A2), (A3), and (A4)

$$\Gamma_l = \frac{1}{2} \alpha_o c (V\alpha - \omega) \qquad (A6)$$

When Γ_1 is determined, wing lift and induced drag are given by

$$L = \int_{-b/2}^{b/2} \rho V \Gamma_1 \, dy \qquad (A7)$$

$$D_i = \int_{-b/2}^{b/2} \rho \omega \Gamma_1 \, dy$$

By making use of Glauert's solution, the circulation may be expressed as a Fouier series. First, the substitutions are made

$$y = -\frac{b}{2} \cos \theta$$

$$dy = \frac{b}{2} \sin \theta \, d\theta$$

such that when $y = b/2$, $\cos \theta = -1$, $\theta = \pi$ and when $y = -b/2$, $\cos \theta = 1$, $\theta = 0^\circ$. The Fourier series expression for circulation is

$$\Gamma = 4 \frac{b}{2} V \sum_{n=1}^{\infty} A_n \sin n\theta \qquad (A8)$$

This series satisfies the condition that the circulation must fall to zero at the tips and, since the wing is symmetrical about its mid-point, odd integral values only of n will be used in the series.

The normal induced velocity at y_1, or θ_1, from equation (A1) now becomes

$$\omega(\theta_1) = \frac{V}{\pi} \int_0^\pi \frac{\sum n A_n \cos n\theta}{\cos \theta_1 - \cos \theta} \, d\theta \qquad (A9)$$

since

$$\int_0^\pi \frac{\cos \theta_1}{\cos \theta_1 - \cos \theta} \, d\theta = \pi \frac{\sin n\theta_1}{\sin \theta_1}$$

equation (A9) reduces to

$$\omega(\theta_1) = V \sum n A_n \frac{\sin n\theta_1}{\sin \theta_1}$$

Utilizing the two equations connecting circulation and normal induced velocity, equations (A6) and (A8), we may write

$$4 \frac{b}{2} V \sum A_n \sin n\theta = \frac{1}{2} a_o c V \left[\alpha - \frac{\sum n A_n \sin n\theta}{\sin \theta} \right]$$

This reduces to

$$\sum A_n \sin n\theta (n\mu + \sin \theta) = \mu a \sin \theta$$

where

$$\mu = \frac{a_o c}{8 \left(\frac{b}{2} \right)}$$

The above fundamental equation may be solved for the coefficients, A_n, knowing the wing geometry and angle of attack. Another expression may be derived for the coefficients in terms of a given span load distribution, $\frac{c_l c}{c_{avg}}$, and the wing geometry. From equations (A5) and (A8), it follows that

$$4 \frac{b}{2} V \sum A_n \sin n\theta = \frac{1}{2} c_l c V$$

This may be reduced algebraically to

$$\sum A_n \sin n\theta = \left(\frac{c_l c}{c_{avg}} \right) \frac{1}{4A}$$

Recalling the equation for the lift of the airfoil, equation (A7), and substituting from equation (A8) for Γ,

$$L = \int_0^\pi 4 \left(\frac{b}{2} \right)^2 \rho V^2 \left(\sum A_n \sin n\theta \right) \sin \theta \ d\theta$$

The value of $\int_0^\pi \sin n\theta \ \sin \theta \ d\theta$ is 0 for all values of n except $n = 1$, for which it is $\pi/2$.

Therefore,

$$L = 2\pi \left(\frac{b}{2} \right)^2 \rho V^2 A_1$$

$$C_L = \pi A A_1$$

where A is the aspect ratio and A_1 is the first coefficient of the Fourier series.

Similarly, it may be shown that the induced drag is

$$D_i = \int_0^\pi 4\left(\frac{b}{2}\right)^2 \rho V^2 \left(\sum n\, A_n \sin n\theta\right)\left(\sum A_n \sin n\theta\right) d\theta$$

$$C_{D_i} = \pi A \sum n\, A_n^2$$

Since $C_L = \pi A A_1$, then $C_L^2 = \pi^2 A^2 A_1^2$, and it follows that

$$C_{D_i} = \frac{1}{\pi A} \frac{\sum n\, A_n^2}{A_1^2} C_L^2$$

Now let

$$\sum \frac{n\, A_n^2}{A_1^2} = 1 + \epsilon$$

Thus, C_{D_i} will be a minimum when $\epsilon = 0$. The wing efficiency in terms of the ideal induced drag is then

$$e = \frac{1}{1 + \epsilon} = \frac{A_1^2}{\sum n\, A_n^2}$$

REFERENCES

1. Treon, S. L.; Steinle, F. W.; and Hagerman, J. R.: Data Correlation from Investigations of a High-Subsonic Speed Transport Aircraft Model in Three Major Transonic Wind Tunnels. AIAA Paper No. 69-794, presented at the Aircraft Design and Operations Meetings, July 14-16, 1969.

2. Bahr, W. C.; Ferrill, R. S.; Nichols, P. M.; and Withers, C. C.: C-141A Engineering Flight Test Data Analysis Methods for Performance and Flying Qualities. ER-4936, Lockheed-Georgia Company, March 1966.

3. Osborne, J.: A Comparison Between Predicted and Measured Profile Drag for a Two-Dimensional Aerofoil at Incompressible Speeds Over a Large Range of Reynolds Number. NPL Aero Report 1052, British, A.R.C. 28,720., 1963.

4. Nash, J. F.; Moulden, T. H.; and Osborne, J.: On the Variation of Profile Drag Coefficient Below the Critical Mach Number. NPL Aero Report 1084, British A.R.C. 25,349., 1963.

5. Nash, J. F.; Osborne, J.; and Macdonald, A. G. J.: A Note on the Prediction of Aerofoil Profile Drag at Subsonic Speeds. NPL Aero Report 1196, British A.R.C. 28,075., 1966.

6. Osborne, J.: The Variation of Profile Drag with Mach Number Up to the Critical Value; A Comparison of Recent Predictions with Early Flight and Wind Tunnel Measurements, and a Comment on an Earlier Prediction. NPL Aero Report 1197, British A.R.C. 28,107., 1966.

7. Bennett, J. A.; and Goradia, S. H.: Methods for Analysis of Two-Dimensional Airfoils with Subsonic and Transonic Applications. ER 8591 (ARO-D Project Number 398, Contract Number DA-31-124-ARO-D-398), Lockheed-Georgia Company, July 1966.

8. Hemenover, Albert D.: The Effects of Camber on the Variation with Mach Number of the Aerodynamic Characteristics of a 10-Percent-Thick Modified NACA Four-Digit-Series Airfoil Section. NACA TN 2998, 1953.

9. Taylor, J. S.; and Schwanebeck, J. D.: C-141A Substantiating Data Report Based on Flight Test Data. ER-8330, Lockheed-Georgia Company., January 1967.

10. JT3D Military Turbofan Handbook, JT3D Engines, Pratt and Whitney Aircraft, April 1959.

11.   Wittel, W. T.; and Cooper, B.L.: Re-Defined Aerodynamic Data for Structural Design Based on In-Flight Measurements. ER 8211, Lockheed-Georgia Company., February 1966.

12.   Hoerner, S. F.: Fluid-Dynamic Drag. Published by the Author, 1965.

13.   Perdue, J. P.; and Maddox, B. W.: C-141 Investigation of Empennage Bullet Modifications Using a 0.044 Scale Model in the NASA-Ames 11 Foot Unitary Wind Tunnel. ER 6130, Lockheed-Georgia Company, July 1963.

14.   Brown, C. E.; and Chen, C. F.: An Analysis of Performance Estimation Methods for Aircraft. NASA CR-921, 1967.

15.   Dean, Jr., R. C.: Aerodynamic Measurements. Gas Turbine Laboratory, Massachusetts Institute of Technology. Eagle Enterprises, 1953.

TABLE 1

C-141A AIRPLANE DIMENSIONAL DATA

Wing

Airfoil section

Root (B.L. = 0.0) . . . . NACA 0013 (Mod)

Break (B.L. = 404.6). . . . . NACA 0011.2 (Mod)

Tip (B.L. = 959.7) . . . . NACA 0010 (Mod)

Average thickness ratio, percent. 11.5

Area, S, ft.^{2} . . . . 3228.

Span, b, ft. 159.92

Aspect ratio, A 7.9

Taper ratio, λ 373

Sweep of 0.25 chord, deg.

Inboard of construction break 23.73

Outboard of construction break 25.03

Incidence, deg.

Root 4.89

Construction break. 2.25

Tip . . . . -0.69

Dihedral, deg.

Inboard of construction break . . . . -0.94

Outboard of construction break . . . . -1.195

Chord lengths, inches

Root 398.80

MAC 266.47

Inboard break 240.70

Tip 131.89

Fuselage

Length, ft. 132.29

Maximum diameter, inches 170.0

Fineness ratio 9.34

Horizontal stabilizer

Airfoil section . . . . NACA 64A(010)010.5

Area, S_H, ft^2 . . . . 483.0

Span, ft 50.17

Aspect ratio, A_{tail} 5.21

Sweep of 0.25 chord, deg. 25.0

Vertical Stabilizer

Airfoil section . . . . NACA 64A(012)013

Area, S_V, ft^2 . . . . 416.0

Span, ft. 22.72

Aspect ratio 1.24

Sweep of 0.25 chord 35.0

TABLE 1.- Continued

C-141A AIRPLANE DIMENSIONAL DATA

Nacelles
    Length, inches 199.22
    Maximum diameter, inches 66.0
    Fineness ratio 3.018
    Inlet area, ft^2 . . . . 12.5
    Exit area, ft^2 . . . . 9.34
    Toe-in angle, deg.
        Inboard 2.0
        Outboard 1.0
    Side area, ft^2 . . . . 86.84
Pylons
    Area, ft^2
        Inboard 46.25
        Outboard 47.87
    Span, inches
        Inboard 33.30
        Outboard 34.47
    MAC, inches 200.0
    Sweep of leading edge, deg. 73.0
Wheel Wells
    Length, inches 404.0
    Equivalent diameter at the maximum area, inches 70.14
    Fineness ratio 5.76
Empennage Bullet
    Length, inches 299.84
    Maximum frontal area, $inches^2$
        (Including horizontal and vertical effects) 1508.3
    Maximum equivalent diameter, inches 43.82
    Fineness ratio 6.84

TABLE 1.- Continued

C-141A AIRPLANE DIMENSIONAL DATA

Wetted areas, ft^2

Wing, basic		6599.50
Deduct for pylons (2 outboard at 12.17 and 2 inboard at 10.72)	45.78	
Deduct for fuselage and fillet intersection	911.32	
Add for planform of wing upper surface, BL 84 left to BL 84 right	424.0	
Wing, net		6066.40
Fuselage, basic		5088.33
Deduct for wing and fillet intersection	545.83	
Add fillet (BL 84 left to 84 right including wing upper surface)	642.01	
Deduct from fillet planform of wing upper surface	424.0	
Deduct for wheel wells	346.0	
Deduct for vertical stabilizer and dorsal intersection	66.99	
Fuselage, net		4347.52
Vertical stabilizer, basic		803.13
Add fin plus part of vertical stabilizer	66.44	
Deduct for dorsal and fuselage intersection	50.17	
Vertical stabilizer, net		819.40
Horizontal stabilizer, basic		980.14
Deduct for bullet intersection	86.40	
Horizontal stabilizer, net		893.74
Nacelles, 4 at 259.68		1038.72
Deduct for pylon intersection	53.56	
Add outboard pylons (2 at 111.62)	223.24	
Add inboard pylons (2 at 107.44)	214.88	
Add net stang area	60.80	
Net pylon/nacelle area		1484.08
Wheel wells, both		822.0
Bullet fairing		136.80
Total airplane		14,569.94

TABLE 1.- Continued

C-141A AIRPLANE DIMENSIONAL DATA

Weights, lb.

Operating weight empty 132,606

Maximum fuel capacity 153,538

Maximum design flight weight 316,100

Maximum ramp weight 318,000

TABLE 2

SUMMARY OF FLIGHT TEST DATA

Flight Number	Pressure Altitude ft.	Temp. °C	Mach Number M	Weight lb.	Fuel Weight lb.	Center of Gravity percent MAC	RN based on wing MAC	Rate of Climb ft/min	Dynamic Pressure lb/ft²	Lift Coeff. C_L	Drag Coeff. C_D
					Speed Power Flights						
106-4A	7,497	2.8	.6736	321,538	139,048	26.06	85.00	8.	508.4	.1961	.0169
4B	7,474	2.6	.6412	317,220	134,730	26.20	81.22	8.	462.9	.2123	.0168
4C	7,399	3.3	.5850	313,752	131,262	26.25	74.20	-8.	387.8	.2506	.0176
4D	7,276	3.4	.5315	311,314	128,824	26.28	67.58	-14.	320.4	.3008	.0191
4E	7,179	3.7	.3989	308,639	126,149	26.32	51.10	-14.	182.9	.5213	.0273
4F	7,101	3.5	.3208	305,695	123,205	26.28	40.96	-29.	116.9	.8046	.0450
4G	8,059	2.6	.4788	303,765	121,275	26.26	59.29	2.	252.4	.3724	.0211
106-5A	15,466	-10.4	.7054	294,007	111,516	26.20	69.34	-9.	409.0	.2228	.0177
5B	15,379	-10.9	.6454	290,122	107,631	26.17	63.78	-9.	343.4	.2617	.0182
5C	15,309	-10.5	.5815	286,631	104,140	26.12	57.54	-5.	279.7	.3172	.0197
5D	15,216	-9.8	.5274	284,401	101,910	26.08	52.20	-14.	230.9	.3811	.0215
5E	15,115	-10.0	.4465	281,791	99,300	26.04	44.47	-19.	166.6	.5226	.0273
5F	15,306	-10.6	.3981	280,404	97,913	26.00	39.43	24.	131.2	.6587	.0352
5G	15,587	-11.6	.4832	277,920	95,429	25.87	47.51	-18.	191.0	.4499	.0242
119-7.1	25,715	-40.0	.8069	303,815	120,199	21.95	59.62	-1.	346.8	.2715	.0244
7.2	25,706	-39.6	.8003	299,747	116,131	21.83	58.96	-1.	340.7	.2727	.0225
7.3	25,682	-40.0	.7897	296,022	112,406	21.75	58.43	4.	332.7	.2757	.0209
7.4	25,661	-40.0	.7672	292,542	108,926	21.65	56.76	-3.	313.6	.2890	.0197
7.5	25,561	-38.8	.7107	289,326	105,710	21.65	52.58	-3.	271.4	.3300	.0195

TABLE 2.– Continued

SUMMARY OF FLIGHT TEST DATA

Flight Number	Pressure Altitude ft.	Temp. °C	Mach Number M	Weight lb.	Fuel Weight lb.	Center of Gravity percent MAC	RN based on wing MAC	Rate of Climb ft/min	Dynamic Pressure lb/ft^2	Lift Coeff. C_L	Drag Coeff. C_D
Speed Power Flights.– Continued
119-7.6	25,488	-38.9	.6589	286,782	103,166	21.55	48.90	-4.	233.7	.3797	.0215
7.7	25,431	-38.8	.5846	284,775	101,159	21.50	43.46	7.	184.3	.4774	.0250
119-8.1	35,552	-55.6	.7939	277,862	94,246	21.15	40.65	6.	213.9	.4022	.0270
8.2	35,552	-55.5	.7815	275,145	91,529	20.97	40.02	-6.	207.5	.4103	.0263
8.3	35,538	-55.2	.7799	272,687	89,071	20.60	39.86	0	206.4	.4089	.0244
8.4	35,504	-55.5	.7586	270,450	86,834	20.45	38.96	-3.	196.2	.4264	.0249
8.5	35,482	-54.6	.7512	267,992	84,376	20.45	38.42	-8.	192.4	.4309	.0244
8.6	35,380	-54.8	.6737	265,135	81,520	20.20	34.66	-10.	155.5	.5268	.0287
123-6.1	11,496	-3.7	.7076	233,365	50,223	18.55	78.96	3.	482.5	.1502	.0170
6.2	11,573	-3.8	.6624	228,843	45,701	18.52	73.72	-3.	421.7	.1686	.0168
123-9A	20,716	-24.3	.8062	219,735	36,593	18.40	68.25	6.	430.1	.1591	.0223
9B	20,613	-23.9	.7598	215,342	32,200	18.20	64.60	-1.	385.3	.1734	.0188
9CR	20,500	-23.5	.6988	208,370	25,228	17.40	59.58	-2.	327.5	.1973	.0173
9D	20,455	-24.4	.6471	205,048	21,906	18.67	55.45	8.	280.7	.2264	.0177
9E	20,373	-23.2	.5987	201,744	18,602	18.25	50.86	±5.	238.2	.2623	.0185
9F	20,331	-22.5	.5568	199,497	16,355	18.00	47.68	7.	210.4	.2936	.0182
9G	20,239	-21.5	.3975	196,222	13,080	17.55	33.76	-5.	106.1	.5705	.0314

TABLE 2.- Continued

SUMMARY OF FLIGHT TEST DATA

Flight Number	Pressure Altitude ft.	Temp. °C	Mach Number M	Weight lb.	Fuel Weight lb.	Center of Gravity percent MAC	RN based on wing MAC	Rate of Climb ft/min	Dynamic Pressure lb/ft^2	Lift Coeff. C_L	Drag Coeff. C_D
				Speed Power Flights.- Continued							
128-5A	30,699	-47.0	.8096	224,273	51,473	20.20	49.64	-3.	279.1	.2489	.0245
5B	30,647	-47.8	.7871	222,059	49,259	20.15	48.52	-8.	265.1	.2595	.0215
5C	30,614	-46.9	.7593	219,425	46,625	20.10	46.76	-1.	247.1	.2751	.0201
5D	30,546	-47.5	.7209	216,792	43,992	20.05	44.69	-2.	223.5	.3005	.0198
5E	30,408	-46.3	.6512	214,295	41,495	20.02	40.63	-8.	184.1	.3605	.0216
5F	30,410	-46.4	.6167	212,297	39,497	20.00	38.23	3.	164.4	.4000	.0225
5GR	30,450	-46.8	.5726	209,449	36,649	19.95	35.51	15.	141.5	.4586	.0254
5H	30,339	-47.3	.4986	207,417	34,617	19.90	31.16	-7.	107.9	.5955	.0335
128-6A	40,481	-55.1	.7978	202,261	29,461	19.60	32.27	-1.	171.1	.3663	.0260
6B	40,476	-54.6	.7835	199,665	26,865	19.30	31.67	-4.	165.7	.3733	.0249
6C	40,512	-54.2	.7736	197,328	24,528	19.05	31.11	9.	160.8	.3799	.0234
6D	40,422	-53.9	.7517	195,101	22,301	18.75	30.28	-1.	152.3	.3964	.0235
6E	40,416	-53.8	.7417	193,217	20,417	18.50	29.86	1.	148.2	.4034	.0237
6F	40,332	-53.3	.6942	191,595	18,795	18.25	28.03	-5.	130.7	.4532	.0248
6G	40,328	-54.6	.6018	190,264	17,464	18.00	24.49	11.	98.3	.5976	.0322
129-5AR	7,518	6.6	.6947	212,075	39,342	21.37	86.37	4.	543.5	.1213	.0172
5B	7,468	5.3	.6578	207,023	34,290	21.30	82.21	3.	485.7	.1324	.0163
5C	7,407	3.6	.6124	203,020	30,287	21.10	77.55	6.	424.8	.1484	.0162
5D	7,317	4.9	.5534	201,011	28,278	20.82	69.96	-4.	348.6	.1788	.0168

TABLE 2.- Continued

SUMMARY OF FLIGHT TEST DATA

Flight Number	Pressure Altitude ft.	Temp. °C	Mach Number M	Weight lb.	Fuel Weight lb.	Center of Gravity percent MAC	RN based on wing MAC	Rate of Climb ft/min	Dynamic Pressure lb/ft^2	Lift Coeff. C_L	Drag Coeff. C_D
				Speed Power Flights.- Continued							
129-5E	7,233	7.5	.4585	197,946	25,213	20.47	57.35	-11.	239.0	.2565	.0183
5F	7,152	7.0	.3582	195,350	22,717	20.15	44.98	-7.	145.9	.4141	.0229
5G	7,681	5.8	.2308	192,821	20,088	19.85	29.62	-55.	61.7	.9583	.0591
129-6R1	20,404	-26.5	.4611	189,730	16,997	19.40	39.97	2.	142.4	.4118	.0235
6R2	19,994	-26.4	.3028	187,535	14,802	19.10	26.67	29.	62.5	.9201	.0581
				Cruise Portion of Range Mission Flights							
187-1	33,536	-52.9	.7261	302,779	120,699	29.30	40.34	-11.	197.2	.4757	.0261
2	33,790	-51.6	.7261	298,436	116,356	29.32	39.56	17.	194.7	.4748	.0260
3	34,364	-50.4	.7255	290,930	108,850	29.35	38.25	26.	189.5	.4757	.0263
4	34,828	-48.2	.7256	284,766	102,686	29.10	37.06	32.	186.2	.4739	.0262
5	35,299	-47.7	.7300	278,805	96,725	28.90	36.24	8.	183.0	.4720	.0257
6	35,788	-48.2	.7344	271,288	89,208	28.50	35.57	14.	179.6	.4679	.0261
7	36,458	-48.7	.7242	261,731	79,615	28.10	34.24	18.	171.0	.4743	.0262
8	37,266	-50.6	.7228	252,520	70,440	27.58	33.22	18.	163.8	.4775	.0264
9	37,975	-53.1	.7241	243,660	61,580	27.50	32.57	13.	158.7	.4757	.0267
10	39,026	-55.9	.7246	234,168	52,088	27.63	31.49	25.	151.0	.4803	.0265
11	39,493	-57.9	.7252	229,221	47,141	27.75	31.08	14.	147.3	.4820	.0265

TABLE 2.- Continued

SUMMARY OF FLIGHT TEST DATA

Flight Number	Pressure Altitude ft.	Temp. °C	Mach Number M	Weight lb.	Fuel Weight lb.	Center of Gravity percent MAC	RN based on wing MAC	Rate of Climb ft/min	Dynamic Pressure lb/ft^2	Lift Coeff. c_L	Drag Coeff. c_D
Cruise Portion of Range Mission Flights.- Continued											
187-12	39,895	-59.9	.7265	223,798	41,718	27.62	30.89	8.	145.1	.4778	.0265
13	40,097	-61.7	.7159	219,453	37,373	27.38	30.61	0.	141.0	.4823	.0271
14	40,075	-58.9	.7156	211,809	29,729	26.78	30.04	-1.	140.0	.4687	.0261
15	39,996	-55.0	.7063	204,519	22,439	26.17	29.17	3.	137.4	.4610	.0250
190-1	34,104	-49.3	.7235	294,937	133,592	28.86	38.41	16.	191.0	.4783	.0262
2	34,812	-49.2	.7242	284,669	123,324	29.03	37.15	15.	185.0	.4766	.0265
3	35,480	-47.9	.7268	274,710	113,365	29.09	35.81	16.	179.8	.4732	.0260
4	36,259	-48.8	.7254	265,071	103,726	29.13	34.64	13.	173.2	.4742	.0264
5	37,100	-49.9	.7221	255,779	94,434	28.90	33.41	13.	165.6	.4784	.0265
6	37,800	-51.9	.7253	246,751	85,406	28.49	32.73	18.	160.9	.4751	.0267
7	38,715	-53.9	.7226	238,065	76,720	28.02	31.51	14.	152.4	.4850	.0270
8	39,424	-55.7	.7258	229,658	68,313	27.51	30.89	18.	148.5	.4790	.0270
9	40,216	-56.3	.7267	221,105	59,760	27.02	29.85	1.	143.2	.4782	.0265
10	40,133	-57.7	.7208	213,399	52,054	26.80	29.98	-2.	141.6	.4668	.0258
11	40,109	-58.9	.7180	205,165	43,820	27.00	30.11	1.	140.8	.4513	.0255
12	40,147	-55.9	.7171	198,535	37,190	27.03	29.48	-2.	139.8	.4398	.0250
13	40,160	-52.8	.7148	191,325	29,980	27.00	28.92	0.	139.3	.4255	.0243
14	40,166	-57.1	.7118	184,306	22,961	26.30	29.39	0.	137.4	.4156	.0242
15	40,130	-52.6	.7083	176,809	15,464	25.58	28.73	-1.	137.7	.3979	.0233

TABLE 2.– Continued

SUMMARY OF FLIGHT TEST DATA

Flight Number	Pressure Altitude ft.	Temp. °C	Mach Number M	Weight lb.	Fuel Weight lb.	Center of Gravity percent MAC	RN based on wing MAC	Rate of Climb ft/min	Dynamic Pressure lb/ft^2	Lift Coeff. C_L	Drag Coeff. C_D
					Continuous Climb Flights						
138-5.1	9,627	-2.3	.4988	309,386	128,915	22.17	59.55	2317.	258.4	.3685	.0188
5.2	15,760	-13.3	.5586	308,025	127,554	22.19	54.74	1784.	251.1	.3785	.0203
5.3	20,254	-24.7	.6072	306,843	126,372	22.21	52.40	1386.	247.9	.3820	.0212
5.4	23,936	-34.4	.6512	305,772	125,301	22.19	50.42	1153.	243.5	.3878	.0214
5.5	27,216	-43.0	.6924	304,785	124,314	22.17	48.31	1005.	235.9	.3991	.0220
5.6	30,163	-49.8	.7027	303,882	123,411	22.15	44.81	888.	215.4	.4359	.0241
5.7	33,285	-56.4	.7053	302,942	122,471	22.13	40.40	619.	188.0	.4928	.0263
139-5.1	14,938	-12.5	.5540	315,368	134,864	22.02	55.98	1698.	255.8	.3799	.0212
5.2	22,103	-29.1	.6333	313,379	132,875	22.05	51.38	1216.	246.6	.3921	.0216
5.3	27,135	-41.1	.6914	311,702	131,198	22.08	47.66	909.	233.2	.4129	.0229
5.4	30,980	-50.1	.7018	310,232	129,728	22.11	43.21	729.	207.2	.4626	.0249
5.5	34,074	-58.0	.7049	308,947	128,443	22.14	39.22	418.	180.8	.5277	.0284
5.6	35,625	-60.5	.7042	307,774	127,270	22.16	35.78	268.	167.9	.5659	.0301
5.7	36,661	-61.6	.7018	306,666	126,162	22.16	35.41	57.	159.8	.5920	.0333
140-5.1	12,196	-7.7	.5279	307,455	127,450	22.15	57.91	1894.	257.0	.3686	.0222
5.2	19,884	-25.2	.6030	305,690	125,685	22.12	52.81	1442.	246.7	.3821	.0221
5.3	25,188	-38.1	.6687	303,859	123,854	22.08	49.62	1001.	239.4	.3919	.0230
5.4	29,365	-48.6	.6989	302,260	122,255	22.05	45.66	848.	218.4	.4272	.0246
5.5	32,702	-56.8	.7024	301,152	121,147	22.00	41.40	577.	191.3	.4860	.0275
5.6	34,894	-61.5	.7011	300,128	120,123	21.98	38.37	362.	172.7	.5365	.0301
5.7	36,025	-63.3	.7019	298,969	118,964	21.96	36.66	236.	163.2	.5655	.0308

TABLE 3

CONFIGURATION MATRIX AND RESULTS FOR
FLEXIBLE DRAG ANALYSIS

Explanation of Items for Table 3	
Item	Explanation
(1)	Trimmed lift coefficient, C_{L_A}
(2)	Mach Number, M
(3)	Dynamic pressure, q, lb/ft^2
(4)	Center of gravity, percent MAC
(5)	Fuel, lbs.
(6), (13)	Tail-off lift coefficient, $C_{L_{A-h}}$
(7), (14)	Exposed wing lift coefficient, C_{L_W}
(8), (15)	Tail lift coefficient, $C_{L_{tail}}$
(9), (16)	Fuselage lift coefficient, C_{L_F}
(10), (17)	Efficiency factor, e
(11), (18)	Trimmed angle of attack, α FRL, deg.
(12), (19)	Downwash angle, ϵ , deg.
(20)	Incremental wing profile drag due to flexibility, $\Delta C_{D_{P_{wing_{rigid-flex}}}}$

TABLE 3.– Continued

CONFIGURATION MATRIX AND RESULTS FOR
FLEXIBLE DRAG ANALYSIS

Item	Configuration									
(1)	.600	.700	.800	.250	.300	.400	.500	.550	.200	.250
(2)	.600	.600	.600	.600	.600	.600	.600	.600	.600	.600
(3)	100.	100.	100.	200.	200.	200.	200.	200.	300.	300.
(4)	18.0	18.0	18.0	18.0	18.0	18.0	18.0	18.0	18.0	18.0
(5)	22,000	22,000	22,000	22,000	22,000	22,000	22,000	22,000	22,000	22,000
Rigid Results										
(6)	.6263	.7277	.8291	.2751	.3249	.4262	.5275	.5782	.2239	.2745
(7)	.5650	.6540	.7429	.2547	.2986	.3877	.4769	.5217	.2091	.2535
(8)	−.0263	−.0276	−.0291	−.0244	−.0249	−.0262	−.0275	−.0283	−.0246	−.0253
(9)	.0613	.0736	.0862	.0204	.0263	.0385	.0506	.0566	.0148	.0210
(10)	.9742	.9778	.9765	.8542	.8955	.9468	.9631	.9655	.7689	.8579
(11)	3.33	4.51	5.68	−0.84	−0.27	0.89	2.04	2.63	−1.45	−0.89
(12)	3.22	3.58	3.94	1.95	2.12	2.51	2.89	3.07	1.80	1.98
Flexible Results										
(13)	.6244	.7255	.8265	.2726	.3222	.4226	.5233	.5736	.2199	.2700
(14)	.5572	.6453	.7337	.2455	.2886	.3758	.4635	.5074	.1963	.2394
(15)	−.0244	−.0254	−.0265	−.0219	−.0222	−.0226	−.0233	−.0237	−.0206	−.0207
(16)	.0672	.0802	.0928	.0271	.0336	.0468	.0598	.0662	.0236	.0306
(17)	.9719	.9662	.9630	.9250	.9373	.9437	.9414	.9397	.9155	.9285
(18)	3.60	4.82	6.04	−0.50	0.12	1.36	2.62	3.25	−0.95	−0.32
(19)	3.12	3.52	3.79	1.82	2.04	2.49	2.96	3.13	1.68	1.92
(20)	–	–	–	−.00008	−.00005	−.00004	−.00004	−.00002	−.00012	−.00016

TABLE 3.- Continued

CONFIGURATION MATRIX AND RESULTS FOR FLEXIBLE DRAG ANALYSIS

Item	Configuration									
(1)	.300	.350	.150	.200	.250	.100	.200	.416	.500	.550
(2)	.600	.600	.600	.600	.600	.600	.600	.600	.600	.600
(3)	300.	300.	400.	400.	400.	500.	500.	200.	200.	200.
(4)	18.0	18.0	18.0	18.0	18.0	18.0	18.0	18.0	18.0	18.0
(5)	22,000	22,000	22,000	22,000	22,000	22,000	22,000	121,000	121,000	121,000
	Rigid Results									
(6)	.3248	.3752	.1739	.2245	.2750	.1239	.2250	.4426	.5277	.5782
(7)	.2977	.3421	.1648	.2092	.2536	.1209	.2097	.4022	.4770	.5216
(8)	-.0259	-.0265	-.0243	-.0250	-.0256	-.0236	-.0250	-.0267	-.0277	-.0283
(9)	.0271	.0331	.0091	.0153	.0214	.0030	.0153	.0404	.0507	.0566
(10)	.9094	.9329	.6138	.7626	.8529	.3894	.7528	.9488	.9634	.9687
(11)	-0.33	0.23	-2.01	-1.46	-0.91	-2.56	-1.46	1.07	2.04	2.63
(12)	2.15	2.33	1.64	1.81	1.99	1.45	1.81	2.55	2.89	3.07
	Flexible Results									
(13)	.3197	.3695	.1689	.2187	.2686	.1185	.2177	.4401	.5245	.5746
(14)	.2824	.3252	.1498	.1924	.2350	.1050	.1894	.3927	.4662	.5100
(15)	-.0208	-.0208	-.0193	-.0192	-.0192	-.0182	-.0177	-.0242	-.0245	-.0247
(16)	.0373	.0443	.1689	.2187	.2686	.0135	.0283	.0474	.0583	.0646
(17)	.9286	.9231	.8474	.8844	.8886	.6927	.8386	.9517	.9527	.9511
(18)	0.31	0.95	-1.41	-0.77	-0.12	-1.92	-0.60	1.42	2.47	3.10
(19)	2.15	2.38	1.45	1.72	1.95	1.13	1.69	2.40	2.80	3.02
(20)	-.00009	-.00005	-.00024	-.00018	-.00021	-.00051	-.00026	-.00003	-.00003	-.00001

TABLE 3.- Continued

CONFIGURATION MATRIX AND RESULTS FOR FLEXIBLE DRAG ANALYSIS

Item	Configuration									
(1)	.400	.500	.550	.400	.550	.400	.550	.400	.550	.400
(2)	.600	.600	.600	.600	.600	.600	.600	.600	.600	.600
(3)	200.	200.	200.	200.	200.	200.	200.	200.	200.	200.
(4)	18.0	18.0	18.0	22.0	22.0	26.0	26.0	22.0	22.0	26.0
(5)	73,000	73,000	73,000	22,000	22,000	22,000	22,000	121,000	121,000	121,000
Rigid Results										
(6)	.4267	.5280	.5786	.4216	.5720	.4170	.5657	.4309	.5720	.4201
(7)	.3882	.4772	.5220	.3836	.5162	.3796	.5106	.3919	.5161	.3824
(8)	-.0267	-.0280	-.0287	-.0216	-.0221	-.0170	-.0158	-.0220	-.0221	-.0174
(9)	.0385	.0508	.0566	.0380	.0558	.0374	.0551	.0390	.0459	.0377
(10)	.9429	.9623	.9628	.9418	.9692	.9437	.9637	.9444	.9643	.9406
(11)	0.89	2.05	2.63	0.83	2.56	0.78	2.48	0.94	2.55	0.82
(12)	2.50	2.89	3.06	2.48	3.05	2.47	3.01	2.52	3.03	2.48
Flexible Results										
(13)	.4240	.5245	.5747	.4181	.5674	.4135	.5611	.4284	.5684	.4177
(14)	.3781	.4656	.5094	.3718	.5019	.3678	.4965	.3826	.5045	.3733
(15)	-.0240	-.0245	-.0248	-.0181	-.0175	-.0135	-.0112	-.0195	-.0185	-.0150
(16)	.0459	.0589	.0653	.0463	.0655	.0457	.0646	.0458	.0639	.0444
(17)	.9471	.9478	.9454	.9402	.9434	.9439	.9394	.9519	.9496	.9540
(18)	1.27	2.53	3.16	1.31	3.17	1.25	3.10	1.27	3.02	1.14
(19)	2.37	2.85	3.05	2.55	3.21	2.61	3.27	2.42	3.11	2.46
(20)	-.00004	-.00003	-.00002	-.00005	-.00003	-.00005	-.00005	-.00004	-.00002	-.00006

TABLE 3.- Continued

CONFIGURATION MATRIX AND RESULTS FOR
FLEXIBLE DRAG ANALYSIS

Item	Configuration									
(1)	.550	.200	.250	.200	.250	.400	.400	.400	.400	.400
(2)	.600	.600	.600	.600	.600	.700	.740	.775	.813	.840
(3)	200.	400.	400.	400.	400.	200.	200.	200.	200.	200.
(4)	26.0	22.0	22.0	26.0	26.0	18.0	18.0	18.0	18.0	18.0
(5)	121,000	22,000	22,000	22,000	22,000	22,000	22,000	22,000	22,000	22,000
	Rigid Results									
(6)	.5657	.2222	.2722	.2199	.2693	.4276	.4277	.4315	.4346	.4349
(7)	.5106	.2072	.2511	.2052	.2486	.3877	.3892	.3914	.4040	.4103
(8)	-.0158	-.0227	-.0228	-.0204	-.0199	-.0276	-.0277	-.0315	-.0346	-.0349
(9)	.0551	.0150	.0211	.0147	.0207	.0399	.0385	.0401	.0306	.0246
(10)	.9607	.7533	.8507	.7506	.8449	.9544	.9277	.8619	.7355	.5567
(11)	2.48	-1.49	-0.94	-1.51	-0.97	0.72	0.57	0.53	0.95	1.84
(12)	3.01	1.79	1.98	1.79	1.96	2.52	2.47	2.80	3.46	3.50
	Flexible Results									
(13)	.5622	.2164	.2656	.2142	.2629	.4234	.4235	.4273	.4304	.4270
(14)	.4991	.1905	.2326	.1885	.2302	.3740	.3805	.3819	.3955	.3940
(15)	-.0123	-.0169	-.0163	-.0147	-.0135	-.0234	-.0235	-.0273	-.0304	-.0270
(16)	.0631	.0259	.0330	.0257	.0327	.0494	.0430	.0454	.0349	.0330
(17)	.9473	.8848	.8928	.8825	.8907	.9507	.9380	.8720	.7894	.6630
(18)	2.94	-0.80	-0.16	-0.83	-0.19	1.26	1.11	1.08	1.62	2.65
(19)	3.19	1.78	2.03	1.85	2.13	2.56	2.52	2.78	3.42	3.76
(20)	-.00004	-.00020	-.00017	-.00022	-.00020	-	-	-	-	-

TABLE 3.– Continued

CONFIGURATION MATRIX AND RESULTS FOR FLEXIBLE DRAG ANALYSIS

Item	Configuration							
(1)	.250	.250	.250	.250	.250	.250	.250	.250
(2)	.740	.775	.810	.840	.740	.775	.810	.840
(3)	200.	200.	200.	200.	400.	400.	400.	400.
(4)	18.0	18.0	18.0	18.0	18.0	18.0	18.0	18.0
(5)	22,000	22,000	22,000	22,000	22,000	22,000	22,000	22,000
Rigid Results								
(6)	.2755	.2784	.2800	.2813	.2758	.2787	.2799	.2808
(7)	.2562	.2578	.2648	.2707	.2566	.2583	.2653	.2708
(8)	-.0255	-.0284	-.0300	-.0313	-.0258	-.0287	-.0299	-.0308
(9)	.0193	.0206	.0152	.0106	.0192	.0204	.0146	.0100
(10)	.7510	.6370	.5477	.3858	.7450	.6301	.5274	.3723
(11)	-0.98	-0.96	-0.78	-0.06	-0.98	-0.96	-0.78	-0.06
(12)	1.96	2.27	2.76	2.81	1.96	2.26	2.76	2.80
Flexible Results								
(13)	.2722	.2751	.2750	.2752	.2684	.2714	.2712	.2702
(14)	.2446	.2445	.2512	.2557	.2360	.2366	.2432	.2472
(15)	-.0222	-.0251	-.0250	-.0252	-.0184	-.0214	-.0212	-.0202
(16)	.0276	.0306	.0238	.0195	.0324	.0348	.0281	.0230
(17)	.9329	.8332	.7462	.5548	.8979	.8115	.7447	.5593
(18)	-0.59	-0.56	-0.31	-0.53	-0.16	-0.12	0.21	1.14
(19)	1.88	2.15	2.68	2.80	1.99	2.23	2.77	3.14
(20)	-	-	-	-	-	-	-	-

TABLE 4

RIGID AND FLEXIBLE COEFFICIENTS AND DRAG INCREMENTS FOR
FIVE SELECTED SPEED POWER FLIGHTS – COMPARISON OF CALCULATED AND INTERPOLATED RESULTS

Flight	C_{L_A}	e_{rigid}	e_{flex}	$C_{D_{i_{rigid}}}$ $\dfrac{①^2}{\pi A\,②}$	$C_{D_{i_{flex}}}$ $\dfrac{①^2}{\pi A\,③}$	$\Delta C_{D_{i_{rigid-flex}}}$ ④-⑤	$C_{L_A-h_{rigid}}$	$C_{L_A-h_{flex}}$	$\Delta C_{D_{i_{trim-rigid}}}$ $\dfrac{⑦}{②}-④$
	①	②	③	④	⑤	⑥	⑦	⑧	⑨
Calculated Results									
106-4A	.1961	.7256	.8399	.00214	.00185	.00029	.2166	.2105	.00047
106-5A	.2228	.7556	.9068	.00265	.00221	.00044	.2433	.2375	.00051
119-7.5	.3300	.8960	.9530	.00490	.00460	.00029	.3538	.3498	.00073
119-8.6	.5268	.9713	.9640	.01151	.01160	-.00009	.5529	.5500	.00117
123-6.1	.1502	.5878	.8356	.00155	.00109	.00046	.1746	.1679	.00054
Interpolated Results									
106-4A	.1961	.6980	.8400	.00222	.00185	.00038	.2151	.2088	.00045
106-5A	.2228	.7312	.9006	.00274	.00222	.00051	.2415	.2358	.00048
119-7.5	.3300	.8913	.9465	.00492	.00464	.00029	.3521	.3479	.00068
119-8.6	.5268	.9583	.9525	.01167	.01174	-.00007	.5533	.5505	.00120
123-6.1	.1502	.5306	.8384	.00171	.00108	.00063	.1737	.1669	.00058

TABLE 4.- Continued

RIGID AND FLEXIBLE COEFFICIENTS AND DRAG INCREMENTS FOR FIVE SELECTED SPEED POWER FLIGHTS – COMPARISON OF CALCULATED AND INTERPOLATED RESULTS

Flight	⑩ $\Delta C_{D_{i_{trim_{flex}}}}$ $\dfrac{\textcircled{8}^2}{\pi A \,\textcircled{3}} - \textcircled{5}$	⑪ $\Delta C_{D_{i_{trim_{rigid-flex}}}}$ $\textcircled{9} - \textcircled{10}$	⑫ $C_{L_{tail_{rigid}}}$	⑬ $C_{L_{tail_{flex}}}$	⑭ $e_{tail_{rigid}}$	⑮ $e_{tail_{flex}}$	⑯ $C_{d_{i_{tail_{rigid}}}}$ $\dfrac{\textcircled{12}^2 \times S/S_H}{\pi A_{tail}\,\textcircled{14}}$
Calculated Results							
106-4A	.00028	.00019	−.0205	−.0144	.7482	.5970	.00023
106-5A	.00030	.00021	−.0205	−.0147	.7630	.6180	.00023
119-7.5	.00057	.00016	−.0238	−.0198	.8452	.7597	.00027
119-8.6	.00104	.00013	−.0261	−.0246	.8382	.8181	.00033
123-6.1	.00027	.00027	−.0244	−.0177	.8274	.7116	.00029
Interpolated Results							
106-4A	.00025	.00020	−.0190	−.0127	.7213	.5423	.00020
106-5A	.00027	.00021	−.0187	−.0130	.7283	.5758	.00020
119-7.5	.00052	.00017	−.0221	−.0179	.7957	.7216	.00025
119-8.6	.00108	.00012	−.0265	−.0237	.8426	.8025	.00034
123-6.1	.00025	.00032	−.0235	−.0167	.8139	.6803	.00028

TABLE 4.– Continued

RIGID AND FLEXIBLE COEFFICIENTS AND DRAG INCREMENTS FOR FIVE SELECTED SPEED POWER FLIGHTS – COMPARISON OF CALCULATED AND INTERPOLATED RESULTS

Flight	⑰ $C_{D_{i_{tail_{flex}}}}$ $\dfrac{⑬^2 \times S/S_H}{\pi\,A_{tail}\ \ ⑮}$	⑱ $\Delta C_{D_{i_{tail_{rigid-flex}}}}$ ⑯ – ⑰	⑲ ϵ rigid deg.	⑳ ϵ flex deg.	㉑ $\left(C_{L_{tail}} \tan \epsilon\right)_{rigid}$ ⑫ × tan ⑲	㉒ $\left(C_{L_{tail}} \tan \epsilon\right)_{flex}$ ⑬ × tan ⑳
			Calculated Results			
106-4A	.00014	.00009	-1.77	-1.66	-.00063	-.00042
106-5A	.00014	.00008	-1.88	-1.85	-.00067	-.00047
119-7.5	.00021	.00006	-2.25	-2.20	-.00093	-.00076
119-8.6	.00030	.00003	-2.99	-2.95	-.00136	-.00127
123-6.1	.00018	.00011	-1.44	-1.35	-.00061	-.00042
			Interpolated Results			
106-4A	.00012	.00008	-1.57	-1.57	-.00052	-.00035
106-5A	.00012	.00008	-1.69	-1.69	-.00055	-.00038
119-7.5	.00018	.00007	-2.19	-2.18	-.00085	-.00068
119-8.6	.00029	.00006	-3.06	-3.07	-.00142	-.00127
123-6.1	.00017	.00011	-1.39	-1.39	-.00057	-.00040

TABLE 4.- Continued

RIGID AND FLEXIBLE COEFFICIENTS AND DRAG INCREMENTS FOR
FIVE SELECTED SPEED POWER FLIGHTS – COMPARISON OF CALCULATED AND INTERPOLATED RESULTS

Flight	㉓	㉔	㉕	㉖	㉗
	$\Delta\left[C_{l_{tail}}\,\tan\varepsilon\right]$ rigid-flex	$C_{D_{trim}}$ rigid	$\Delta C_{D_{trim}}$ rigid-flex	$\Delta C_{D_{P\,wing}}$ rigid-flex	ΔC_{D} rigid-flex
	㉑ - ㉒	⑥ + ⑯ + ㉑	⑪ + ⑱ + ㉓		⑨ + ㉕ + ㉖
Calculated Results					
106-4A	-.00021	.00007	.00007	-.00022	.00014
106-5A	-.00020	.00006	.00009	-.00016	.00037
119-7.5	-.00017	.00008	.00006	-.00004	.00031
119-8.6	-.00009	.00014	.00007	.00003	.0001
123-6.1	-.00019	.00023	.00020	-.00030	.00035
Interpolated Results					
106-4A	-.00017	.00014	.00012	-.00026	.00023
106-5A	-.00017	.00012	.00012	-.00017	.00046
119-7.5	-.00017	.00008	.00006	-.00008	.00027
119-8.6	-.00015	.00012	.00003	-.00003	-.00007
123-6.1	-.00017	.00029	.00026	-.00037	.00052

TABLE 5

DRAG INCREMENTS DUE TO EXTERNAL CONFIGURATION CHANGES FOR FLIGHT TEST OPERATIONS

External Change	ΔC_D
Instrumentation nose boom airspeed system	0.000059
Trailing static airspeed cone, with 36 feet of cable	.000116
Takeoff and landing camera located immediately aft of nose gear wheel well	.000026
Two tail skegs, located underneath the rear fuselage to prevent skin damage during rotation	.000413
Various test airspeed and free air temperature probes	.000004
Anti-spin drag chute, located in the aft fuselage tail cone section	.000008
Stick shaker installation with two angle of attack sensing vanes	.000003
Water ballast drain holes	.000014
Two closure plates on pedal door	.000021
Various external straps, conduit, brackets and switches	.000016
Forty vortex generators per wing spaced at intervals on the 25 percent chord line between wing station 33.5 and wing station 644.4	.000180[a]
One 24-inch stall strip located 6 inches outboard of each wing leading edge air conditioning inlet scoop	.000020[a]
Total drag increment due to flight test instrumentation	.000680

[a]These items were installed during the flight test program and subsequently became part of the production configuration; consequently, drag of these items is part of the overall roughness drag and is not included in instrumentation drag.

TABLE 6

REDUCTION OF FLIGHT TEST DRAG COEFFICIENT
TO EQUIVALENT RIGID MINIMUM PROFILE DRAG COEFFICIENT

Flight	$C_{D_{flex}}$	C_{D_i}	$C_{D_{trim}}$	$C_{Dp_{C_L}}$	C_{Dp_C}	$\Delta C_{D_{rigid-flex}}$	$\Delta C_{D_{trim_{cg}}}$	$\Delta C_{D_{inst}}$	$C_{Dp_{min,rigid}}$
Speed Power Flights									
106-4A	.017269	.002220	.000141	.000773	.000430	.000231	.000015	.089000	.013271
4B	.017120	.002393	.000116	.000192	.000671	.000166	.000021	.089000	.013256
4C	.017640	.003023	.000088	0.	.000457	.000106	.000028	.089000	.013525
4D	.018949	.004100	.000071	0.	.000243	.000068	.000032	.089000	.013955
4E	.026575	.011355	.000049	0.	.000076	-.000114	.000206	.089000	.014507
4G	.020734	.005976	.000049	0.	.000052	-.000049	.000048	.089000	.013977
106-5A	.018067	.002735	.000124	.000712	.000610	.000475	.000023	.089000	.013693
5B	.018400	.003289	.000089	.000179	.000402	.000218	.000027	.089000	.014005
5C	.019737	.004489	.000065	0.	.000186	.000077	.000030	.089000	.014424
5D	.021254	.006237	.000048	0.	.000037	-.000044	.000045	.089000	.014253
5E	.026725	.011414	.000052	0.	.000080	-.000082	.000164	.089000	.014581
5F	.034536	.019327	.000327	0.	.000714	.001057	.000320	.089000	.014865
5G	.023589	.008492	.000039	0.	.000000	-.000133	.000078	.089000	.014323
119-7.1	.024221	.005444	.000195	.000337	.004999	.001717	-.000073	.089000	.014210
7.2	.022458	.005001	.000143	.000332	.003870	.001257	-.000076	.089000	.013614
7.3	.020988	.004900	.000181	.000320	.002775	.001201	-.000078	.089000	.013254
7.4	.019934	.004452	.000131	.000070	.001545	.000640	-.000083	.089000	.013411
7.5	.019797	.004923	.000087	.000136	.004456	.000278	-.000099	.089000	.013694
7.6	.021683	.006232	.000081	.000033	.000060	-.000005	-.000158	.089000	.014434
7.7	.024916	.009518	.000072	.000017	0.	-.001135	-.000472	.089000	.014065

TABLE 6.- Continued

REDUCTION OF FLIGHT TEST DRAG COEFFICIENT
TO EQUIVALENT RIGID MINIMUM PROFILE DRAG COEFFICIENT

Flight	$C_{D_{flex}}$	C_{D_i}	$C_{D_{trim}}$	$C_{D_{pCL}}$	$C_{D_{pC}}$	$\Delta C_{D_{rigid-flex}}$	$\Delta C_{D_{trim.cg}}$	$\Delta C_{D_{inst}}$	$C_{D_{p_{min-rigid}}}$
Speed Power Flights.- Continued									
119-8.1	.026535	.008148	-.000022	.000005	.003093	.000225	-.000228	.000680	.014629
8.2	.026136	.008089	.000036	.000002	.002138	.000097	-.000261	.000680	.015077
8.3	.024256	.007950	.000048	.000002	.002030	.000098	-.000273	.000680	.013371
8.4	.024808	.007935	.000020	0.	.001079	-.000046	-.000336	.000680	.014713
8.5	.024386	.007969	.000014	0.	.000854	-.000066	-.000363	.000680	.014439
8.6	.028750	.011668	.000129	.000111	.001124	-.000070	-.000834	.000680	.015134
123-6.1	.017458	.001713	.000284	.001056	.000851	.000524	-.000007	.000680	.013390
6.2	.017127	.001770	.000209	.000920	.000358	.000383	-.000039	.000680	.013533
123-9A	.022263	.003437	.000626	.000990	.005393	.002396	-.000023	.000680	.013509
9B	.019115	.002243	.000267	.000889	.001832	.000880	-.000050	.000680	.014035
9CR	.017595	.002280	.000200	.000723	.000678	.000579	-.000096	.000680	.013517
9D	.017879	.002619	.000148	.000546	.000218	.000359	-.001117	.000680	.013910
9E	.018451	.003251	.000133	.000362	0.	.000240	-.001156	.000680	.014109
9F	.018016	.003943	.000131	.000233	0.	.000186	-.001176	.000680	.013039
9G	.030495	.014029	.000329	.000304	0.	.000235	-.001623	.000680	.013765
128-5A	.024262	.005145	.000293	.000426	.005676	.002134	-.000104	.000680	.014072
5B	.021549	.004524	.000234	.000379	.002673	.001351	-.000110	.000680	.014299
5C	.020230	.003904	.000114	.000320	.001394	.000587	-.000118	.000680	.014289
5D	.019962	.004217	.000107	.000223	.000658	.000420	-.000125	.000680	.014372
5E	.021639	.005646	.000096	.000059	.000047	.000108	-.000190	.000680	.015028
5F	.022523	.006808	.000090	.000009	0.	-.000016	-.000299	.000680	.014676

TABLE 6.- Continued

REDUCTION OF FLIGHT TEST DRAG COEFFICIENT
TO EQUIVALENT RIGID MINIMUM PROFILE DRAG COEFFICIENT

Flight	$C_{D_{flex}}$	C_{D_i}	$C_{D_{trim}}$	$C_{D_{PC_L}}$	$C_{D_{PC}}$	$\Delta C_{D_{rigid-flex}}$	$\Delta C_{D_{trim_{cg}}}$	$\Delta C_{D_{inst}}$	$C_{DP_{min_{rigid}}}$
				Speed Power Flights.- Continued					
128-5GR	.025286	.008798	.000089	.000006	.0	-.000061	-.000522	.000680	.015130
5H	.033124	.015224	.000319	.000391	.0	.000350	-.001203	.000680	.015657
128-6A	.025996	.007165	.000008	.000040	.003418	.000488	-.000222	.000680	.014952
6B	.024676	.006989	.000077	.000030	.002164	.000337	-.000255	.000680	.014817
6C	.023371	.006898	.000108	.000023	.001589	.000236	-.000289	.000680	.014021
6D	.023384	.006866	.000040	.000011	.000841	.000081	-.000370	.000680	.014657
6E	.023828	.007041	.000063	.000006	.000675	.000061	-.000417	.000680	.015006
6F	.025120	.008661	.000106	.000004	.000205	-.000134	-.000671	.000680	.014658
6G	.032232	.015373	.000409	.000419	.0	.000402	-.001726	.000680	.014031
129-5AR	.017661	.001393	.000339	.001278	.000707	.000281	.000032	.000680	.013577
5B	.016641	.001338	.000251	.001187	.000330	.000259	.000018	.000680	.013133
5C	.016371	.001431	.000198	.001066	.000049	.000264	-.000002	.000680	.013210
5D	.016748	.001816	.000160	.000853	.0	.000303	-.000038	.000680	.013504
5E	.017881	.003113	.000117	.000401	.0	.000251	-.000102	.000680	.013720
5F	.022454	.007248	.000086	.000002	.0	-.000023	-.000332	.000680	.014084
129-6R1	.022873	.007171	.000095	.000002	.0	-.000016	-.000381	.000680	.014529

TABLE 6.- Continued

REDUCTION OF FLIGHT TEST DRAG COEFFICIENT
TO EQUIVALENT RIGID MINIMUM PROFILE DRAG COEFFICIENT

Flight	$C_{D_{flex}}$	C_{D_i}	$C_{D_{trim}}$	$C_{D_{p_{C_L}}}$	$C_{D_{p_C}}$	$\Delta C_{D_{rigid\text{-}flex}}$	$\Delta C_{D_{trim,cg}}$	$\Delta C_{D_{inst}}$	$C_{D_{p,min,rigid}}$
				Cruise Portion of Range Mission Flights					
187-1	.026805	.009553	-.000007	.000008	.000500	-.000244	.000478	.000680	.016304
2	.027243	.009519	-.000007	.000007	.000499	-.000237	.000476	.000680	.015784
3	.027121	.009653	-.000007	.000008	.000491	-.000232	.000483	.000680	.016647
4	.026879	.009483	-.000006	.000007	.000490	-.000221	.000449	.000680	.016452
5	.026155	.009415	-.000009	.000006	.000552	-.000203	.000421	.000680	.015730
6	.026431	.009265	-.000011	.000004	.000613	-.000178	.000366	.000680	.016607
7	.026298	.009495	-.000002	.000008	.000472	-.000204	.000344	.000680	.015786
8	.026776	.009616	.000001	.000010	.000457	-.000207	.000299	.000680	.016105
9	.027198	.009547	-.000000	.000009	.000472	-.000190	.000283	.000680	.016582
10	.026619	.009725	-.000001	.000012	.000485	-.000189	.000309	.000680	.015839
11	.026721	.009792	-.000002	.000013	.000496	-.000185	.000327	.000680	.015884
12	.026743	.009629	-.000003	.000011	.000508	-.000170	.000302	.000680	.016050
13	.027812	.009798	.000007	.000014	.000385	-.000198	.000285	.000680	.017014
14	.026613	.009273	.000011	.000006	.000371	-.000166	.000191	.000680	.016297
15	.026931	.008977	.000023	.000003	.000289	-.000159	.000117	.000680	.016917
190-1	.026468	.009650	-.000004	.000010	.000467	-.000249	.000440	.000680	.015856
2	.026187	.009585	-.000005	.000009	.000474	-.000231	.000452	.000680	.015565
3	.025857	.009457	-.000007	.000007	.000506	-.000206	.000446	.000680	.016543
4	.026094	.009494	-.000006	.000007	.000488	-.000207	.000454	.000680	.015683
5	.026433	.009653	-.000003	.000010	.000448	-.000211	.000445	.000680	.015879
6	.025556	.009526	-.000005	.000008	.000488	-.000187	.000389	.000680	.016060
7	.027232	.009909	-.000001	.000016	.000464	-.000207	.000368	.000680	.016326
8	.027244	.009625	-.000002	.000012	.000500	-.000129	.000292	.000680	.016493

TABLE 6.– Continued

REDUCTION OF FLIGHT TEST DRAG COEFFICIENT
TO EQUIVALENT RIGID MINIMUM PROFILE DRAG COEFFICIENT

Flight	$C_{D_{flex}}$	C_{D_i}	$C_{D_{trim}}$	$C_{DP_{C_L}}$	C_{DP_C}	$\Delta C_{D_{rigid-flex}}$	$\Delta C_{D_{trim_{cg}}}$	$\Delta C_{D_{inst}}$	$C_{DP_{min_{rigid}}}$
Cruise Portion of Range Mission Flights.– Continued
190–9	.026221	.009643	–.000001	.000012	.000512	–.000168	.000235	.000680	.015442
10	.026220	.009204	.000006	.000005	.000420	–.000152	.000189	.000680	.015942
11	.025557	.008636	.000009	.0	.000383	–.000113	.000181	.000680	.015917
12	.025530	.008231	.000011	.000000	.000374	–.000078	.000161	.000680	.016317
13	.023426	.007745	.000016	.000001	.000358	–.000033	.000133	.000680	.014727
14	.023625	.007416	.000023	.000004	.000338	–.000004	.000078	.000680	.015237
15	.023300	.006854	.000034	.000016	.000319	.000055	.000029	.000680	.015480
Continuous Climb Flights
138–5.1	.018753	.005850	.000076	.000051	.0	–.000049	–.000113	.000680	.011933
5.2	.020109	.006149	.000074	.000035	.0	–.000068	–.000125	.000680	.012977
5.3	.020949	.006260	.000074	.000031	.0	–.000074	–.000129	.000680	.013706
5.4	.021095	.006471	.000075	.000023	.000039	–.000061	–.000139	.000680	.013606
5.5	.021666	.006863	.000069	.000013	.000216	–.000035	–.000158	.000680	.013633
5.6	.023720	.008069	.000060	.0	.000265	–.000168	–.000232	.000680	.014245
5.7	.025840	.010212	.000057	.000033	.000299	–.000315	–.000401	.000680	.013844
139–5.1	.021331	.006191	.000076	.000033	.0	–.000080	–.000135	.000680	.014136
5.2	.021389	.006585	.000075	.000019	.000006	–.000097	–.000153	.000680	.013774
5.3	.022689	.007295	.000068	.000003	.000205	–.000098	–.000189	.000680	.014151
5.4	.024585	.009025	.000060	.000006	.000256	–.000265	–.000305	.000680	.013988
5.5	.028073	.011745	.000092	.000105	.000340	–.000310	–.000486	.000680	.014314

TABLE 6.– Continued

REDUCTION OF FLIGHT TEST DRAG COEFFICIENT
TO EQUIVALENT RIGID MINIMUM PROFILE DRAG COEFFICIENT

Flight	$C_{D_{flex}}$	C_{D_i}	$C_{D_{trim}}$	$C_{D_{P_{C_L}}}$	$C_{D_{P_C}}$	$\Delta C_{D_{rigid-flex}}$	$\Delta C_{D_{trim_{cg}}}$	$\Delta C_{D_{inst}}$	$C_{D_{P_{min_{rigid}}}}$
				Continuous Climb Flights.– Continued					
139-5.6	.029543	.013682	.000166	.000234	.000413	-.000101	-.000560	.000680	.013707
5.7	.032675	.015196	.000243	.000352	.000457	.000211	-.000646	.000680	.015312
140-5.1	.022098	.005853	.000076	.000051	.0	-.000048	-.000114	.000680	.015275
5.2	.021802	.006261	.000075	.000030	.0	-.000072	-.000134	.000680	.014554
5.3	.022654	.006614	.000074	.000019	.000097	-.000048	-.000151	.000680	.014972
5.4	.024210	.007771	.000065	.0	.000244	-.000137	-.000221	.000680	.015093
5.5	.027029	.009933	.000061	.000024	.000270	-.000307	-.000395	.000680	.015358
5.6	.029591	.012166	.000113	.000132	.000319	-.000256	-.000530	.000680	.015394
5.7	.030380	.013663	.000173	.000234	.000387	-.000073	-.000599	.000680	.014571

TABLE 7

FLIGHT TEST DRAG COEFFICIENTS CORRECTED TO
CONSTANT MACH NUMBERS AND TO
$RN = 55 \times 10^6/MAC$ AND C.G. = .25 MAC

Explanation of Items for Table 7	
Item	Explanation
(1)	Flight number
(2)	Airplane trimmed lift coefficient, C_{L_A}
(3)	Flight test measured drag coefficient, $C_{D_{flex}}$
(4)	Constant Mach Number to which data is being corrected, M_{corr}.
(5)	Incremental drag due to Mach Number, ΔC_{D_M}
(6)	Incremental drag due to Reynolds Number, $\Delta C_{D_{RN}}$
(7)	Incremental trim drag due to c.g. position, $\Delta C_{D_{trim_{c.g.}}}$
(8)	Incremental drag due to flexibility, $\Delta C_{D_{rigid-flex}}$
(9)	Incremental drag due to instrumentation, $\Delta C_{D_{inst}}$
(10)	Rigid drag coefficient, corrected to a constant Mach Number, $RN = 55 \times 10^6/MAC$, and c.g. = .25 MAC, $C_{D_{rigid}}$ c.g. = .25 MAC less inst M $= M_{corr}$ RN $= 55 \times 10^6/Mac$

TABLE 7.- Continued

FLIGHT TEST DRAG COEFFICIENTS CORRECTED TO CONSTANT MACH NUMBERS AND TO

RN = 55×10⁶/MAC AND C.G. = .25 MAC

(1)	(2)	(3)	(4)	(5)	(6)	(7)	(8)	(9)	(10)
106-4A	.1961	.017269	.600	-.000570	.000685	.000015	.000231	.000680	.016950
4A	.1961	.017269	.700	.000430	.000685	.000015	.000231	.000680	.017950
4B	.2123	.017120	.600	-.000192	.000612	.000021	.000166	.000680	.017047
4B	.2123	.017120	.700	.000749	.000612	.000021	.000166	.000680	.017989
4C	.2506	.017640	.600	0.	.000471	.000028	.000106	.000680	.017564
4C	.2506	.017640	.700	.000748	.000471	.000028	.000106	.000680	.018312
4D	.3008	.018949	.600	0.	.000322	.000032	.000068	.000680	.018691
4D	.3008	.018949	.700	.000616	.000322	.000032	.000068	.000680	.019307
4F	.5213	.026575	.600	0.	-.000117	.000206	-.000114	.000680	.025871
4G	.3724	.020734	.600	0.	.000114	.000048	-.000049	.000680	.020167
106-5A	.2228	.018067	.600	-.000991	.000363	.000023	.000465	.000680	.017247
5A	.2228	.018067	.700	-.000095	.000363	.000023	.000465	.000680	.018143
5A	.2228	.018067	.750	.001051	.000363	.000023	.000465	.000680	.019289
5B	.2617	.018400	.600	-.000179	.000229	.000077	.000218	.000680	.018015
5B	.2617	.018400	.700	.000531	.000229	.000077	.000218	.000680	.018725
5C	.3172	.019737	.600	0.	.000069	.000030	.000077	.000680	.019233
5C	.3172	.019737	.700	.000555	.000069	.000030	.000077	.000680	.019788
5D	.3811	.021254	.600	0.	-.000082	.000045	-.000044	.000680	.020493
5E	.5226	.026725	.600	0.	-.000342	.000164	-.000082	.000680	.025786
5F	.4587	.034536	.600	0.	-.000540	-.000320	.001056	.000680	.034693
5G	.4499	.023589	.600	0.	-.000234	.000078	-.000133	.000680	.022621
119-7.1	.2715	.024221	.008	-.001619	.000122	-.000073	.001717	.000680	.023688
7.1	.2715	.024221	.810	.000879	.000122	-.000073	.001717	.000680	.026187
7.2	.2727	.022458	.775	-.003011	.000106	-.000076	.001257	.000680	.020054

TABLE 7.- Continued

FLIGHT TEST DRAG COEFFICIENTS CORRECTED TO CONSTANT MACH NUMBERS AND TO
RN = 55×10^6/MAC AND C.G. = .25 MAC

(1)	(2)	(3)	(4)	(5)	(6)	(7)	(8)	(9)	(10)
119-7.2	.2727	.022458	.800	-.000061	.000106	-.000076	.001257	.000680	.023004
7.2	.2727	.022458	.810	.002442	.000106	-.000076	.001257	.000680	.025507
7.3	.2757	.020988	.775	-.001398	.000092	-.000078	.001201	.000680	.020125
7.3	.2757	.020988	.800	.001575	.000092	-.000078	.001201	.000680	.023097
7.3	.2757	.020988	.810	.004090	.000092	-.000078	.001201	.000680	.025613
7.4	.2890	.019934	.750	-.000686	.000049	-.000083	.000640	.000680	.019173
7.4	.2890	.019934	.775	.000498	.000049	-.000083	.000640	.000680	.020357
7.4	.2890	.019934	.800	.003594	.000049	-.000083	.000640	.000680	.023453
7.5	.3300	.019797	.600	-.000621	-.000071	-.000099	.000278	.000680	.018604
7.5	.3300	.019797	.700	-.000120	-.000071	-.000099	.000278	.000680	.019105
7.5	.3300	.019797	.750	.000651	-.000071	-.000099	.000278	.000680	.019876
7.6	.3797	.021683	.600	-.000093	-.000187	-.000158	-.000005	.000680	.020550
7.6	.3797	.021683	.700	.002177	-.000187	-.000158	-.000005	.000680	.026980
7.7	.4774	.024916	.600	0.	-.000380	-.000427	-.000135	.000680	.023294
7.7	.4774	.024916	.700	.000166	-.000380	-.000427	-.000135	.000680	.023460
119-8.1	.4022	.026535	.775	-.002703	-.000490	-.000228	.000225	.000680	.022659
8.1	.4022	.026535	.800	-.001729	-.000490	-.000228	.000225	.000680	.027091
8.1	.4022	.026535	.810	.007017	-.000490	-.000228	.000225	.000680	.032379
8.2	.4103	.021636	.750	-.001927	-.000516	-.000261	.000097	.000680	.022849
8.2	.4103	.021636	.775	-.000701	-.000516	-.000261	.000097	.000680	.024075
8.2	.4103	.021636	.800	.003929	-.000516	-.000261	.000097	.000680	.028705
8.3	.4089	.024256	.750	-.001736	-.000523	-.000273	.000098	.000680	.021143
8.3	.4089	.024256	.775	-.000511	-.000523	-.000273	.000098	.000680	.022368
8.3	.4089	.024256	.800	.004083	-.000523	-.000273	.000098	.000680	.026962
8.4	.4264	.024808	.750	-.000285	-.000560	-.000336	-.000046	.000680	.022901
8.4	.4264	.024808	.775	.000951	-.000560	-.000336	-.000046	.000680	.024137

TABLE 7.- Continued

FLIGHT TEST DRAG COEFFICIENTS CORRECTED TO CONSTANT MACH NUMBERS AND TO

$RN = 55 \times 10^6 / MAC$ AND C.G. = .25 MAC

(1)	(2)	(3)	(4)	(5)	(6)	(7)	(8)	(9)	(10)
119-8.5	.4309	.024386	.700	-.000536	-.000583	-.000363	-.000066	.000680	.022158
8.5	.4309	.024386	.750	-.000035	-.000583	-.000363	-.000066	.000680	.022659
8.5	.4309	.024386	.775	.001204	-.000583	-.000363	-.000066	.000680	.023898
8.6	.5268	.028750	.600	-.000100	-.000751	-.000834	-.000070	.000680	.026316
8.6	.5268	.028750	.700	.001142	-.000751	-.000834	-.000070	.000680	.026558
123-6.1	.1502	.017458	.600	-.001235	.000568	-.000007	.000524	.000680	.016628
6.1	.1502	.017458	.700	-.000148	.000568	-.000007	.000524	.000680	.017715
6.1	.1502	.017458	.750	.001164	.000568	-.000007	.000524	.000680	.019027
6.2	.1686	.017127	.600	-.000490	.000461	-.000039	.000383	.000680	.016760
6.2	.1686	.017127	.700	.000576	.000461	-.000039	.000383	.000680	.017827
123-9A	.1591	.022263	.775	-.004431	.000338	-.000023	.002396	.000680	.019863
9A	.1591	.022263	.800	-.001300	.000338	-.000023	.002396	.000680	.022994
9A	.1591	.022263	.810	.000977	.000338	-.000023	.002396	.000680	.025521
9B	.1739	.019115	.750	-.000389	-.000249	-.000050	.000880	.000680	.019125
9B	.1739	.019115	.775	.000850	-.000249	-.000050	.000880	.000680	.020365
9B	.1739	.019115	.800	.003949	-.000249	-.000050	.000880	.000680	.023463
9CR	.1980	.017595	.700	.000022	.000121	-.000096	.000579	.000680	.017541
9CR	.1980	.017595	.750	.001240	.000121	-.000096	.000579	.000680	.018758
9D	.2273	.017829	.600	-.000221	.000013	-.000117	.000359	.000680	.017233
9D	.2273	.017829	.700	.000654	.000013	-.000117	.000359	.000680	.018107
9D	.2273	.017829	.750	.001785	.000013	-.000117	.000359	.000680	.019239
9D	.2636	.018451	.600	0.	-.000124	-.000156	.000240	.000680	.017731
9D	.2636	.018451	.700	.000704	-.000124	-.000156	.000240	.000680	.018434
9F	.2954	.018016	.600	0.	-.000228	-.000176	.000186	.000680	.017117

TABLE 7.- Continued

FLIGHT TEST DRAG COEFFICIENTS CORRECTED TO CONSTANT MACH NUMBERS AND TO
RN = 55×10⁶/MAC AND C.G. = .25 MAC

(1)	(2)	(3)	(4)	(5)	(6)	(7)	(8)	(9)	(10)
123-9F	.2954	.018016	.700	.000626	-.000228	-.000176	.000186	.000680	.017744
9G	.5742	.030495	.600	0.	-.000793	-.001623	.000235	.000680	.027634
128-5A	.2489	.024262	.800	-.002275	-.000163	-.000104	.002134	.000680	.023174
5A	.2489	.024262	.810	.000113	-.000163	-.000104	.002134	.000680	.025562
5B	.2595	.021549	.775	-.001091	-.000200	-.000110	.001351	.000680	.020819
5B	.2595	.021549	.800	.001785	-.000200	-.000110	.001351	.000680	.023695
5B	.2595	.021549	.810	-.004231	-.000200	-.000110	.001351	.000680	.026140
5C	.2751	.020230	.750	-.000352	-.000259	-.000118	.000587	.000680	.019409
5C	.2751	.020230	.775	-.000844	-.000259	-.000118	.000587	.000680	.020604
5C	.2751	.020230	.800	-.003812	-.000259	-.000118	.000587	.000680	.023572
5D	.3005	.019962	.600	-.000913	-.000334	-.000125	.000420	.000680	.018331
5D	.3005	.019962	.700	-.000296	-.000334	-.000125	.000420	.000680	.018948
5D	.3005	.019962	.750	-.000584	-.000334	-.000125	.000420	.000680	.019827
5E	.3605	.021639	.600	-.000079	-.000499	-.000190	.000108	.000680	.020299
5E	.3605	.021639	.700	.000291	-.000499	-.000190	.000108	.000680	.020668
5F	.4000	.022523	.600	-.000015	-.000591	-.000299	-.000016	.000680	.020921
5F	.4000	.022523	.700	.000241	-.000591	-.000299	-.000016	.000680	.021178
5GR	.4586	.025286	.600	0.	-.000712	-.000522	-.000061	.000680	.023312
5GR	.4586	.025286	.700	.000164	-.000712	-.000522	-.000061	.000680	.023476
5H	.5955	.033124	.600	0.	-.000919	-.001203	.000350	.000680	.030673
128-6A	.3663	.025996	.775	-.003241	-.000864	-.000222	.000488	.000680	.021477
6A	.3663	.025996	.800	-.000542	-.000864	-.000222	.000488	.000680	.025260
6A	.3663	.025996	.810	-.004330	-.000864	-.000222	.000488	.000680	.029048
6B	.3733	.024676	.750	-.002042	-.000893	-.000255	.000337	.000680	.021142

TABLE 7.- Continued

FLIGHT TEST DRAG COEFFICIENTS CORRECTED TO CONSTANT MACH NUMBERS AND TO
RN = 55x10^6/MAC AND C.G. = .25 MAC

(1)	(2)	(3)	(4)	(5)	(6)	(7)	(8)	(9)	(10)
128-6B	.3733	.024676	.775	-.000848	-.000893	-.000255	.000337	.000680	.022336
6B	.3733	.024676	.800	.003042	-.000893	-.000255	.000337	.000680	.026226
6C	.3799	.023371	.750	-.001079	-.000921	-.000289	.000236	.000680	.020638
6C	.3799	.023371	.775	.000120	-.000921	-.000289	.000236	.000680	.021838
6C	.3799	.023371	.800	.004119	-.000921	-.000289	.000236	.000680	.025837
6D	.3964	.023384	.700	-.000651	-.000963	-.000370	.000081	.000680	.020802
6D	.3964	.023384	.750	-.000052	-.000963	-.000370	.000081	.000680	.021400
6D	.3964	.023384	.775	.001162	-.000963	-.000370	.000081	.000680	.022615
6E	.4034	.023828	.700	-.000439	-.000984	-.000417	.000061	.000680	.021368
6E	.4034	.023828	.750	.000146	-.000984	-.000417	.000061	.000680	.021953
6E	.4034	.023828	.775	.001367	-.000984	-.000417	.000061	.000680	.023174
6F	.4532	.025120	.600	-.000146	-.001079	-.000671	-.000134	.000680	.022410
6F	.4532	.025120	.700	.000021	-.001079	-.000671	-.000134	.000680	.022577
6F	.4532	.025120	.750	.000445	-.001079	-.000671	-.000134	.000680	.023001
6G	.5976	.032232	.600	-.000007	-.001271	-.001726	.000402	.000680	.028949
6G	.5976	.032232	.700	.000523	-.001271	-.001726	.000402	.000680	.029480
129-5AR	.1213	.017661	.600	-.000998	.000710	.000032	.000281	.000680	.017006
5AR	.1213	.017661	.700	.000085	.000710	.000032	.000281	.000680	.018089
5AR	.1213	.017661	.750	.001427	.000710	.000032	.000281	.000680	.019431
5B	.1324	.016641	.600	-.000527	.000632	.000018	.000259	.000680	.016342
5B	.1324	.016641	.700	.000563	.000632	.000018	.000259	.000680	.017432
5C	.1484	.016371	.600	-.000079	.000540	-.000002	.000264	.000680	.016415
5C	.1484	.016371	.700	.001010	.000540	-.000002	.000264	.000680	.017503
5D	.1788	.016748	.600	.0	.000377	-.000038	.000303	.000680	.016710
5E	.2565	.017881	.600	.0	.000064	-.000102	.000251	.000680	.017415
5F	.4141	.022454	.600	.0	-.000323	-.000332	-.000023	.000680	.021096
6R1	.4118	.022873	.600	.0	-.000518	-.000381	-.000016	.000680	.021278

TABLE 8

INDICATOR ACCURACY

Measured Parameter	Root-sum-square Error
Airspeed, knots	$\pm$ 1.8
Altitude, feet	$\pm$ 49.5
Pressure, P_{TO}, inches of H_2O	$\pm$ 0.28
Pressure, $P_{T2.5}$, inches of H_2O	$\pm$ 0.65
Pressure, P_{T7}, inches of H_2O	$\pm$ 0.65
Temperature, T_{TO}, degrees C	$\pm$ 1.1
Temperature, $T_{T2.5}$, degrees C	$\pm$ 2.2
Temperature, T_{T7}, degrees C	$\pm$ 2.2

TABLE 9

THRUST INFLUENCE COEFFICIENTS[a]

Flight Condition		Engine Parameter					
h feet	M	EPR	M	h	T_{TO}	N_1	FPR
Lockheed Calculation Method							
20,000	0.6	[a]1.54	0.240	0.830	0	–	0.832
	.7	1.58	.350	.840	0	–	.837
	.8	1.56	.420	.840	0	–	.797
30,000	.6	1.48	.235	1.350	0	–	.777
	.7	1.47	.328	1.360	0	–	.759
	.8	1.50	.428	1.350	0	–	.690
40,000	.6	1.43	.242	1.890	0	–	.727
	.7	1.44	.334	1.900	0	–	.694
	.8	1.47	.445	1.890	0	–	.709
P&WA Calculation Method							
20,000	0.6	1.62	0.243	0.842	0	0.409	1.290
	.7	1.63	.359	.837	0	.638	1.435
	.8	1.65	.405	.850	0	.747	1.469
30,000	.6	1.55	.237	1.350	0	.291	1.202
	.7	1.53	.348	1.340	0	.347	1.250
	.8	1.57	.430	1.340	0	.414	1.273
40,000	.6	1.54	.243	1.890	0	.081	1.131
	.7	1.57	.360	1.880	0	.103	1.156
	.8	1.58	.422	1.900	0	.395	1.266

[a]All values are $\pm$ $\dfrac{\text{percent change in net thrust}}{\text{percent change in parameter}}$

TABLE 10

TOTAL RANDOM ERRORS DUE TO INSTRUMENTATION
INACCURACY AND READABILITY

Flight Condition		Engine Parameter					
h feet	M	EPR	M	h	T_{TO}	N_1	FPR
20,000	0.6	[a]0.165	0.592	0.260	0.552	1.0	0.5
	.7	.154	.539	.260	.552	1.025	.5
	.8	.140	.493	.260	.531	1.005	.5
30,000	.6	.246	.618	.173	.595	1.012	.5
	.7	.227	.565	.173	.595	1.012	.5
	.8	.207	.515	.173	.574	0.990	.5
40,000	.6	.390	.655	.130	.650	1.028	.5
	.7	.358	.577	.130	.617	1.005	.5
	.8	.332	.538	.130	.617	1.030	.5

[a]All values are $\pm$ (percent error in parameter).

TABLE 11

TOTAL THRUST ERROR DUE TO INSTRUMENTATION
INACCURACY AND READABILITY

Flight Condition		($\pm$) Percent Error in Thrust	
h feet	M	Lockheed Method	P&WA Method
20,000	0.6	0.551	0.854
	.7	.564	1.045
	.8	.545	1.120
30,000	.6	.600	0.818
	.7	.588	.853
	.8	.565	.885
40,000	.6	.726	.880
	.7	.695	.875
	.8	.667	.977

TABLE 12

TOTAL ESTIMATED RANDOM ERROR AND
MAXIMUM OVERALL ERROR FOR
THREE TYPICAL FLIGHT CONDITIONS

Flight Conditions	(1)	(2)	(3)
Weight, lb.	181,500	299,000	300,000
Alt. feet	30,000	30,000	30,000
M	0.8	0.775	0.65
C_L	0.2	0.35	0.5
C_D	0.0214	0.0225	0.0270
Errors Due to Instrumentation Inaccuracies			
Weight, lb.	[a]180	300	300
Thrust, random, lb.	130	128	113
Thrust, overall, lb.	500	490	420
q, lb/ft^2	2.61	2.56	2.04
M	0.0036	0.0036	0.0036
Angle of attack, deg.	0.3	0.3	0.3
Rate of climb, ft/min[b]	8.0	8.0	8.0
Random error in C_D	[a]0.000455	0.00031	0.00084
Overall maximum error in C_D	[a]0.00074	0.00074	0.00115

[a]All values are ($\pm$).

[b]Error under level flight conditions.
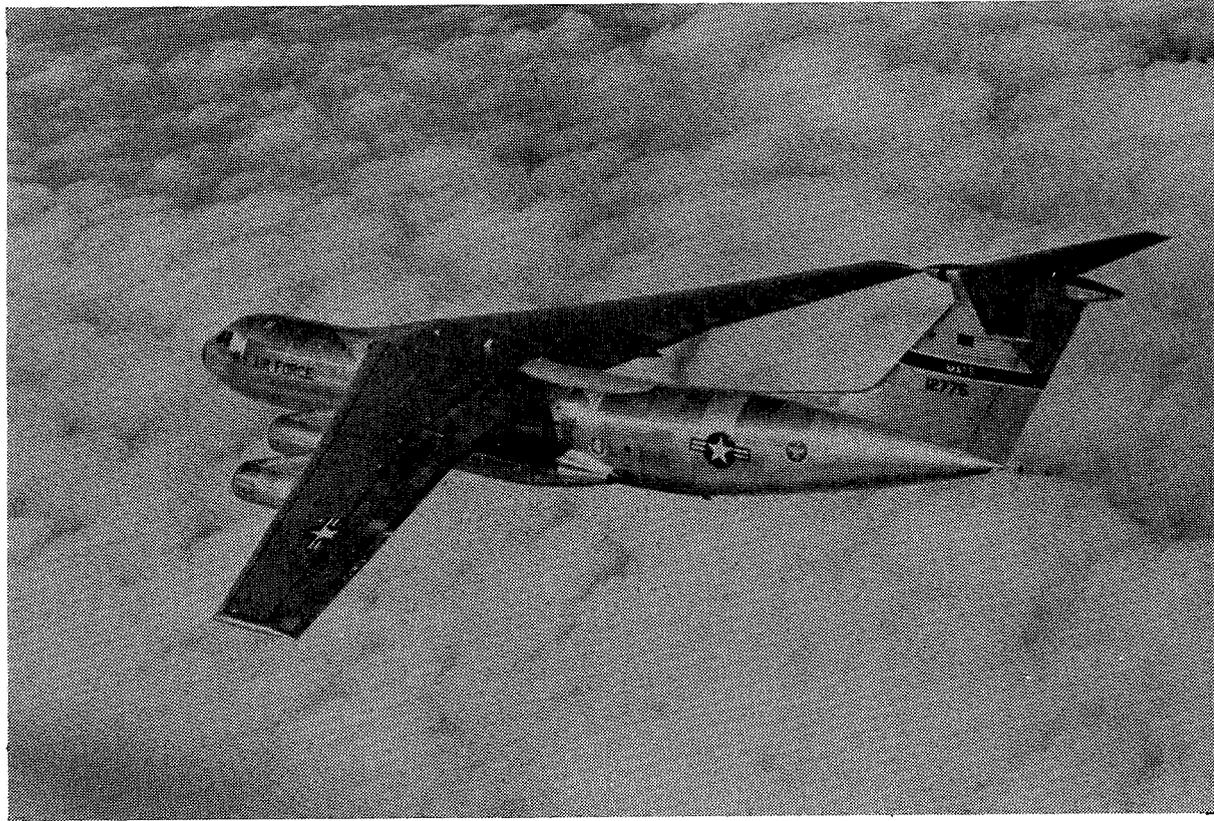
Figure 1.- Test article, C-141A Starlifter.
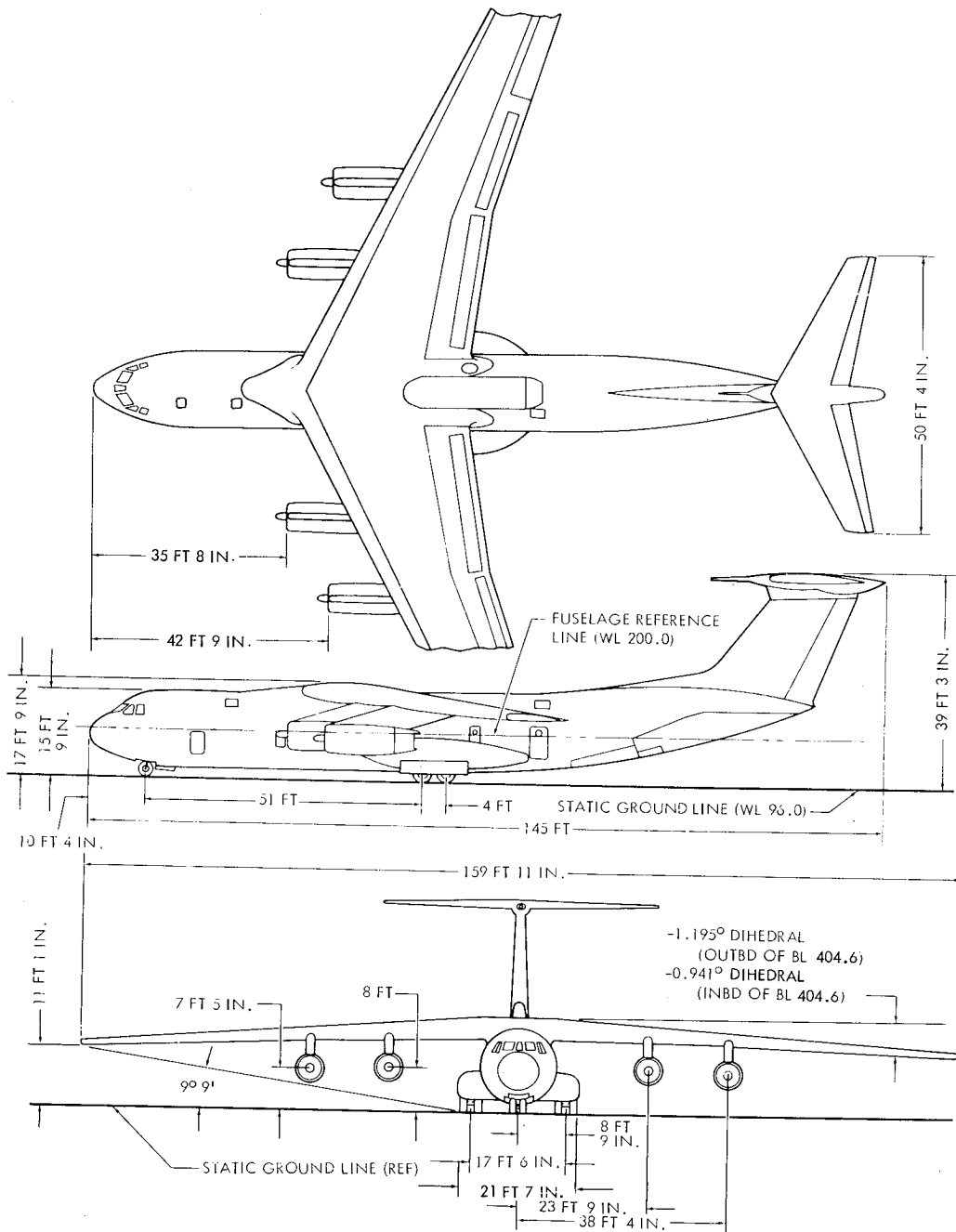
Figure 2.- C-141A general arrangement.

α_{TL}

$F_N \sin(\alpha_{FRL} + \alpha_{TL})$

α_{FRL}

V

L

F_N

V'

ϵ

V

γ

Horizontal

$F_N \cos(\alpha_{FRL} + \alpha_{TL})$

D

$W \cos \gamma$

W

$W \sin \gamma$
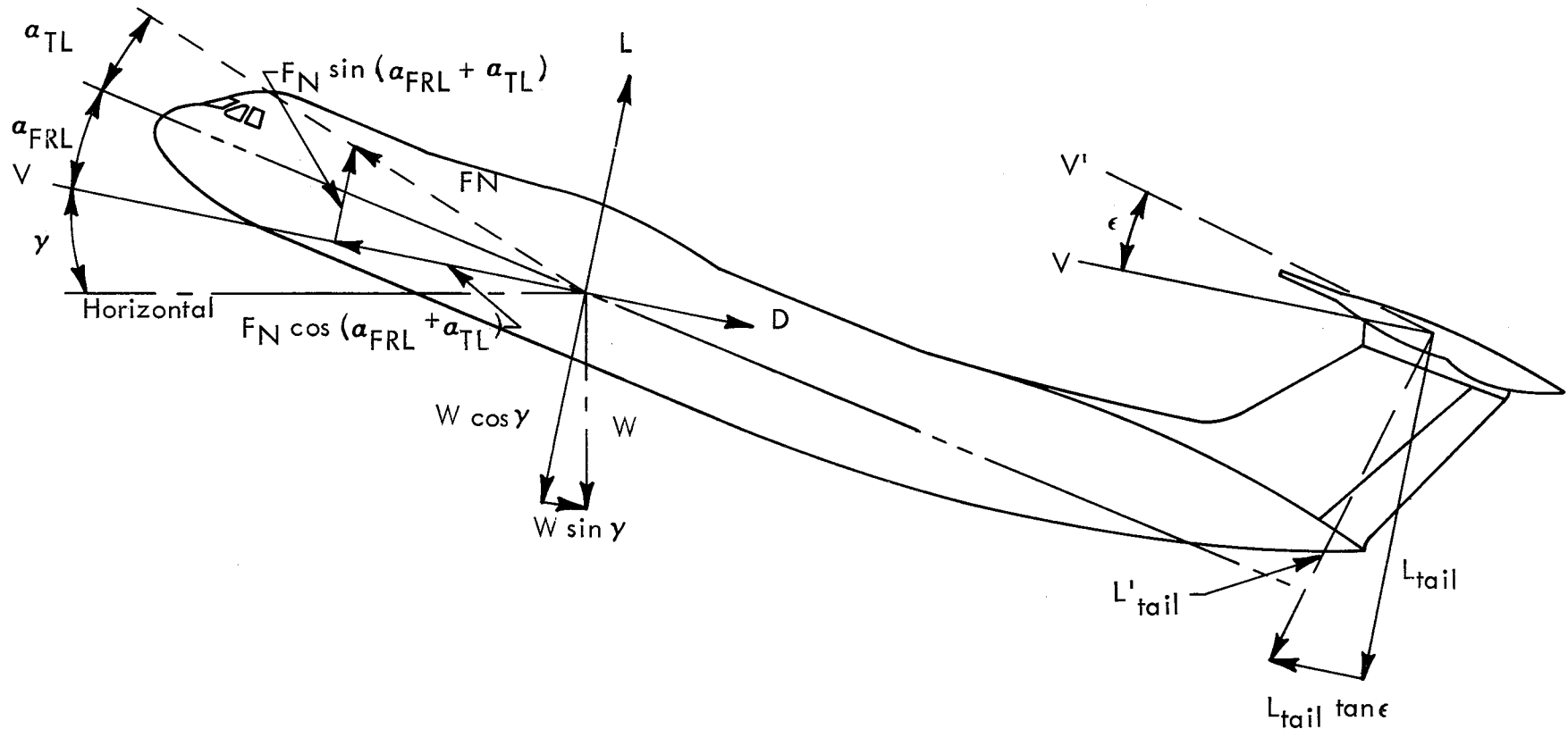
L'_{tail}

L_{tail}

$L_{tail} \tan \epsilon$

V	= relative wind
V'	= relative wind at the tail
L'_{tail}	= that amount of tail lift required to balance the aircraft pitching moment.
$L_{tail} \tan \epsilon$	= drag component of tail lift along the drag axis.

Figure 3.– Sketch of C–141A lift and drag vectors.
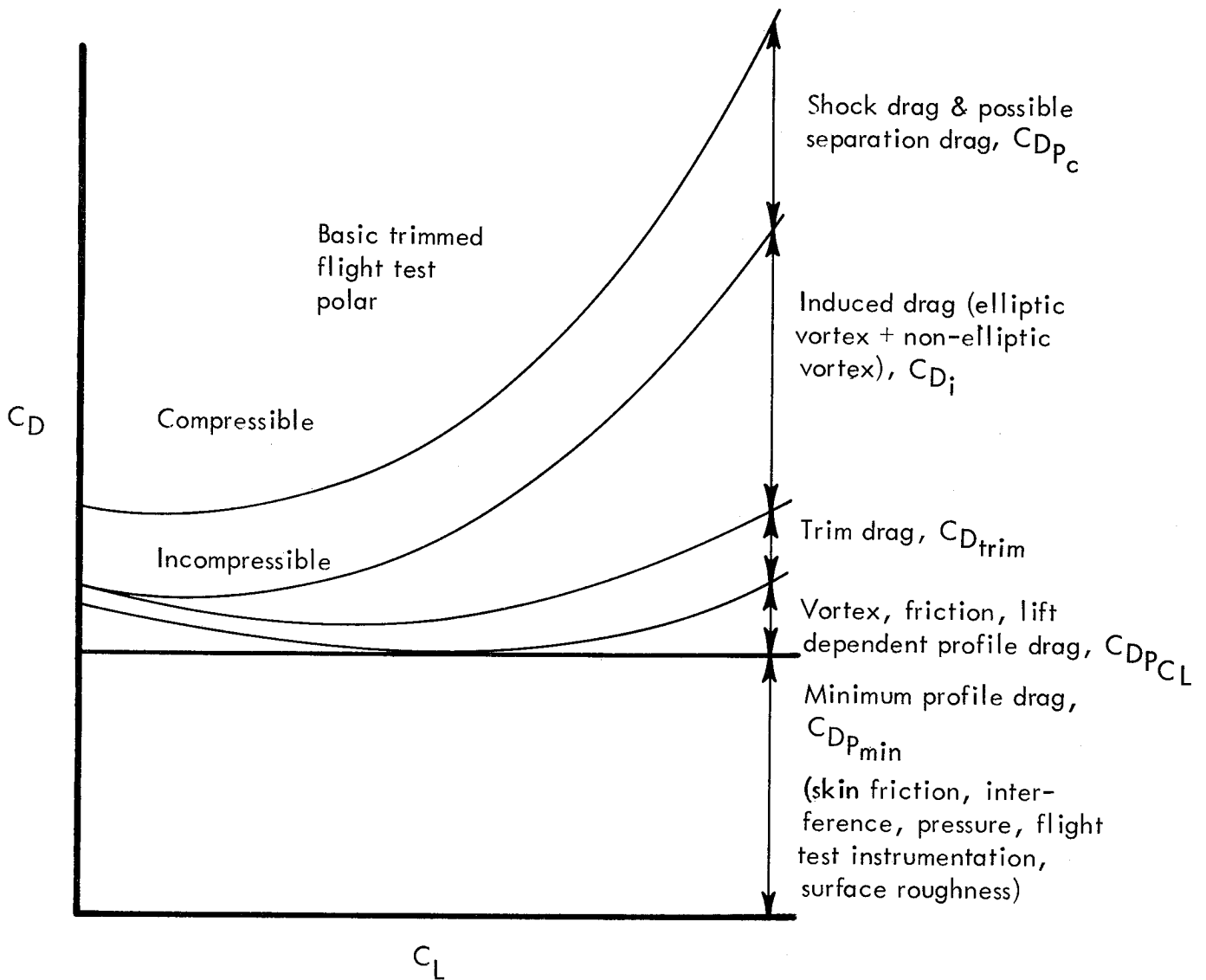
Figure 4.- Breakdown of typical subsonic jet aircraft drag polar.
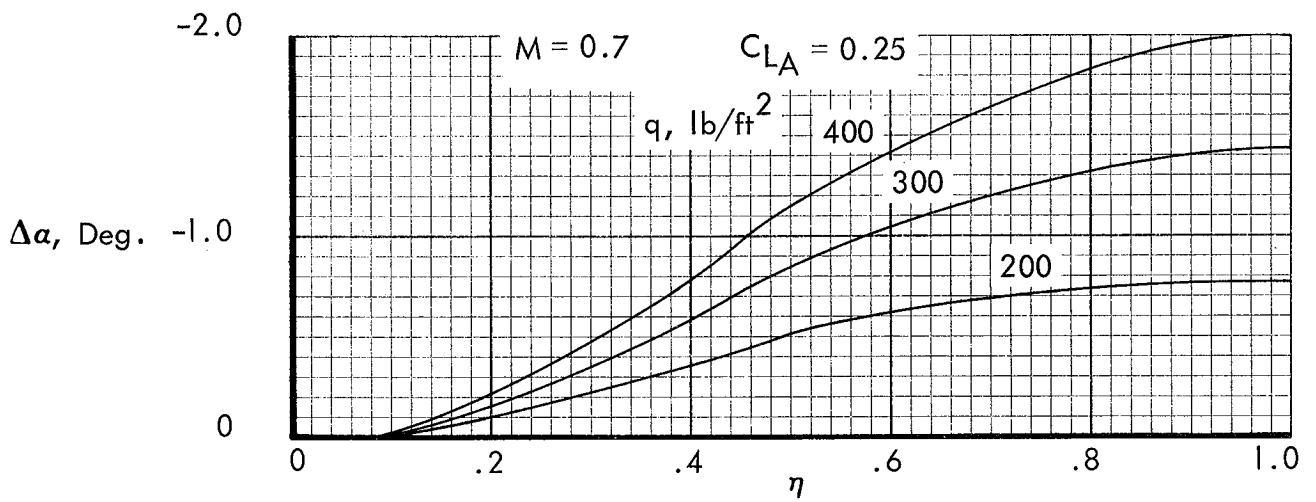
Figure 5.- Effect of aeroelasticity on wing twist.
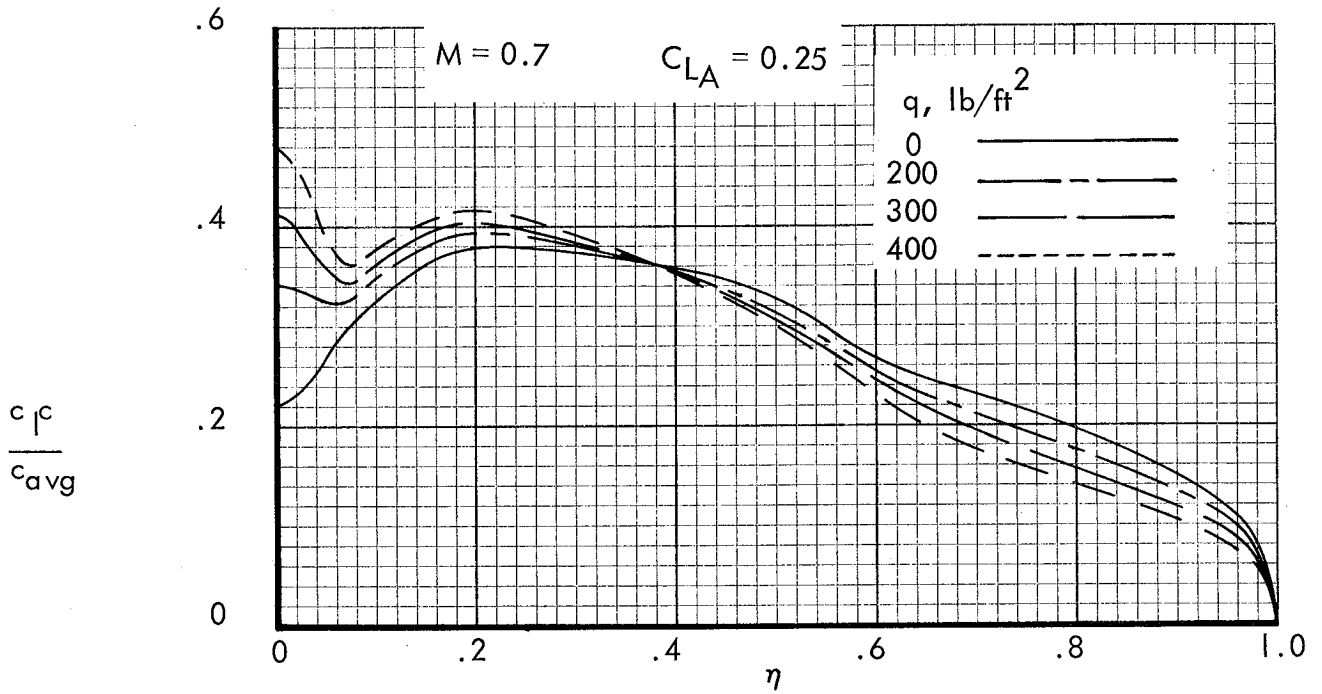
Figure 6.- Effect of aeroelasticity on wing spanwise
load distribution
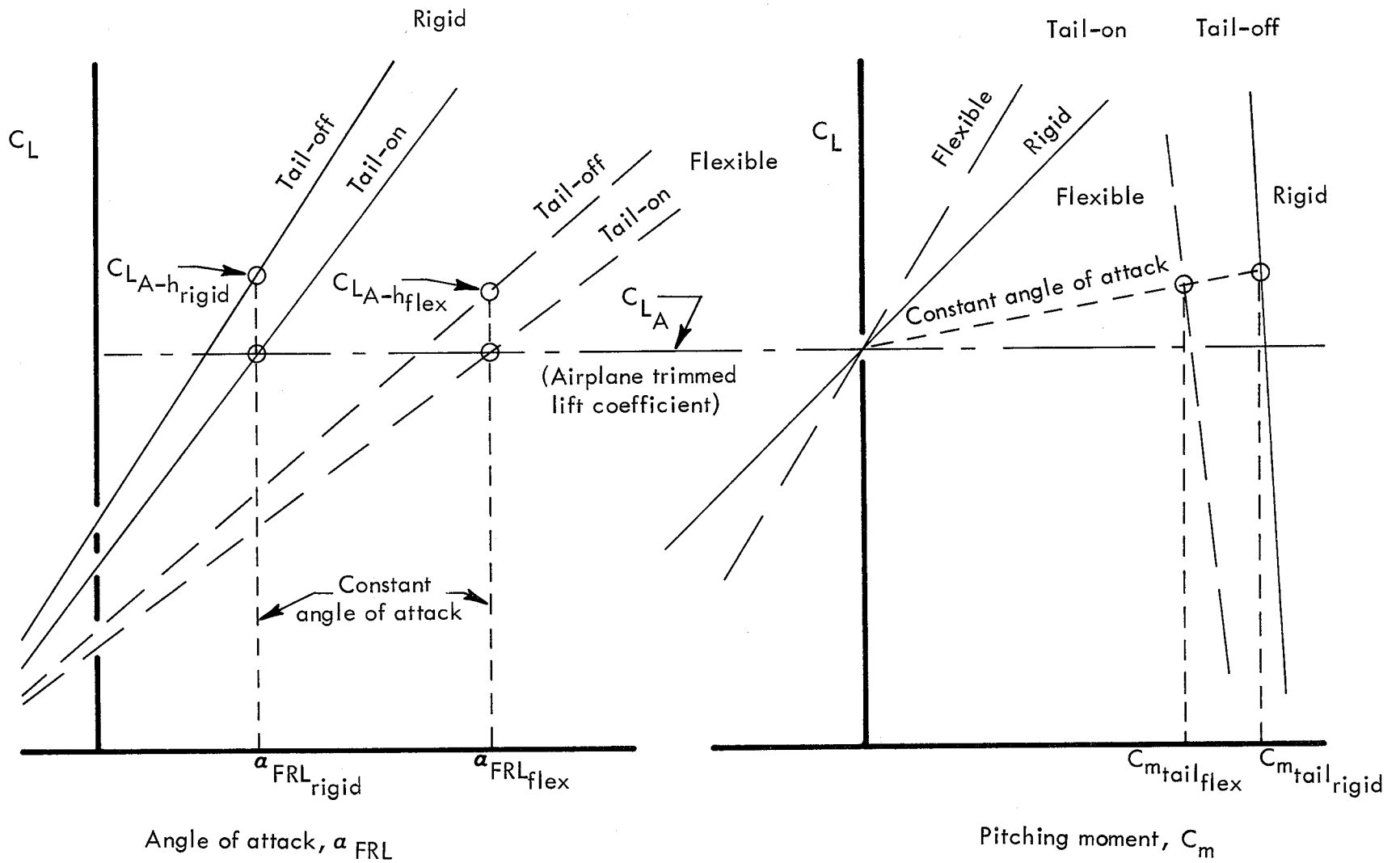
(a) Pitching moment and lift curve.

Figure 7.- Sketch of C-141A trim conditions.
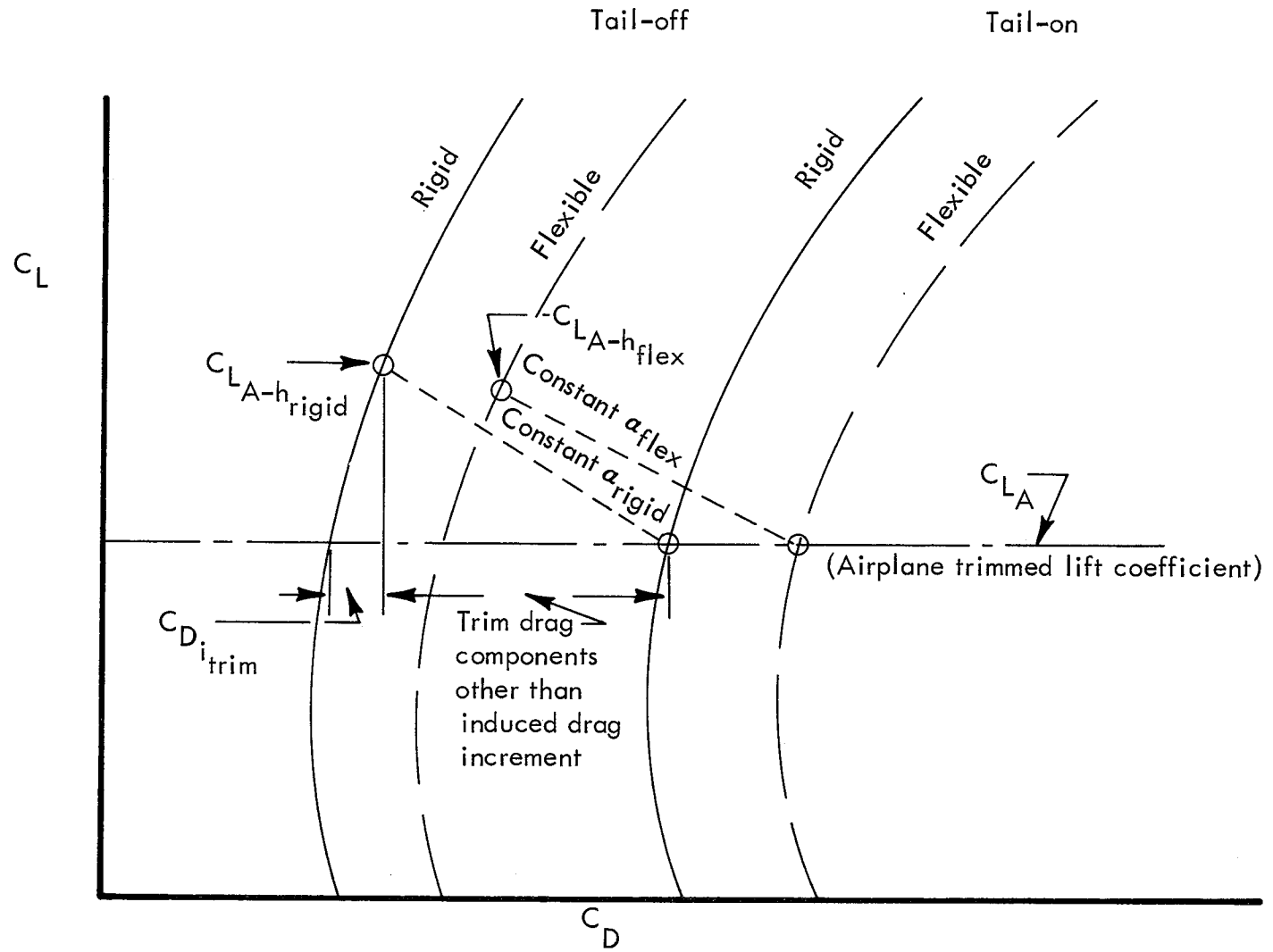
(b) Drag polar.

Figure 7.- Continued
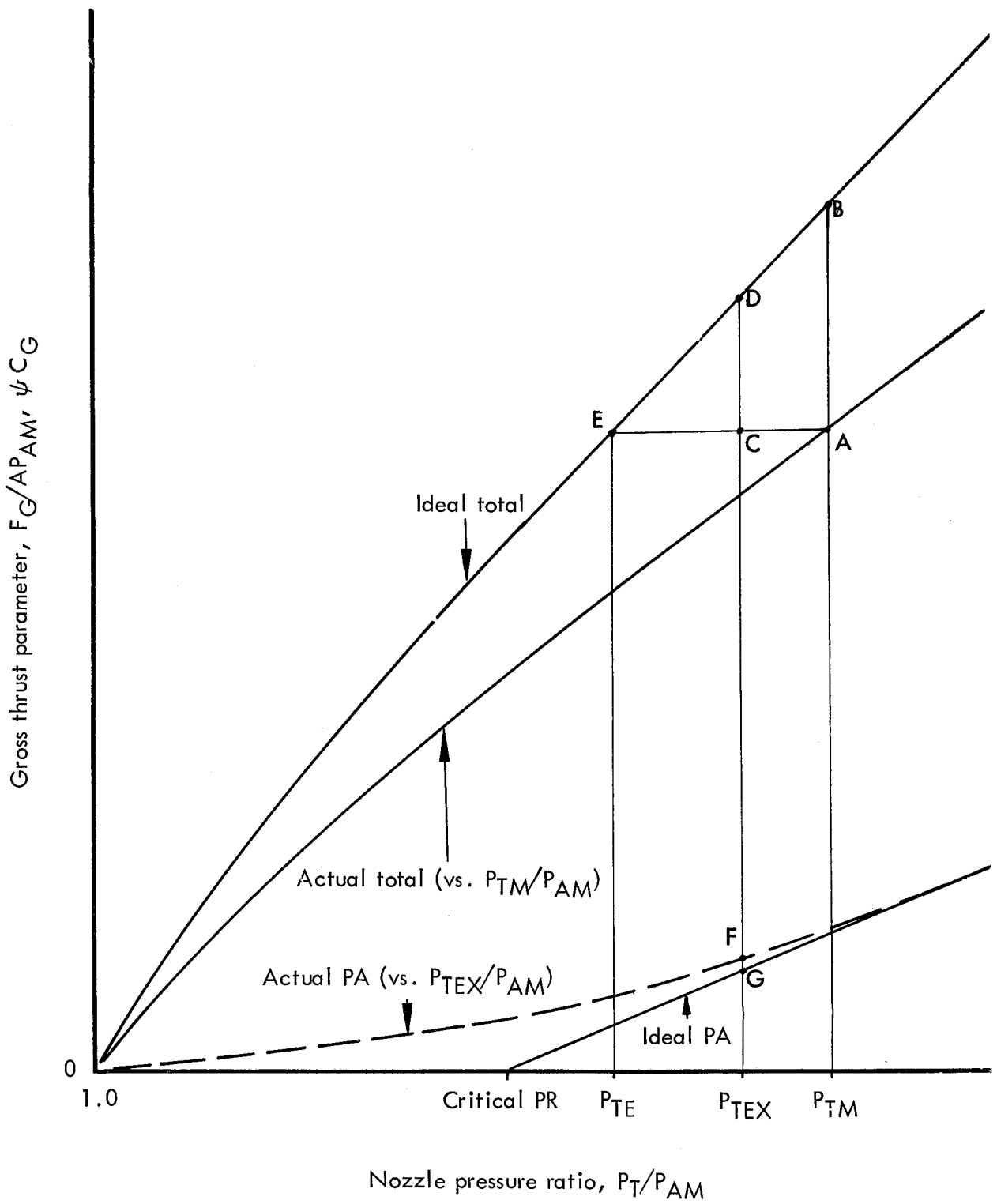
Figure 8.— Nozzle gross thrust parameter
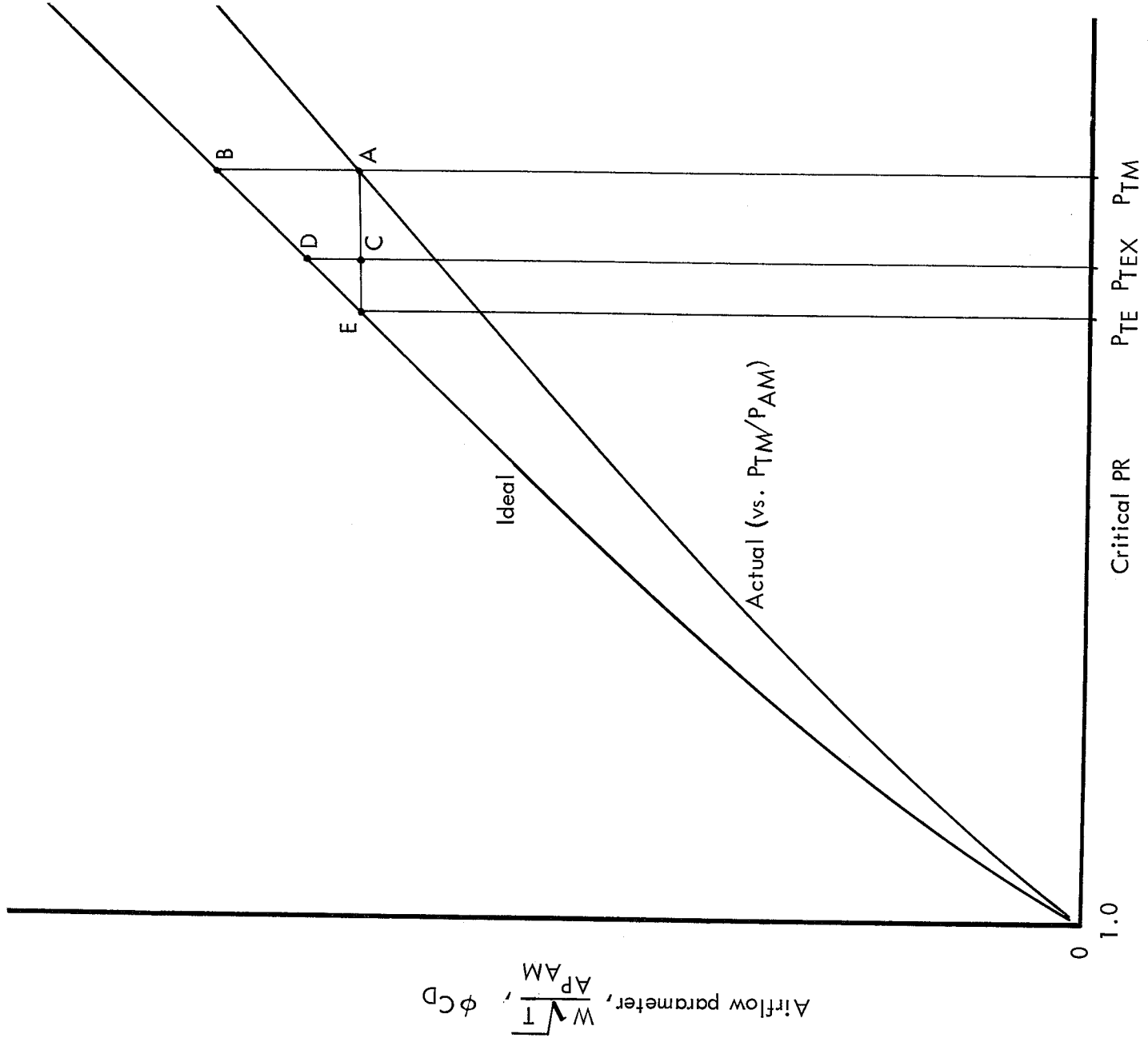
Figure 9.- Nozzle airflow parameter.

100

Fan nozzle coefficients
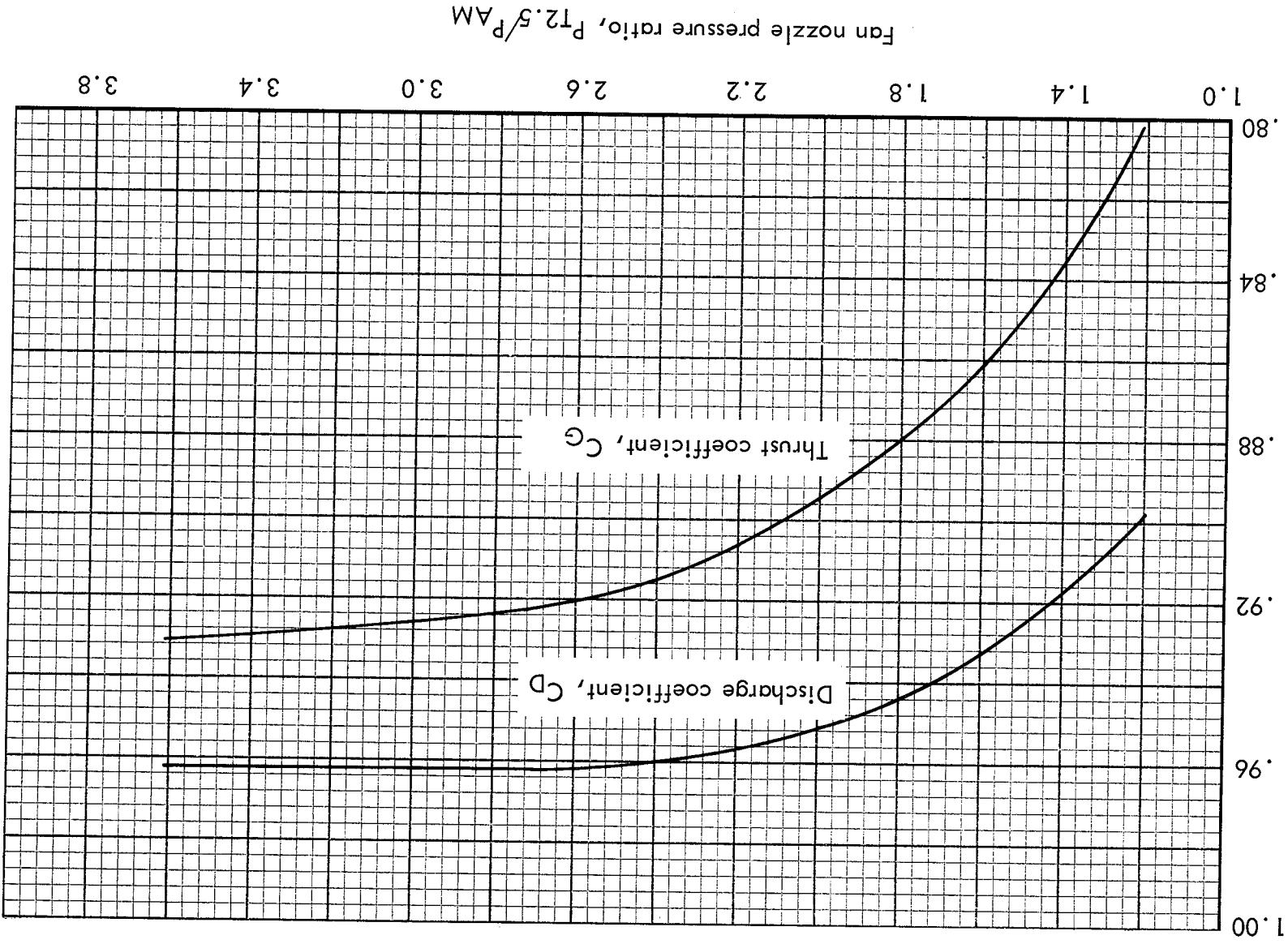
Figure 10.- 1/10 scale fan nozzle coefficients.

Fan nozzle pressure ratio, $P_{T2.5}/P_{AM}$

Thrust coefficient, C_G

Discharge coefficient, C_D
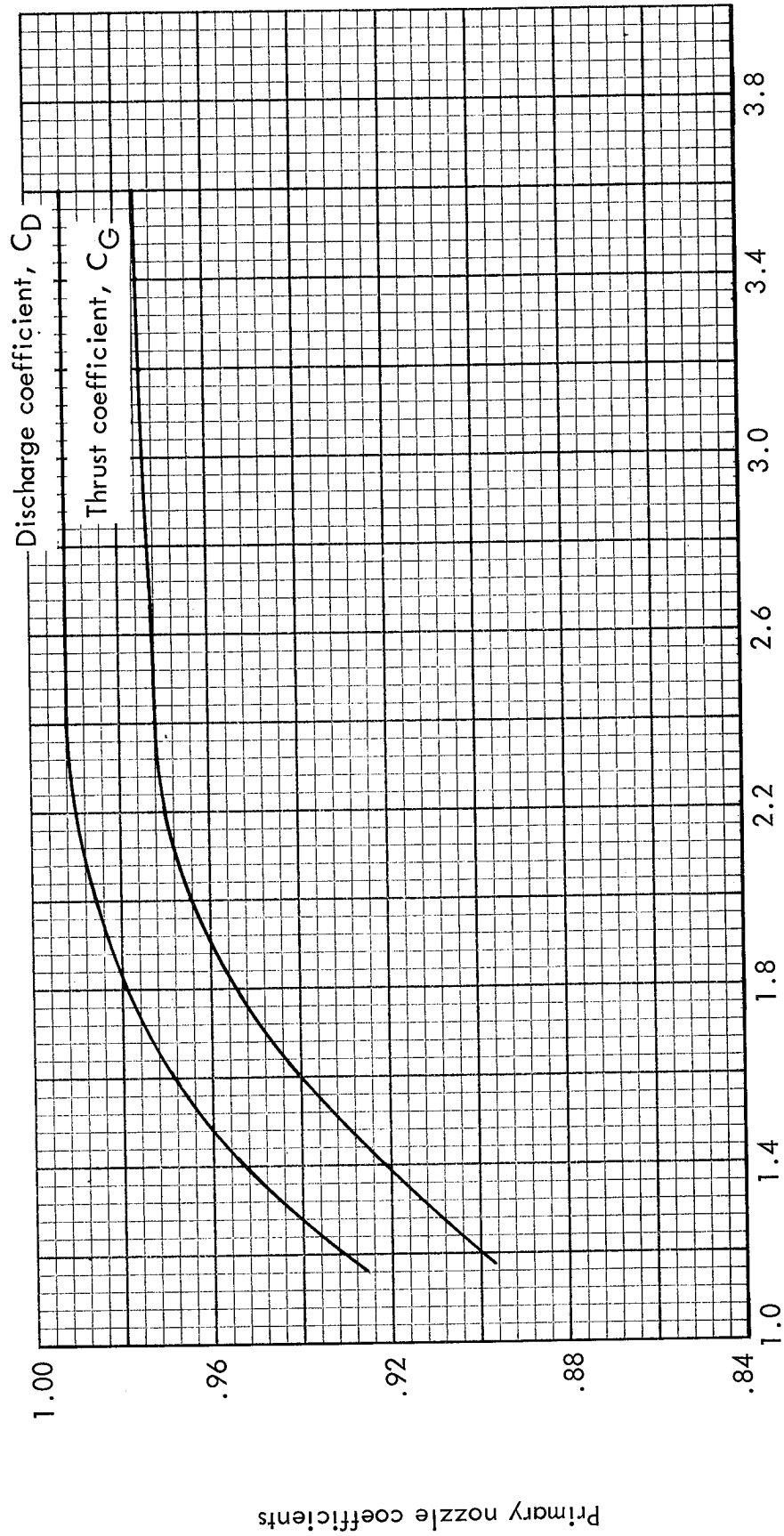
Figure 11. – 1/10 scale unsuppressed primary nozzle coefficients.

102
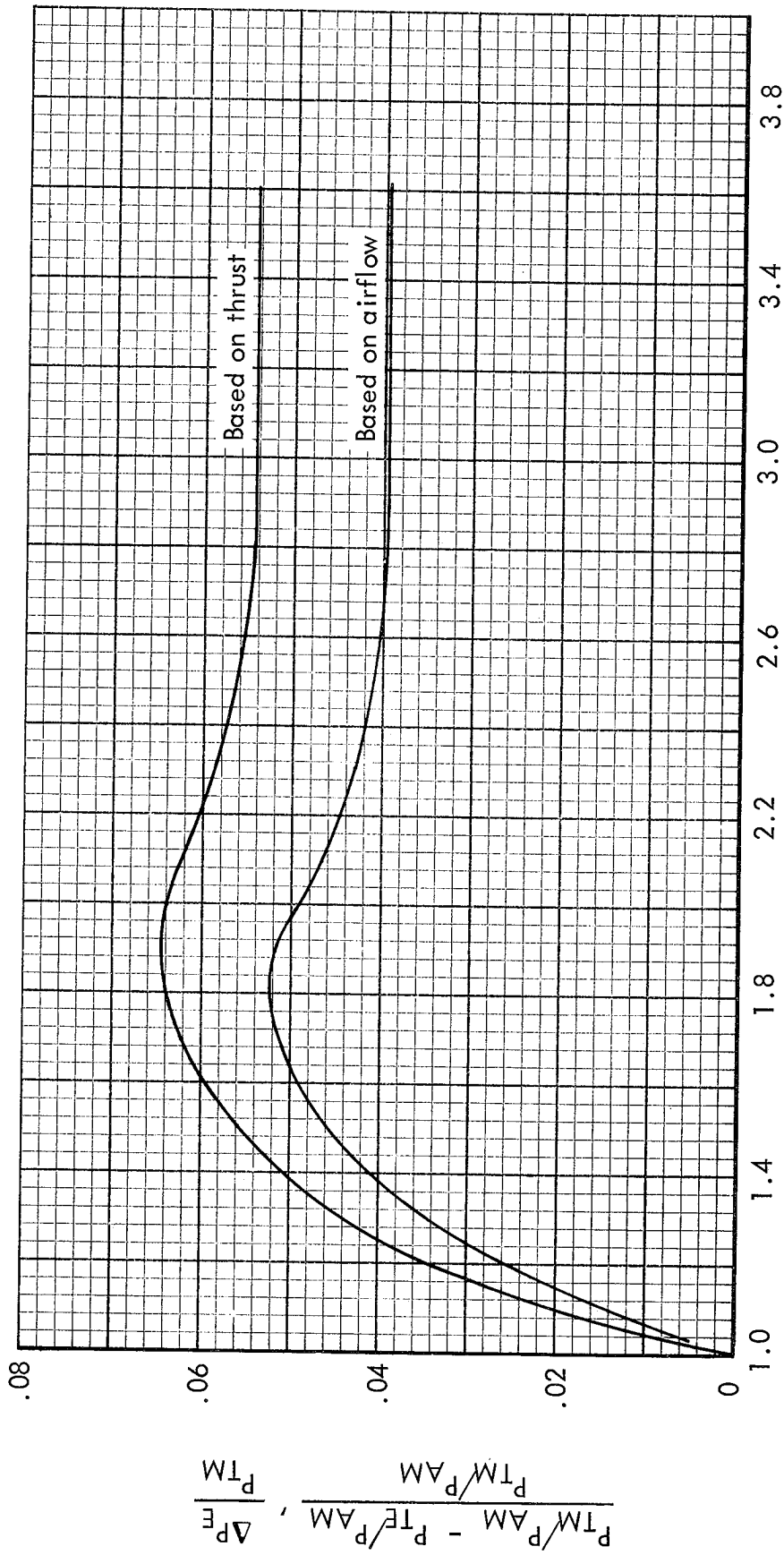
Figure 12.- 1/10 scale fan nozzle effective pressure losses.
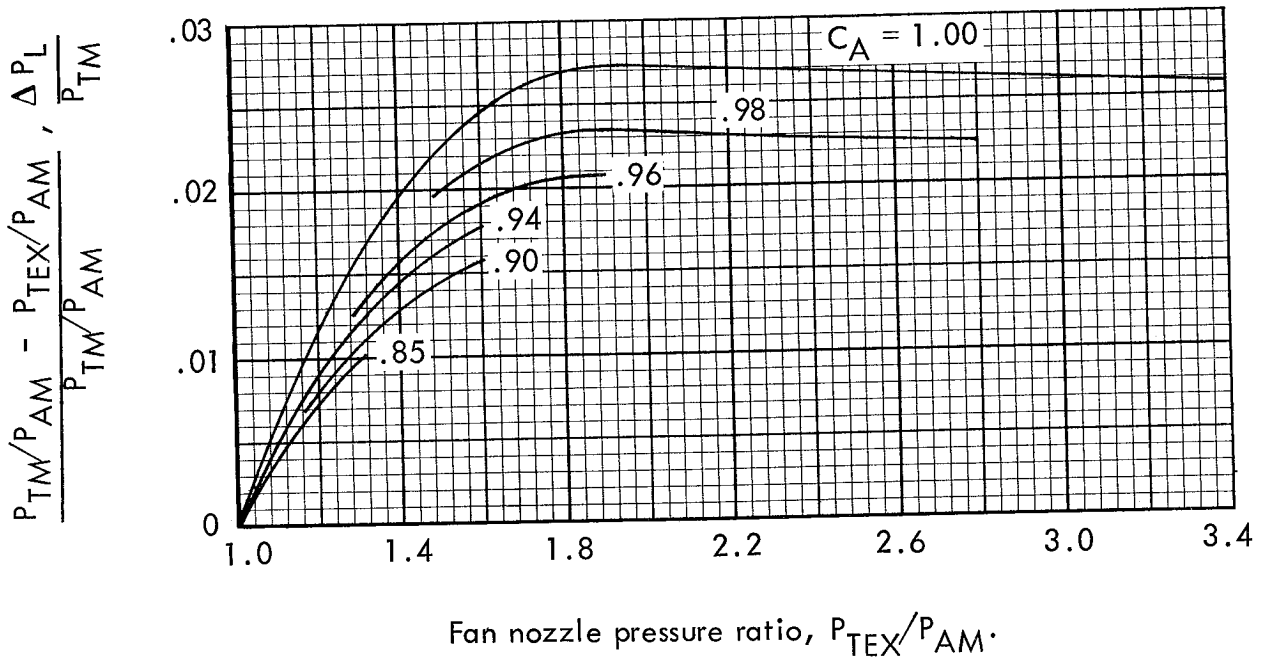
Figure 13.- Effect of area coefficient on duct pressure loss.
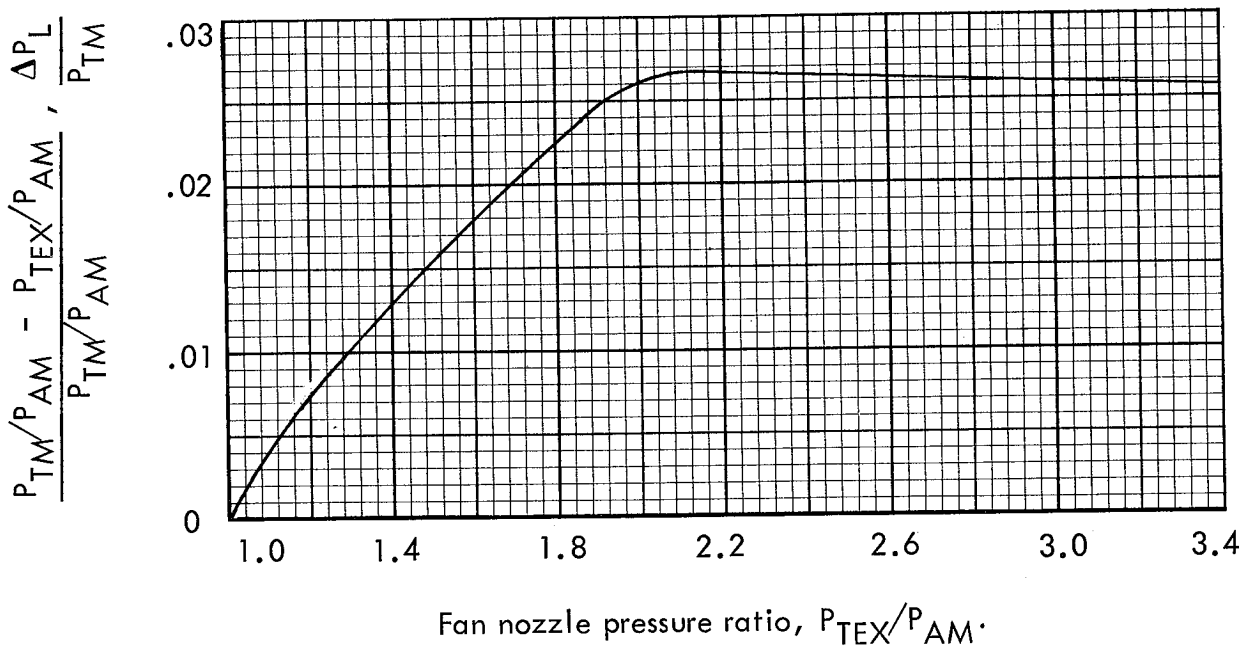
Figure 14.- 1/10 scale fan nozzle pressure loss.
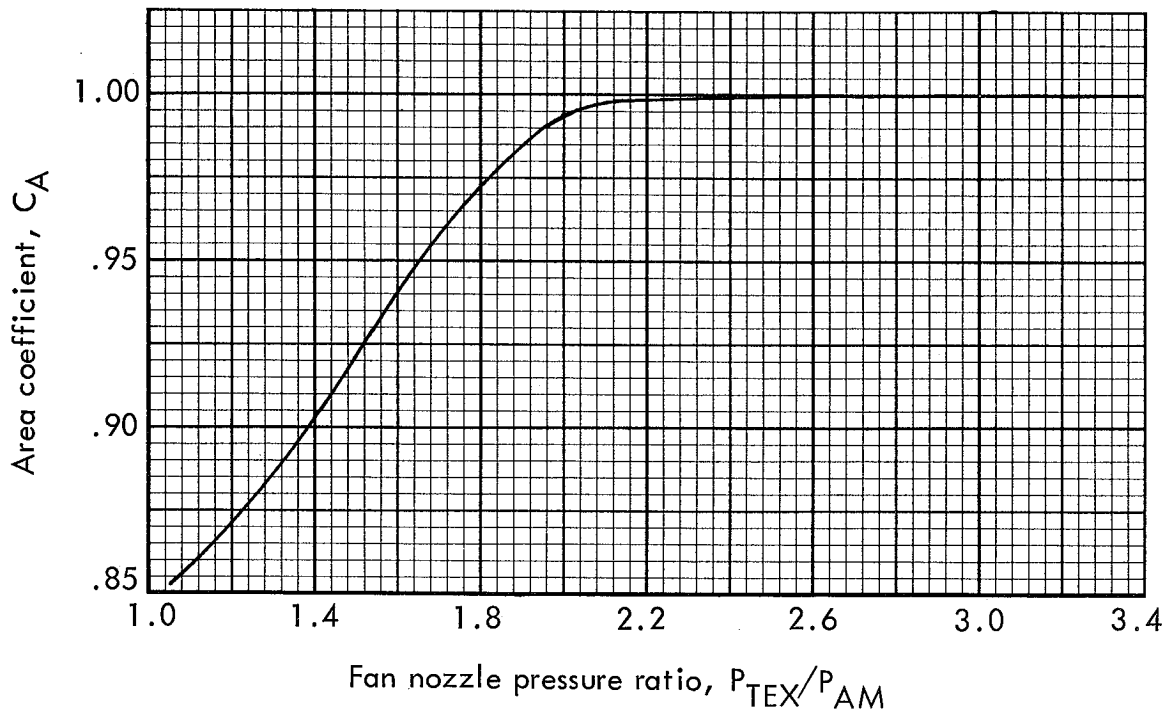
Figure 15.- 1/10 scale and full scale fan nozzle area coefficient.
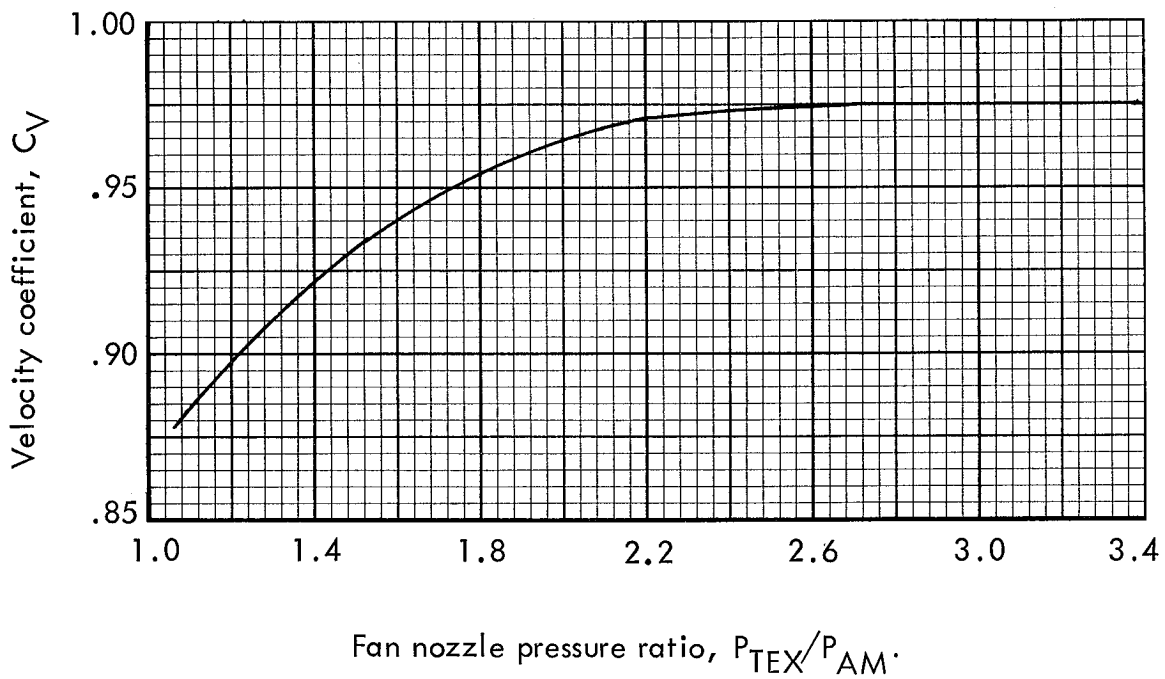
Figure 16.- 1/10 scale fan nozzle velocity coefficient.
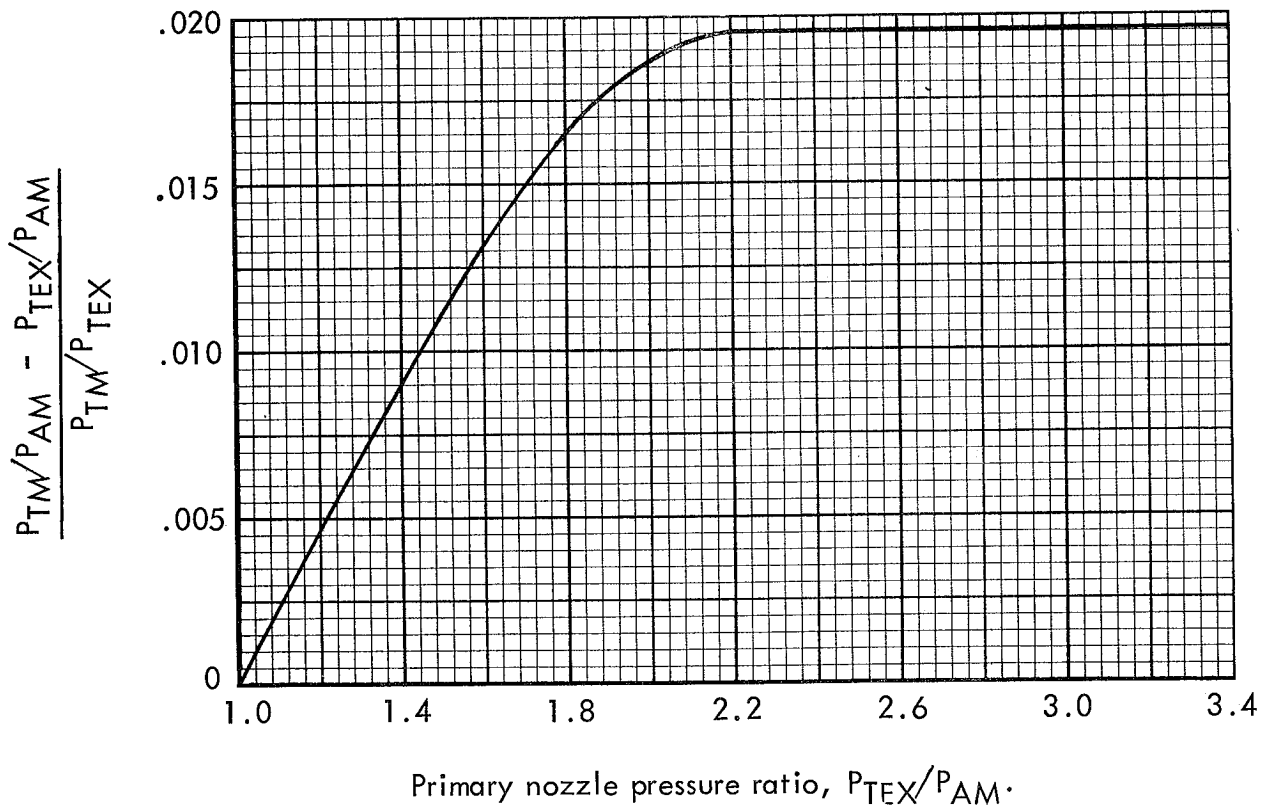
Figure 17.- 1/10 scale primary nozzle pressure loss.
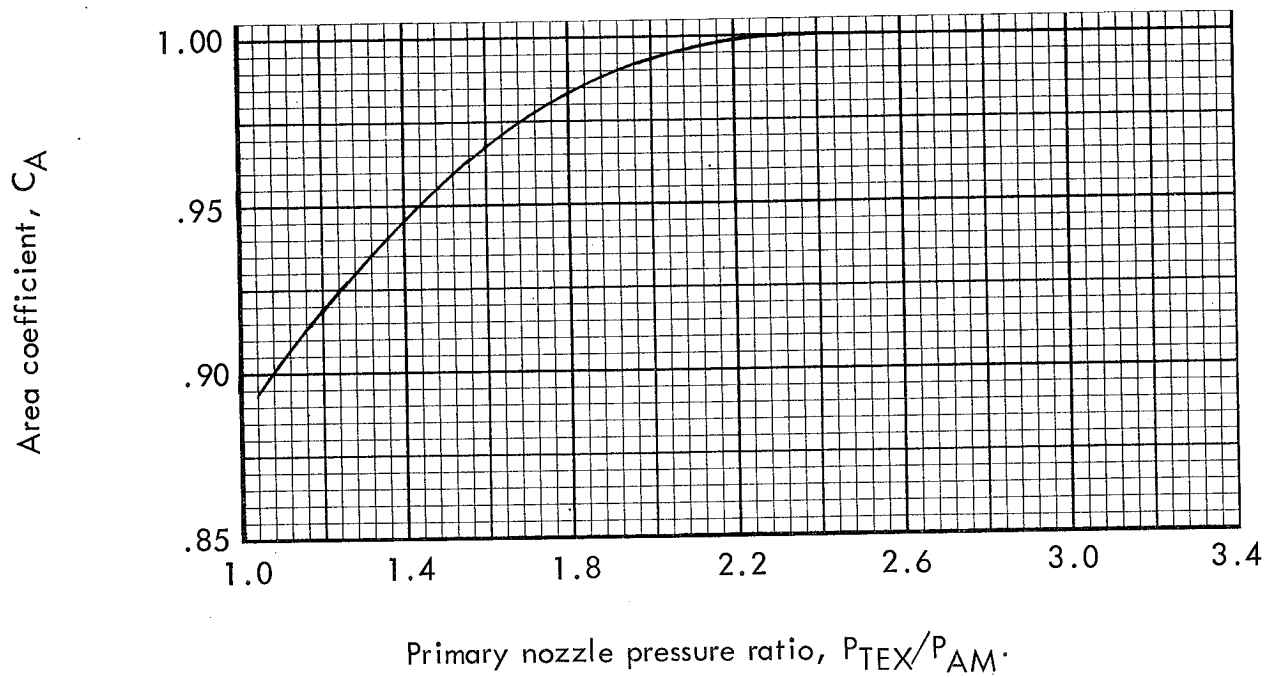
Figure 18.- 1/10 scale and full scale primary nozzle area coefficient.
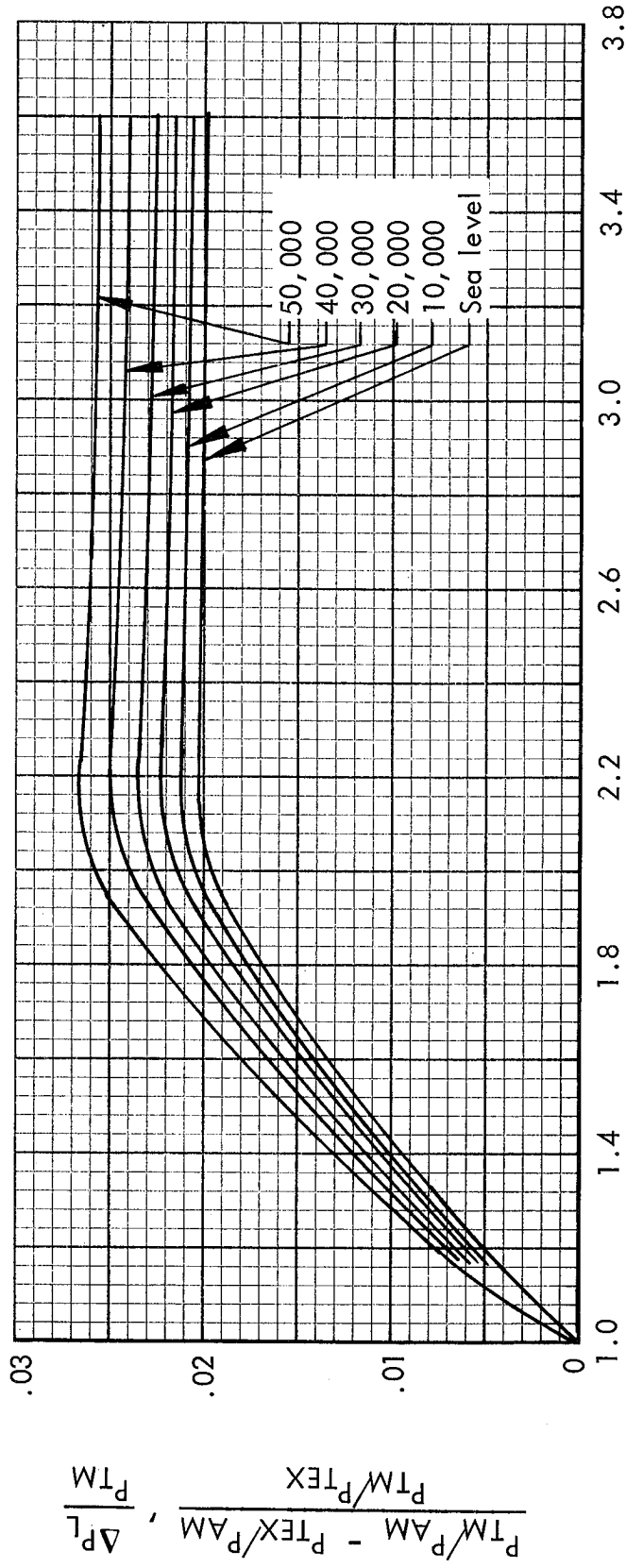
Fan nozzle pressure ratio, P_{TEX}/P_{AM}.

Figure 19.- Full scale fan nozzle pressure loss.

107

$$\Delta C_V = (C_V) \text{ FULL SCALE} - (C_V) \text{ 1/10 SCALE}$$

Fan nozzle pressure ratio, P_{TEX}/P_{AM}.
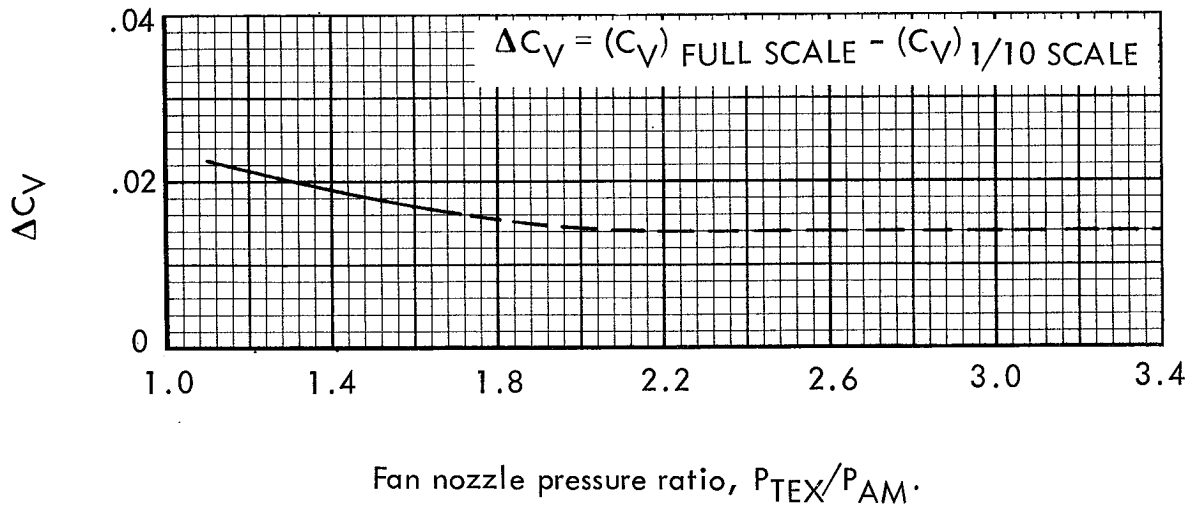
Figure 20.- Velocity coefficient difference between
1/10 scale and full scale fan nozzle.

Fan nozzle pressure ratio, P_{TEX}/P_{AM}.
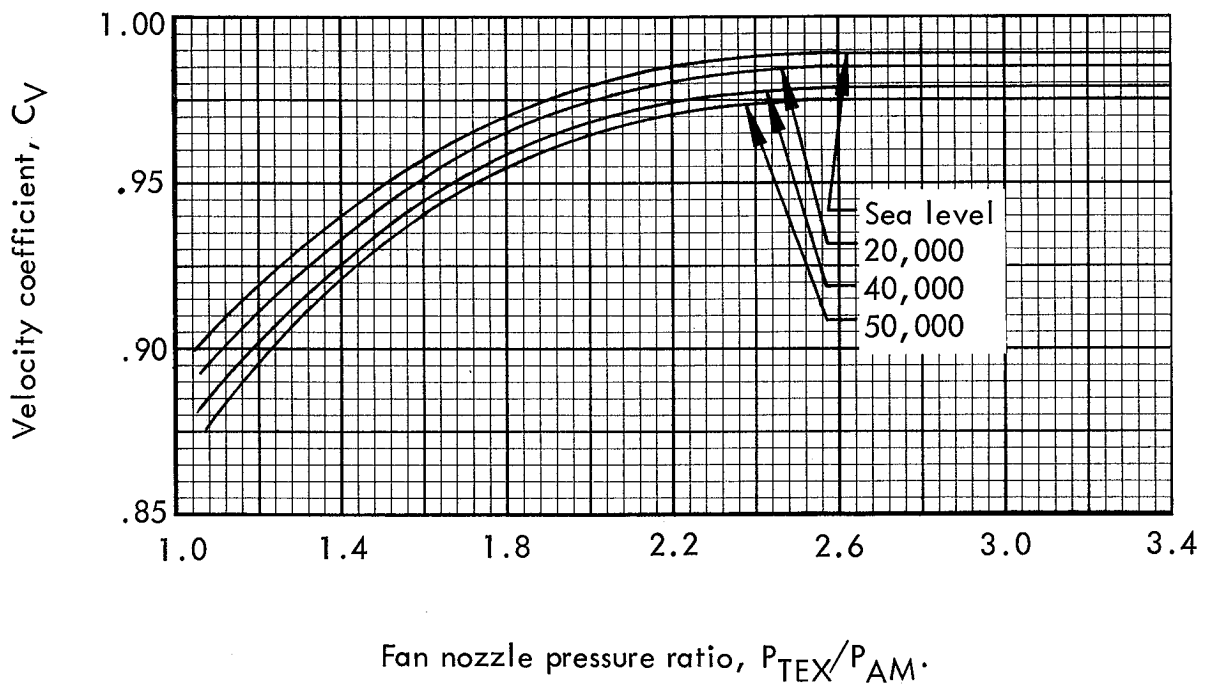
Figure 21.- Full scale fan nozzle velocity coefficient.
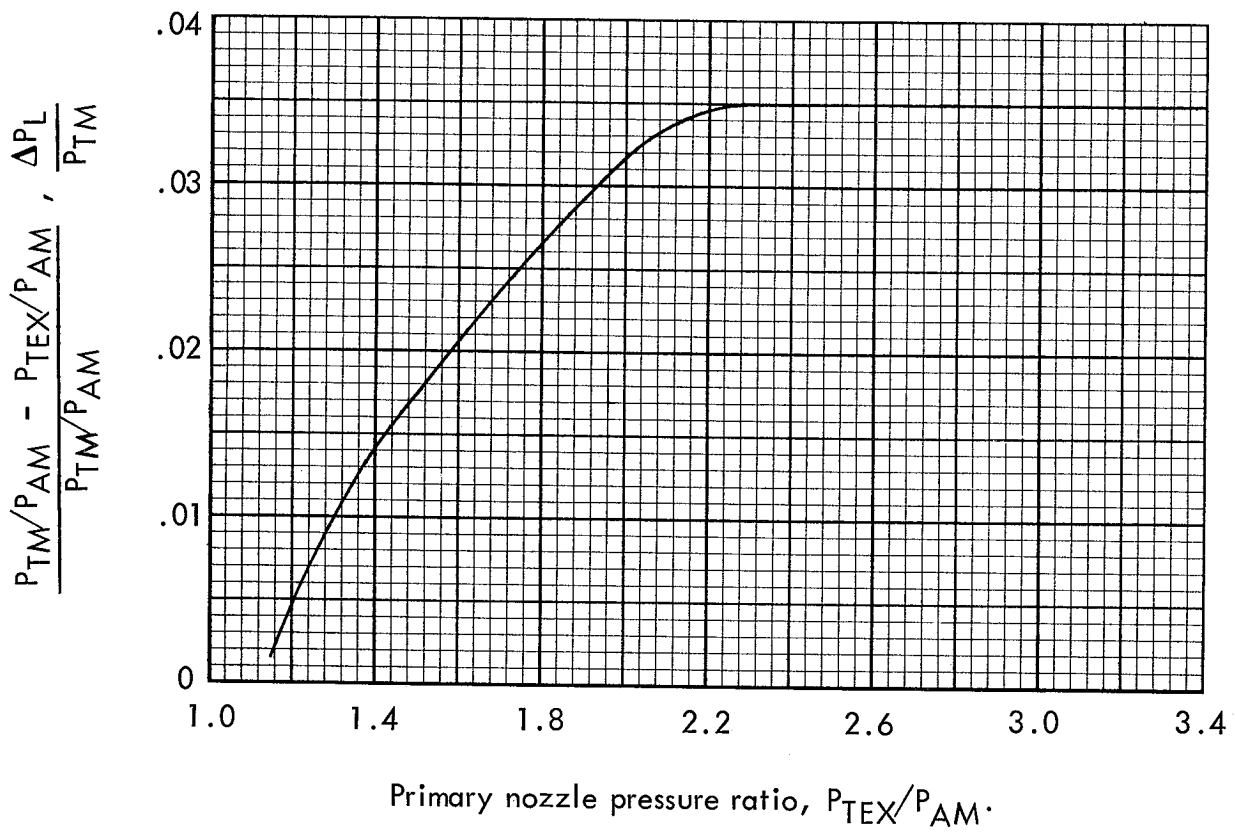
Figure 22.- Full scale primary nozzle pressure loss.
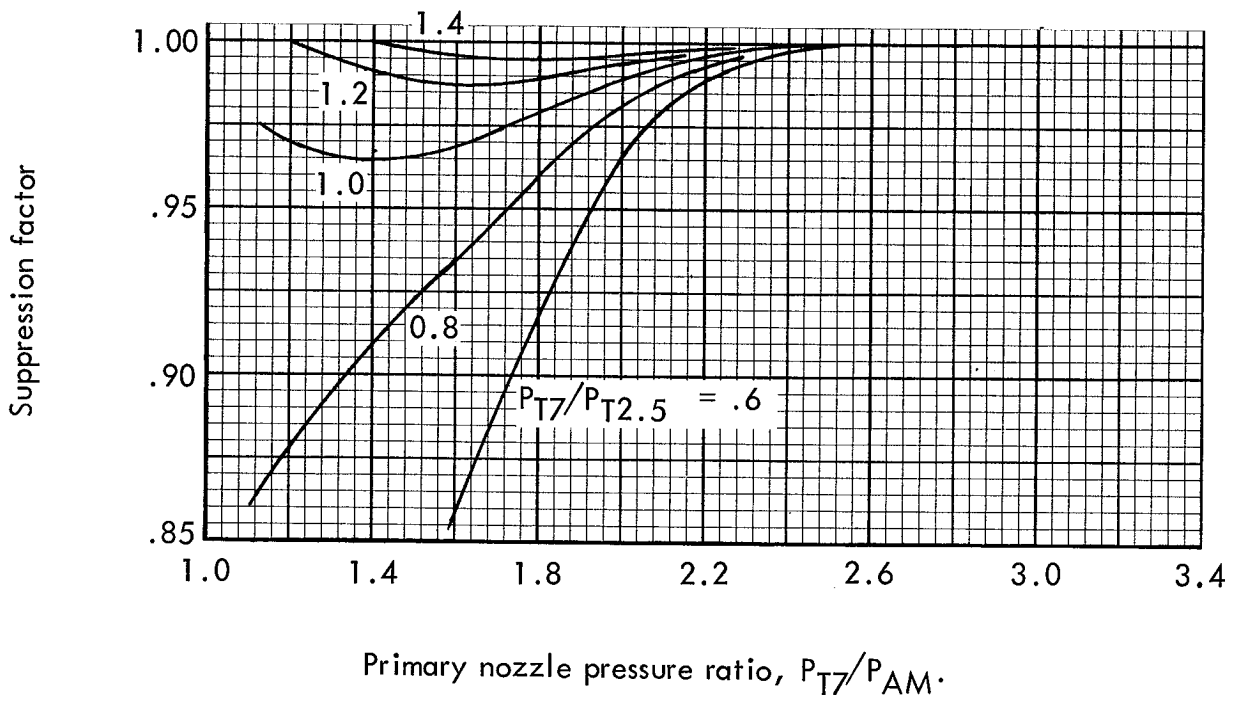
Figure 23.- Full scale primary nozzle suppression factor.

Fan nozzle discharge coefficient, C_{DF}
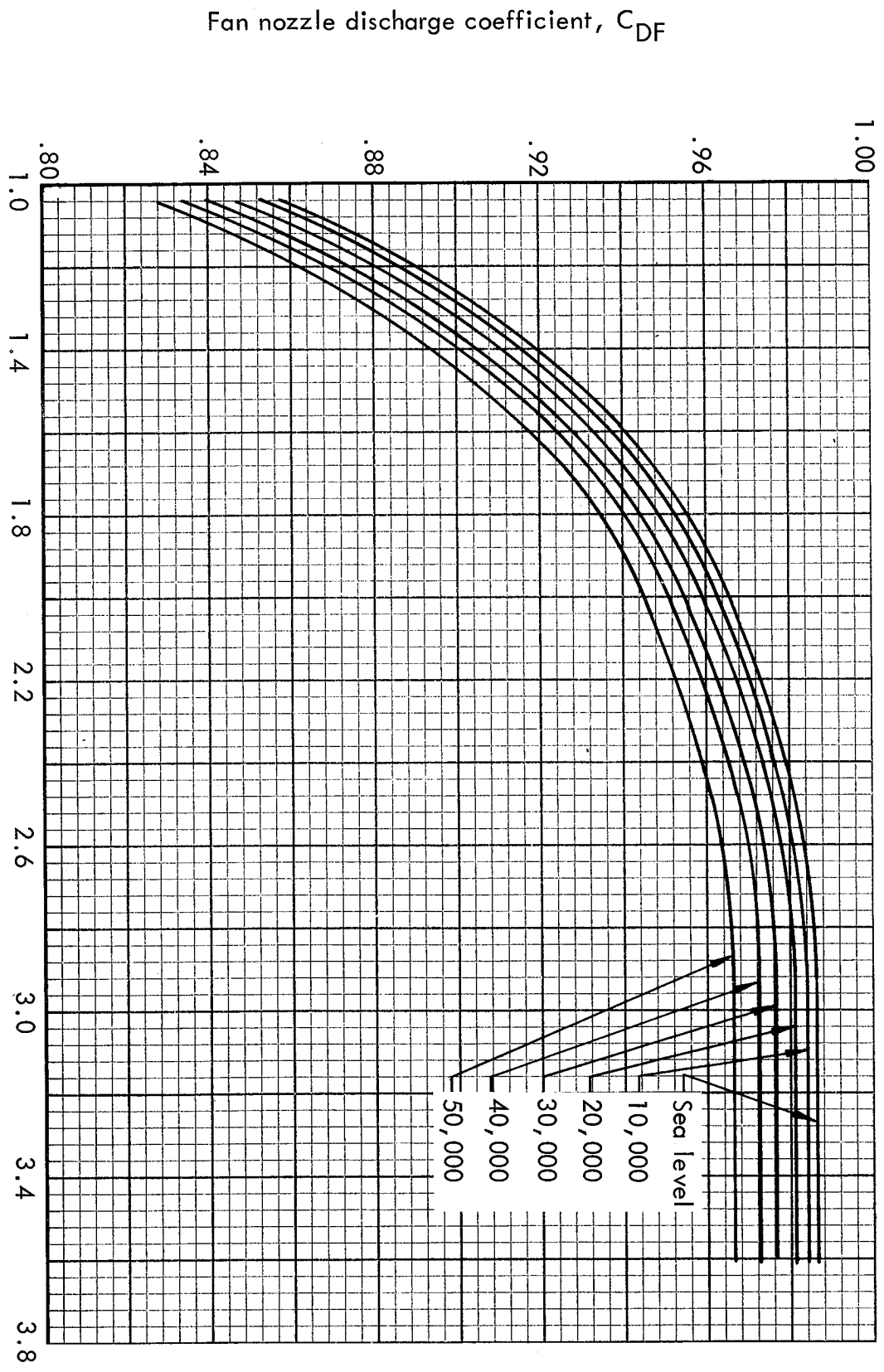
Fan nozzle pressure ratio, $P_{T2.5}/P_{AM}$.

Figure 24. - Full scale fan nozzle discharge coefficient.
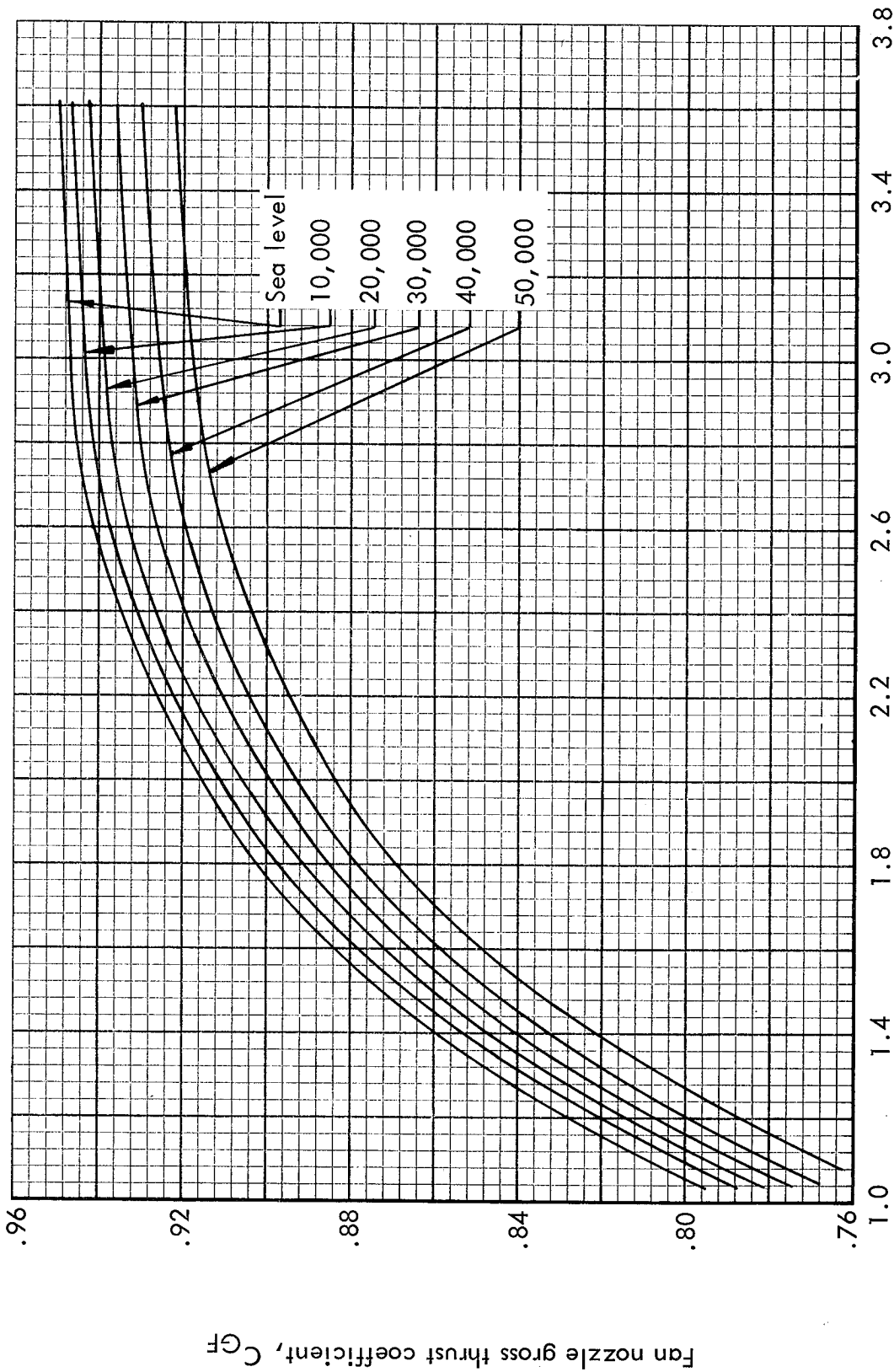
Fan nozzle pressure ratio, $P_{T2.5}/P_{AM}$.

Figure 25. - Full scale fan nozzle gross thrust coefficient.

111
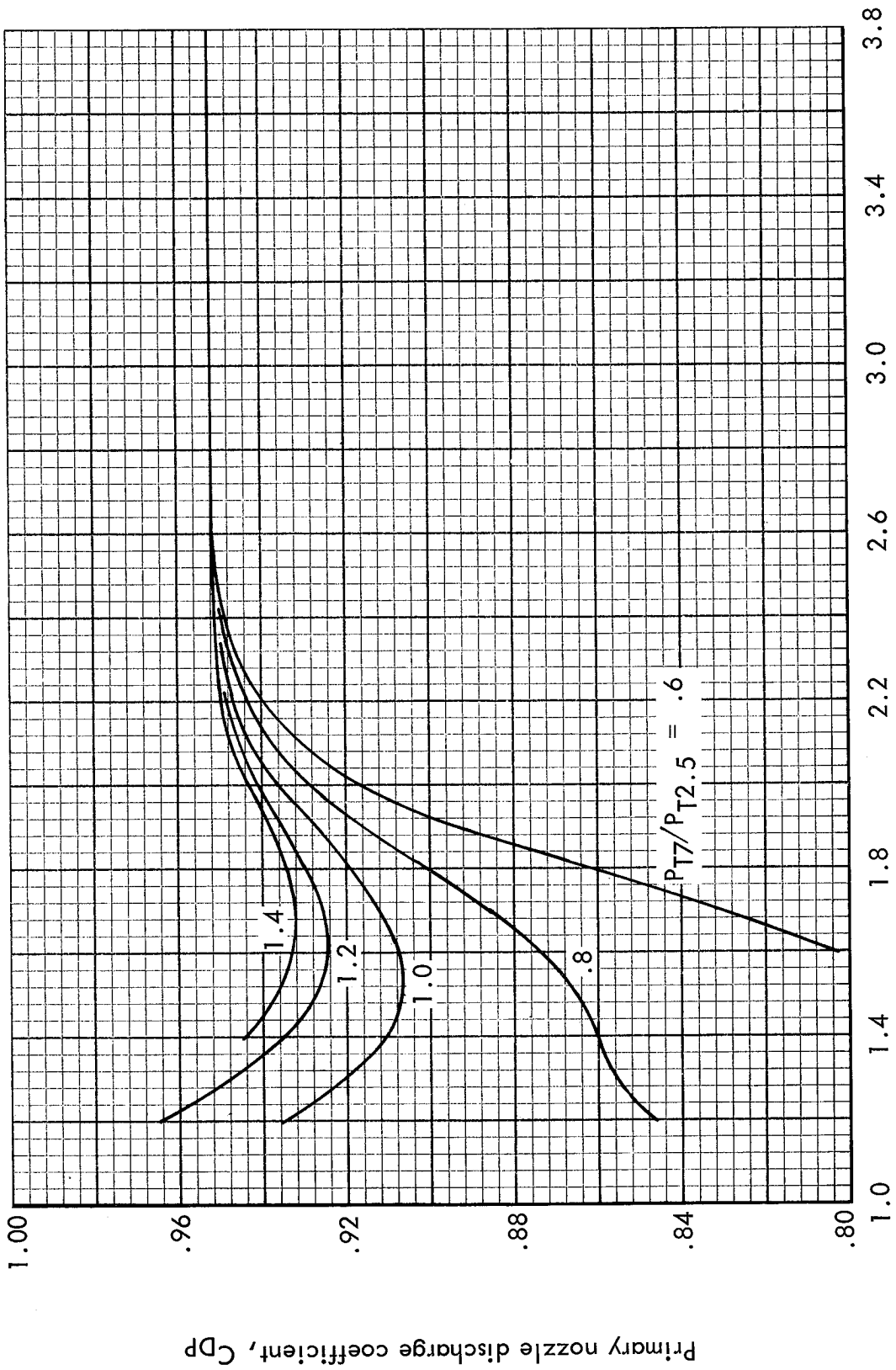
Figure 26.- Full scale primary nozzle discharge coefficient.

112
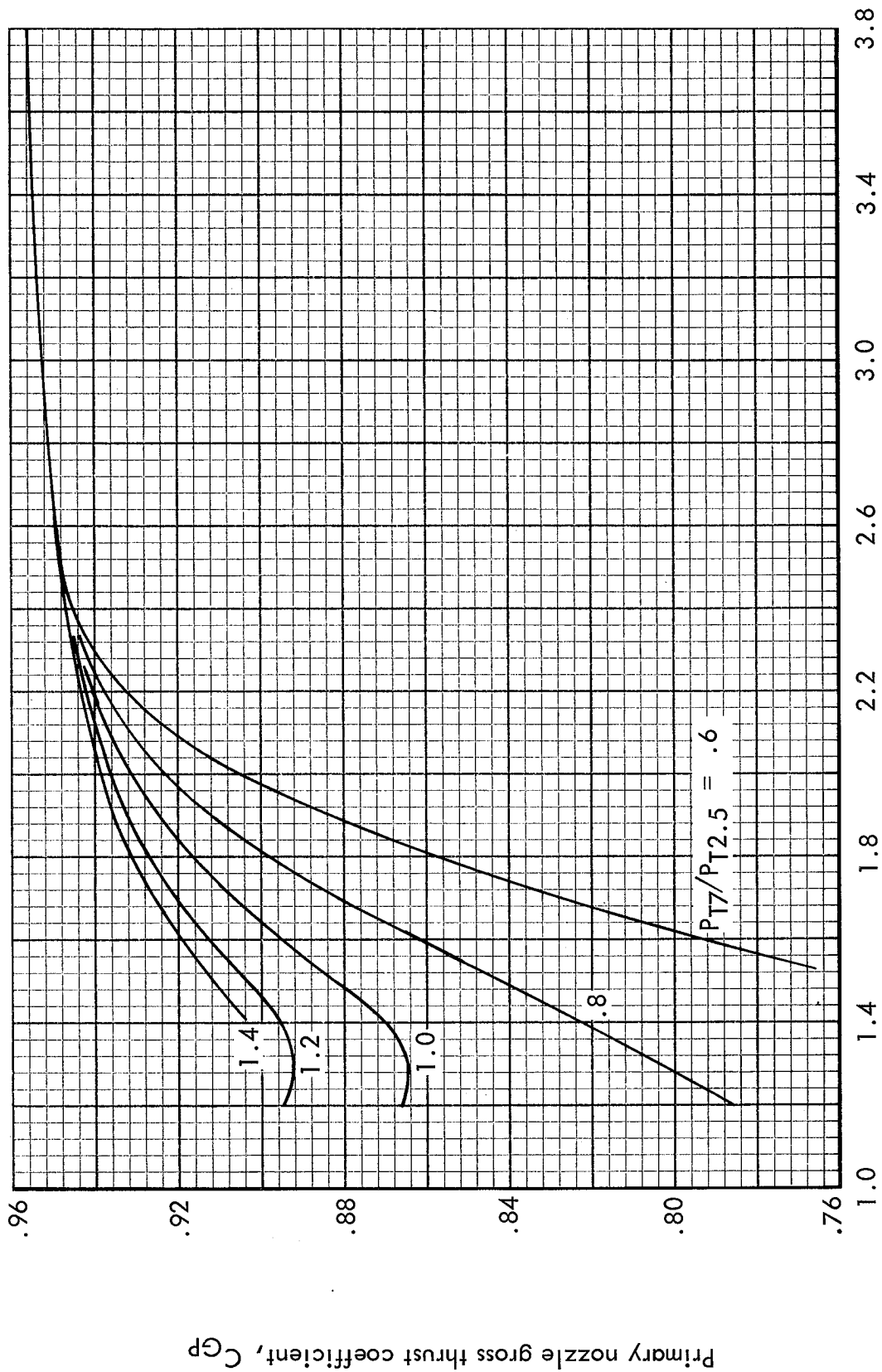
Figure 27. - Full scale primary nozzle gross thrust coefficient.
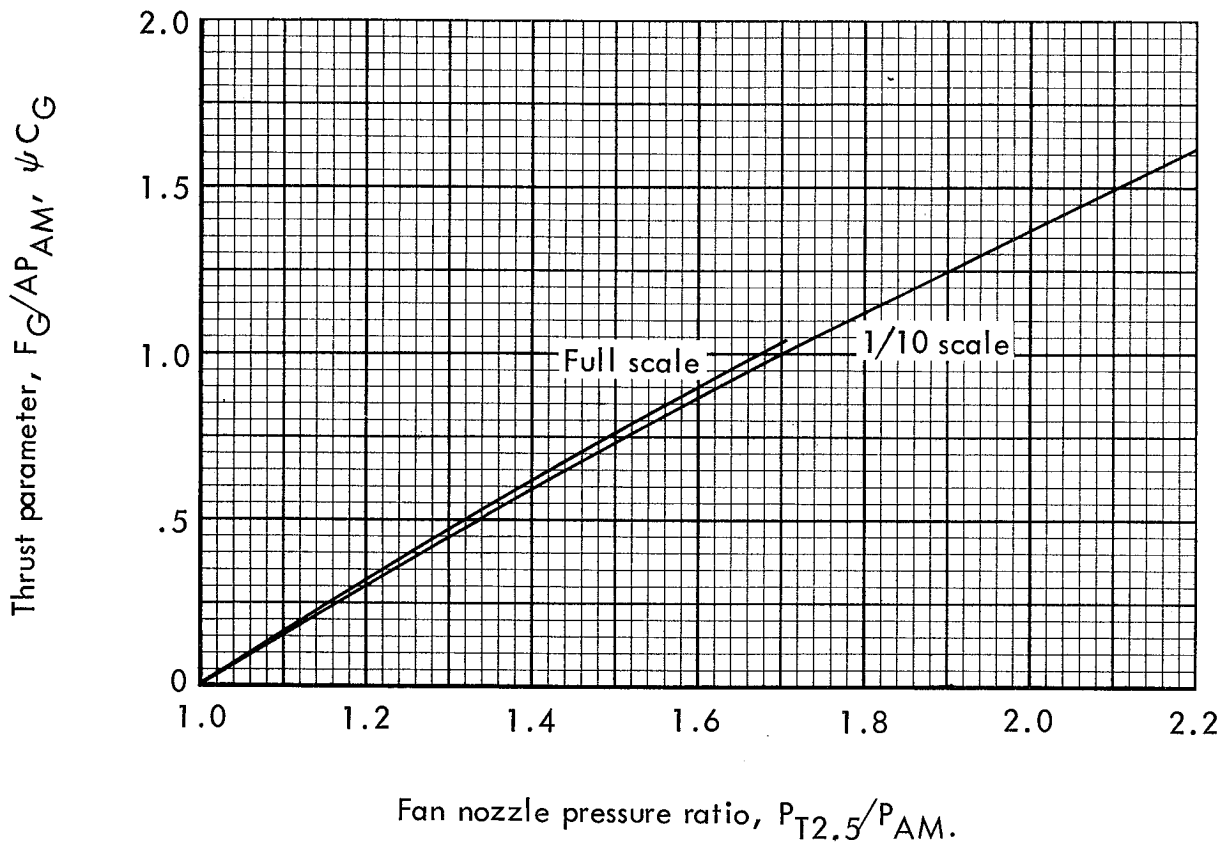
Figure 28.- 1/10 scale and full scale fan nozzle thrust parameter.
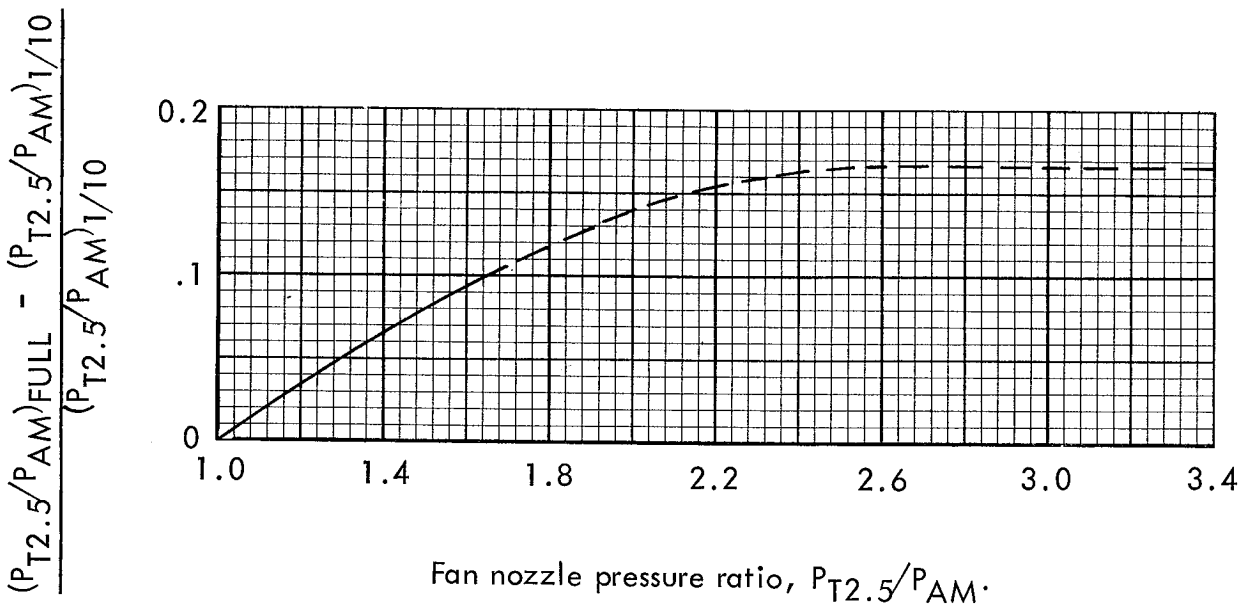
Figure 29.- Extrapolation parameter from 1/10 scale to full scale fan nozzle.
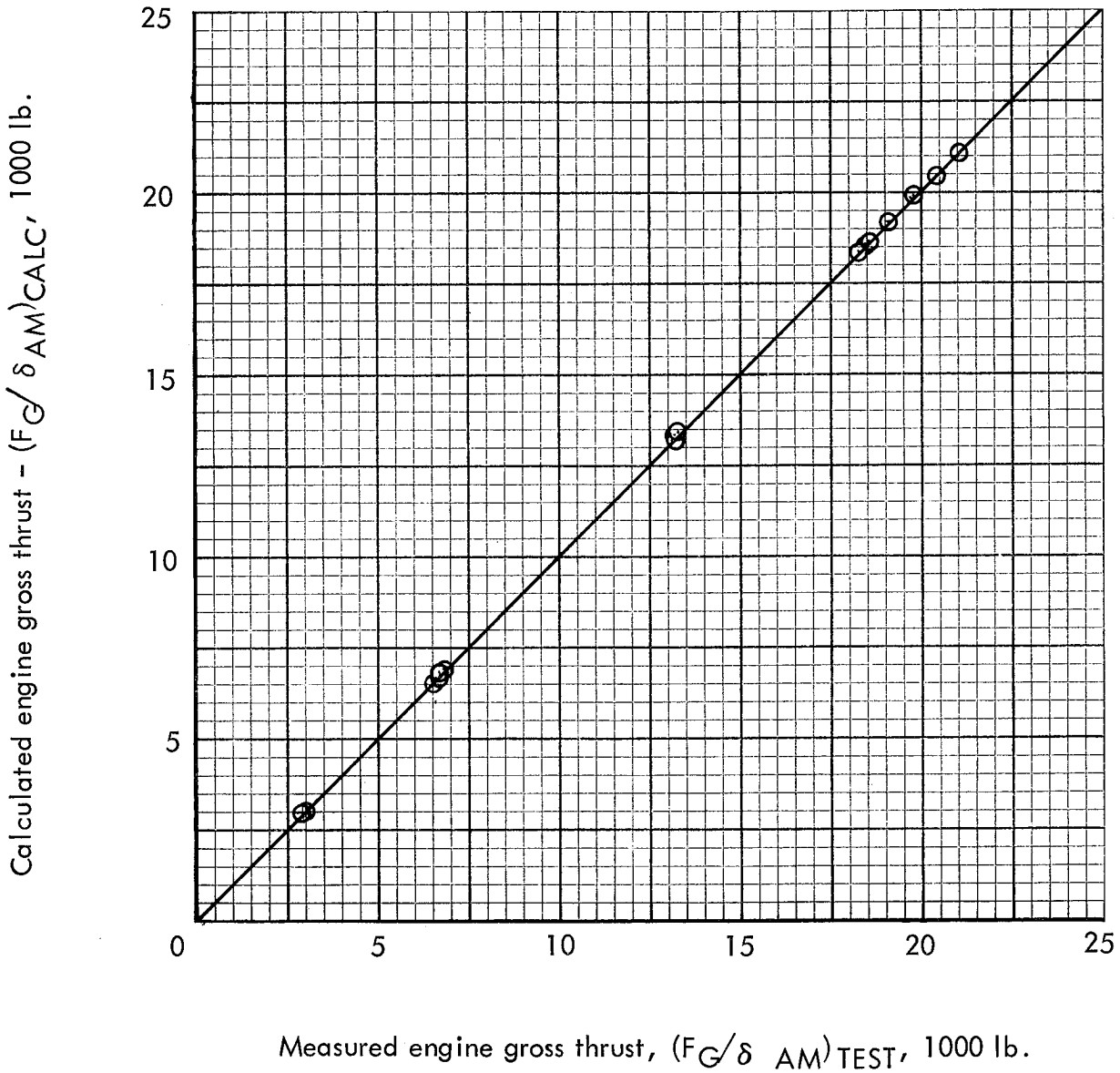
Figure 30.- Comparison of measured and calculated total engine
thrust based on engine test stand data.
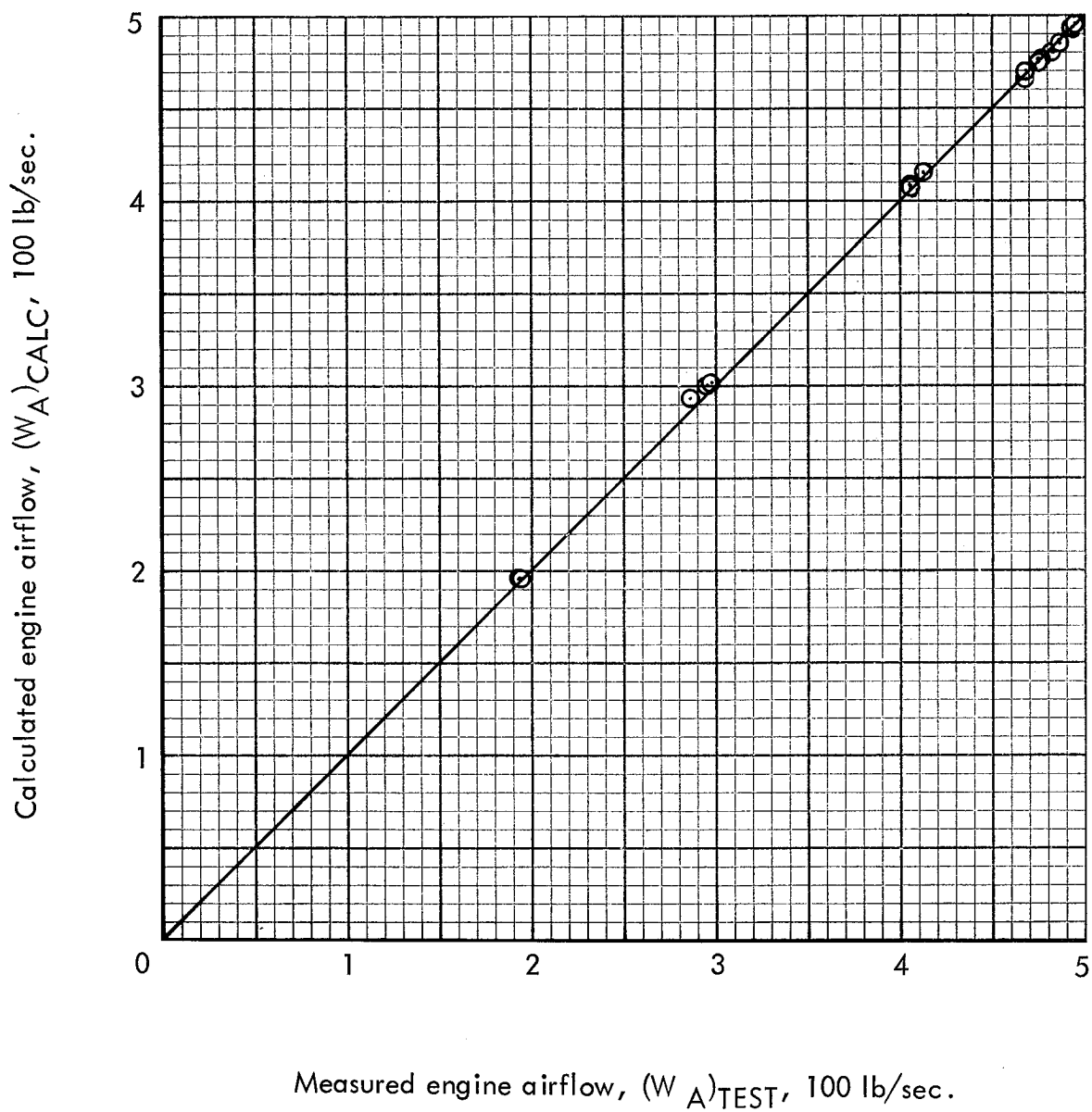
Figure 31.— Comparison of measured and calculated engine airflow based on engine test stand data.
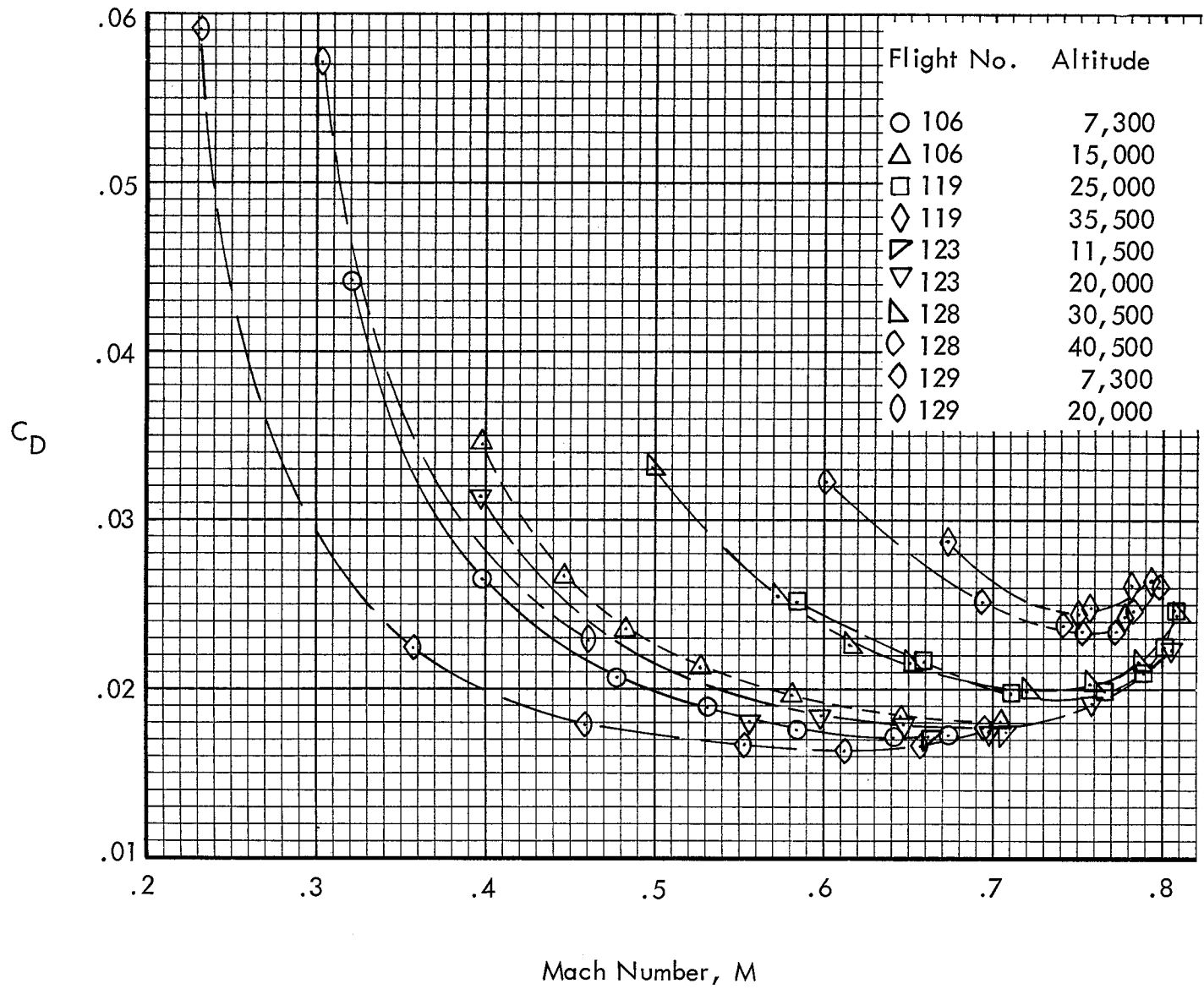
Mach Number, M

(a) C_D versus Mach Number

Figure 32.- Speed power flights.

Flight No.	Altitude
○ 106	7,300
△ 106	15,000
□ 119	25,000
◇ 119	35,500
▽ 123	11,500
▽ 123	20,000
◁ 128	30,500
◇ 128	40,500
◊ 129	7,300
◊ 129	20,000
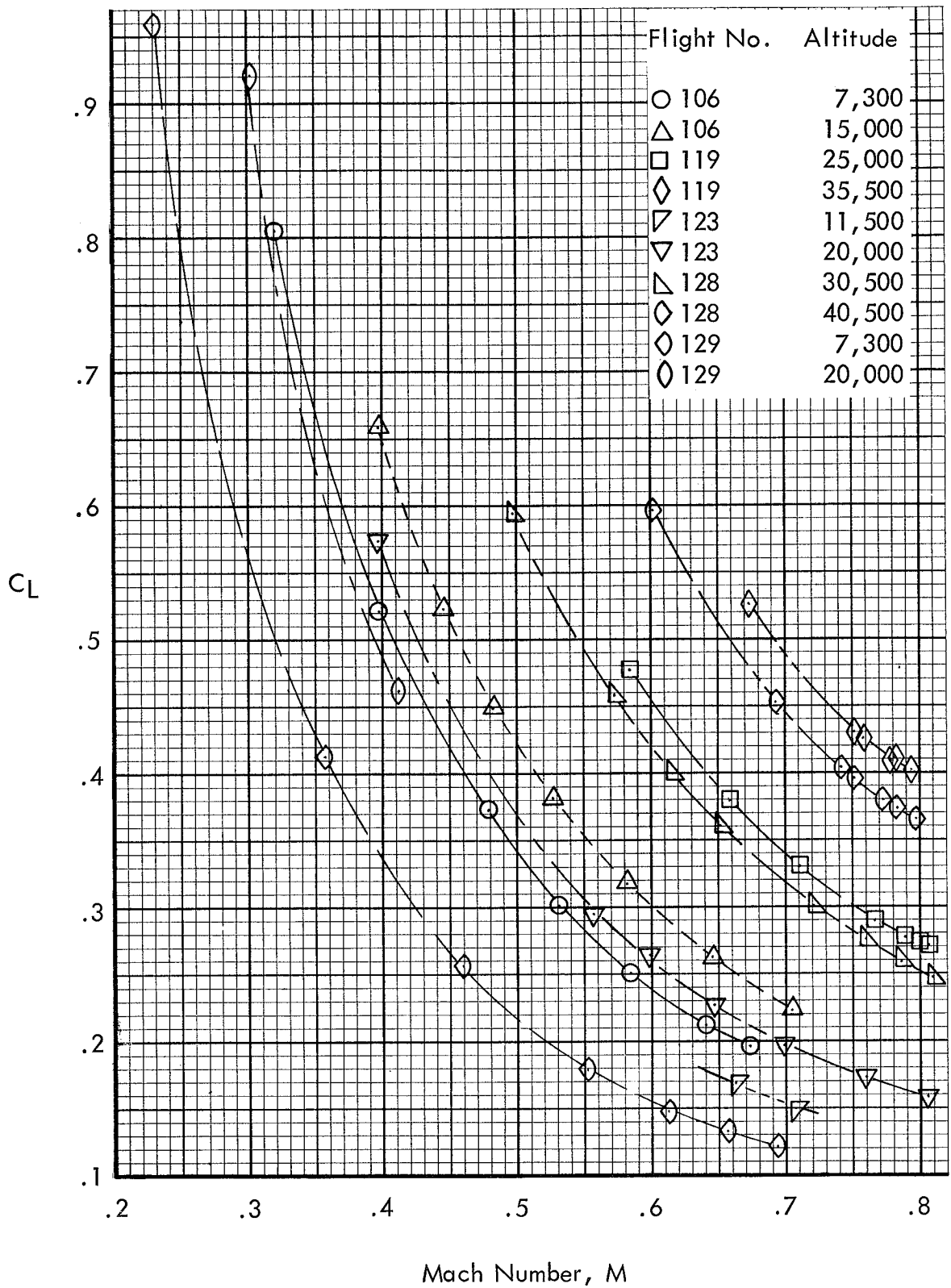
Mach Number, M

(b) C_L versus Mach Number

Figure 32.- Continued

$$\frac{c_l c}{c_{avg}}$$

Rigid $C_{L_{A-h}}$ = .1746
Flexible $C_{L_{A-h}}$ = .1679

Flight Conditions

Weight = 233,365 lb.   M = .7076
Alt.   = 11,496 ft.   RN = 78.96×10⁶
c.g.   = 18.55%MAC C_{L_A} = .1502
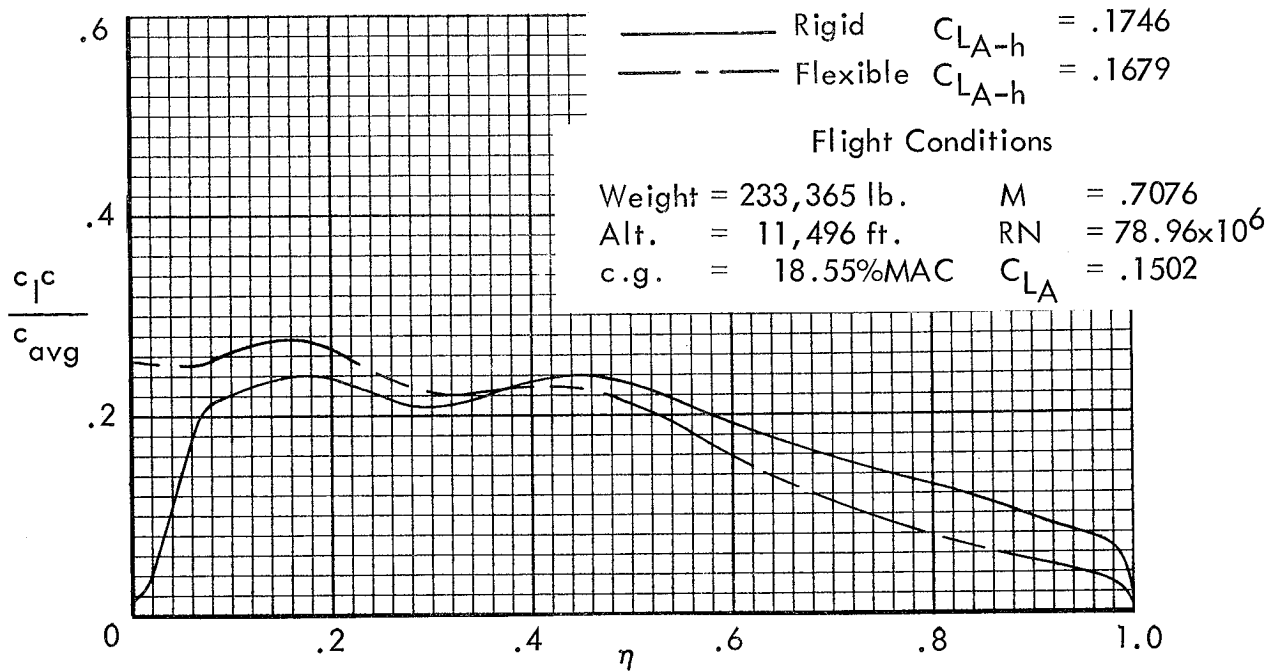
(a) Flight number 123-6.1.

Figure 33.- Rigid and flexible spanwise load distributions for five
selected speed power points.

$$\frac{c_l c}{c_{avg}}$$

Rigid $C_{L_{A-h}}$ = .2166
Flexible $C_{L_{A-h}}$ = .2105

Flight Conditions

Weight = 321,538 lb.   M = .6736
Alt.   = 7,497 ft.   RN = 85.00×10⁶
c.g.   = 26.06%MAC C_{L_A} = .1961
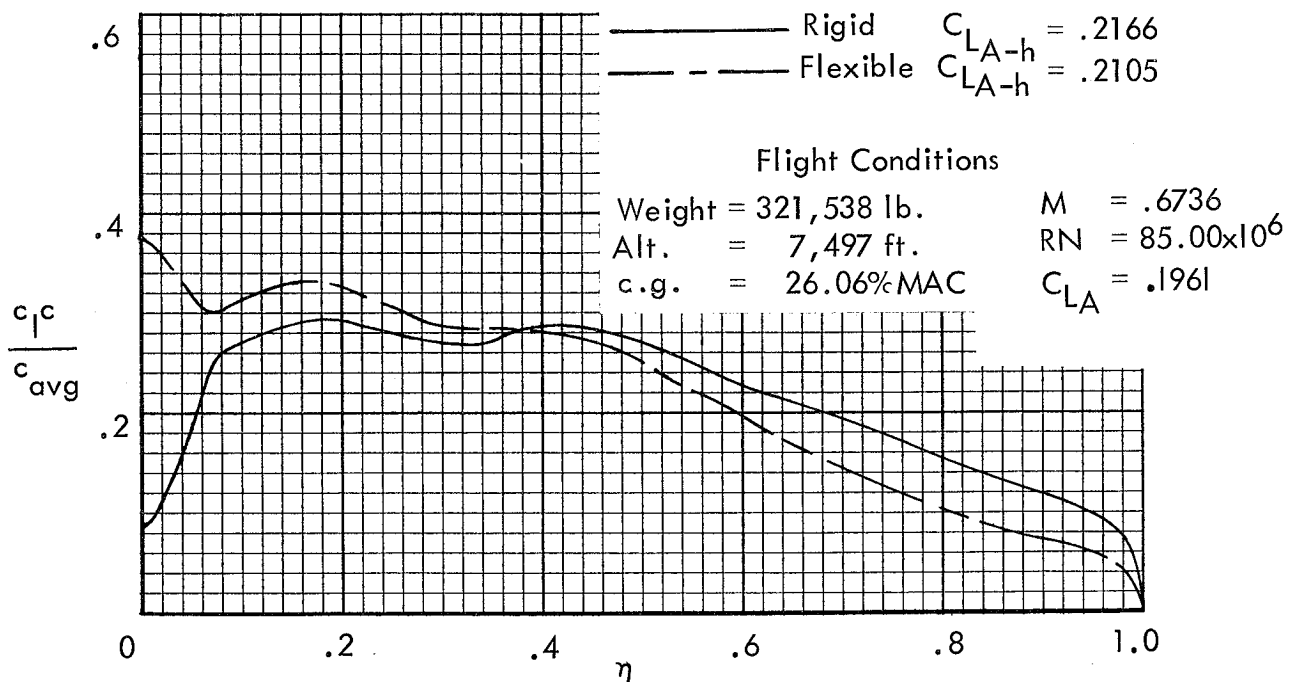
(b) Flight number 106-4A.

Figure 33.- Continued.

Flight Conditions

Weight = 289,326 lb.   M   = .7107
Alt.   = 25,561 ft.   RN = 52.58x10^6
c.g.   =   21.65%MAC C_{L_A} = .3300

Rigid $C_{L_{A-h}}$ = .3538
Flexible $C_{L_{A-h}}$ = .3498
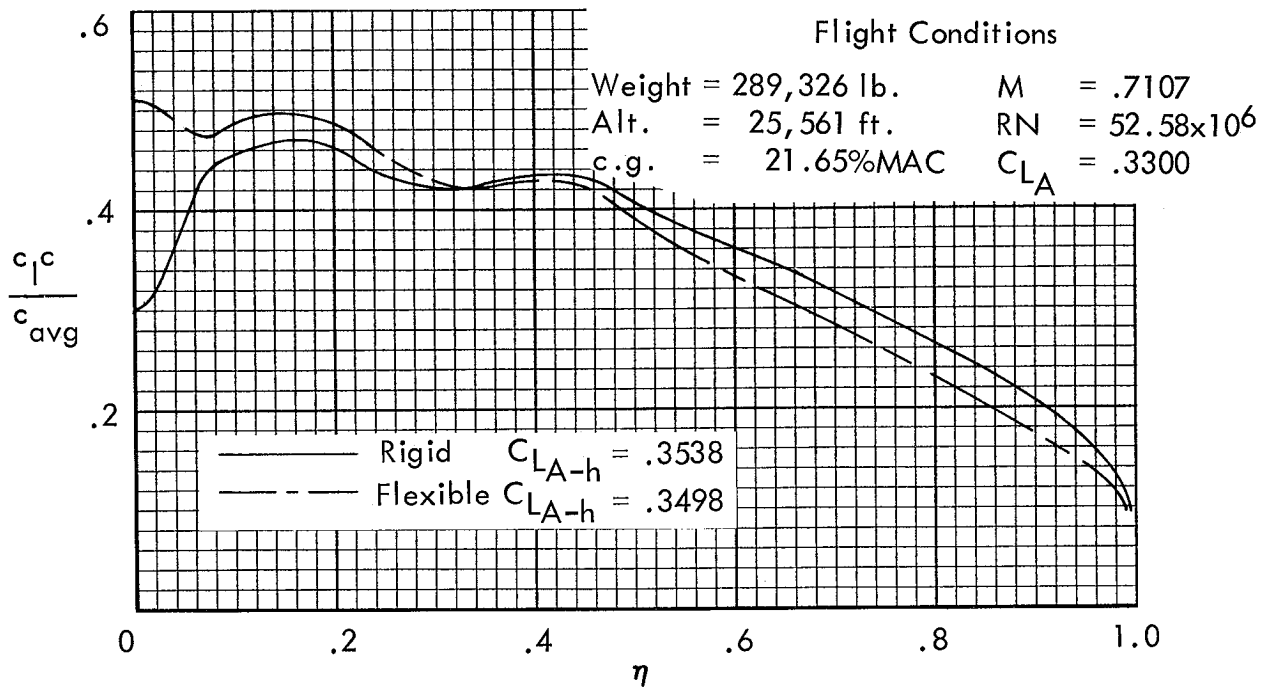
(c) Flight number 119-7.5.

Figure 33.- Continued.

Flight Conditions

Weight = 294,007 lb.   M   = .7054
Alt.   = 15,466 ft.   RN = 69.34x10^6
c.g.   =   26.20%MAC C_{L_A} = .2228

Rigid $C_{L_{A-h}}$ = .2433
Flexible $C_{L_{A-h}}$ = .2375
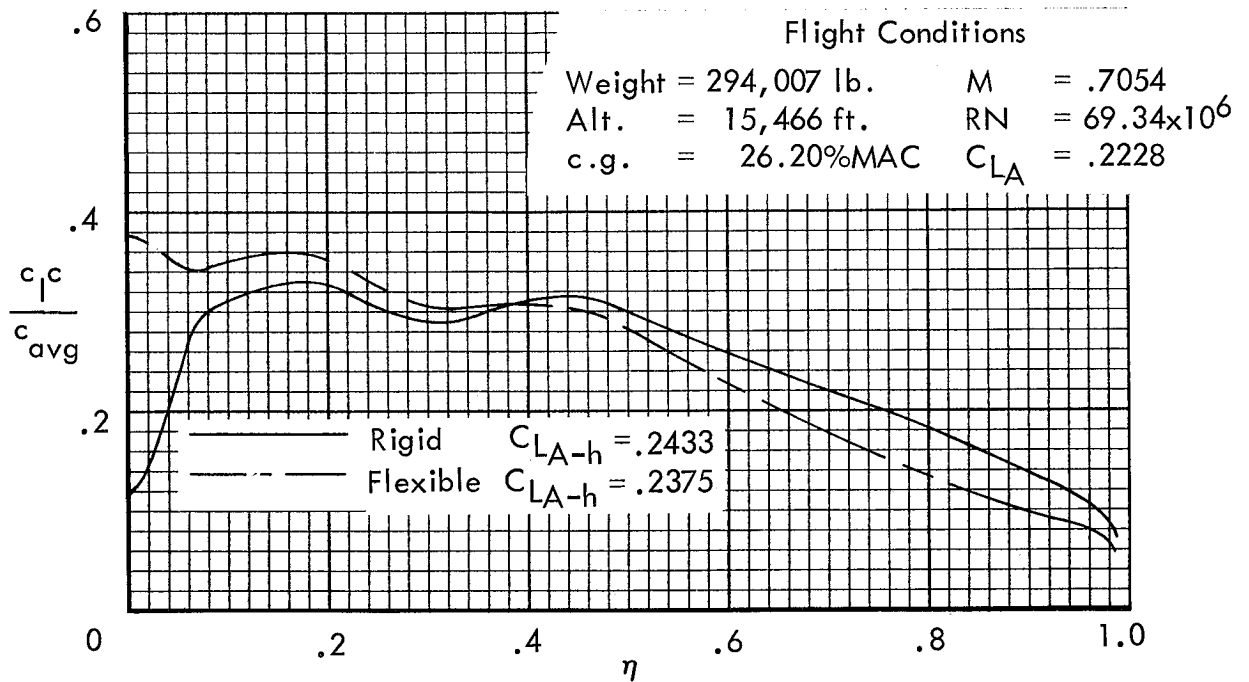
(d) Flight number 106-5A.

Figure 33.- Continued.

Rigid $C_{L_{A-h}} = .5543$
Flexible $C_{L_{A-h}} = .5500$
Flight Conditions

Weight = 265,135 lb.   M = .6737
Alt.   = 35,380 ft.   RN = 34.66x10^6
c.g.   = 20.20%MAC C_{L_A} = .5268
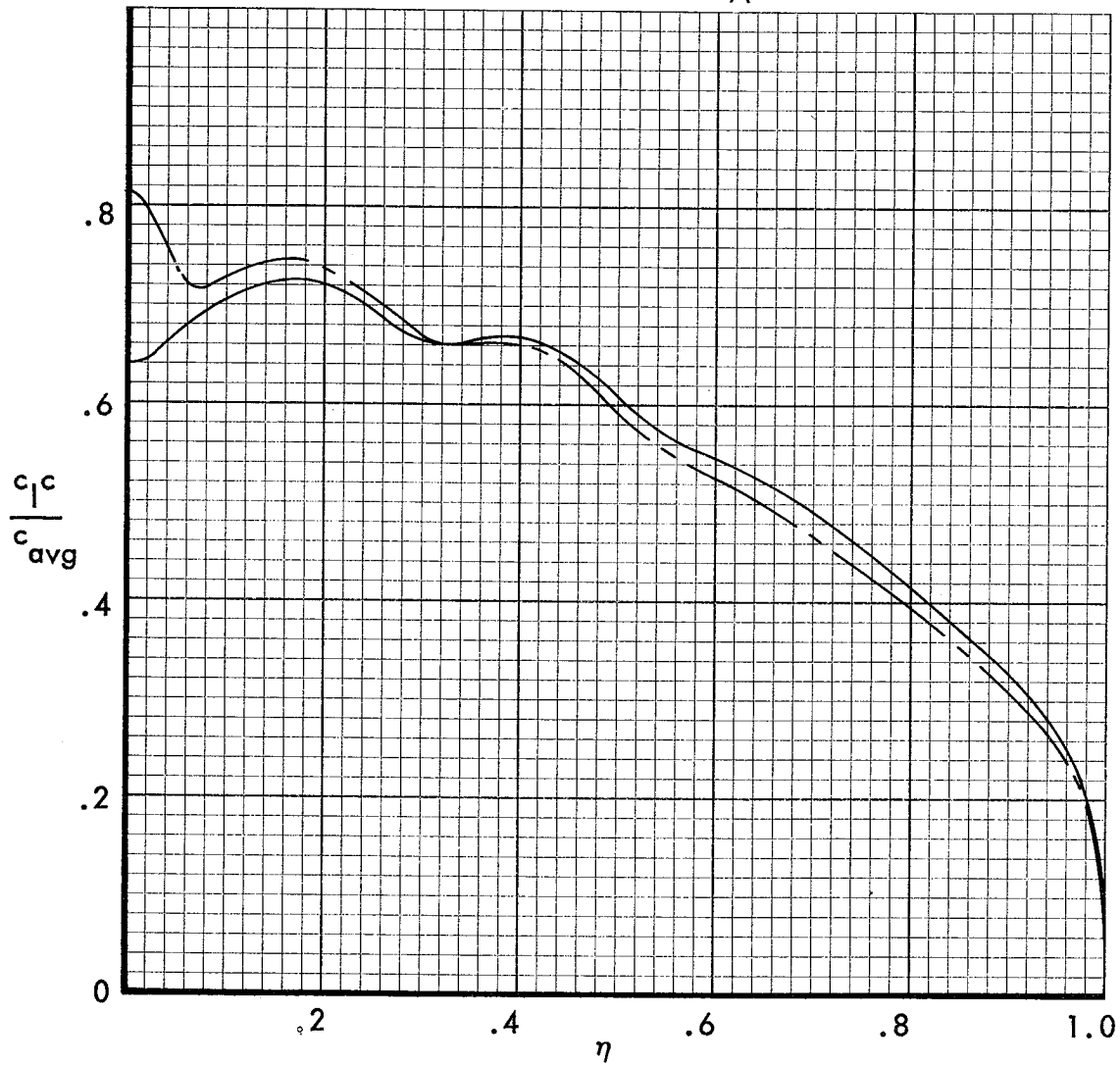
(e) Flight number 119-8.6.

Figure 33.- Continued.
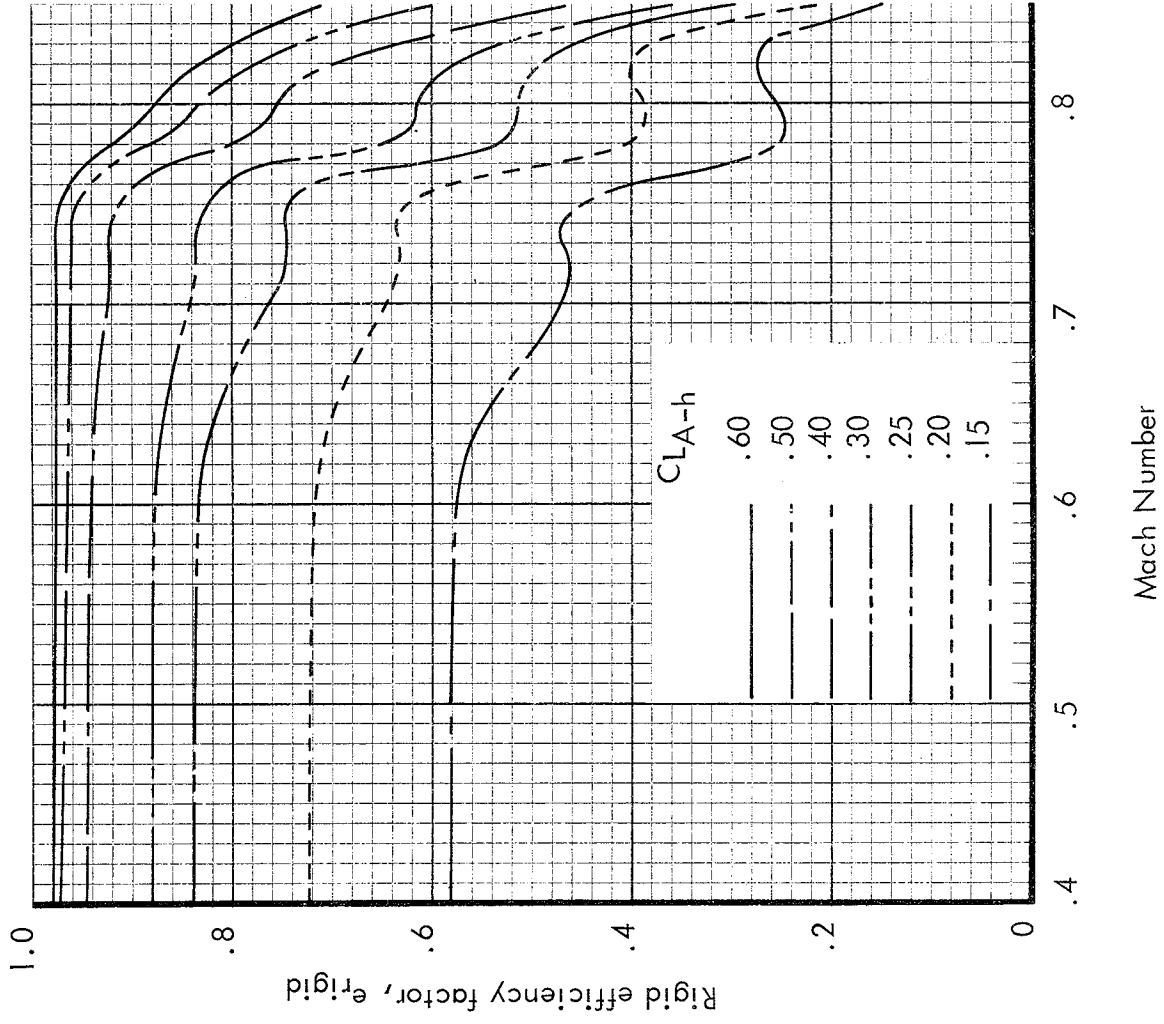
(a) Constant lift coefficient

Figure 34.- Rigid efficiency factor
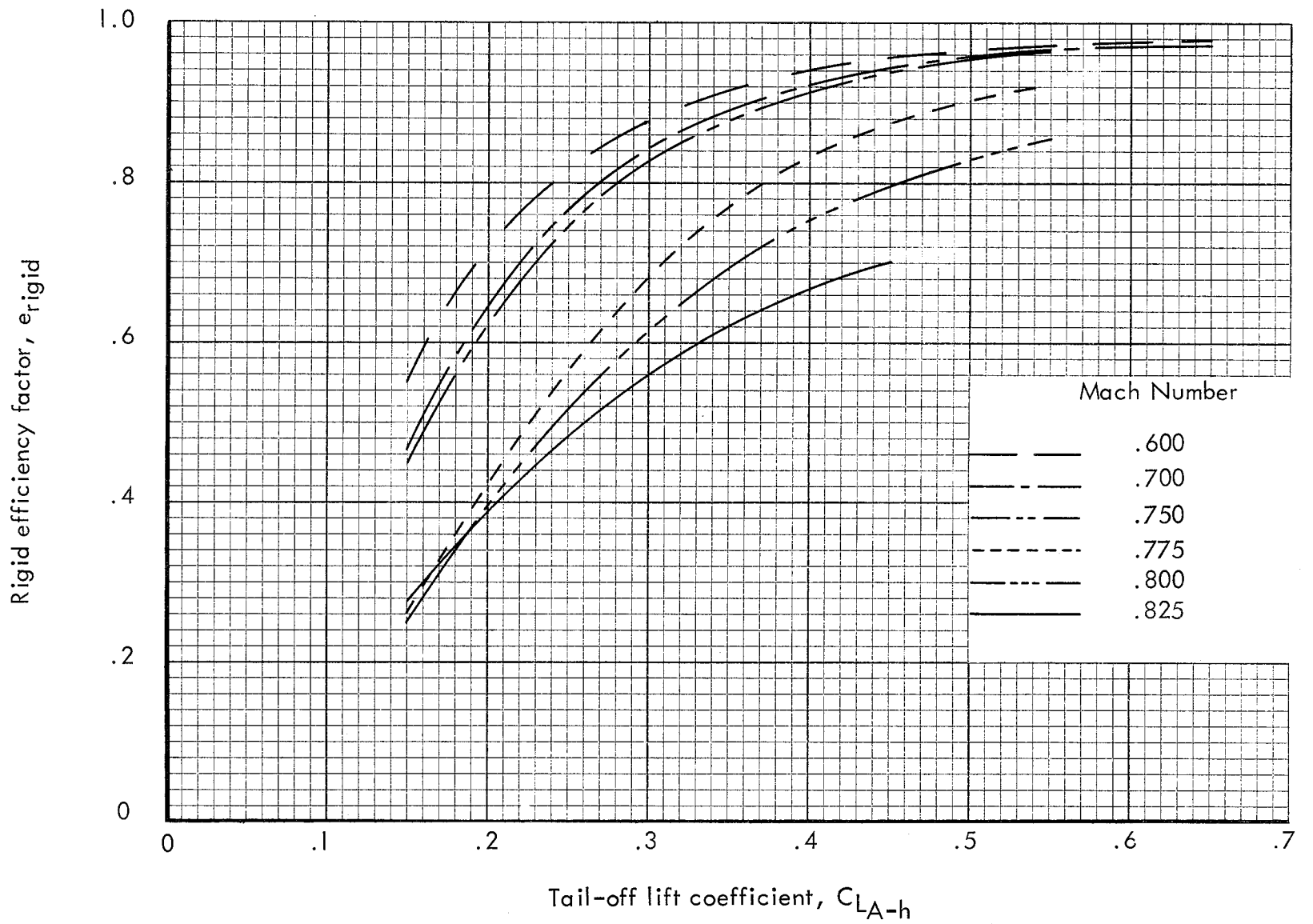
(b) Constant Mach Number.

Figure 34.- Continued
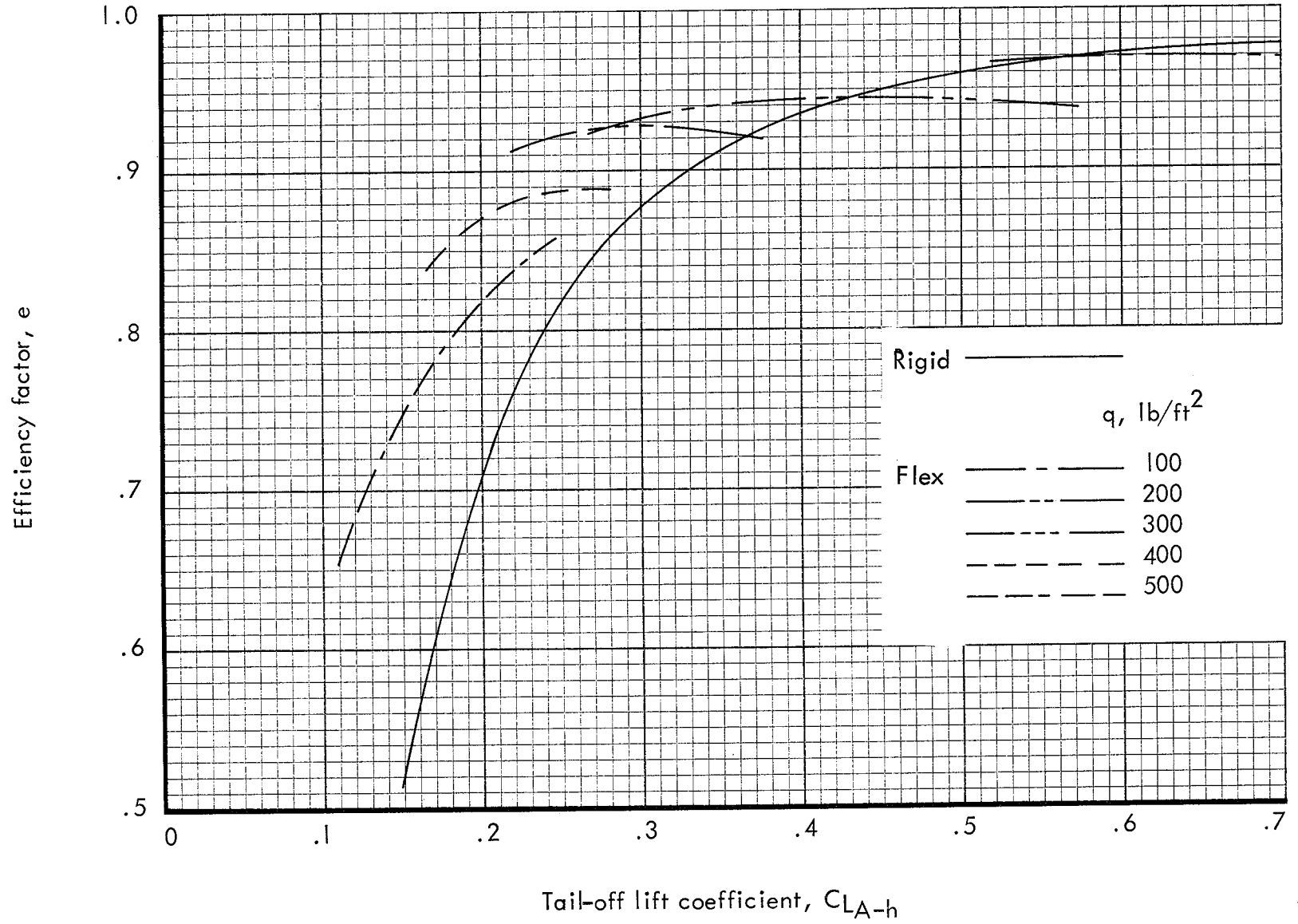
Figure 35.- Effect of dynamic pressure on efficiency
factor at M = 0.6.
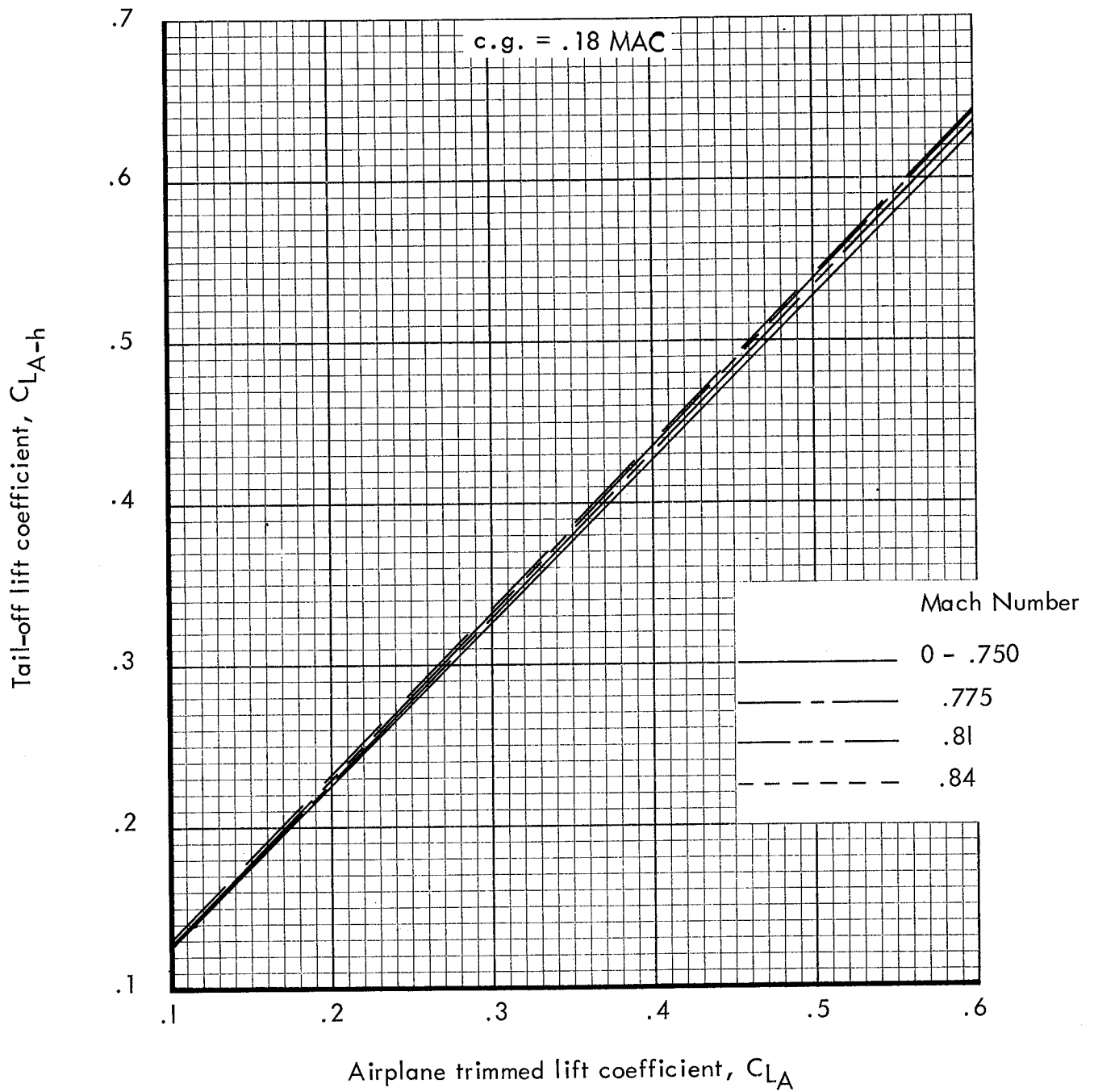
Figure 37.- Rigid tail-off lift coefficient variation
with trimmed lift coefficient and Mach
Number for c.g. = 0.18 MAC.
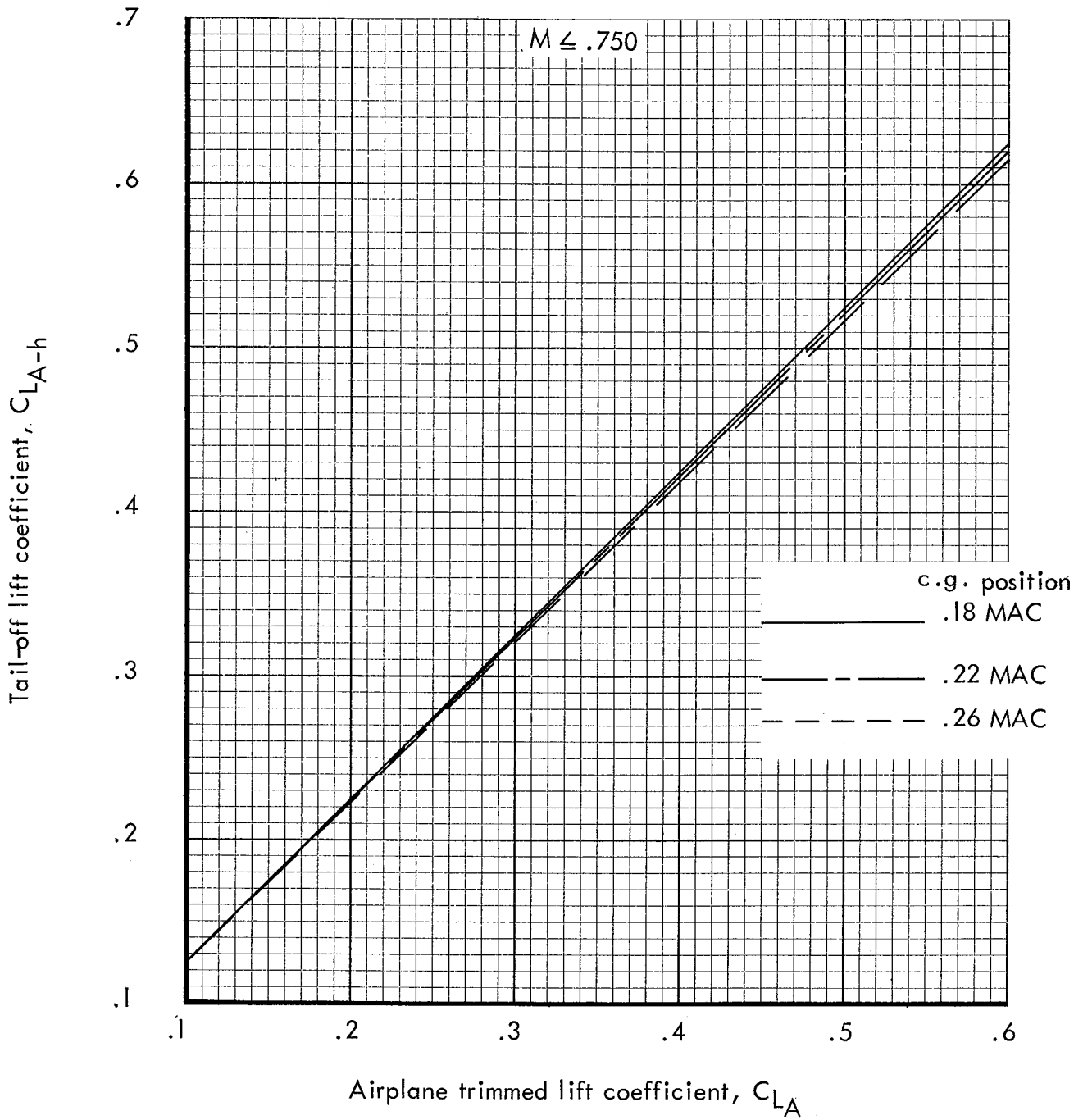
Figure 38.- Effect of trim c.g. position on tail-off lift coefficient.
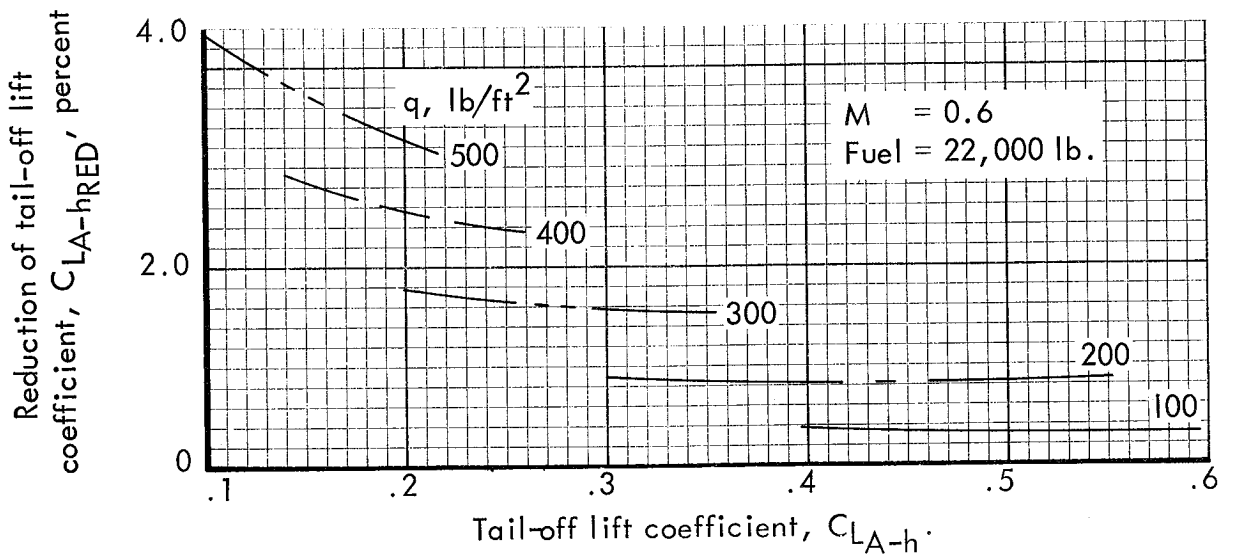
(a) Reduction of $C_{L_{A-h}}$ at $M = 0.6$ and low fuel.

Figure 39.- Effect of flexibility on tail-off lift coefficient.
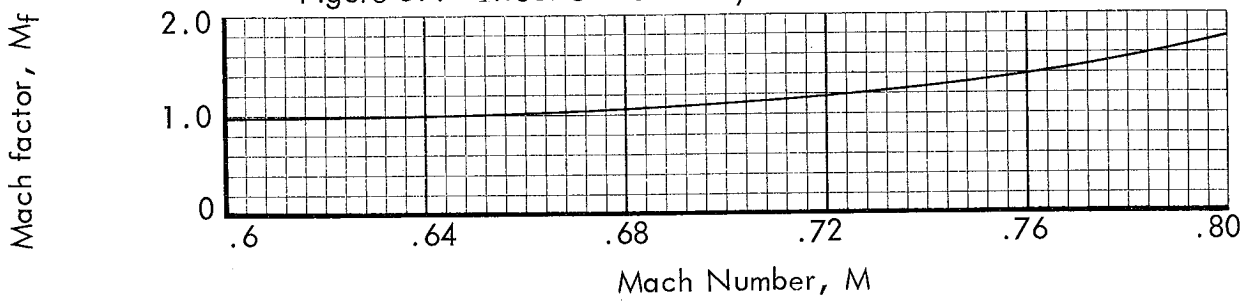
(b) Mach Number effect on percent reduction.

Figure 39.- Continued.
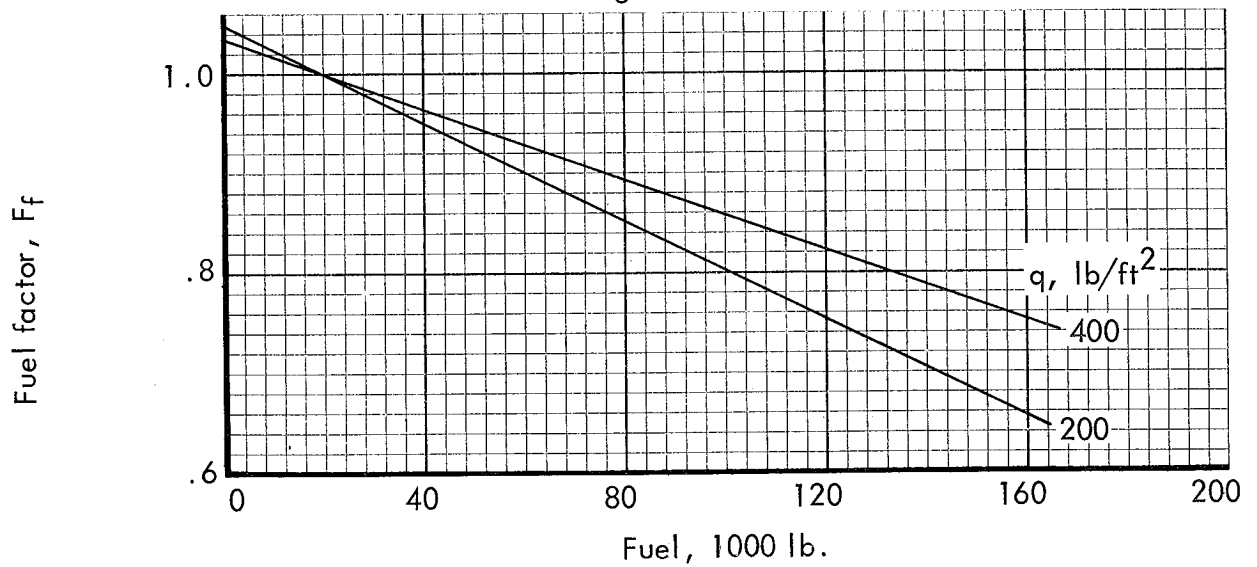
(c) Effect of fuel load on percent reduction.

Figure 39.- Continued.
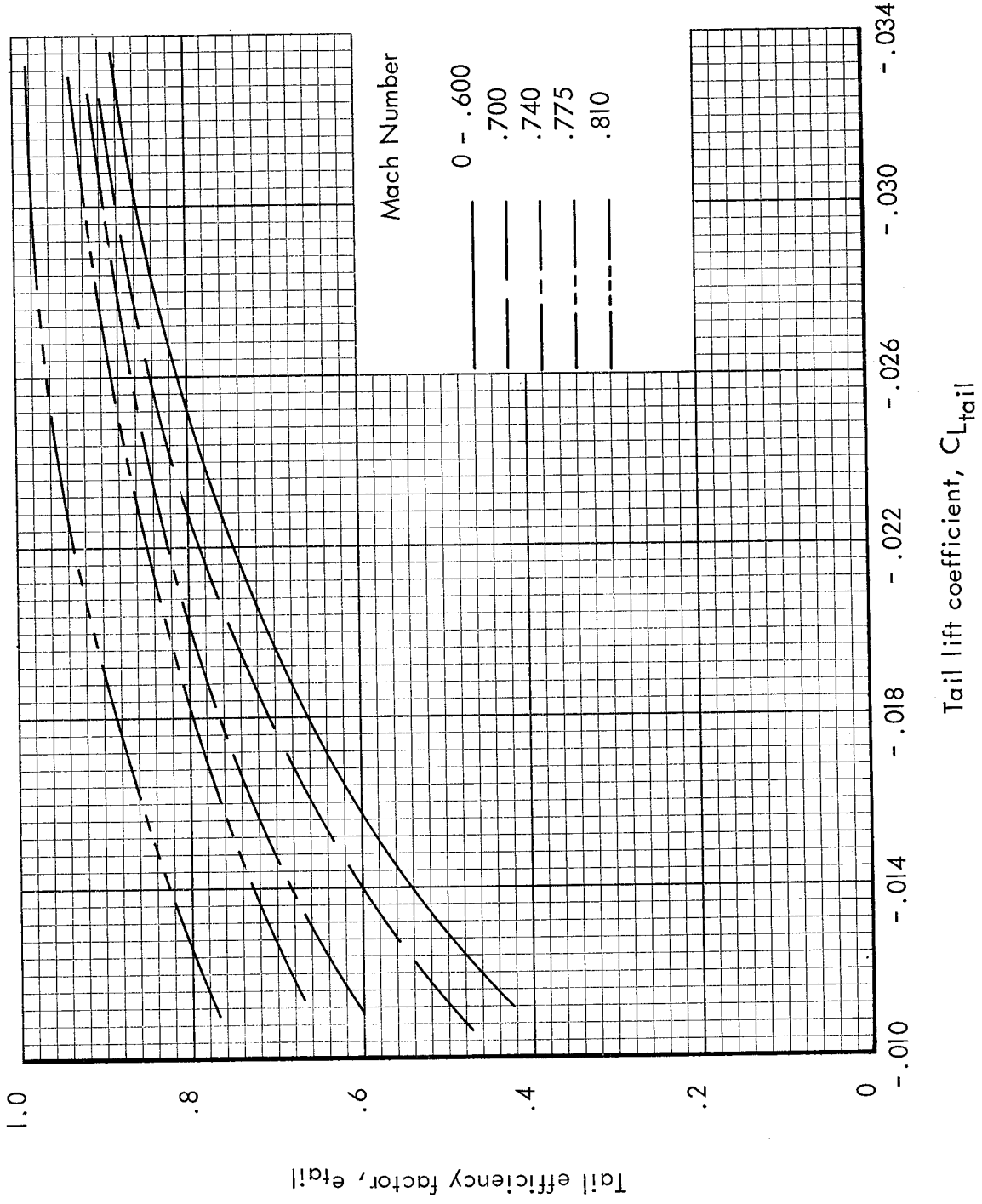
Figure 40. - Horizontal tail efficiency factor.

129
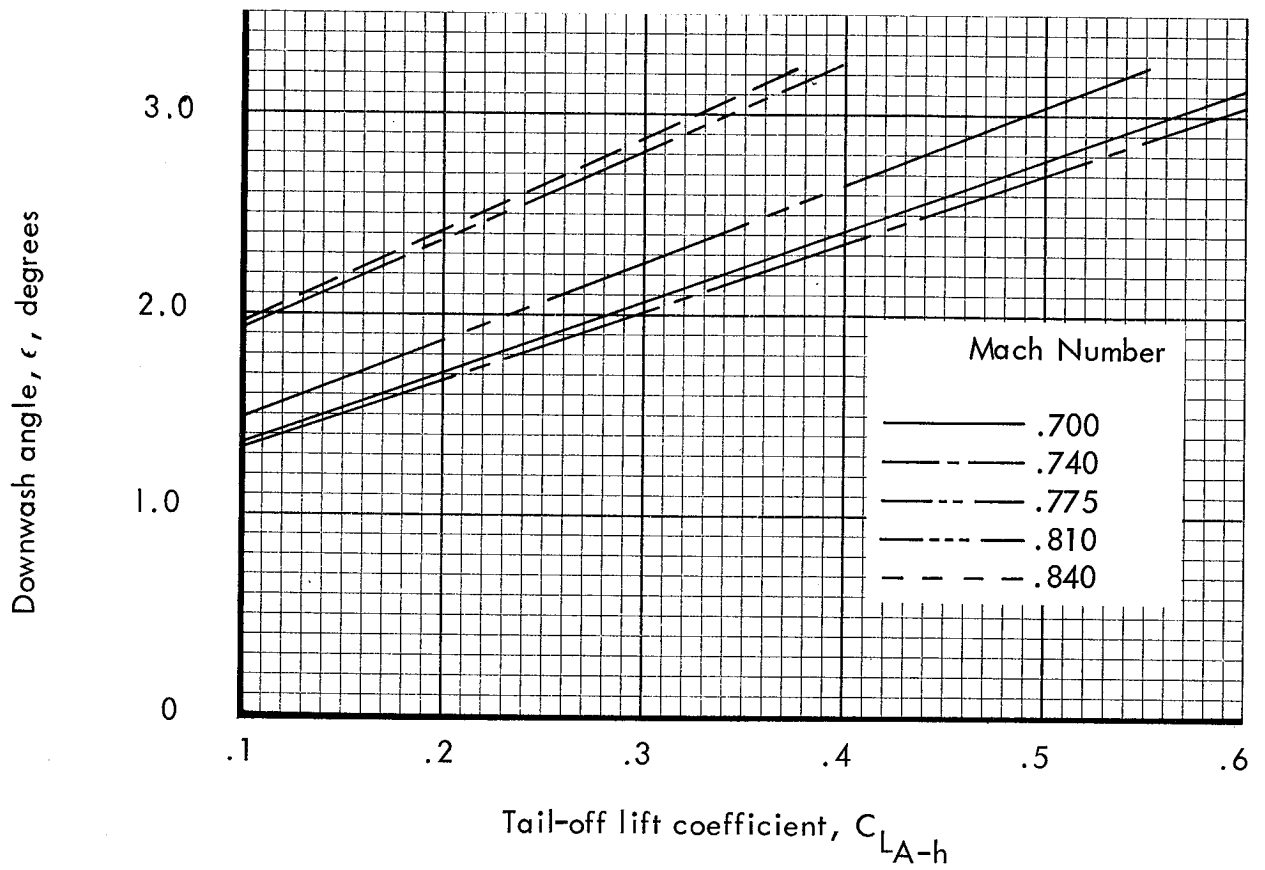
Figure 41.- Downwash angle at the tail for the rigid configuration.
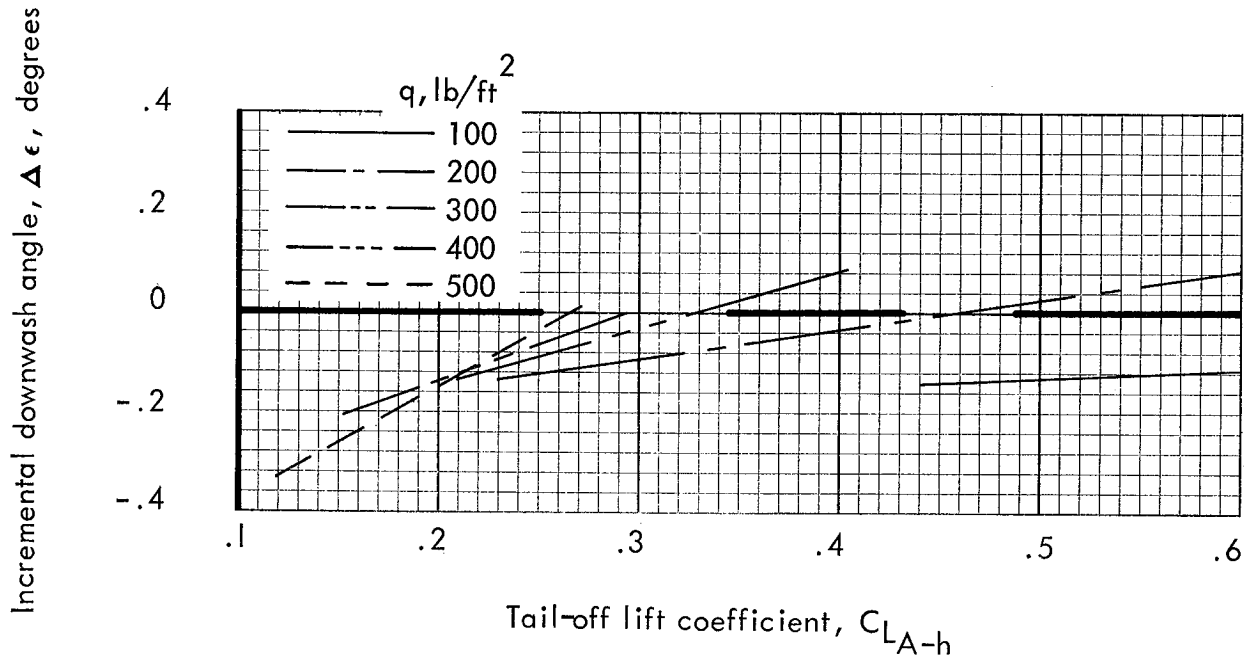
Figure 42.- Effect of flexibility on the downwash angle.
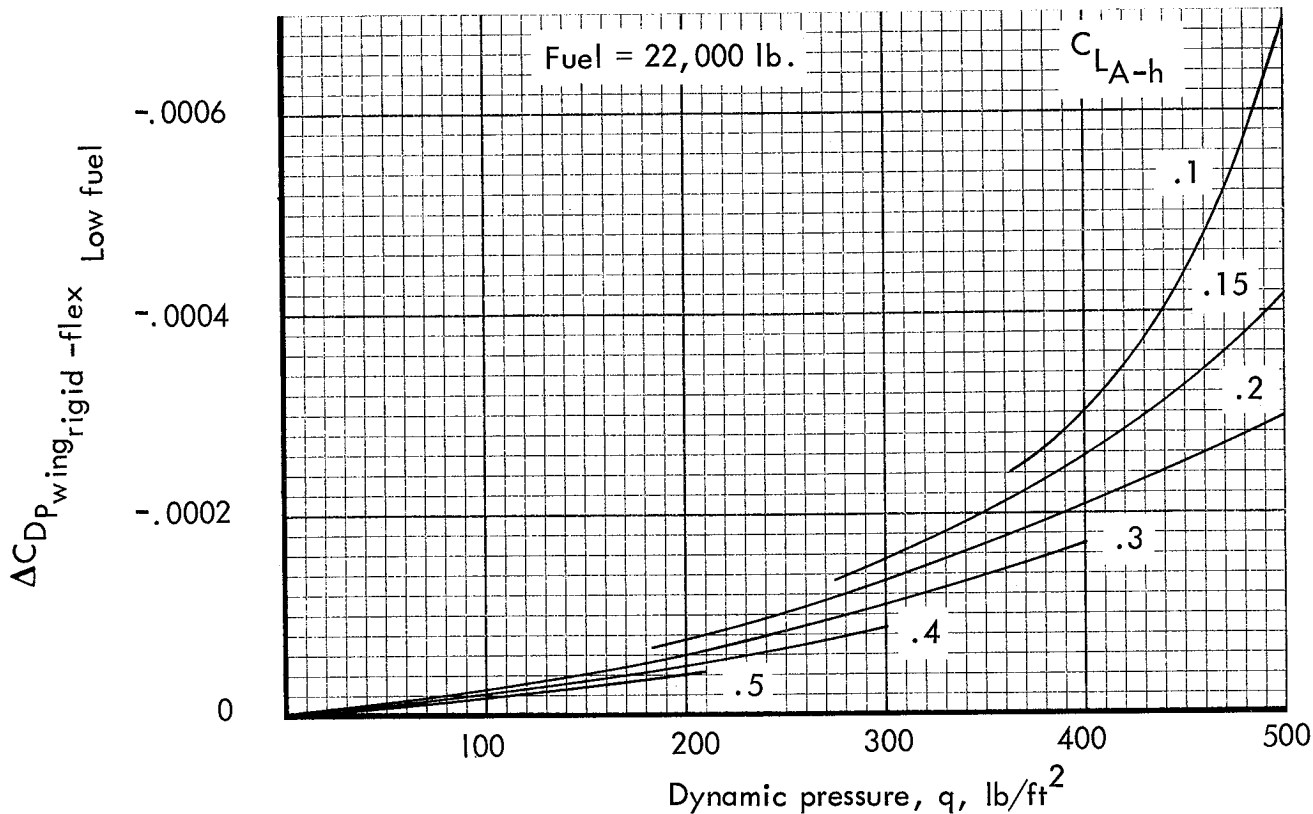
(a) Effect at low fuel.

Figure 43.- Wing profile drag increment due to aeroelastic distortion.
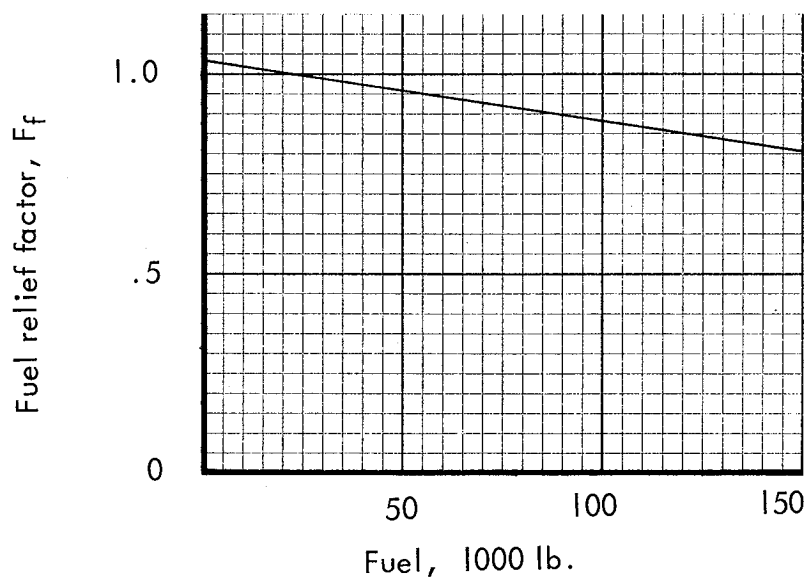
(b) Relief factor due to fuel load.

Figure 43.- Continued

Conduit 1" dia.
6' long on rear
bullet

Bracket on top of
vertical tail 30%C

Angle of attack vanes

Trailing cone
with 36' cable

Line of vortex generators

Spin chute installation

Stall strip

Skegs (on ramp door)

Nose
Boom

Temperature
probe (along
B.L.O)

T.O.L. Camera
(along B.L.O)

Additional items:

Water ballast drain holes
Closure plate on petal door
Micro switch on fuel drain mast
External straps

Figure 44.- Flight test instrumentation.
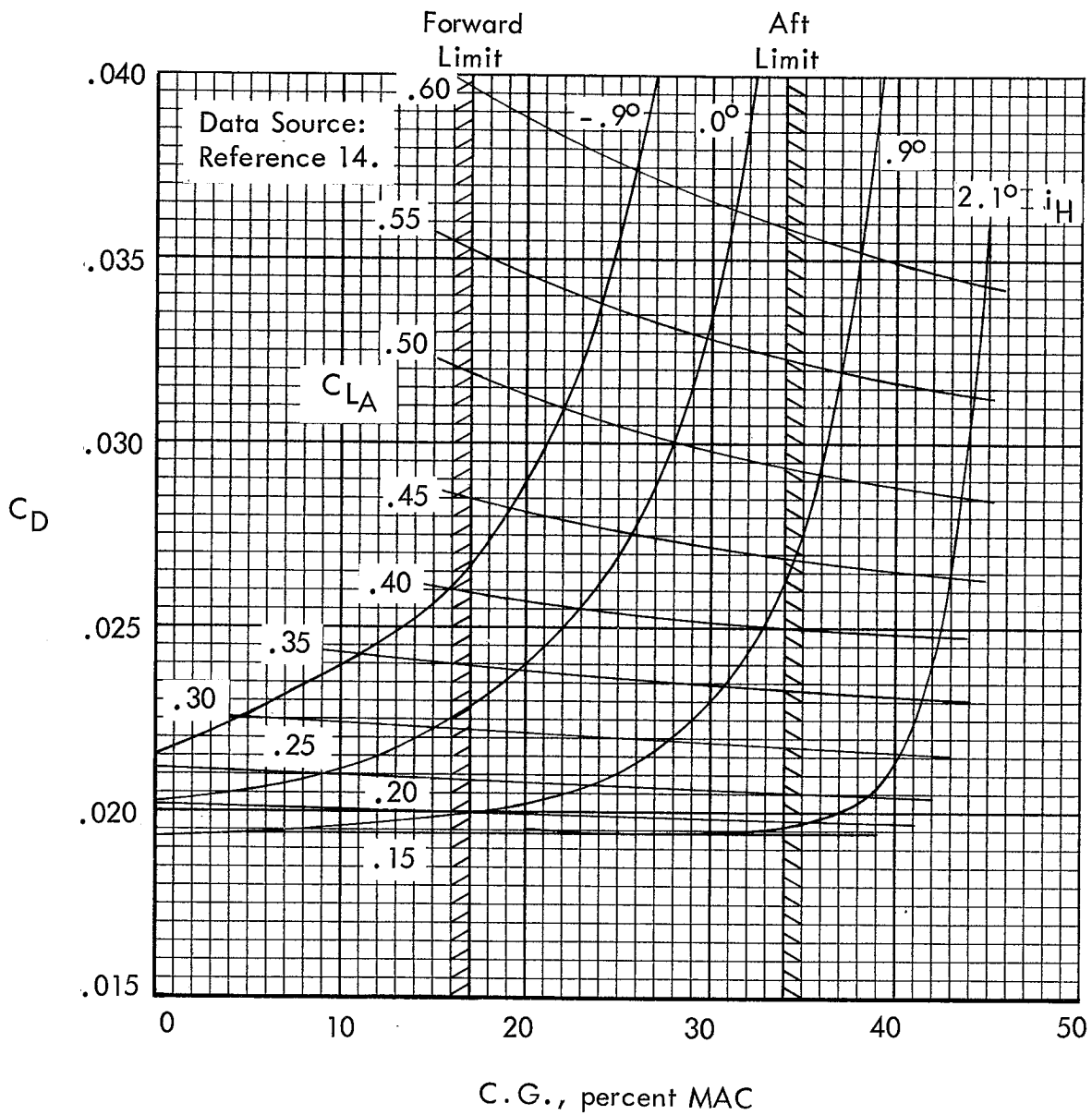
Figure 45.— Effect of center of gravity location on trimmed cruise drag based on wind tunnel data.
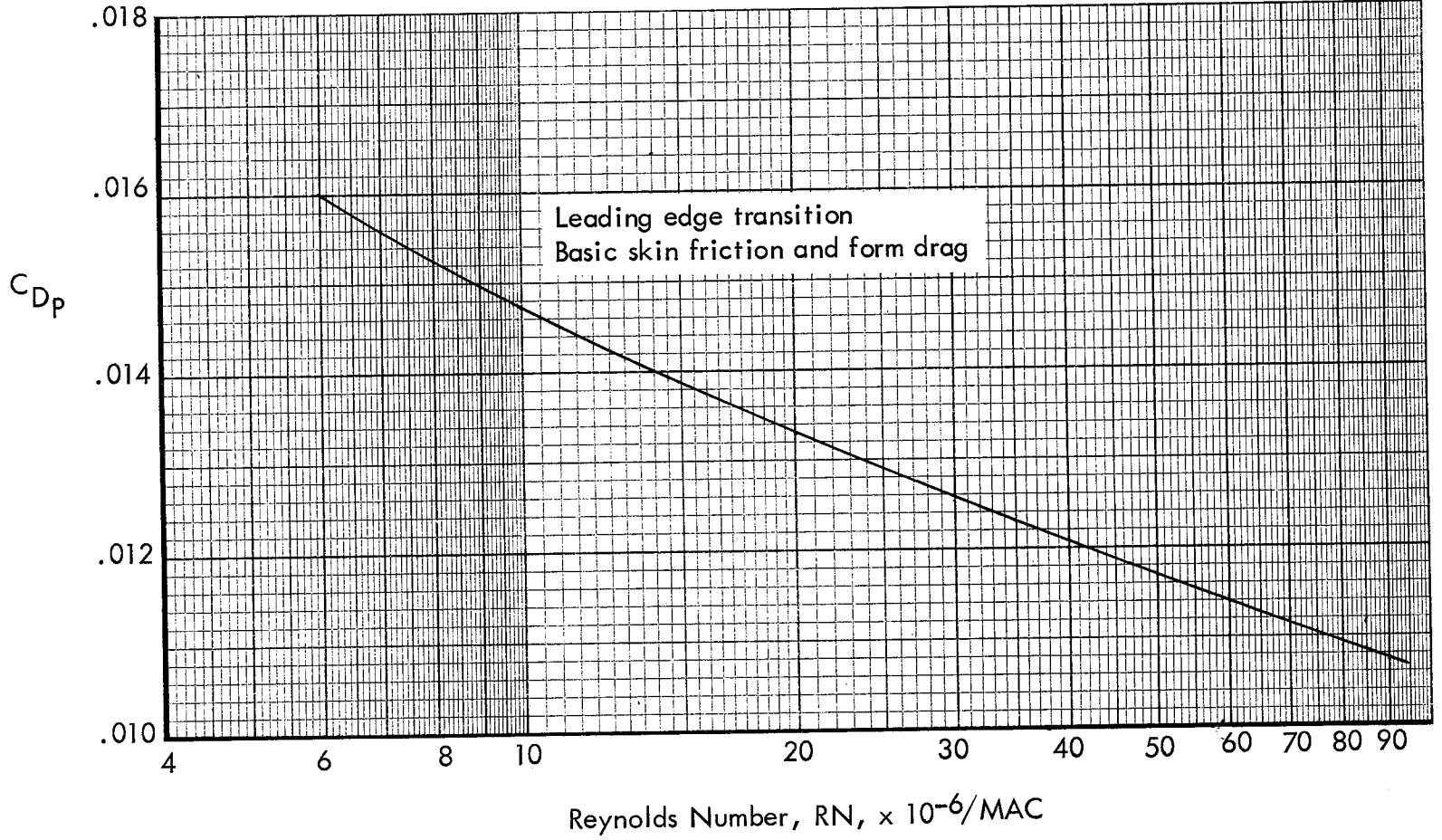
Figure 46.- Estimated C-141A profile drag variation with Reynolds Number.
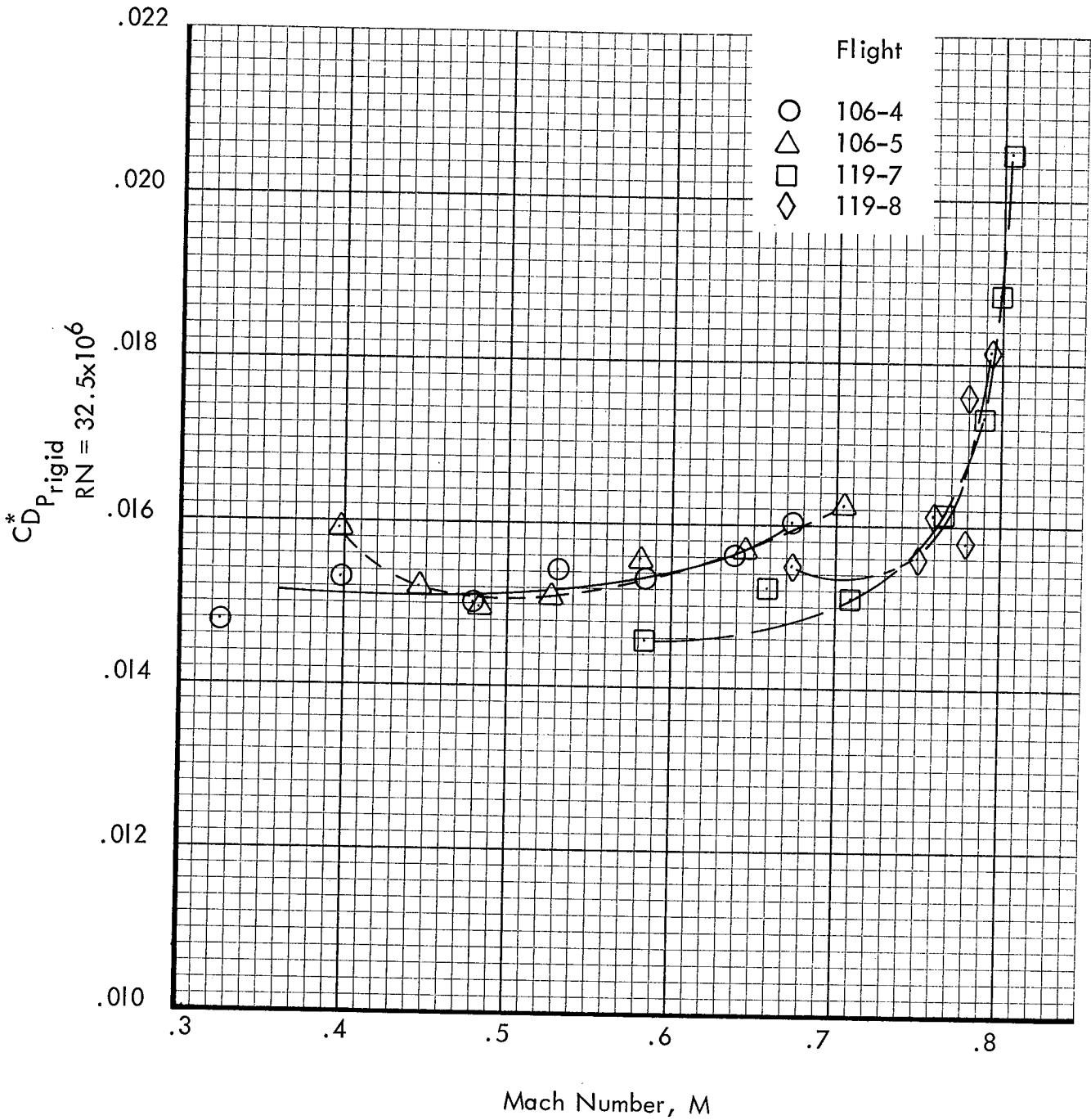
Mach Number, M

(a) Flights 106-4, 106-5, 119-7, 119-8.

Figure 47.- Profile drag variation with Mach Number.
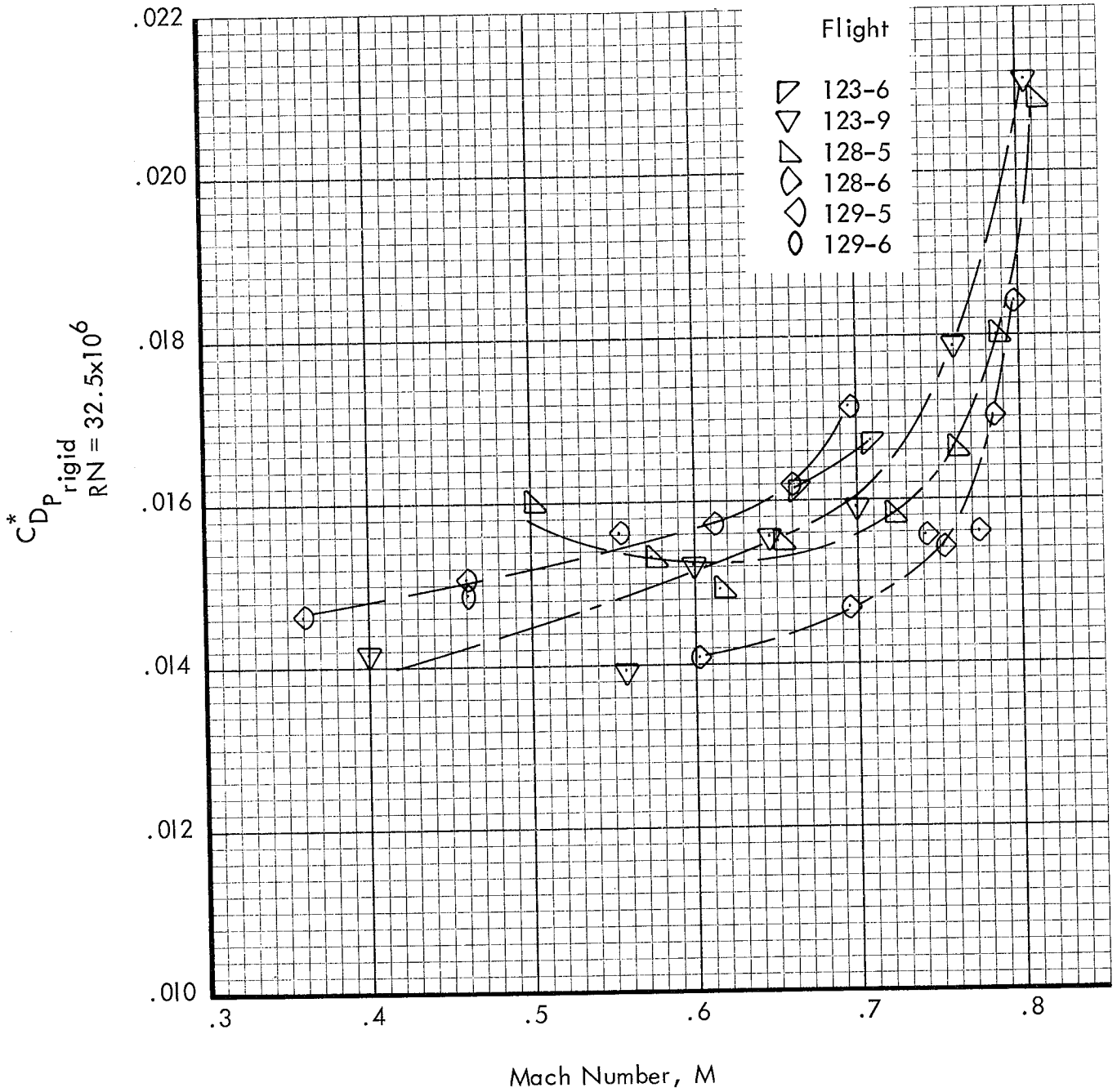
(b) Flights 123-6, 123-9, 128-5, 128-6, 129-5, and 129-6

Figure 47.- Continued
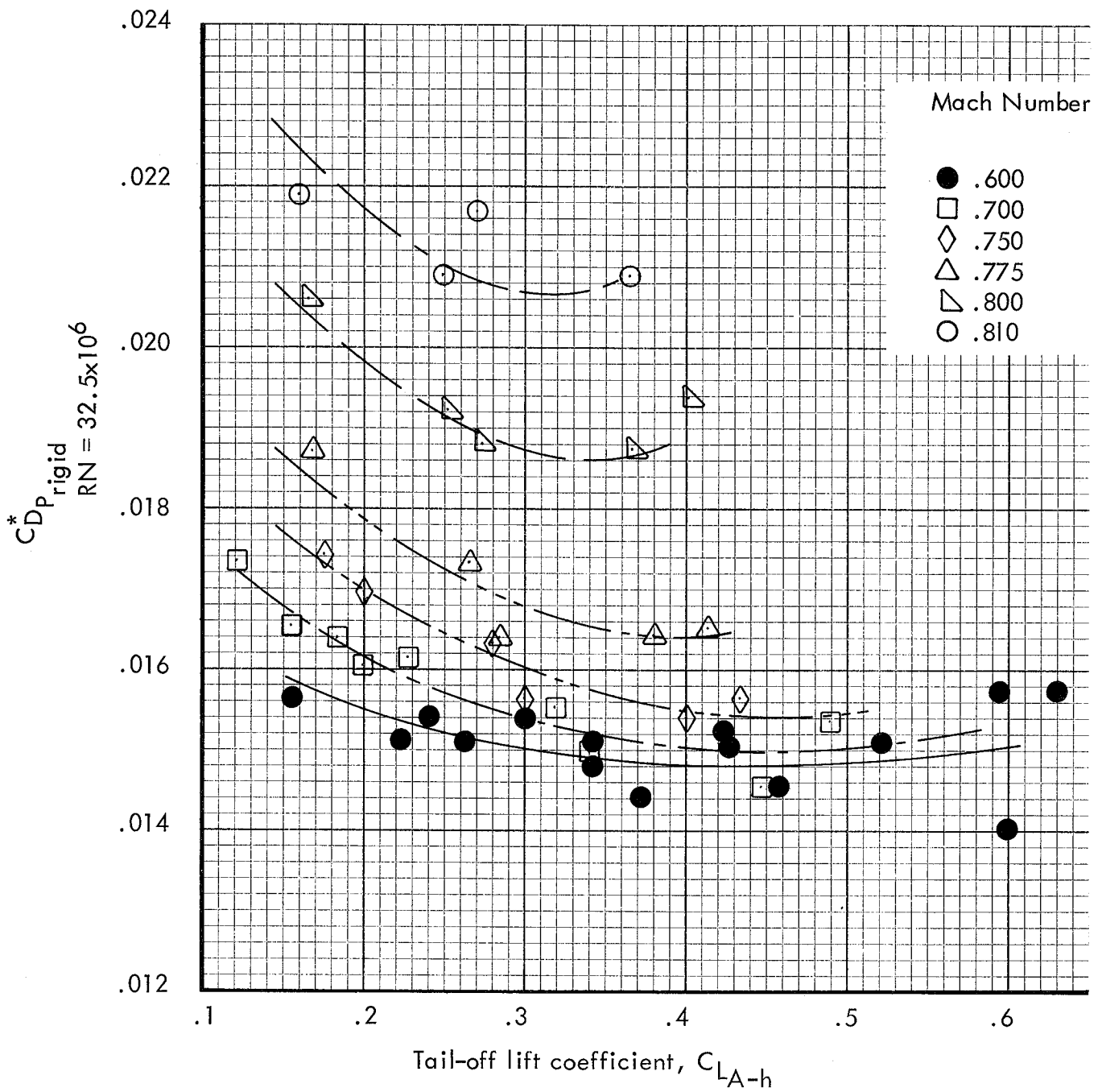
Figure 48.– Profile drag variation with lift coefficient at constant Mach Numbers.
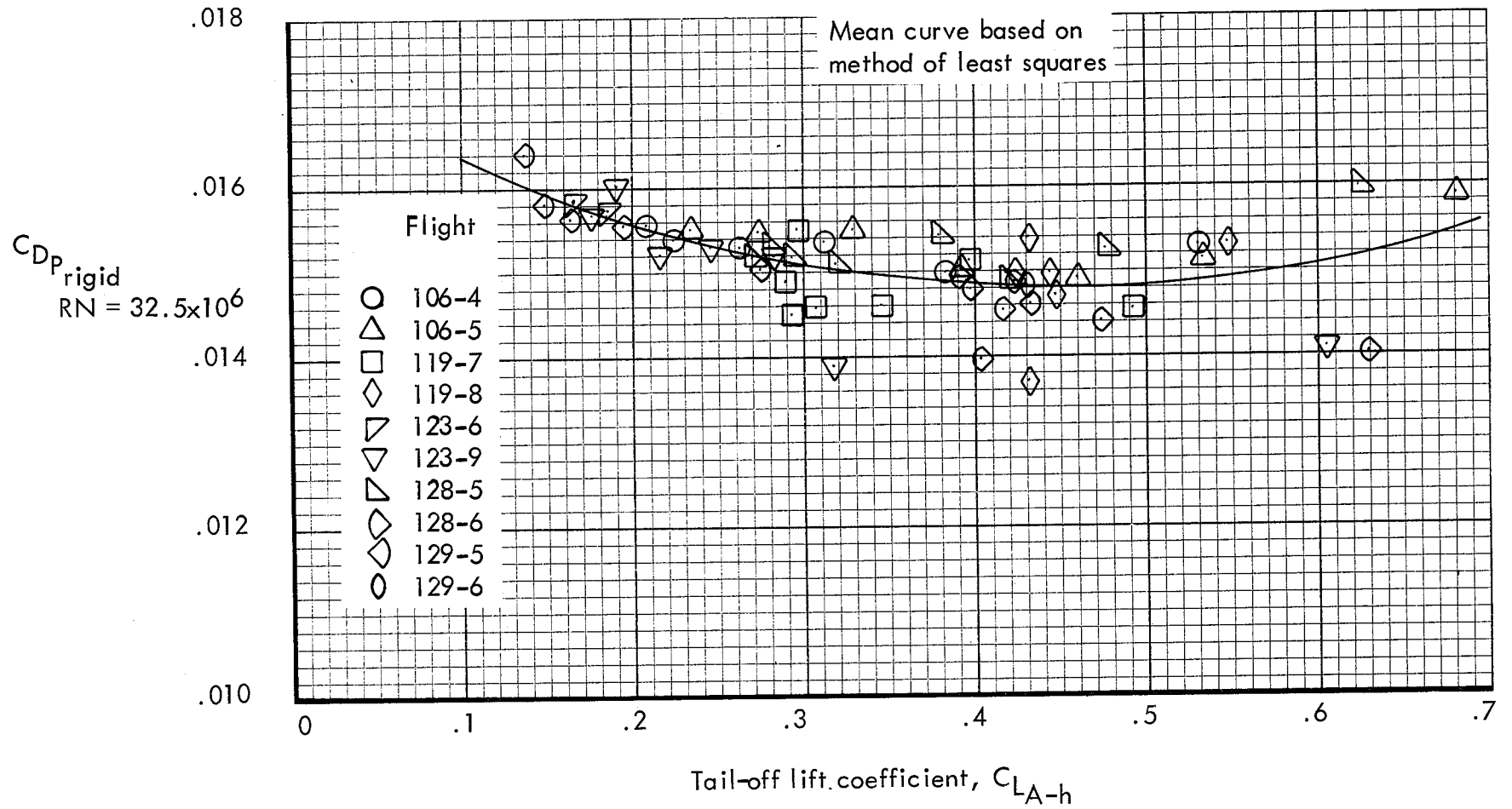
Figure 49.- Profile drag coefficient variation with tail off lift coefficient.
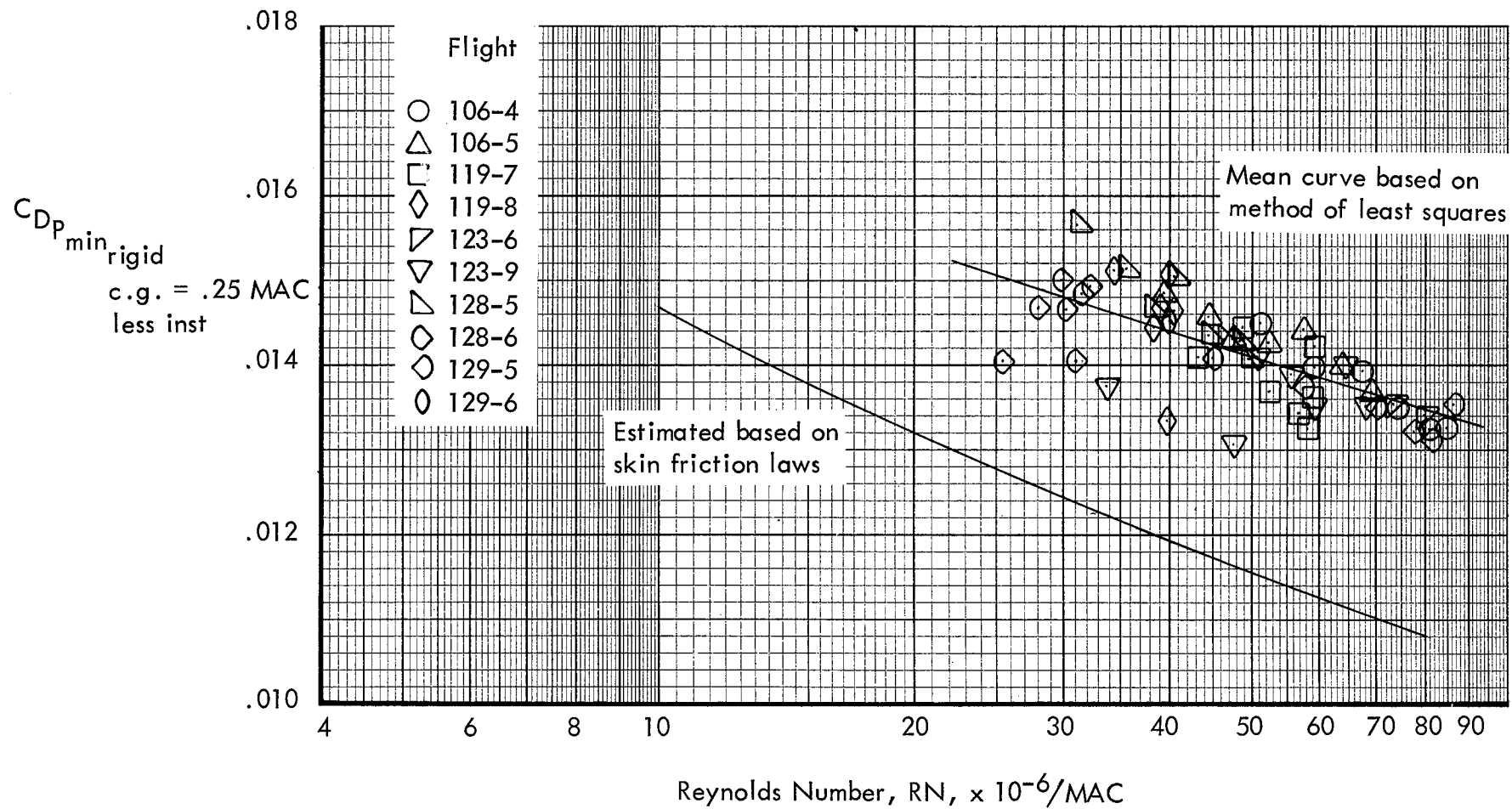
(a) Speed power flights.

Figure 50.- Minimum profile drag coefficient variation with Reynolds Number.
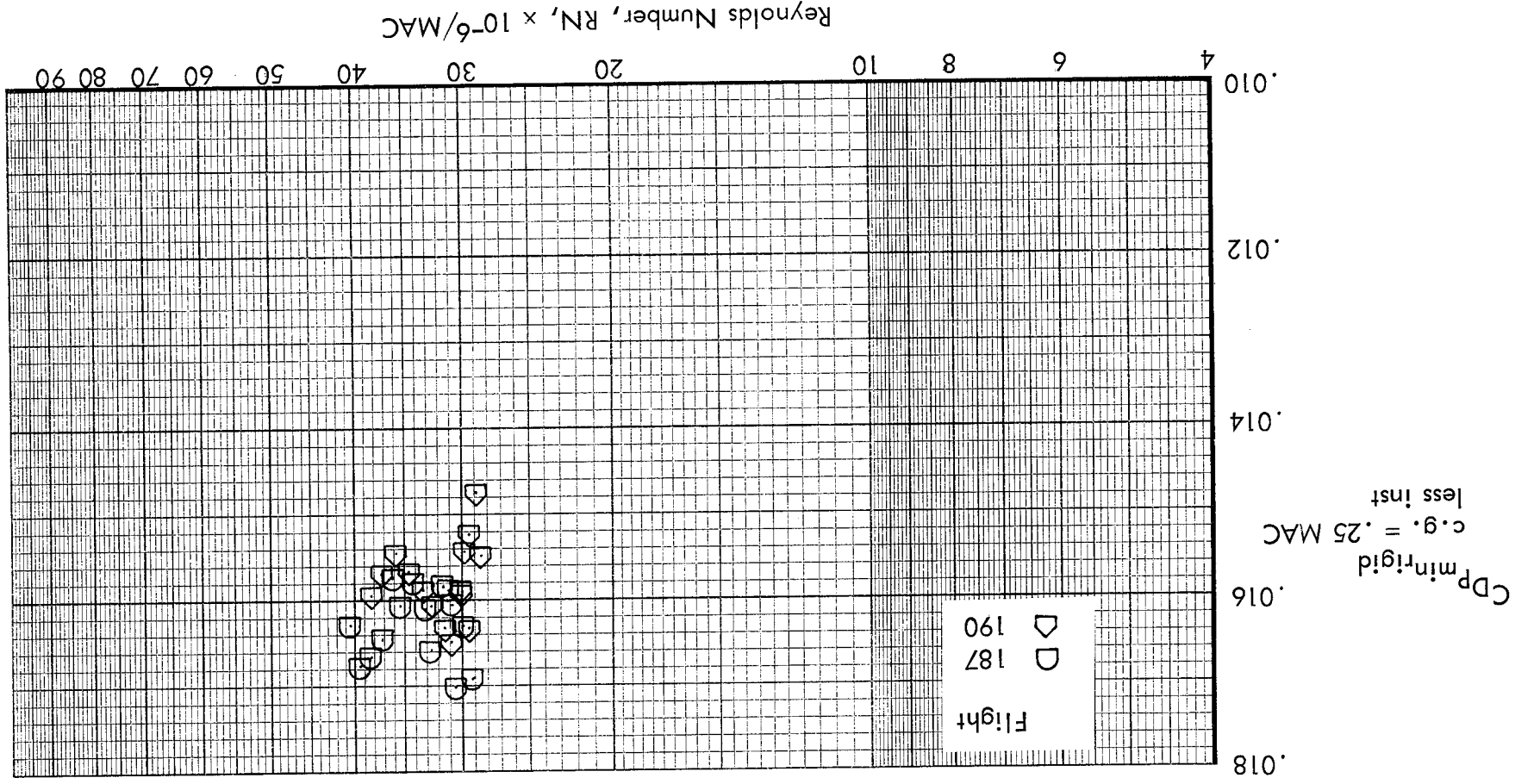
(b) Cruise portion of range mission flights.

Figure 50.- Continued.
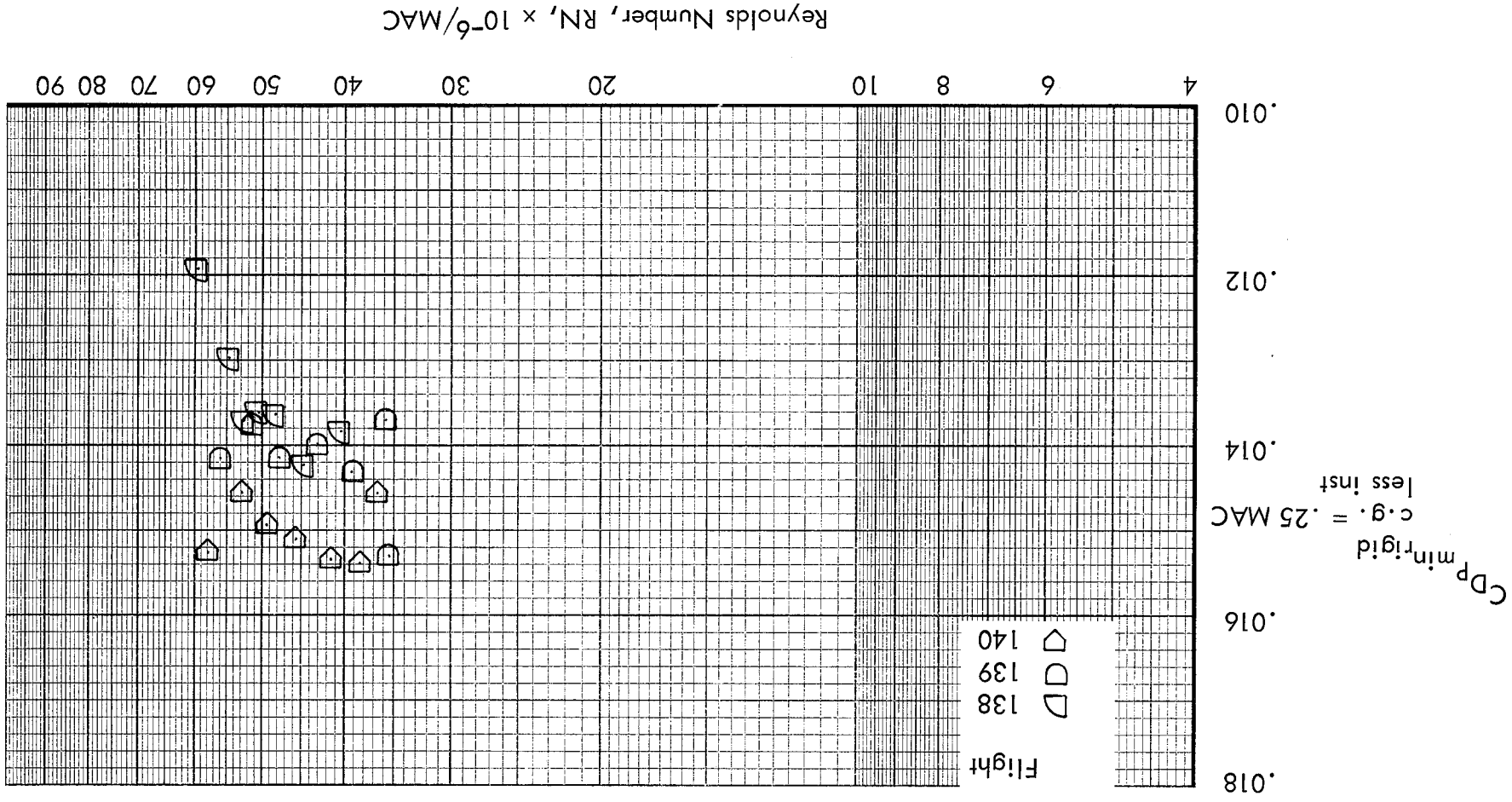
(c) Continuous climb flights.

Figure 50.- Continued.
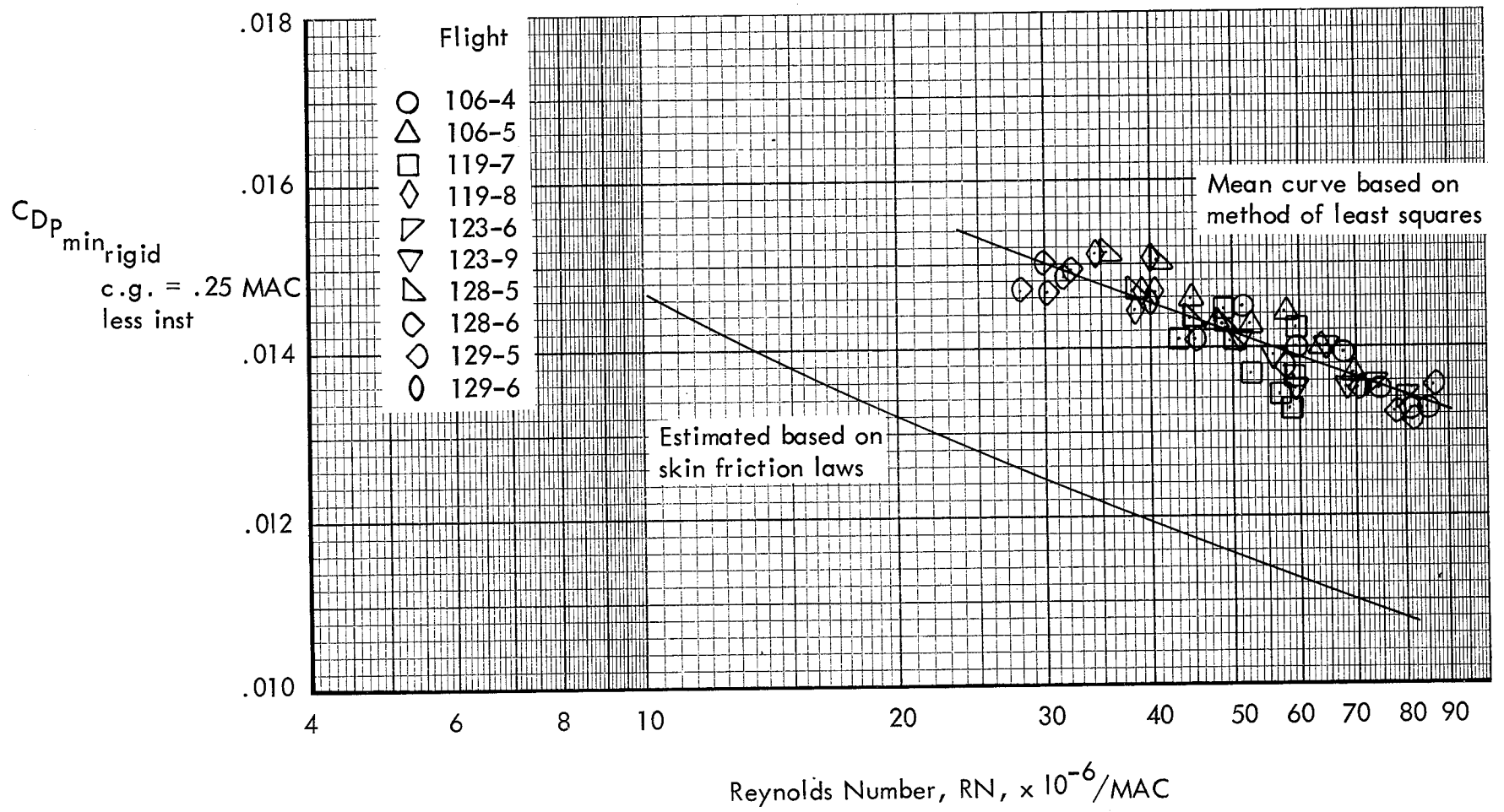
Figure 51.- Minimum profile drag coefficient variation with Reynolds Number after eliminating high C_L test points and obvious wild scatter.
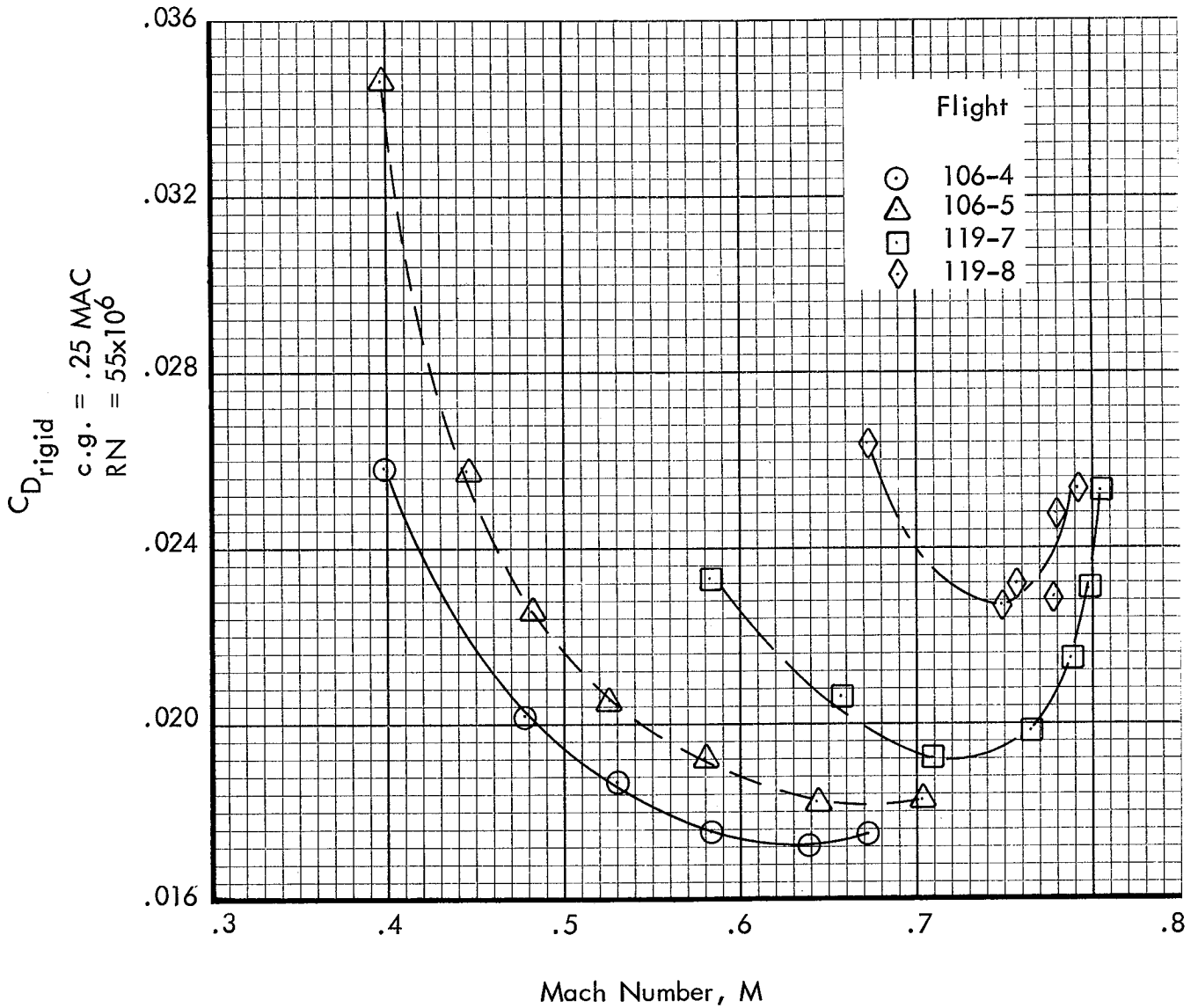
(a) Flights 106-4, 106-5, 119-7, 119-8

Figure 52. – Flight test drag coefficient variation with Mach Number.

$RN = 55.0 \times 10^6$ based on MAC

Rigid

y-axis: $C_{D_{rigid}}$ c.g. = .25 MAC   less inst $RN = 55 \times 10^6$

Flight
▽ 123-6
▽ 123-9
◁ 128-5
◇ 128-6
◇ 129-5
◊ 129-6

x-axis: Mach Number, M
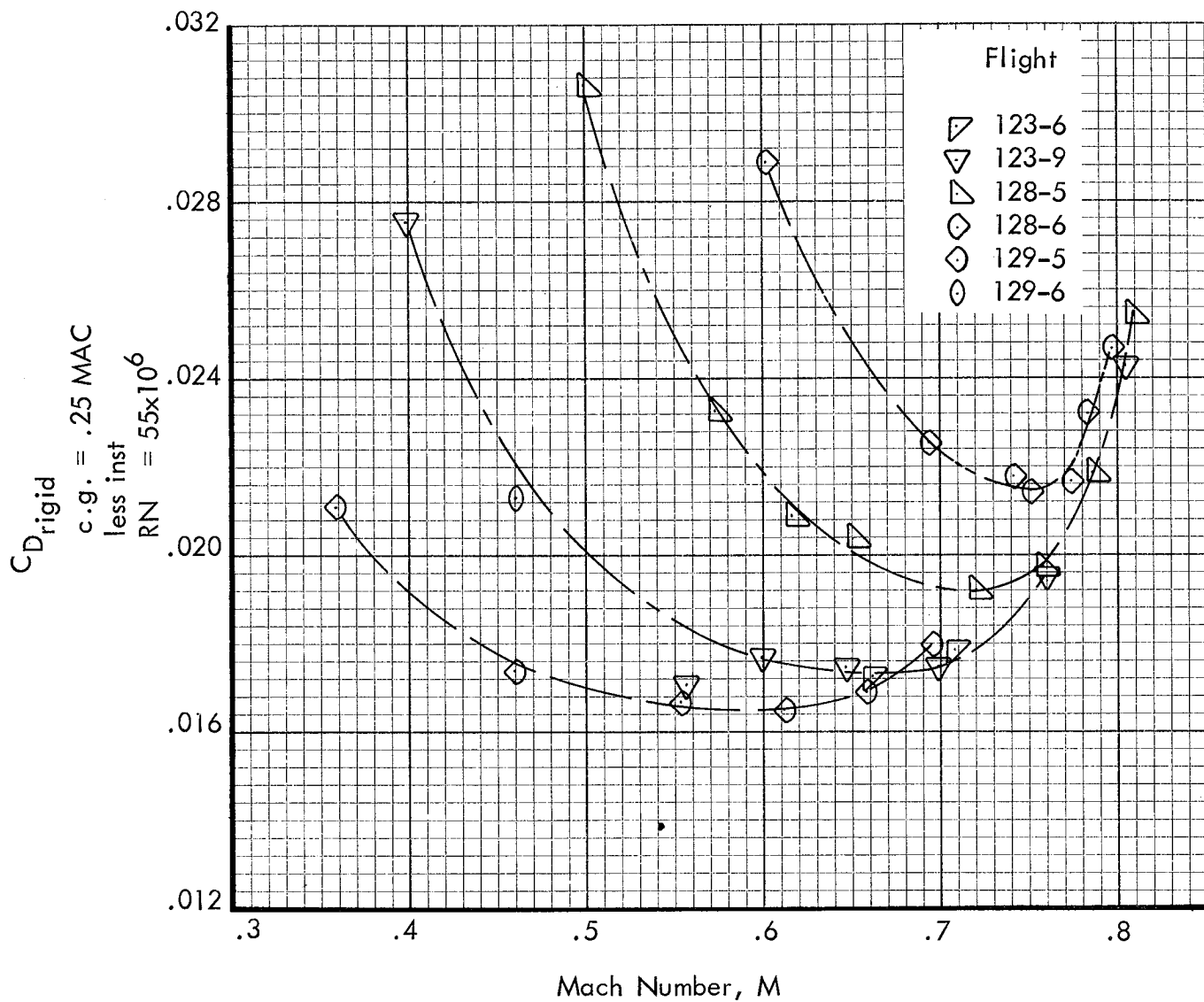
(b) Flights 123-6, 123-9, 128-5, 128-6, 129-5, 129-6

Figure 52.- Continued.

Rigid
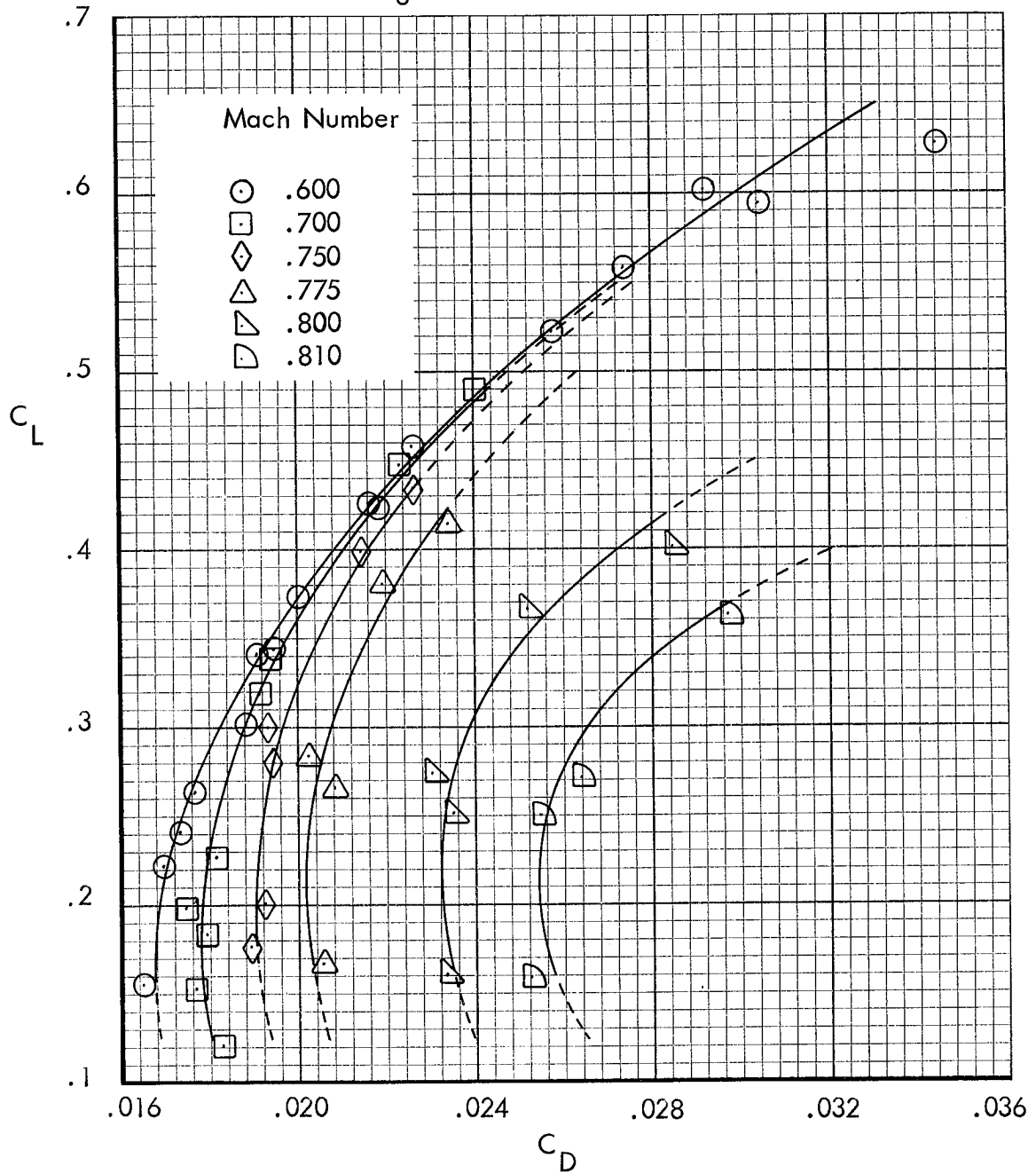
Figure 53.- Initial flight test results at constant Mach Numbers.
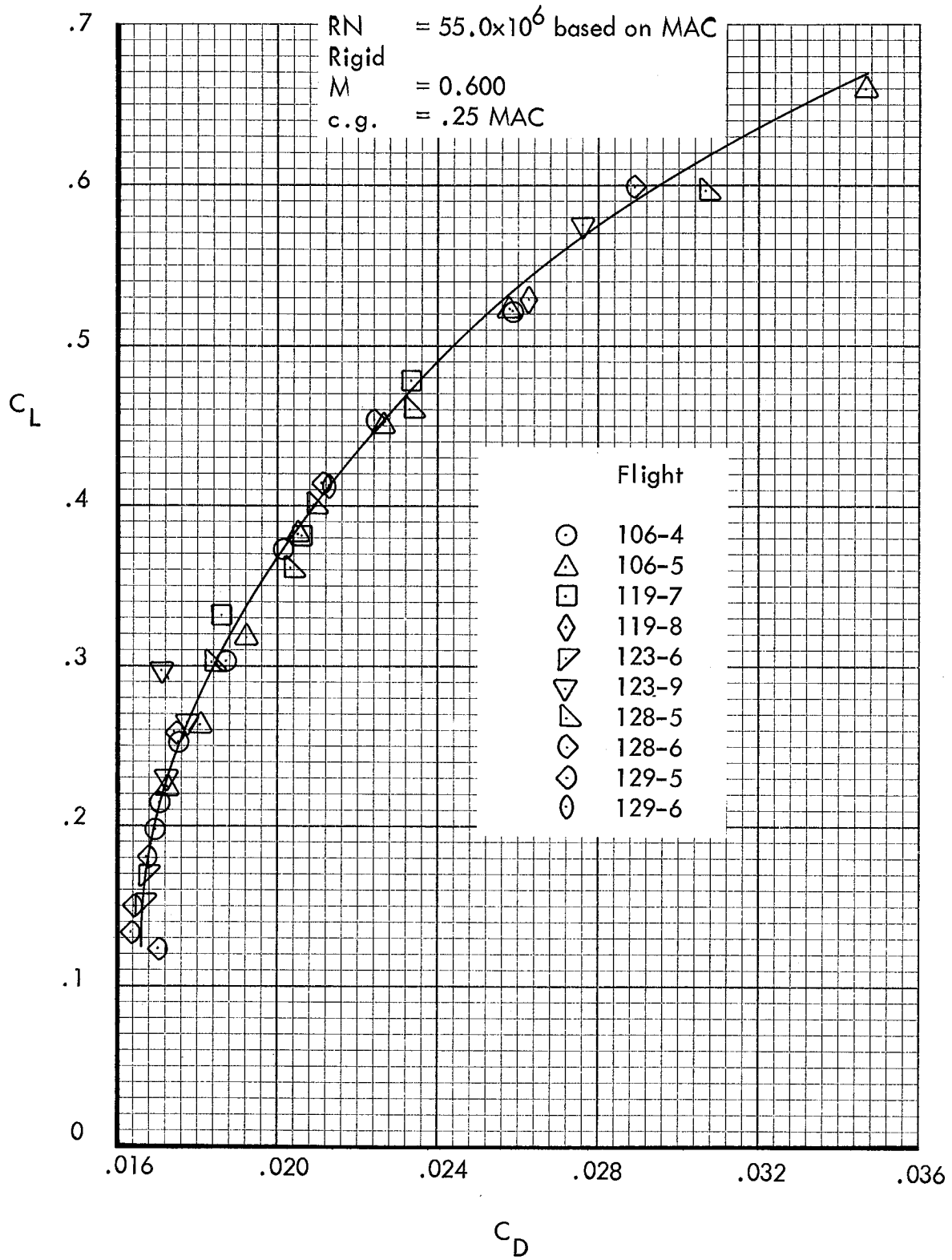
(a) M = 0.600

Figure 54.- Flight test drag polars at constant Mach Numbers.

(b) M = 0.700

Figure 54.- Continued.
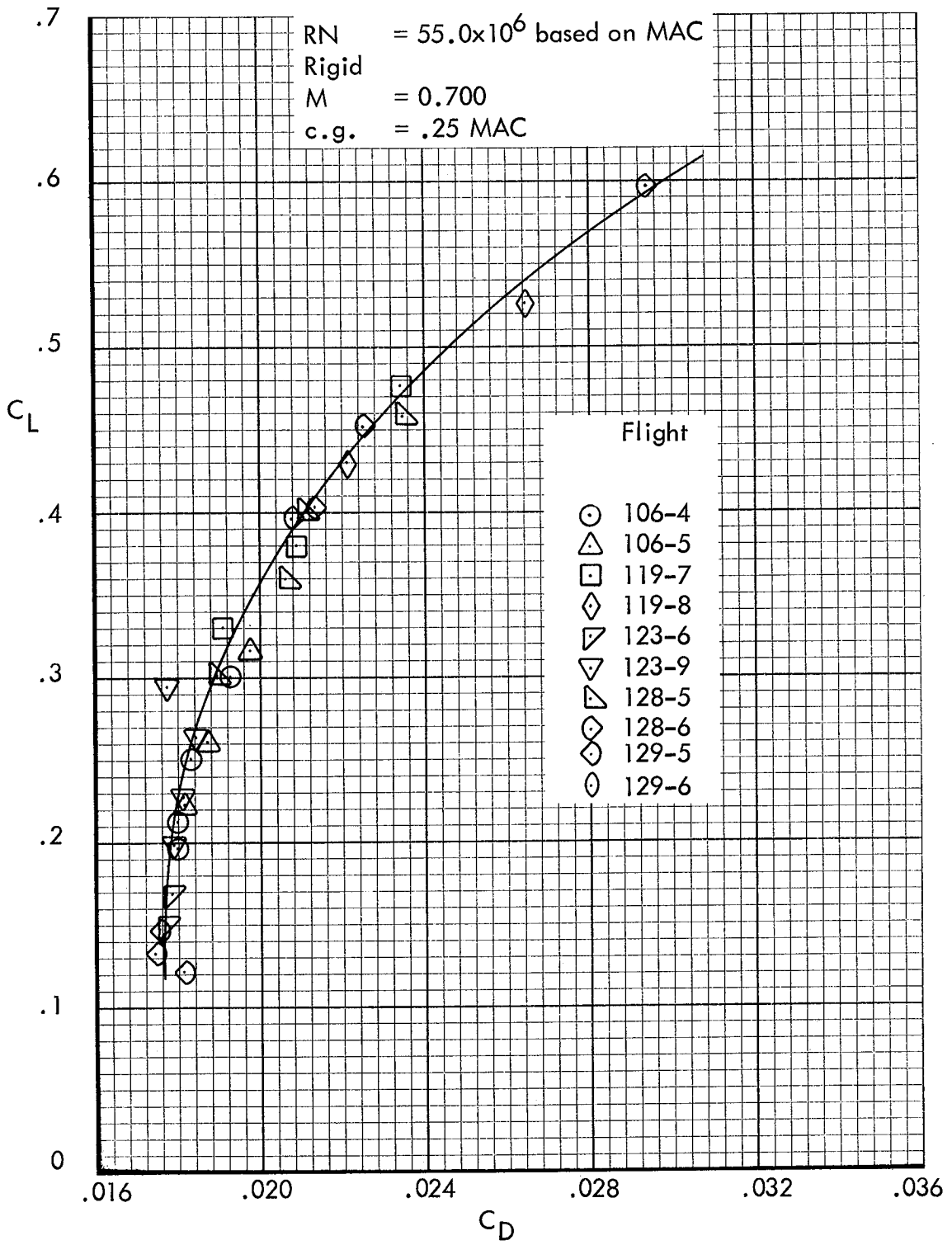
RN = 55.0x10^6 based on MAC
Rigid
M = 0.750
c.g. = .25 MAC

Flight

△ 106-5
⊡ 119-7
◇ 119-8
▽ 123-6
▽ 123-9
◁ 128-5
◊ 128-6
◇ 129-5
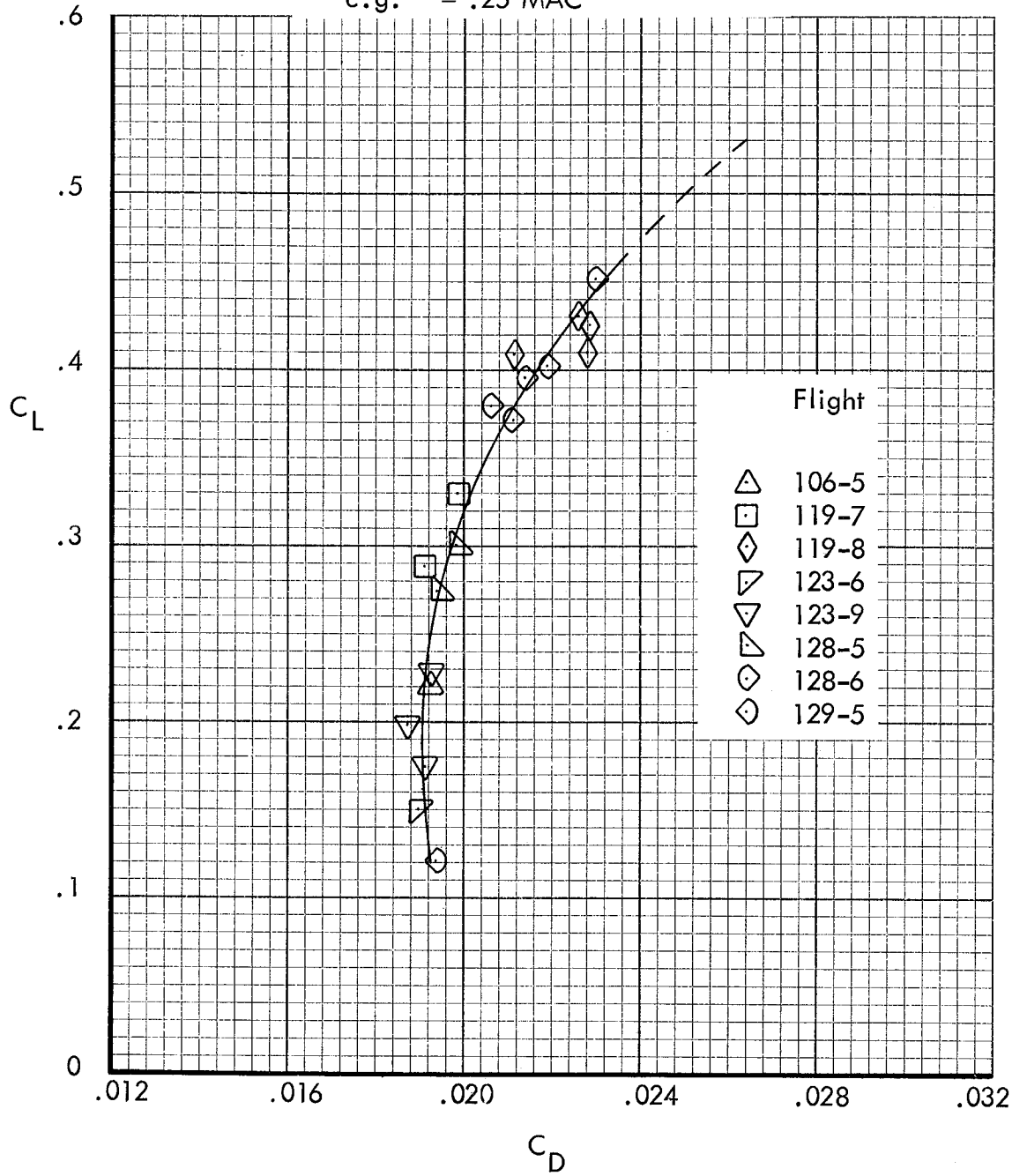
(c) M = 0.750

Figure 54.- Continued.

RN = 55.0×10^6 based on MAC
Rigid
M = 0.775
c.g. = .25 MAC
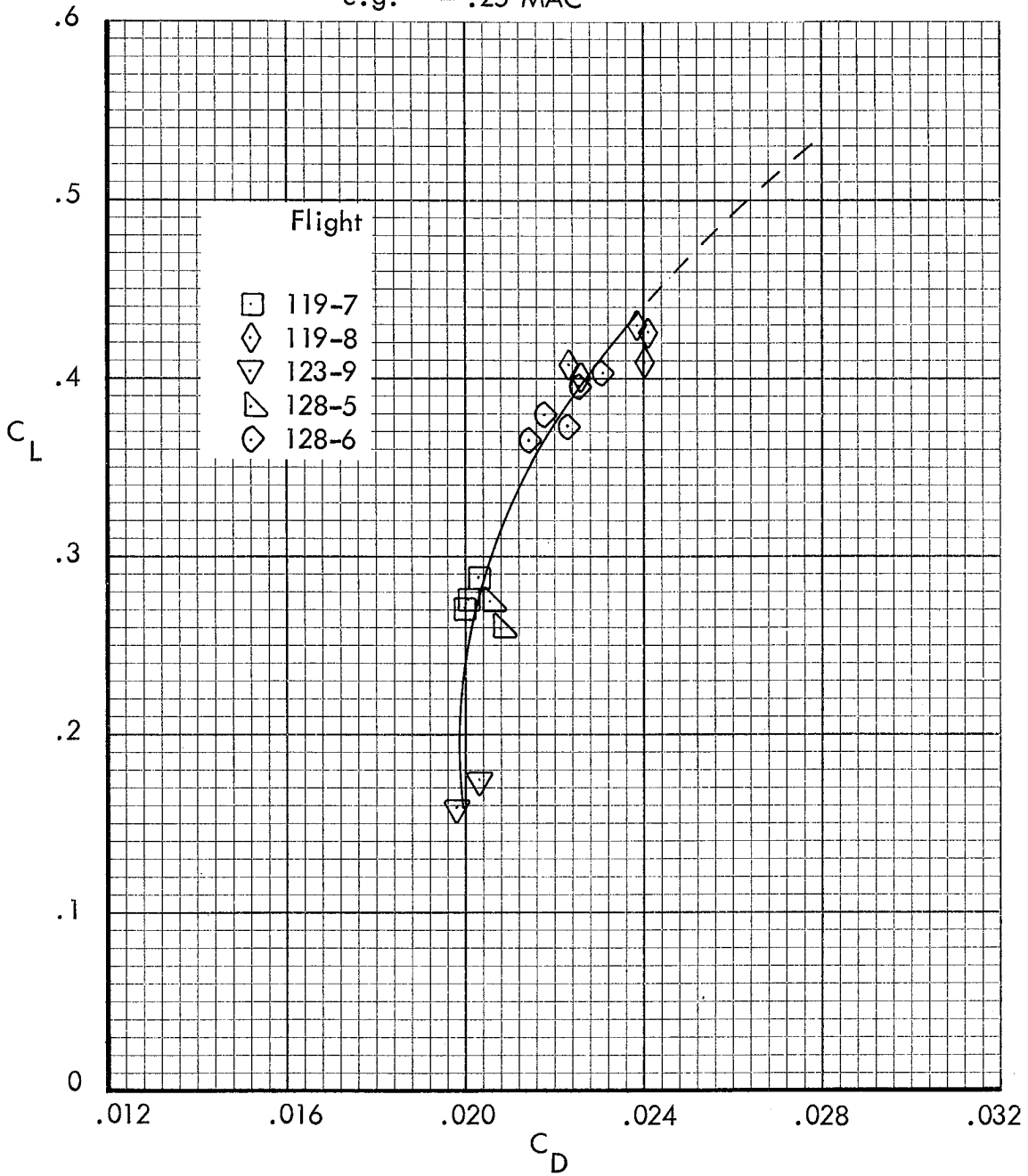
(d) M = 0.775

Figure 54.- Continued.

RN = 55.0×10⁶ based on MAC
Rigid
M = 0.800
c.g. = .25 MAC

(e) M = 0.800

Figure 54.- Continued.

RN $= 55.0 \times 10^6$ based on MAC
Rigid
M   = 0.810
c.g.   = .25 MAC

Flight

□ 119-7
◇ 119-8
▽ 123-9
◁ 128-5
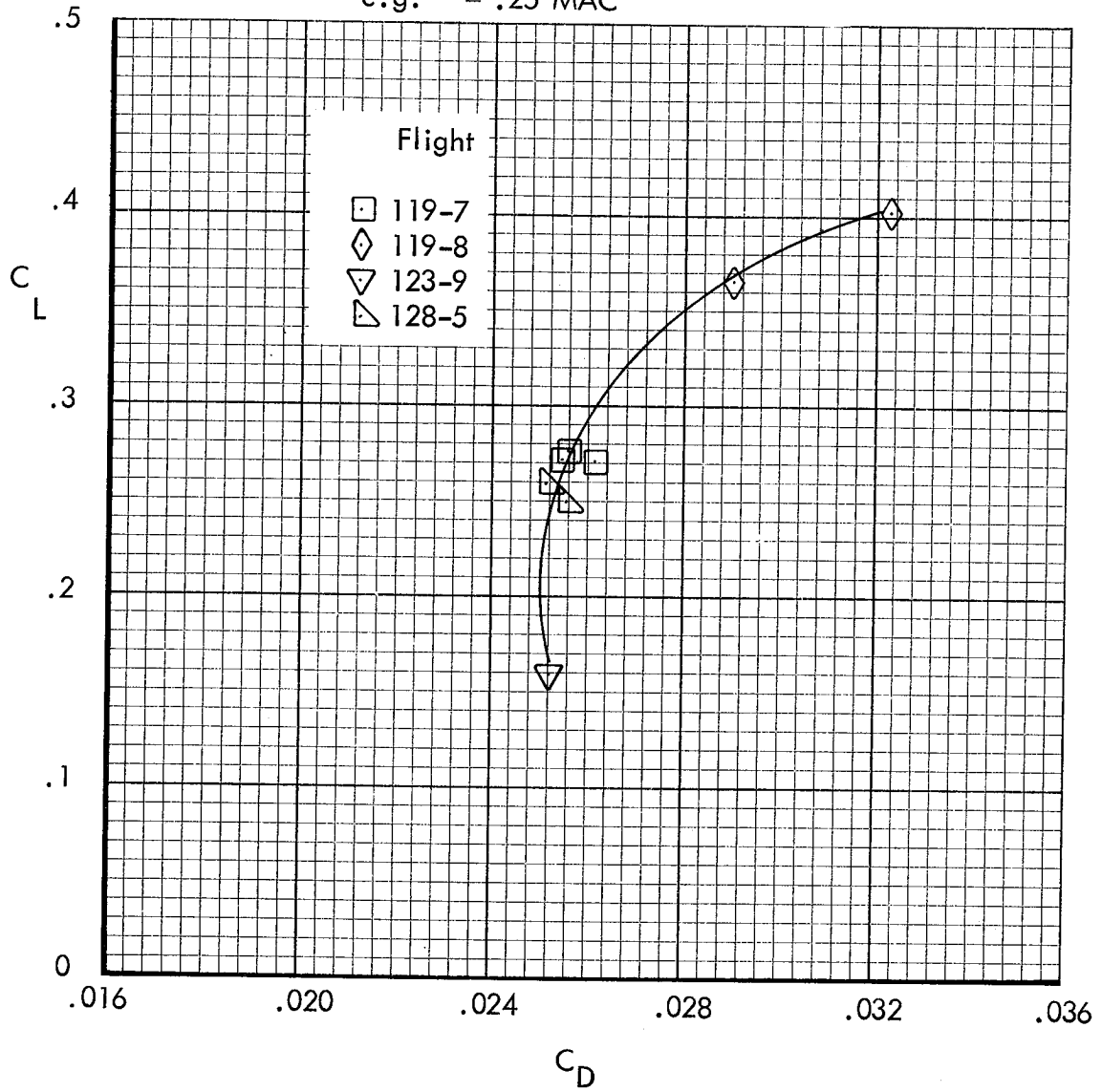
(f) M = 0.810

Figure 54.- Continued.
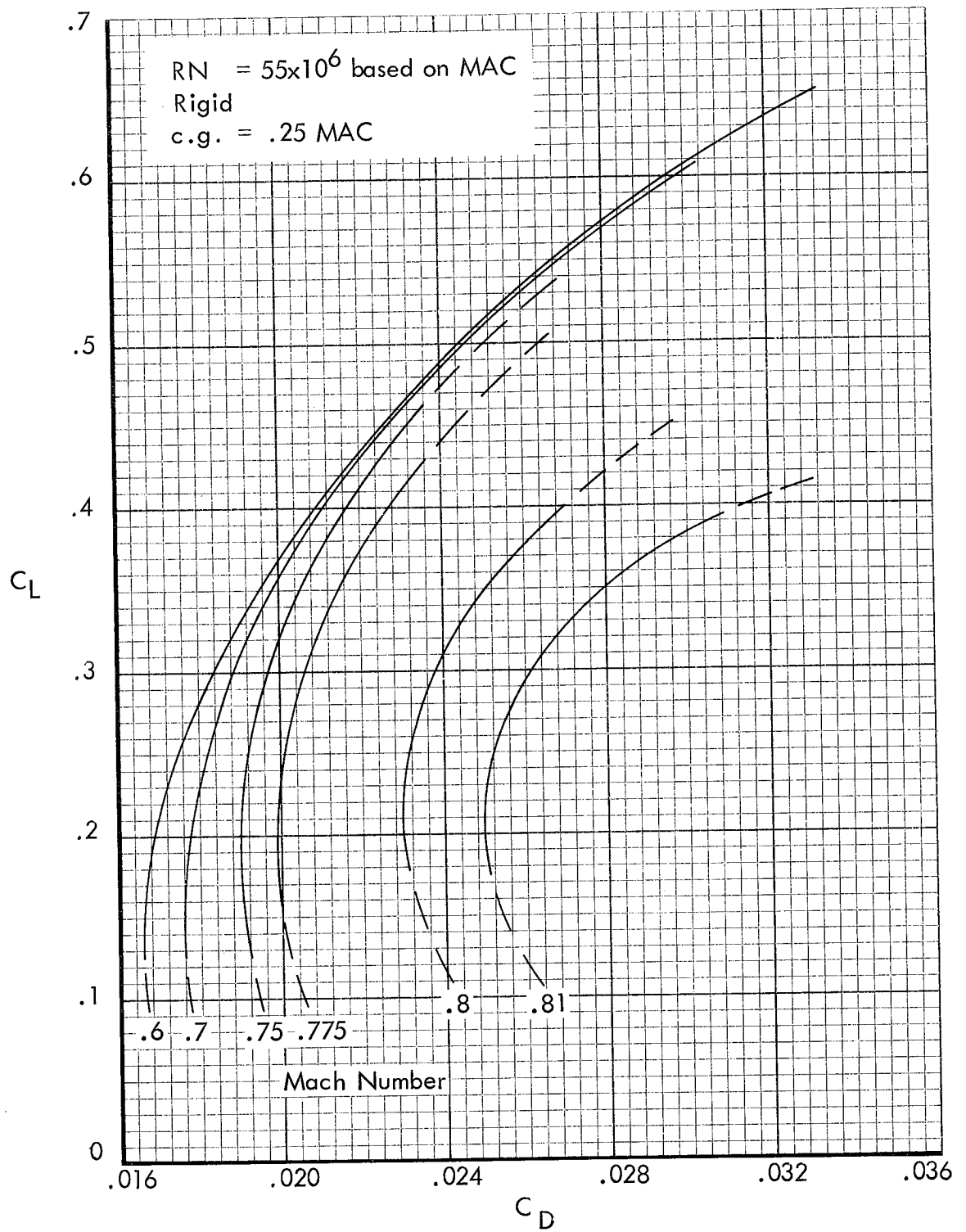
Figure 55.- Summary of flight test drag polars at RN = 55.0×10^6.
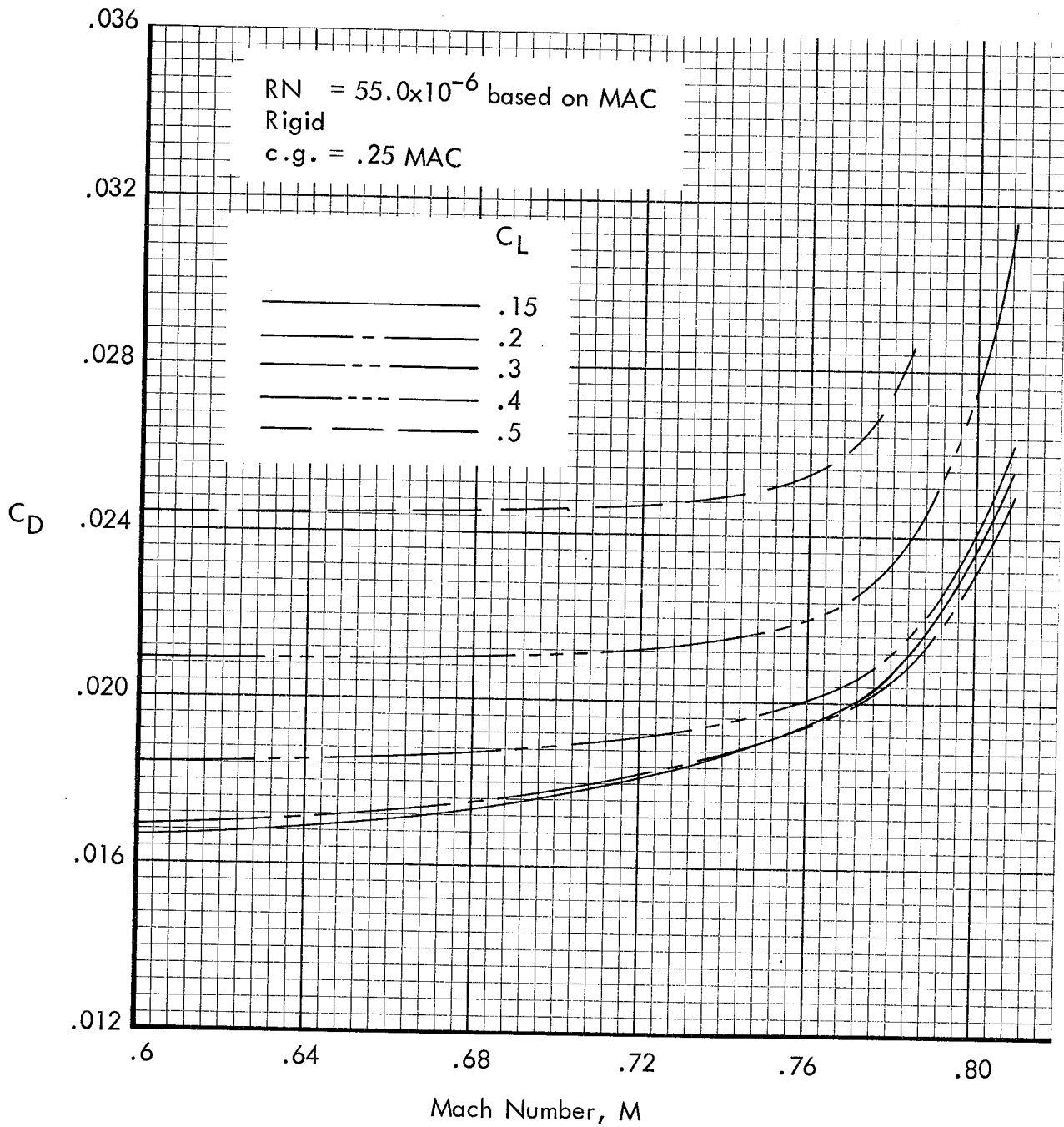
Figure 56.- Drag coefficient variation with Mach Number for constant lift coefficients at RN = 55x10^6.

RN = 55x10⁶ based on MAC
Rigid
M = 0.6
c.g. = .25 MAC

Faired curve based on speed power
data analysis, figure 54 (a)
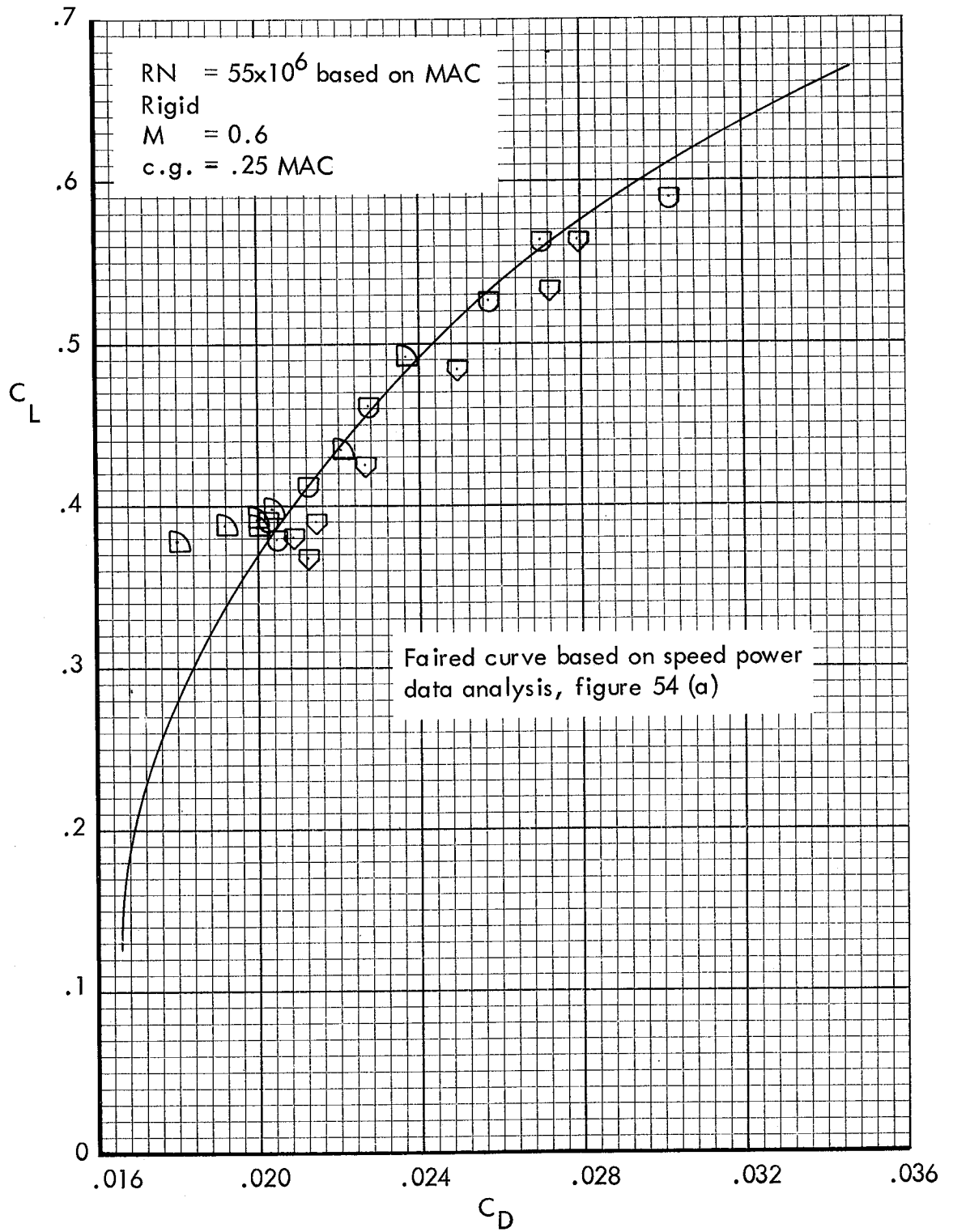
(a) M = 0.6

Figure 57.- Continuous climb drag coefficient data corrected to constant Mach Numbers at RN = 55x10⁶/MAC.

The figure shows a plot of C_L versus C_D.

RN = 55x10^6 based on MAC
Rigid
M = 0.7
c.g.= .25 MAC

Faired curve based on speed power
data analysis, figure 54 (b)

C_L

C_D
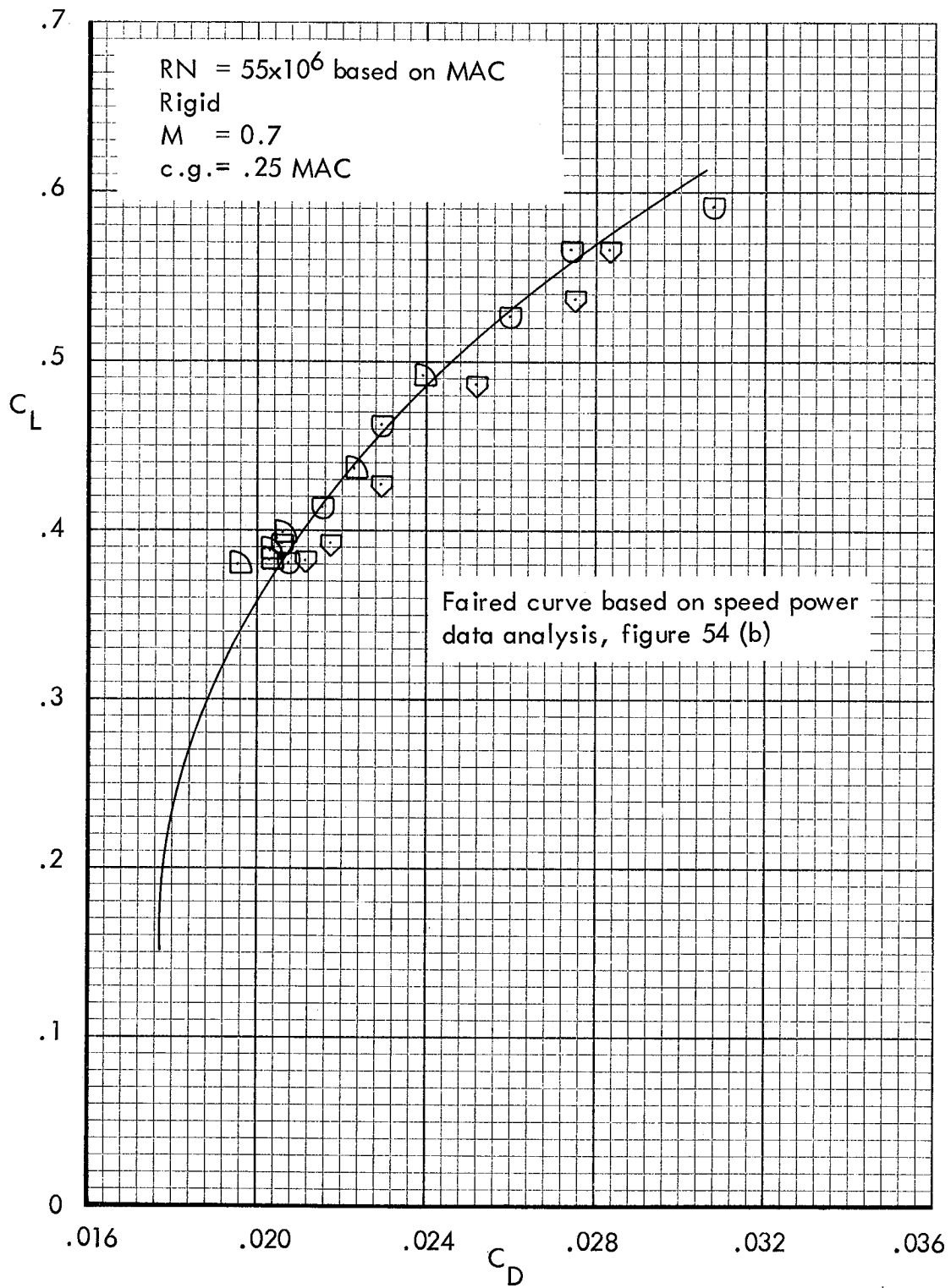
(b) M = 0.7

Figure 57.- Continued.

155

C_D

.016 .020 .024 .028 .032 .036

0 .1 .2 .3 .4 .5 .6 .7

C_L

Figure 57.- Continued.

(c) M = 0.75

Faired curve based on
speed power data analysis,
figure 54 (c)

RN = 55x10^6 based on MAC
Rigid
M = 0.75
c.g. = .25 MAC

(a) M = 0.7
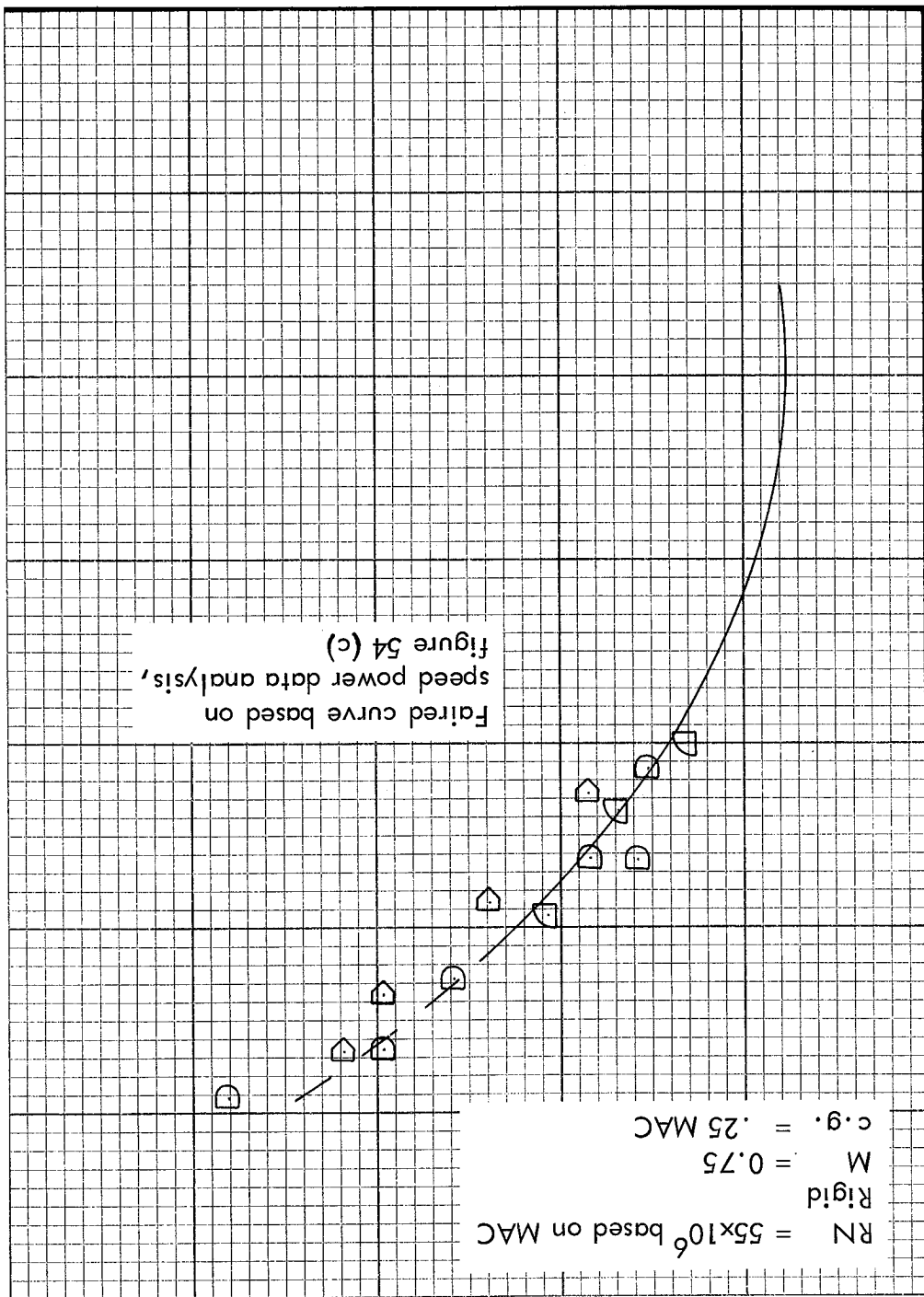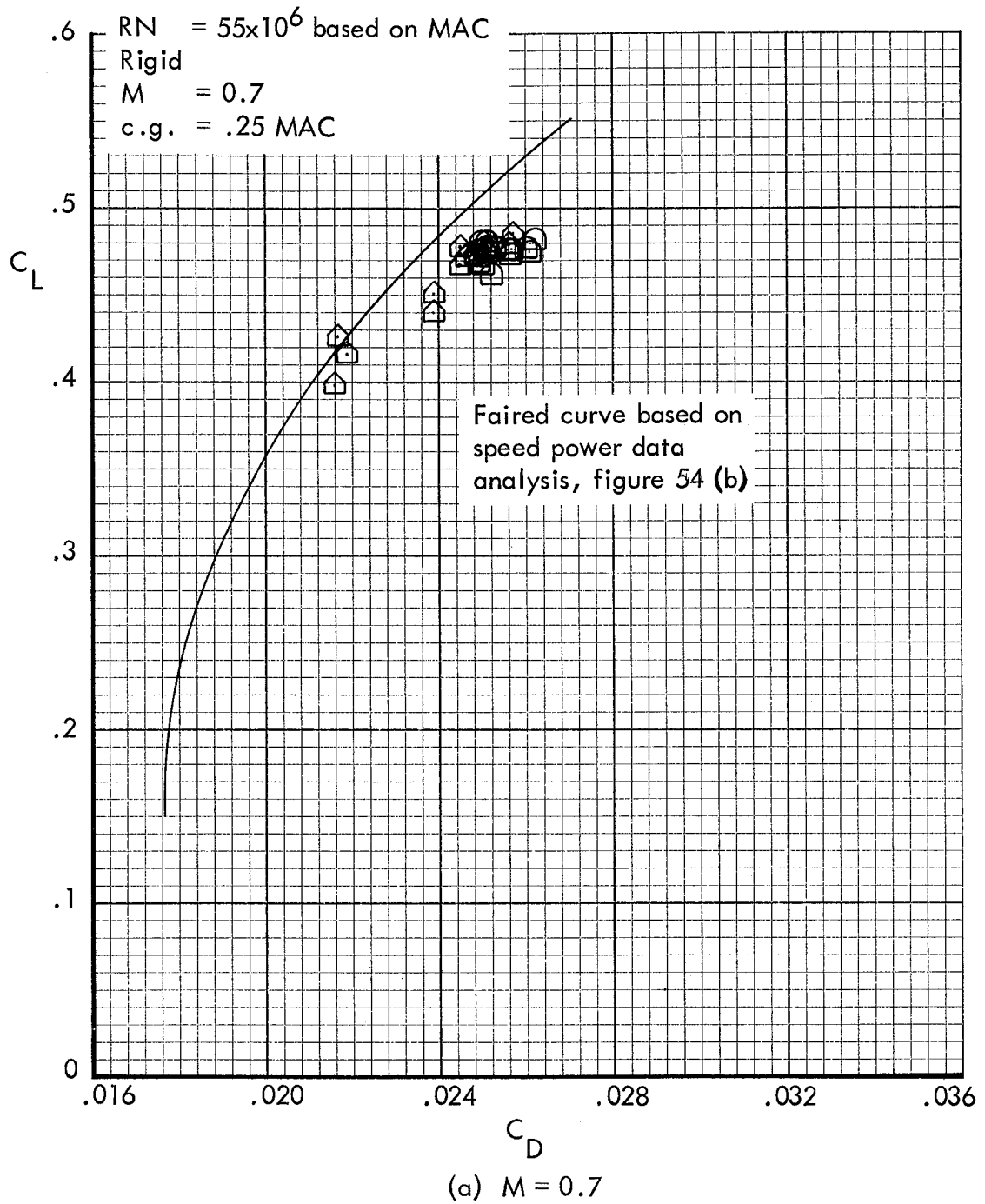
Figure 58.- Range mission cruise drag coefficient data corrected to
constant Mach Numbers at RN = 55x10⁶/MAC.
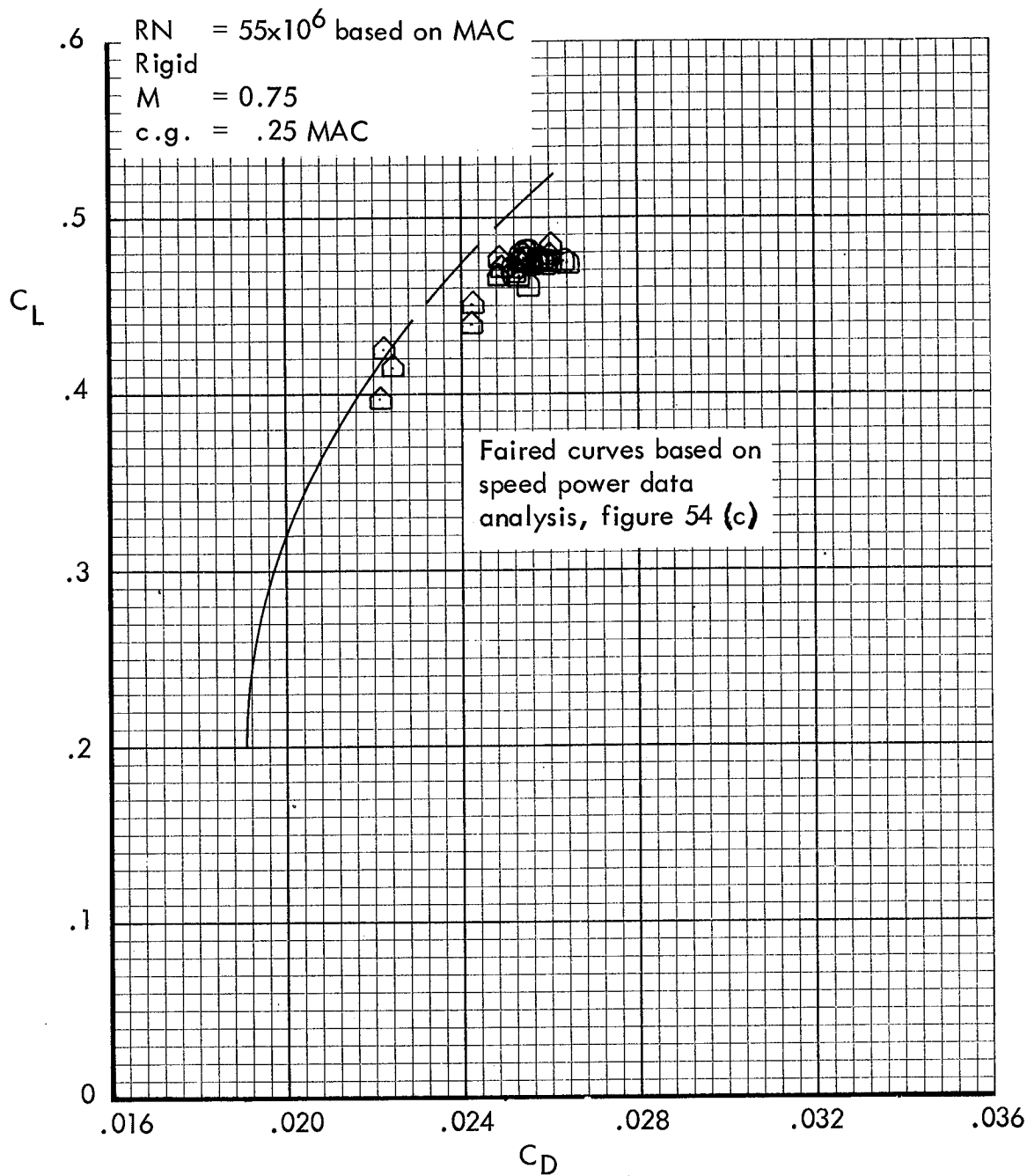
(b) M = 0.75

Figure 58.- Continued.
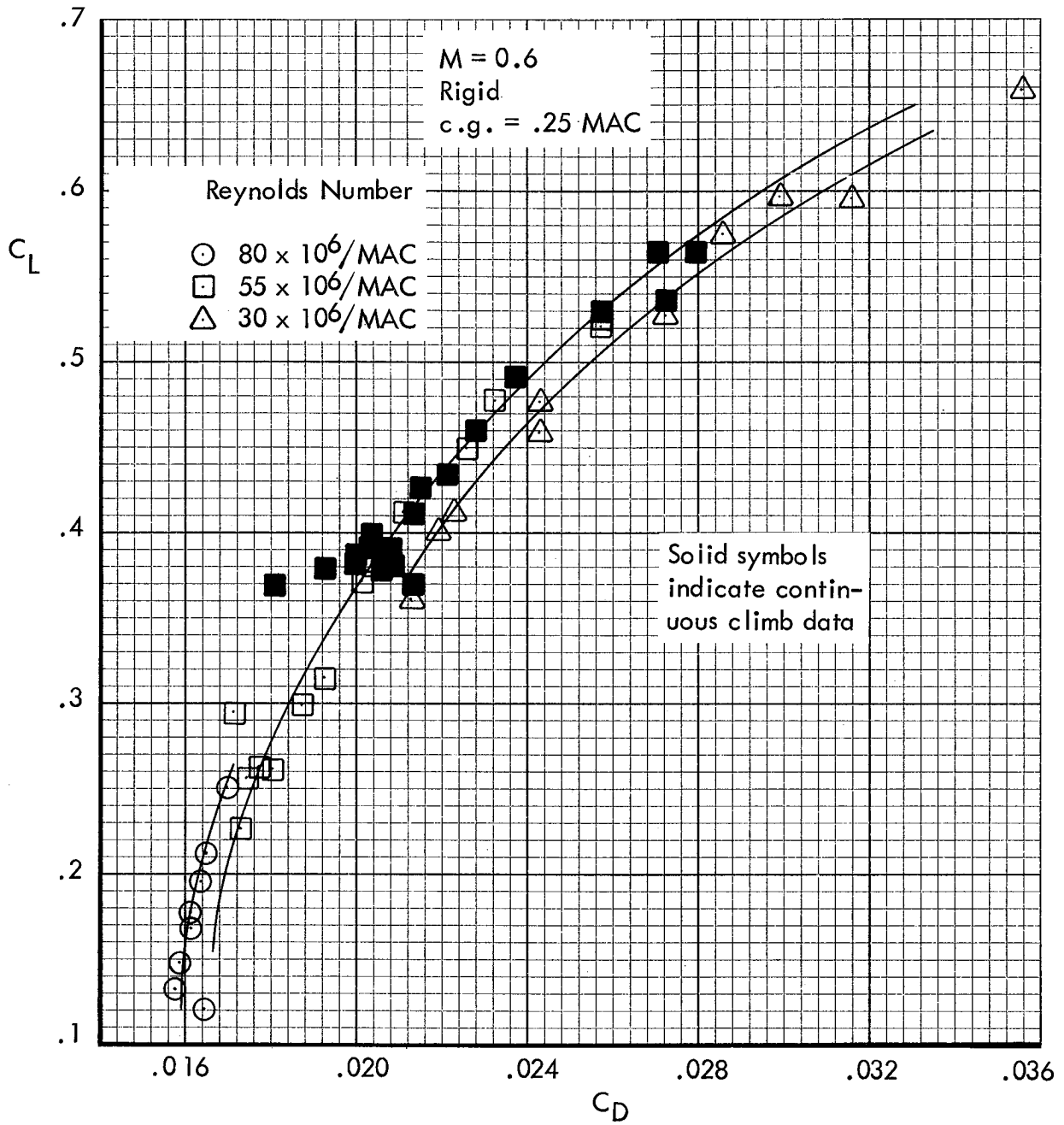
(a) M = 0.6

Figure 59.- Drag polars for several Reynolds Numbers and at constant Mach Numbers.
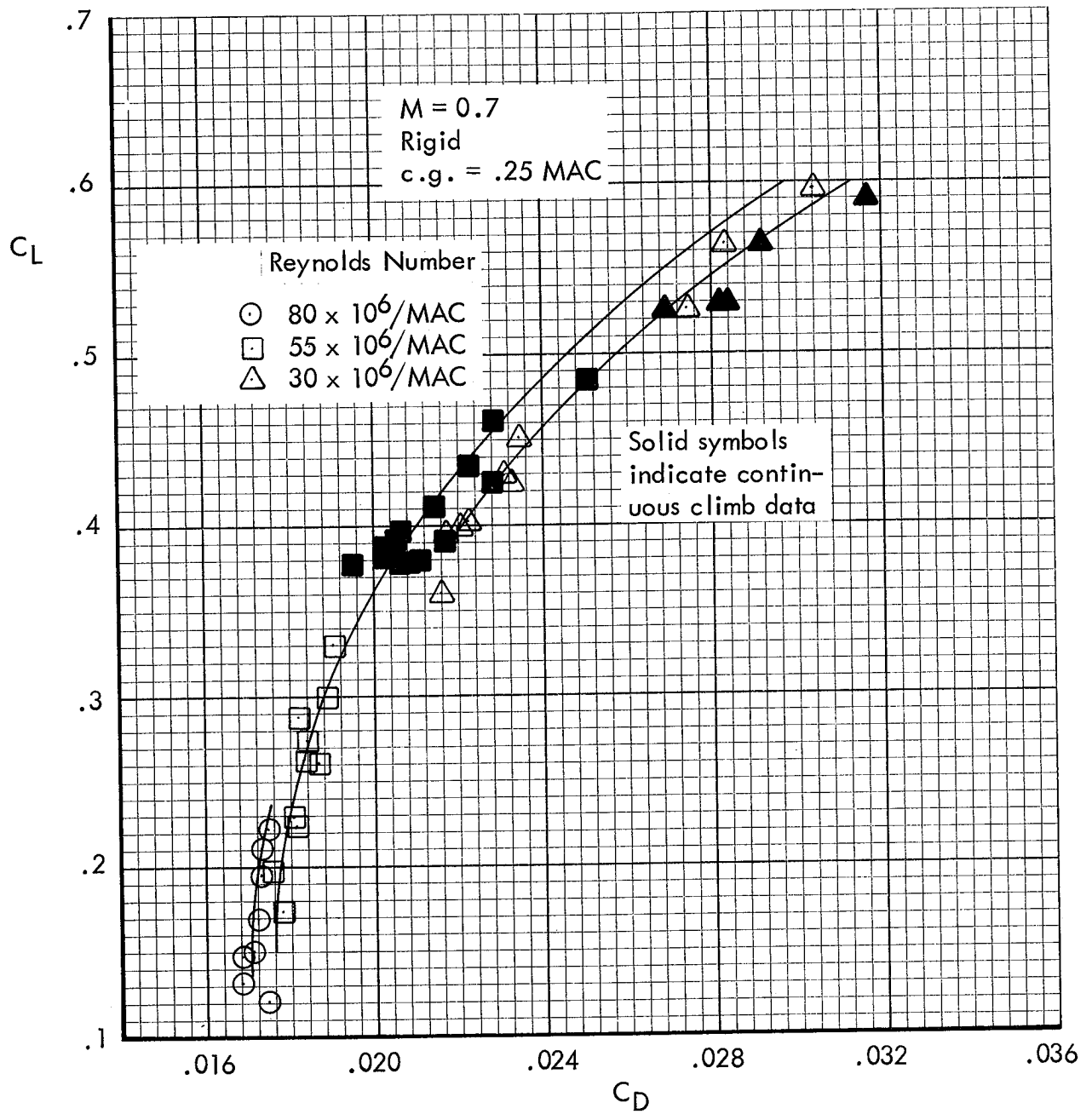
(b) M = 0.7

Figure 59.- Continued.

Correction, knots

Indicated airspeed, knots
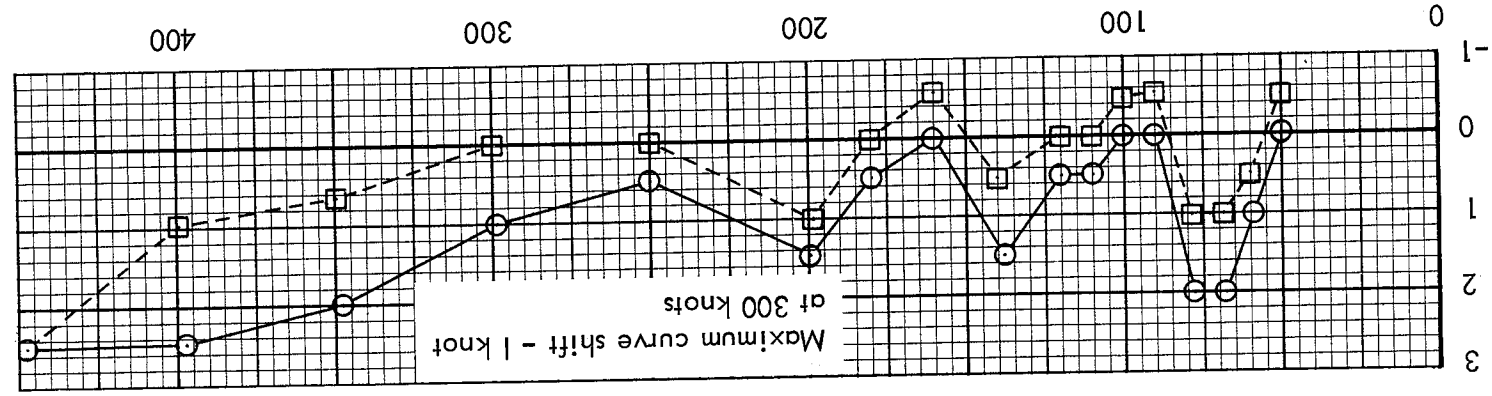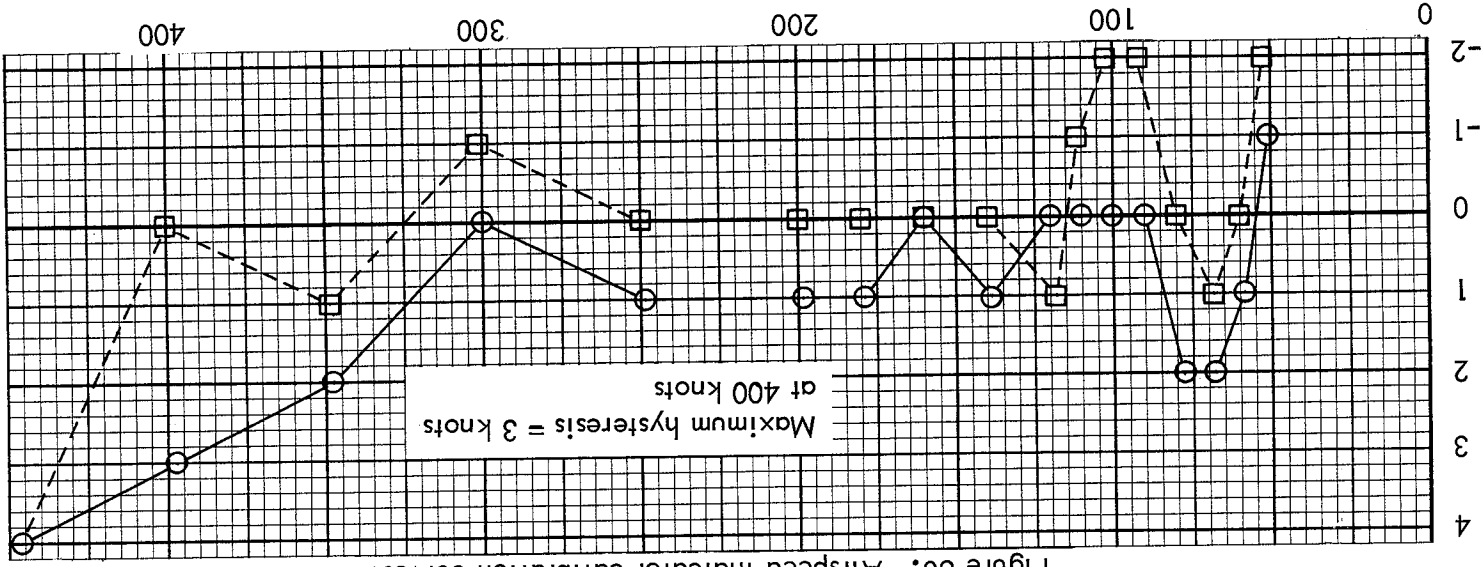
(b) Calibration curve No. 2.

Figure 60.- Continued.

Maximum hysteresis = 3 knots
at 400 knots

Figure 60.- Airspeed indicator calibration curves.

(a) Calibration curve No. 1.

Indicated airspeed, knots.

Correction, knots

Maximum curve shift = 1 knot
at 300 knots

Correction, ft.

Maximum hystersis = 70 ft. at 35,000 ft.

Indicated altitude, 1000 ft.
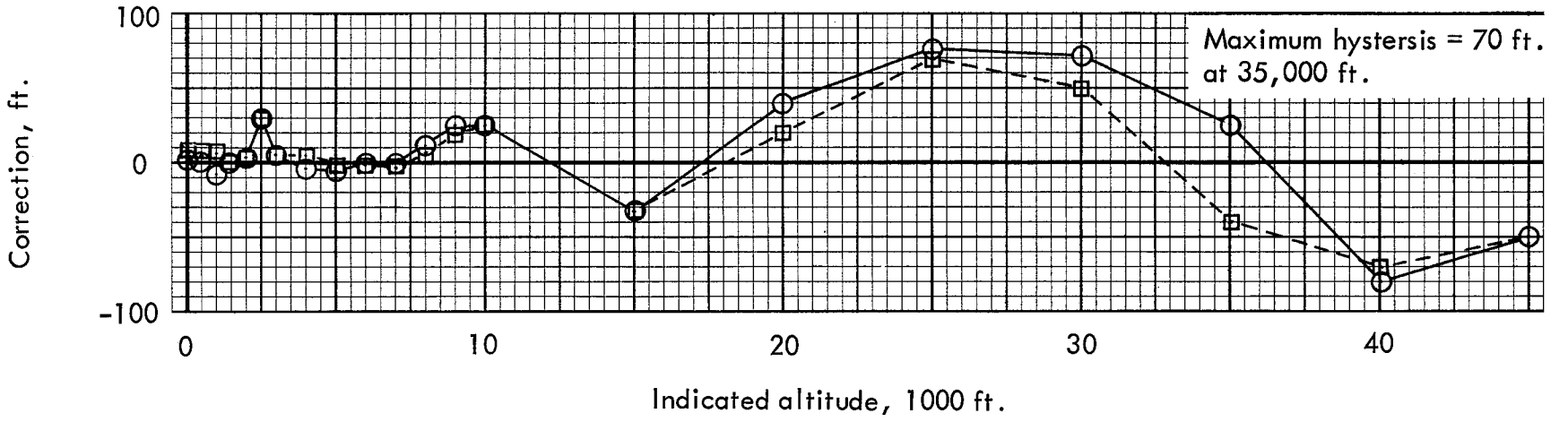
(a) Calibration curve No. 1.

Figure 6.- Altimeter calibration curves.

Correction, ft.

Maximum curve shift = 35 ft. at 35,000 ft.

Indicated altitude, 1000 ft.
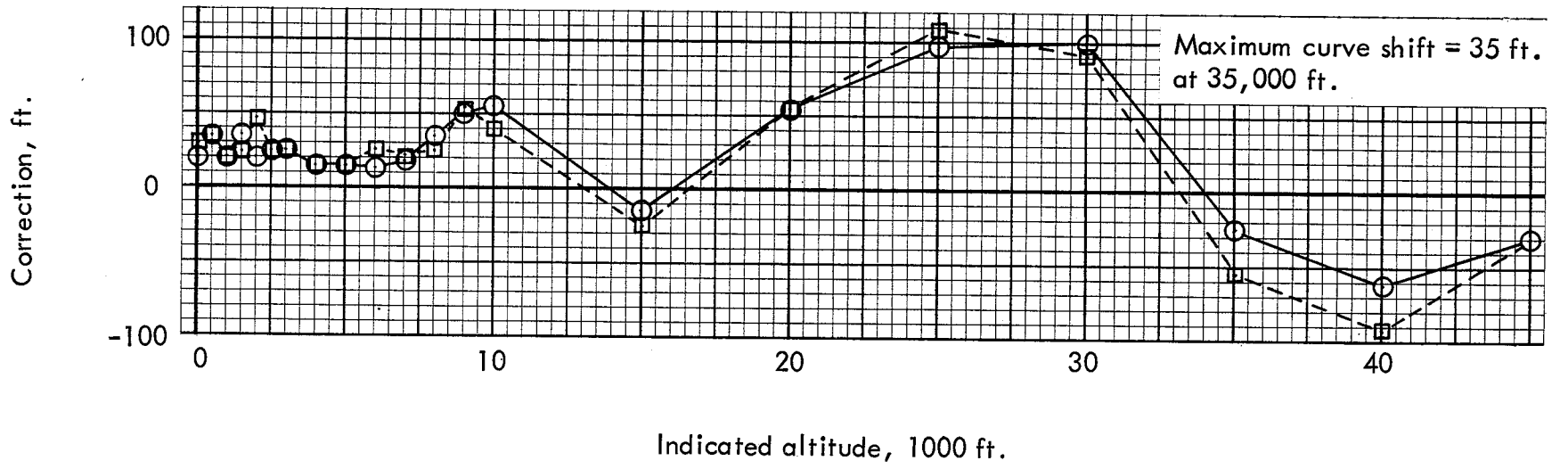
(b) Calibration curve No. 2.

Figure 61.- Continued.
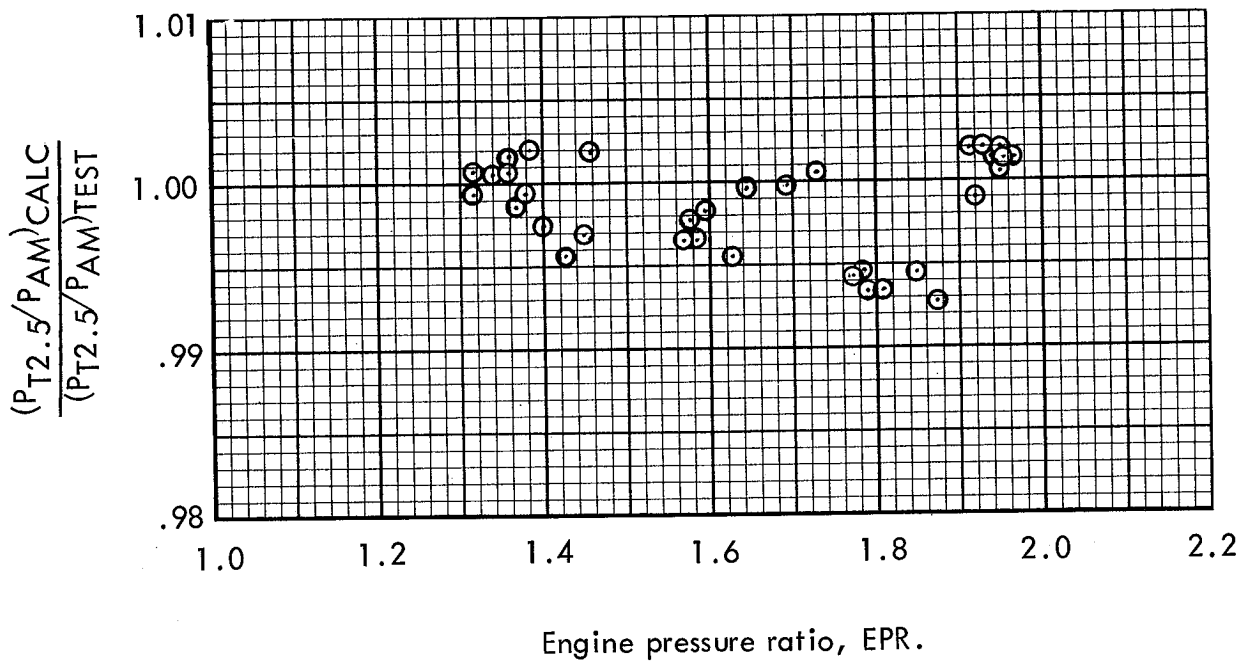
Figure 62.- Comparison of measured and calculated fan
nozzle pressure ratio based on flight data.
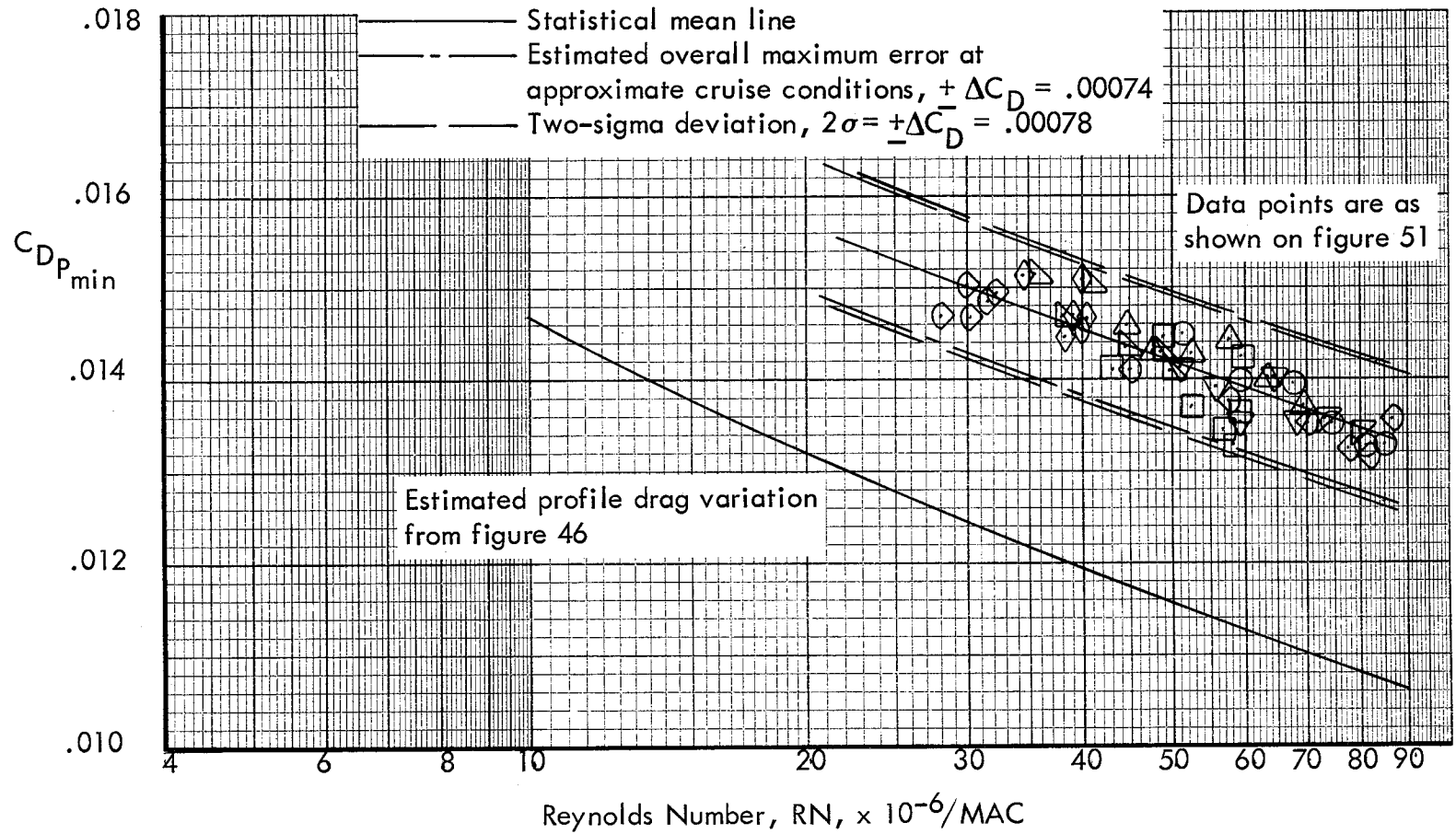
Figure 63.- Comparison of predicted deviation and actual data scatter on profile drag variation with Reynolds Number.

Figure 64.- Comparison of predicted deviation and actual data scatter on flight drag polars.

(a) M = 0.6
RN = 55×10⁶

Faired mean line
Estimated overall maximum error at
approximate cruise conditions, $+ \Delta C_D = .00074$
Two-sigma deviation, $2\sigma = \pm \Delta \bar{C}_D = .00070$

C_L

C_D
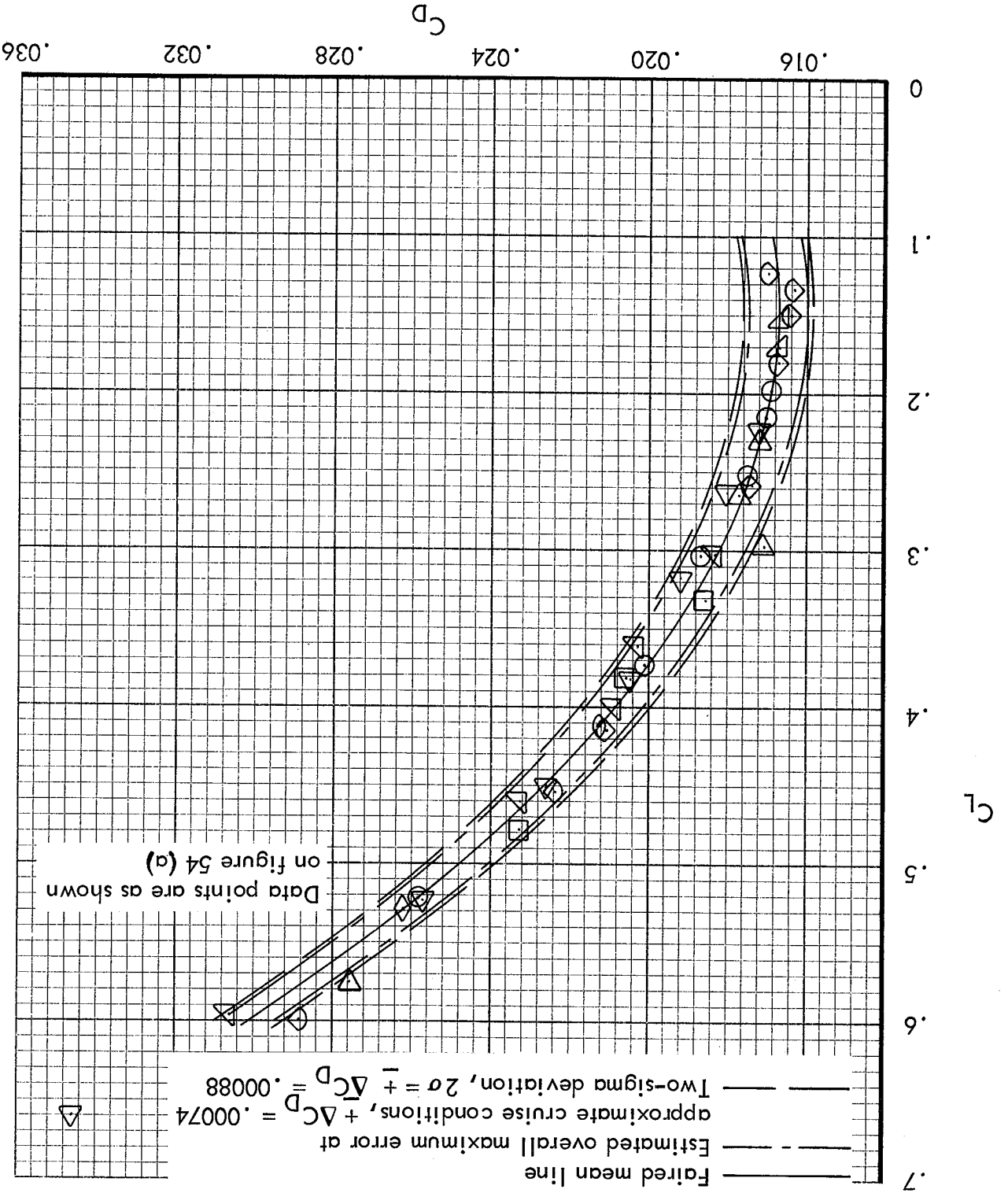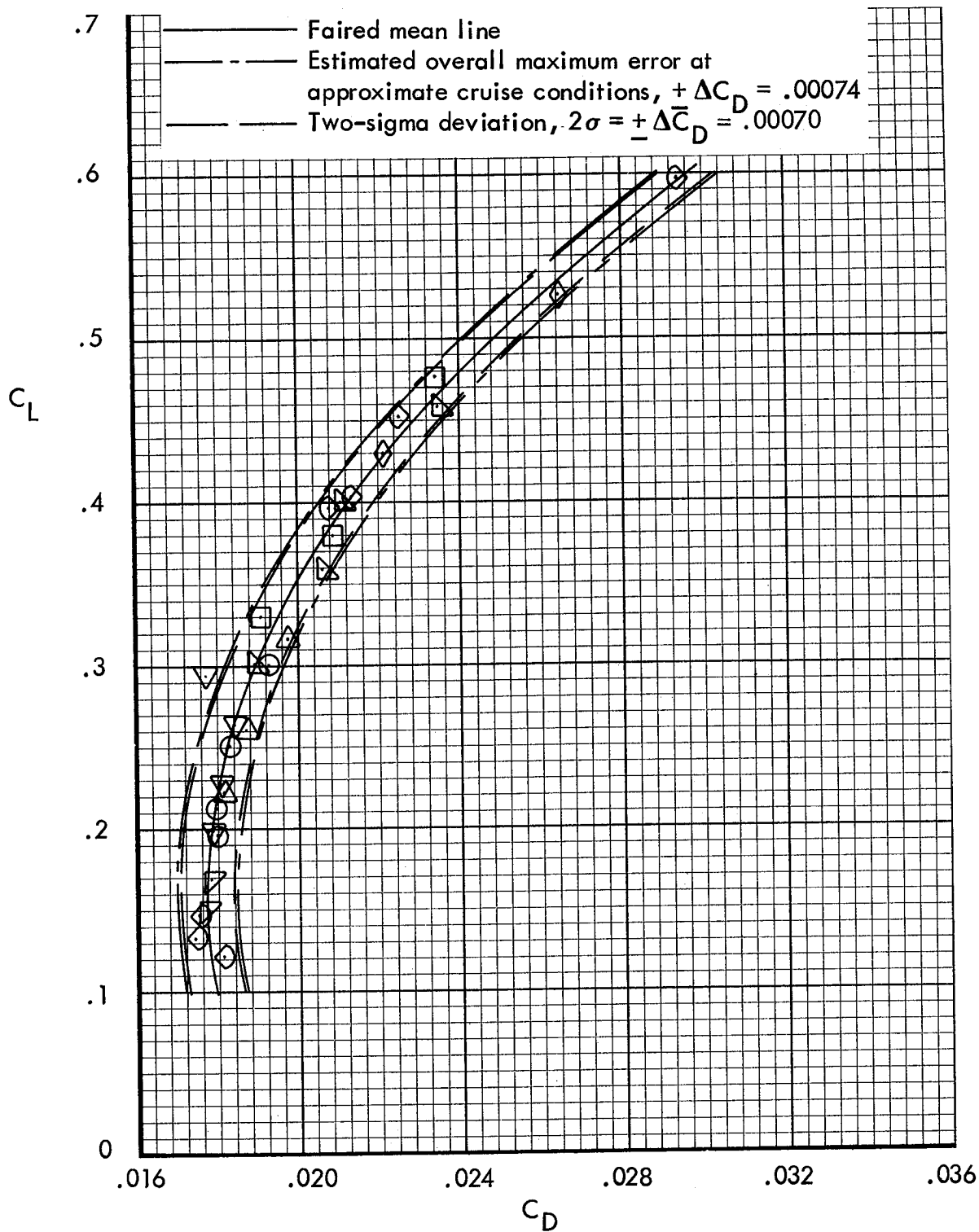
(b) $M = 0.7$
$RN = 55 \times 10^6$

Figure 64.- Continued.